INVESTIGATION OF MECHANICAL BEHAVIOURS OF *EUCALYPTUS NITENS* TIMBER

YINGYAO CHENG

BEng. (Hons), MPhil., M. ASCE

A dissertation submitted for the degree of

Doctor of Philosophy

School of Engineering, University of Tasmania, Australia

May 2022

ABSTRACT

This research focuses on the investigation of the mechanical properties of plantation *Eucalyptus nitens* timber and the understanding of its underlying failure mechanism above and below the fibre saturation point both experimentally and numerically.

Fast-growing eucalypts are now considered potential building materials; one such resource is plantation *Eucalyptus nitens*. To use such a resource as structural or engineered timber, that is to establish design codes and specifications, its compressive and bending strengths need to be studied as they are two important mechanical properties for structural elements in buildings, bridges and decks. For timber members when submerged in water or immersed in soil near the river but above the water table, water can be drawn into the wood by capillary action and lead to moisture contents (*MC*) above fibre saturation point, *FSP*, which is normally at *MC* of 25 - 30%. In this study, compression and four-point bending experiments were undertaken with a Universal Testing Machine to examine for the first time the anisotropic and/or nonlinear mechanical behaviour of fibre-managed plantation *Eucalyptus nitens* (*E. nitens*) samples for low and high *MC*. Here, low *MC* means that the *MC* is less than 15%, which is the normal situation for *E. nitens* timber as used in the building industry, and high *MC* means that the *MC* is above *FSP*, which is the extreme situation for *E. nitens* in structural applications when exposed to water.

As the effect of the moisture dependent material properties are very difficult to examine separately using an experimental approach, sophisticated methods, such as finite element method (FEM) techniques combined with constitutive modelling, are needed to predict ultimate strength more accurately and to assess failure mechanisms in timber under complex loading situations. A newly developed constitutive model extended from an existing constitutive model, namely, a moisture-dependent anisotropic elasto-plasticity model, was proposed in order to display more realistically the short-term deformation and more accurately the failure mechanisms in *E. nitens* timber with different moisture contents and varying grain angles. In this model, a criterion which combined the Hill yield criterion with the Drucker–Prager yield criterion was introduced to exam the anisotropic ultimate capacity of wood with consideration of differences in tension

and compression. Variation of material properties of *E. nitens* timber with varying moisture contents is included in a new moisture-dependent anisotropic elasto-plasticity model in order to predict the short-term anisotropic material behaviour of *E. nitens* timber more accurately when moisture content changes. All these parameters can be derived from experimental data. A UMAT (User-defined mechanical material behaviour in ABAQUS) subroutine within the commercial software ABAQUS was coded to execute the constitutive model for compression, tension and bending. The observed agreement between numerical predictions and experimental investigations shows that the developed constitutive model can be used for *E. nitens* timber with varying moisture contents. The underlying anisotropic behaviour of *E. nitens* timber was also examined numerically.

The key findings of this research were that fibre-managed plantation *E. nitens* timber was highly anisotropic with respect to grain angle and its ductility increased as *MC* increased. The *E. nitens* timber with high moisture content exhibited considerably larger deflections at lower maximum loads, while that with low moisture content showed quite abrupt failures at relatively higher ultimate loads. For both tension and compression, stiffness and strength were dependent on moisture content and loading direction, while the failure mode depended mainly on loading direction. That the anisotropy of *E. nitens* timber was dependent on moisture content sensitivity was proven both numerically and experimentally. The yield surface of *E. nitens* timber enlarged with a decrease in moisture content, while different failure strengths under tension and compression were found. Compared with moisture content, grain angle had a stronger effect on the anisotropic behaviour of *E. nitens* timber due to a difference in the stresses state. At a grain angle of 0°, the normal stress along the grain was dominant compared with the corresponding shear stress and the normal stress across the grain. At loading directions of 30°, 45° and 60°, shear stresses played an important role, and for 90°, the effect of normal stress across the grain was significant. Parametric investigation showed that Young's modulus parallel to the grain and yield stress affected the stiffness and strength significantly when loads were at grain angles between 0° and 15°. Their effects weakened as the grain angle increased from 15° to 45° with almost no effect on compressive strength after 45°. The effect of shear modulus and shear yield stress along wood fibre became the largest contributing factor from 15° to 30°, while after 45° the radial Young's modulus and yield stress took a dominant role in determining stiffness and strength, respectively, compared with the effects of longitudinal Young's modulus and shear modulus. The risk of damage to an *E. nitens* member is expected to increase in high moisture conditions.

The moisture modification factors of Eucalyptus timber at mean level are higher than those of the traditional construction material, Pinus radiata, implying that *E. nitens* was promising as a material to be used for compressive or bending members in the construction industry, especially in water saturated conditions, for example, in wood piling foundations of buildings near the coast for a long time.

This research will provide basic data for *E. nitens* in structural applications, and the approaches introduced can be used in future research for assessing the vulnerability of *E. nitens* members in normal or fully water-saturated states for building and structural applications. The moisture dependent composite plastic constitutive model, by providing results for a comprehensive study of anisotropic plasticity material behaviour incorporating anisotropic and moisture effects, overcame the limitations of the von Mises model and the Hill model with nonlinear isotropic hardening, as they were not always appropriate for *E. nitens* timber. For example, experiments found that the load-deformation behaviour changed from unsteady-state "softening" behaviour at compression parallel to the grain to steady-state "hardening" behaviour at compression perpendicular to the grain. The numerical investigation into the short-term response of *E. nitens* under compression, tension and bending with high and low moisture contents, compared with the experimental data, demonstrated acceptable agreement, showing that the constitutive model works well for Eucalyptus wood.

Keywords: *Eucalyptus nitens; Wood anisotropy; Hardening and softening; Yield criterions; Compression; Bending; High moisture content; Fibre saturation point*

STATEMENTS AND DECLARATIONS

Declaration of Originality

This thesis contains no material which has been accepted for a degree or diploma by the University or any other institution, except by way of background information and duly acknowledged in the thesis, and to the best of my knowledge and belief no material previously published or written by another person except where due acknowledgement is made in the text of the thesis, nor does the thesis contain any material that infringes copyright."

Authority of Access

This thesis may be made available for loan and limited copying and communication in accordance with the *Copyright Act 1968*.

Statement regarding published work contained in thesis

The statement of co-authorship for the research papers in this thesis is given in the following STATE OF CO-AUTHORSHIP. The publishers of Paper 1-4 will hold the copyright for that content and access to the material should be sought from the respective journals. The non-published content of the thesis may be made available for loan and limited copying and communication in accordance with the Statement of Access and the Copyright Act 1968.

Signed

2021/Nov/30

STATE OF CO-AUTHORSHIP

The following people and institutions contributed to the publication of work undertaken as part of this thesis:

- **Candidate:** Yingyao Cheng, School of Engineering, University of Tasmania, Tasmania, Australia.
- **Author 1:** Prof. Andrew Chan, School of Engineering, University of Tasmania, Tasmania, Australia, Primary Supervisor.
- **Author 2:** A/Prof Damien Holloway, School of Engineering, University of Tasmania, Tasmania, Australia, Co-Supervisor.
- **Author 3:** Prof. Gregory Nolan, Centre for Sustainable Architecture with Wood (CSAW), University of Tasmania, Tasmania, Australia, Co-Supervisor.
- **Author 4:** Ms Jaskiran Kaur, School of Engineering, University of Tasmania, Tasmania, Australia.
- **Author 5**: Mr Michael Lee, CLTP Pty Ltd, Tasmania, Australia, Operations manager

Author details and their roles (Corresponding author):*

Paper 1: Located in Chapter 1 and Chapter 3

Yingyao Cheng*, Andrew H.C. Chan, Damien Holloway, Gregory Nolan. Anisotropic material behaviour under compression of *Eucalyptus nitens* with high moisture content. *Construction and building material*, Volume 314, Part B, 2022 DOI: https://doi.org/10.1016/j.conbuildmat.2021.124788

Authors and their roles: The candidate was the primary author of this paper with 75% contribution. Author 1, Author 2, and Author 3 contributed respectively 10%, 10%, and 5%. Candidate: Conceptualization, Methodology, Investigation, Writing original draft & editing. Author 1, Author 2 and Author 3 contributed to the idea behind the paper, provided supervision, technical expertise and edited the draft paper.

Paper 2: Located in Chapter 1 and Chapter 4

Yingyao Cheng*, Gregory Nolan, Damien Holloway, Jaskiran Kaur, Michael Lee and Andrew H.C. Chan. Flexural Characteristics of Eucalyptus nitens Timber with High Moisture Content. BioResources 2021, 16, 2921-2936. DOI: 10.15376/biores.16.2.2921-2936

Authors and their roles: The candidate was the primary author of the paper who conceptualised the research presented in the papers, performed the literature review, developed the methodology, conducted the experimental investigations, analyse the data, and prepared the original draft paper. Author 1, Author 2, Author 3 contributed to the idea behind the paper, provided supervision and edited the draft paper. Author 4 and Author 5 assisted with the experimental investigations and collaborated with the candidate in contributing through discussions and participations to the idea behind the paper.

Paper 3: Located in Chapter 4

Yingyao Cheng*, Gregory Nolan, Damien Holloway, Jaskiran Kaur, Andrew H.C. Chan. Experimental study of *Eucalyptus nitens* timber with high moisture content for its bending design values. World conference on timber Engineering 2021. Santiago, Chile, Aug. 9-12, 2021.

Authors and their roles: The candidate was the primary author of this paper, who conceptualised the research presented in the paper, performed the literature review, developed the methodology, conducted the experimental investigations, analyse the data, and prepared the original draft paper. Author 1, Author 2, Author 3 contributed to the idea behind the paper, provided supervision, edited the draft paper. Author 4 collaborated with the candidate in experimental investigations and contributed through discussions and participations to the idea behind the paper.

Paper 4: Located in Chapter 5

Yingyao Cheng*, Andrew H.C. Chan, Damien Holloway, Gregory Nolan. A moisture dependent elastoplastic fibre composite model for compressive wood members, its finite element method implementation and validation, Fourth Australasian Conference on Computational Mechanics, Hobart, Australian, Nov. 27-29, 2019.

Authors and their roles: The candidate was the primary author of this paper, who conceptualised the research presented in the paper, performed the literature review, developed the constitutive model, conducted the numerical investigations, and prepared the original draft paper. Author 1, Author 2, and Author 3, contributed to the idea behind the paper, provided supervision, technical expertise, and edited the draft paper.

We, the undersigned, endorse the above stated contribution of work undertaken for each of the published (or submitted) peer-reviewed manuscripts contributing to this thesis:

Signed:

Yingyao Cheng	***Professor Andrew Chan***	***Professor Tim Finnigan***
Candidate	*Primary Supervisor*	*Head of School*
School of Engineering	*School of Engineering*	*School of Engineering*
University of Tasmania	*University of Tasmania*	*University of Tasmania*

Date: 25/11/2021

ACKNOWLEDGEMENTS

I sincerely thank my supervisor Prof. Andrew Chan, for his encouraging support and far-sighted guidance in my research. Thanks also go to my cooperating supervisors A/Prof. Damien Holloway and Prof. Gregory Nolan for their valuable feedback, patient advice and constant support during the period of my studies. They are all role models in my daily life. I greatly appreciate all the time and ideas that they have contributed.

While doing my PhD, I was invited by A/Prof. Damien Holloway as a teacher on a structural mechanics course at the University of Tasmania's School of Engineering and by Professor Andrew Chan as a co-supervisor on master projects regarding testing of timber. Thank you, Damien and Andrew, for giving me such valuable teaching opportunities. I have developed a set of skills that will support me well in my future academic career.

I would like to thank Dr Mohammad Derikvand, Dr. Nathan Kotlarewski and Mr. Michael Lee from the Centre for Sustainable Architecture with Wood (CSAW) for their advice and support when designing the experiments and preparing the test specimens. My special thanks to Mr Andrew Bylett, our workshop manager, and Mr Calverly Gerard, our lab expert, in the School of Engineering workshop at the University of Tasmania for constructing the apparatus and providing technical support throughout all the testing.

Special gratitude also goes to ARC CFV director Prof. Mark Hunt, my supervisor Prof. Gregory Nolan and the Centre's manager Dr. Mark Neyland for giving me the opportunity to work closely with people from the University of Tasmania's ARC Centre for Forest Value (CFV) and their industry partners. Without your support and encouragement, it would have been hard for me to link my research to industrial applications and for this PhD research to run as smoothly and cleanly as it did.

Appreciation is also expressed to Dr Chris Beadle for valuable feedback on my papers, Mr Peter Meyer and Ms Barbara Meyer for constant support in my daily life, and all the people of the Royal Society of Tasmania. I enjoyed the time spent with them.

Last but not least, I wish to extend my thanks to all the people in the School of Engineering for their help in providing a good environment for my research. My thanks also go to all my family members for their love and unconditional support throughout the period of my PhD research.

CONTENTS

LIST OF FIGURES

LIST OF TABLES

Chapter 1

1 INTRODUCTION

1.1 BACKGROUND AND AIMS OF THE RESEARCH

Timbers from fast-growing eucalypts are now considered to be building materials with extensive potential [1-4]; and one such resource is plantation Eucalyptus *nitens* (*E. nitens*) [5, 6]. In order to use such eucalyptus timber to produce structural timber or engineered timber, the mechanical properties of *E. nitens* need to be known in order to establish design codes and specifications. For many practical applications, compressive and bending behaviours are particularly of interest as they determine the mechanical performance of timber members, which are widely used in the building industry [4, 6-8]. For example, compressive and bending strengths are two important mechanical properties for piles in buildings, bridges and decks. This study, therefore, uses compression and bending tests to examine the compressive and bending behaviour of wood from plantation-grown *E. nitens*.

Much attention is currently being paid to a reassessment of the safety of timber structures in consideration of high moisture content [9]. Being a hygroscopic material, the strength of wood decreases significantly until reaching a moisture content above fibre saturation point (*FSP*), when there is an absence of any free water in the cell lumina, and the cell walls are saturated with chemically and physically bound water [9, 10]. If moisture content rises above *FSP* to a completely saturated state, compressive strength parallel and perpendicular to the grain direction decreases up to 50%, and consequently, the risk of failure increases [13, 33]. Apart from those design standards for fully immersed piles [28, 34, 35], few provide strength and stiffness values for round wood at moisture content above *FSP*. Those that do are for coniferous species [13, 28, 34] and it is now necessary to develop the same standards for plantation eucalypts. The design values for wood strength are useful indicators for assessing the safety of structural members based on design codes, and these are generally determined by small clear specimen testing according to current STANDARDS [11]. For this study therefore, small clear specimens will be used as a first development towards design values for *E. nitens* timber both below and above *FSP*.

Wood has an orthotropic structure and because of this its mechanical properties are dependent on the grain direction [12-14]. The common structural usage of wood in timber engineering exploits the longitudinal direction as this has the highest strength values

[14, 15]; the lowest strength values are in material which is perpendicular to the grain, and failure mainly occurs in the radial and tangential planes [14, 16]. This is because failure modes perpendicular to the grain differ from those parallel to the grain. Long and narrow cells are oriented in a longitudinal direction and act like columns of fibre, with hemicellulose acting as fibril networks; however, this structure results in minimum strength when compression or tension are perpendicular to the grain, as the bonds between the fibres break [17]. To better understand mechanical failure in timber, the failure behaviour for all material directions must be examined. For plantation eucalypts, examination of wood strength has focused on the effects of site, tree age, silvicultural management [18, 19], and basic mechanical properties such as compressive stiffness and strength under short- or long-term loading [3, 5, 20, 21]. As plantation eucalypts offer some significant advantages for structural applications relative to other timber species, such as sustainable supply [22], a comprehensive examination of anisotropic behaviours of *E. nitens* timber is essential.

Current standards assume a linear elastic behaviour for timber and, based on this assumption, linear ultimate strength is determined. However, this method was not always appropriate as ductile behaviour can be observed in compression perpendicular to the grain [23, 24]. Sophisticated methods are needed to learn more about failure modes and to more accurately predict ultimate strength [24]. FEM (Finite Element Method) techniques combined with constitutive modelling have proven to be valuable tools in assessing and predicting possible failure in wood objects and in timber structures [23-27]. Large amounts of evidence have shown that wood is a three dimensional, orthotropic, elastoplastic, visco-elastic, mechano-sorptive, creep material [23, 24, 28-31], and its mechanical properties are dependent on the grain direction [12-14] and the moisture content [23, 32]. Hence to obtain reliable predictions for the behaviour of timber where the moisture content is very high, the effect of moisture should be included. In order to numerically model strain amplitude correctly, a new constitutive model is needed, which takes anisotropic and hygroscopic features of timber into account.

To deal with these problems, this current research focuses on the investigation of the mechanical properties of plantation *E. nitens* timber and the understanding of its underlying failure mechanism above and below fibre saturation point both experimentally and numerically. The samples were obtained from a 16-year-old fibre managed plantation *E. nitens* resource in Tasmania, Australia. This is because fibre managed plantations are aimed at producing high-quality structural timber, for which there is currently high demand. With fibre-management, the compressive and bending strengths of the *E. nitens* timber are increased for meeting the requirement of building industry. Older plantations exist, but young trees have less growth stresses and split less [33]. In addition, a decline in supply of eucalypt timber from native forest in Australia has led to a need to develop solid-wood products from plantations for applications in building construction [22]. Therefore, the scope of this thesis is confined to the results from 16-year-old *E. nitens*, but the extent to which the findings can be generalised to other plantations and to native eucalyptus forests may be the subject of future research.

The thesis aims to determine the compressive and flexural characteristics of plantation *E. nitens* timber, since currently, fast-growing plantation Eucalyptus species, such as *E. nitens*, are drawing much attention due to their potential for structural building applications and availability [3, 6, 21, 34, 35]. It further aims to model the anisotropic plasticity of *E. nitens* timber and to show the effect of moisture content on this, and to understand the underlying failure mechanism of *E. nitens* timber above and below fibre saturation point. These aims are expanded in the next section into the specific research objectives of this study. It should be noted that this study focuses on idealised (i.e., defect-free) *E. nitens* material.

1.2 RESEARCH OBJECTIVES

To achieve these aims, five objectives are to be addressed:

Objective One: To quantify the anisotropic short-term response under compression of Eucalyptus *nitens* with high and low moisture contents. Objective One links with the first aim and will be investigated using an experimental approach. In Chapter 3 the comprehensive compression behaviour of plantation Eucalyptus for all directions, covering different load-to-annual ring directions as well as grain orientations, was examined systematically. The anisotropy of plantation *E. nitens* under compression with high and low moisture contents was determined.

Objective Two: To ascertain the flexural characteristics of plantation *E. nitens* timber in bending with high and low moisture contents and determine the design values for the application of *E. nitens* wood in water-saturated conditions. Objective Two combines experimental and theoretical approaches, which together with Objective One achieves the first aim of this thesis. *MOE, MOR*, four-point bending load-deflection curves of fibre managed *E. nitens* timber with high moisture content were determined experimentally in Chapter 4. The design characteristic values for *E. nitens* bending members for both low and high moisture contents were obtained.

Objective Three: To determine the anisotropic and hygroscopic material behaviour of *E. nitens* timber in order to display its short-term response in deformation and failure mode with low and high moistures more realistically. Objective Three links with the second aim and will investigate using theoretical and numerical approaches. The moisture-dependent anisotropic elasto-plasticity model will be proposed and validated with experimental data, e.g., De Borst et al. [36], Hering et al. [14] and the data from *E. nitens* from Chapter 3. Details will be provided in Chapter 5.

Objective Four: To understand the failure mechanism of *E. nitens* timber in compression covering a broad range of the grain angles during conditions of both high and low moisture content. This Objective, together with Objective Five, attain the third aim and mainly uses a numerical approach as this approach combined with constitutive modelling overcomes the limitations of the experiments due to the non-uniformity of wood.

Objective Five: To quantify the effect of grain angle and high moisture on the bending performance of *E. nitens* timber. This objective mainly uses a numerical approach together with data from experiments in this study and from the literature. As the final objective in this research project, this task is presented in Chapter 7 and shows the application of the moisture-dependent anisotropic elasto-plasticity model to *E. nitens* timber.

1.3 RESEARCH ORIGINALITY AND INNOVATIONS

Based on the reasons mentioned above, the key innovations in my research are given below.

- The anisotropic material behaviour of plantation *E. nitens* timber under compression with low and high moisture contents is examined for the first time. Timber, a very useful material in building construction, currently receives much attention as to the safety of timber structures possessing high moisture content, since the stiffness and strength are reduced in high moisture content conditions [9]. Although regarded as having great potential for structural applications [3, 6], plantation Eucalyptus *E. nitens* has not yet been systematically studied regarding the effects of high moisture content on its compressive properties, such as strength and stiffness.

- This research provides data for *E. nitens*, and for the first time suggests the design values for this timber, when containing a high moisture content, as the basis for establishing relevant design codes and specifications for using *E. nitens* in fully water saturated applications. This study also introduces approaches which can be used in future research for assessing the vulnerability of *E. nitens* bending members in normal or fully water-saturated states for structural applications.

- A new, moisture dependent anisotropic elasto-plasticity constitutive model is proposed to describe the timber material. Much research showed that, for short term loading, wood is a moisture dependent, anisotropic and elastoplastic tension–compression asymmetrical material [14, 23, 36]. This behaviour has not been systematically studied and described until now. In this study the proposed constitutive model is described in detail, numerically implemented, and experimentally calibrated and validated. The proposed constitutive model has overcome the limitations of the Von Mise model and the Hill model with nonlinear isotropic hardening, as they were not always appropriate for *E. nitens* timber. The application of this material model is not only limited to *E. nitens* but can also be extended to other wood species.

- A comprehensive study of anisotropic plasticity material behaviour incorporating anisotropic and moisture effects using the moisture dependent anisotropic elasto-plasticity constitutive model for *E. nitens* timber was undertaken for the first time. The work here provided a more accurate numerical predictions regarding *E. nitens* timber both below and above *FSP*, in compression, tension and bending, with specific consideration of differences in tension and compression.

1.4 LAYOUT OF THE THESIS

The layout of the remainder of this thesis is as follows.

- Chapter 2 outlines fundamental information on timber, especially Eucalyptus. Previous attempts at constitutive models of timber, moisture adjustment models of timber, and previous experimental studies on Eucalyptus are also documented.

- Chapter 3 examines experimentally the anisotropic behaviour of *E. nitens* under compression with high and low moisture contents. Compression experiments on *E. nitens* wood were carried out with loading direction varying according to the grain direction, ie. with grain angles of 0, 30, 45, 60, 90 degrees, and with different annual growth ring directions. The compressive behaviour of this fibre-managed Eucalyptus wood (*E. nitens*) was determined, whilst values for compressive stiffness, and strength from parallel to perpendicular to the wood fibre (grain) with low and high moisture contents were obtained.

- Chapter 4 determines the flexural characteristics of fibre-managed *E. nitens* beams with different annual ring orientations in high and low moisture content conditions. The material behaviour of *E. nitens* with low and high moisture content under four-point bending was examined and failure modes for high and low moisture contents were identified. *MOE*, *MOR* and design characteristic values for *E. nitens* bending members for both low and high moisture contents were obtained.

- Chapter 5 mainly focuses on modelling the anisotropic behaviour of wood to examine the compressive and flexural characteristics of *E. nitens* timber more realistically. A moisture dependent, anisotropic elasto-plasticity model was proposed. The data from previous experimental studies was also used to validate the modelling.

- Chapter 6 provides a numerical investigation into the short-term response of Eucalyptus under compression with high and low moisture contents. In this chapter, numerical modelling investigating compression in Eucalyptus specimens with varying load-grain directions was presented. Parameters identified from the experimental data were used in the FEM models. Numerical results for compression in high and low moisture content conditions were used to compare with experimental data. The effect of the parameters used in the constitutive model on stiffness and strength in the loading direction were illustrated.

- Chapter 7 examines the damage to Eucalyptus timber in bending, during dry and high moisture content conditions, to explore its underlying failure mechanism. Firstly, a numerical simulation on off-axis tension for *E. nitens* timber with low and high moisture contents was undertaken using Finite Element Method with a moisture content dependent anisotropic elasto-plasticity model. The simulated results were then compared with the predictions from isotropic Hill and von Mises models. Numerical modelling of four-point bending in *E. nitens* specimens with low and high moisture content was then undertaken with consideration of the differences between tension and compression for *E. nitens* timber. A discussion of the effect of moisture content and grain angle on damage to *E. nitens* beams in bending was examined. This work can provide a more accurate prediction regarding *E. nitens* in bending both below and above *FSP*.

- Chapter 8 concludes the findings of this study and suggests further work.

Chapter 2

2 LITERATURE REVIEW

2.1 INTRODUCTION

This chapter provides the background information on which this research project is based, including the mechanical characteristics of timber and previous constitutive modelling for wood. The mechanical behaviour of wood is introduced in Section 2.2, while Section 2.3 provides previous constitutive models. Section 2.4 focuses on previous attempts to determine Eucalyptus properties, such as the Modulus of Elasticity, MOE, and strength, followed by Section 2.5 which discusses moisture adjustment models for wood. A summary follows at the end.

2.2 MECHANICAL BEHAVIOUR OF WOOD

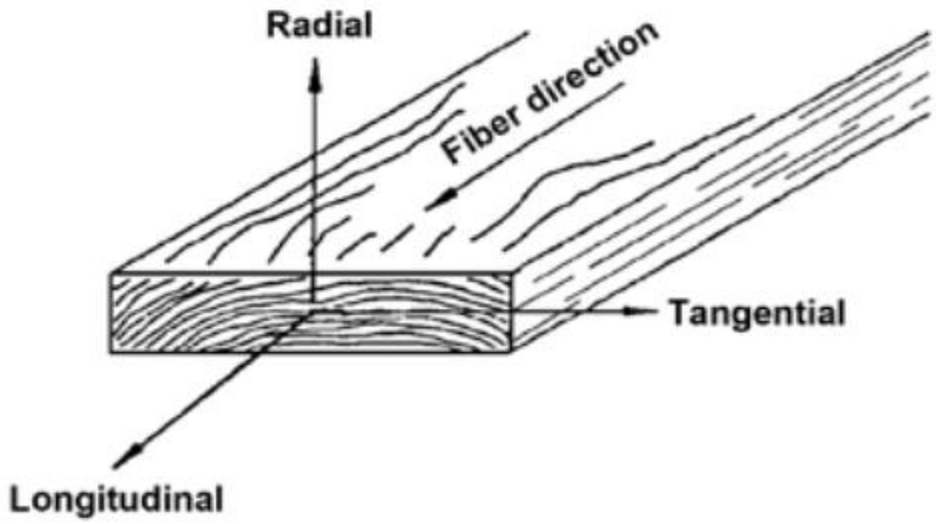

Fig. 2.1 Principal axes of wood with respect to tree stem structure [10]

The important mechanical characteristics of wood are summarised below, providing a basic background for the literature review. Wood is usually considered to be a three-dimensional, orthotropic material measured by a system of cylindrical orthogonal coordinates where the three principal directions correspond to the natural arrangement of the cells in tree stems (see *Fig. 2.1*). Referring to the growth rings, which are approximately defined by swept radii, the tangential direction is tangential to the rings, and normal to the radial direction, while the longitudinal direction is parallel to the direction of the pith (approximately vertical in a growing tree). Each orthotropic direction has different mechanical properties and, within each direction, also differs in tension and in compression [37, 38]. Ductile behaviour in compression can be observed, particularly in the radial and tangential directions [24].

The three-dimensional, orthotropic model is a simple model, which is able to be used to examine the mechanical behaviour of a small specimen. However, due to the way trees grow [39, 40], the three-dimensional orthotropic model may be problematic when applied to trees. It assumes that wood is homogenous, ignoring the differences between earlywood and latewood, as well as its inherent discontinuities. Earlywood is caused by rapid growth at the beginning of summer or during the wet season, and features larger cells and lower density - while slower growth at the end of summer or during the dry season generates latewood, with smaller cells and higher density [41]. Therefore, an anisotropic model, which assumes different material properties in different directions, will be applied in this study.

The behaviour of wood is also influenced by its water content, which is not only found within cell cavities as free water, but also found as bound water within the cell walls. *The total mass of water relative to the mass of dry wood fibre in a piece* is referred to as its moisture content [9]. Moisture in wood can cause elastic and creep deformation [23]. This produces differential strains, which in turn may cause some pre-stress in the wood. The moisture content in the wood can also have an influence on its mechanical properties, such as the modulus of elasticity and its strength, which are key factors when examining damage to timber members vulnerable to water. *Fig 2.2* shows that, as the moisture content increases, the tensile, compressive, and bending strengths of the wood decrease. These situations will be examined in this research into fully water saturated *E. nitens* timber members.

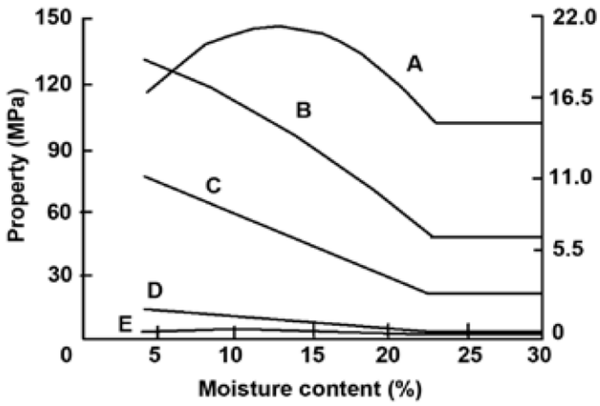

Fig. 2.2 Effect of moisture content on wood strength properties. A, tension parallel to grain; B, bending; C, compression parallel to grain; D, compression perpendicular to grain; E, tension perpendicular to grain [10]

2.3 CONSTITUTIVE MODELS FOR WOOD

As discussed in the last Section, wood is a complex material, and is influenced by its water content [23, 30, 42]. A huge amount of study has already been undertaken to model the material characteristics of wood. For example, the creep and mechano-sorption features of wood were addressed by Leicester (*1971*) [43], Toratti (*1992*) [44], and Hassani (*2015*) [23] with regard to wood's time dependent characteristics, while other researchers focused on short time period behaviour [24, 28, 29]. These constitutive models for wood are provided as follows.

2.3.1 Creep and mechano-sorption models

At unsealed surfaces, wood absorbs or desorbs moisture with changes in air humidity, and this kinetic process is called isothermal sorption. The rate of creep deformation depends on the temperature (*T)* and the relative humidity (*RH)* at any surface [10]. The ratio between the humidity in the air and the moisture the air can hold before it begins condensing into water in the surrounding climate is defined as relative humidity (*RH)*. Because of the temporal nature of what is happening, i.e., mechano-sorptive creep occurs over a time period, strains and deformations caused by this creep can be analysed based on predictions of the effects of variable heat and water transfers within relevant regions of the wood. Since the 1970's, creep and the mechano-sorptive effect have been modelled by several researchers to help improve the performance of structural timber [23, 42-44]. Most of these models are based on phenomenological approaches. For example, Leicester (*1971*) [43] presented a first approximation rheological model and found that 85% of the total deformation during the initial drying was able to be predicted by the proposed model. By tests on small stringy bark beams, the validity of this model was confirmed. Combining a creep limit model with an irrecoverable model, Toratti (*1992*) [44] developed a 2D model which treated separately the duration of load and creep phenomena. Hassani et al. (*2014*) [23] proposed a 3D orthotropic elasto-plastic, visco-elastic, mechano-sorptive constitutive model for wood. In this model, all material parameters were defined as a function of moisture content. With the help of the Finite Element Method (FEM), the capability of the Hassani et al. model was assessed and validated by comparisons with experimental data.

As this study examines the moisture-dependent anisotropic behaviour of *E. nitens* timber for the first time, creep and mechano-sorption are not the effects being investigated here, and therefore the effects of water transfers, non-stationary heat and long-time force action will not be studied in this research.

2.3.2 Elasticity-based models

According to the literature, linear orthotropic material theory, which describes material properties differing along three mutually orthogonal axes, has been widely used to describe the material behaviour of wood at a macroscopic level. For example, Patton-Mallory (*1996*) [45] used a tri-linear constitutive relationship incorporated into an orthotropic elastic material and used this relationship to model bolted wooden connections. The research of Patton-Mallory provided a feasible way to study the material behaviour of wood products at a macroscopic level. However, the material relationships used by Patton-Mallory depended strictly on several material parameters, such as Poisson's ratio and breakpoints in the tri-linear curves. If the parameters were not defined properly, a problem with the convergence to the solution arose, as negative stiffness coefficients could occur on the diagonal terms of the stiffness matrix.

To overcome this problem, Tabiei (*2000*) [46] developed an orthotropic model using an incremental-iterative secant stiffness approach. The model showed close agreement with the experimental shear and compression data of wooden specimens for the given species, and thus proved that the linear elastic orthotropic model worked properly within an elastic range.

However, the wood showed a nonlinear response during testing [47]. Ductile behaviour was observed in compression perpendicular to the grain and failure behaviour was different in tension and compression [36]. Also, as noted above, with wood being a hygroscopic material, its stiffness and strength usually decrease with an increase in its moisture content [10]. For example, European beech, an important softwood species, shows a significant reduction in strength and excessive plastic deformation in high moisture situations [9]. Therefore, plasticity theory-based models needed to be considered.

2.3.3 Plasticity-based models

Perhaps the earliest research to examine the behaviour of the elasto-plastic features of wood was undertaken by Clouston and Lam in *2002* [28]. In their paper, the nonlinear material behaviour of strand-based wood composites with varying grain-angles was examined, see *Fig 2.3*. The numerical results of angle-ply laminates for the stress–strain curves were validated by experimental results in tension, compression and 3-point bending.

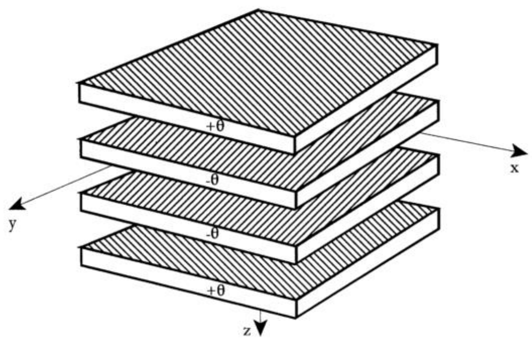

Fig. 2.3 Exploded view of a symmetric angle-ply laminate [28]

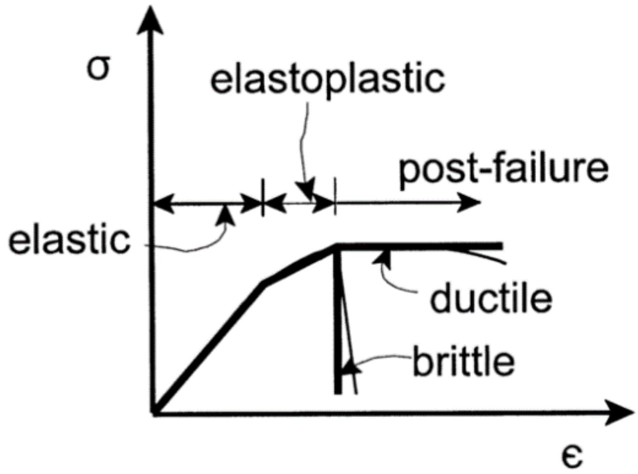

Fig. 2.4 Idealized constitutive behaviour of material [28]

They adopted a hardening material relationship with a Tsai–Wu criterion [48], i.e., a quadratic and interactive stress-based criterion that identified failure while differentiating the modes of failure. This failure criterion reasonably suits the damage characteristics of angle-ply laminate with its different failure modes in tension and in compression (see *Fig 2.4*). The influence of the variation in grain angle on the ultimate strength of wood was found in *Fig 2.5*.

One of the latest studies on the behaviour of the elasto-plastic features of timber both in compression and bending was by Milch, et al [24]. They studied, both numerically and experimentally, the damage to Norway spruce and European beech wood by static loading, examining their elastoplastic material characteristics with nonlinear isotropic hardening, the Hill yield criterion [49] and an extension of the von Mises criterion, [50] in order to describe accurately the ductile behaviour which could be observed in compression perpendicular to the grain. An acceptable agreement between numerical data and experimental results demonstrated the broad capability of the constitutive model for predicting wood's ultimate strength (*Fig. 2.6*-*Fig. 2.8*) with a relative error of up to 16%. This relative error resulted perhaps mainly from the heterogeneous material characteristics of the wood specimens, which were not considered in the research.

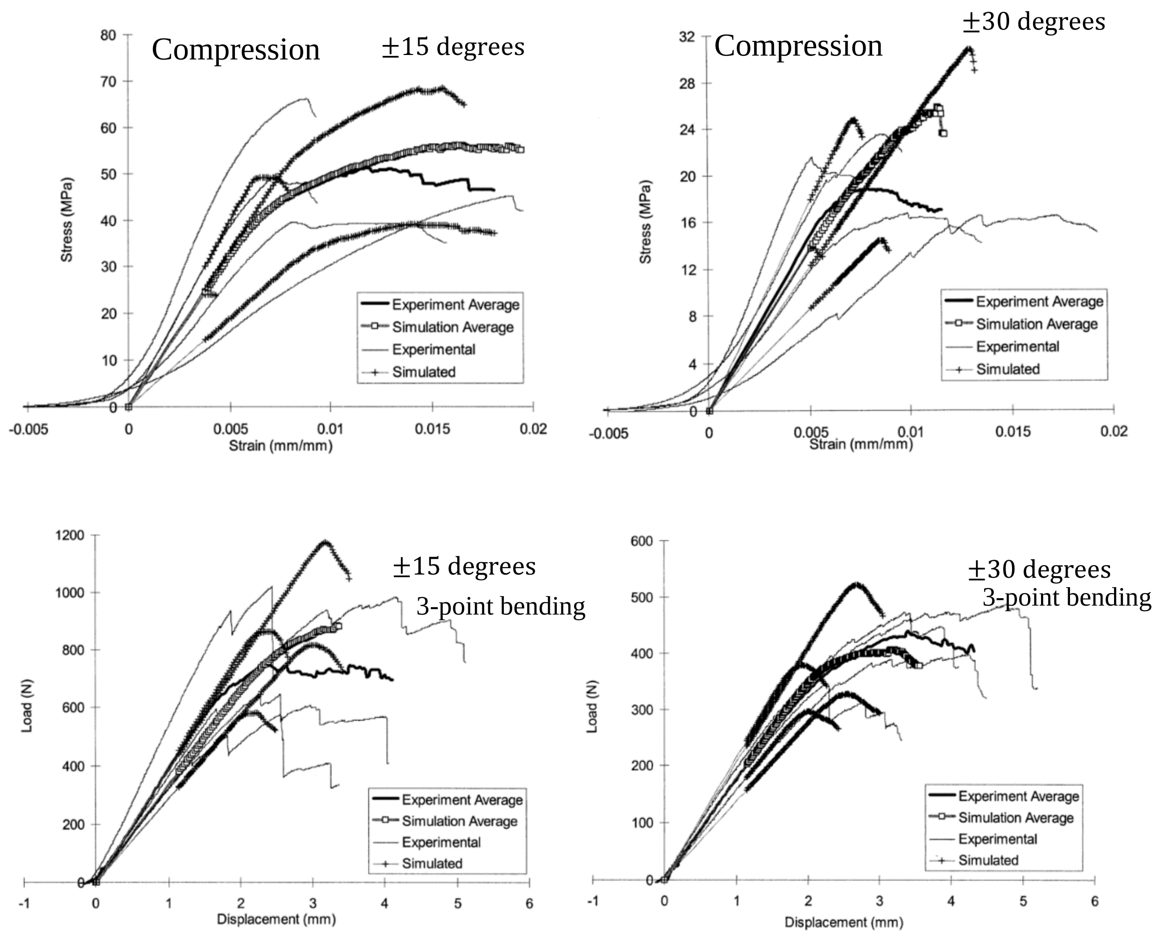

Fig. 2.5 Stress-strain curves of angle-ply laminate [28]

Moreover, when it comes to stress and strain along wood fibre, the hardening law is not always appropriate. The compression behaviour of wood in the longitudinal direction and in both anatomical directions is different: the stress-strain curve changes from "softening" to "hardening" from the longitudinal direction to that perpendicular to the grain [51, 52]. In order to numerically model strain amplitude correctly, a new constitutive model is needed, which takes elastoplastic wood anisotropy into account.

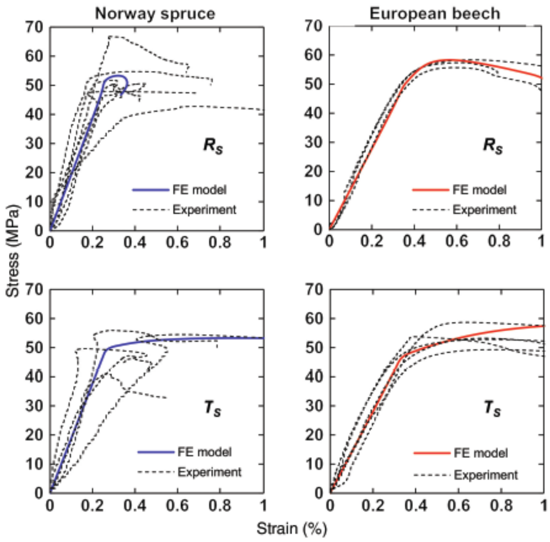

Fig. 2.6 Stress-strain curves of compression parallel to the grain [24]; The blue and red curves represent FE predictions of elasto-plastic deformation behavior. Symbols R_S and T_S represent the extensometer position fixed on the radial and tangential surfaces, respectively

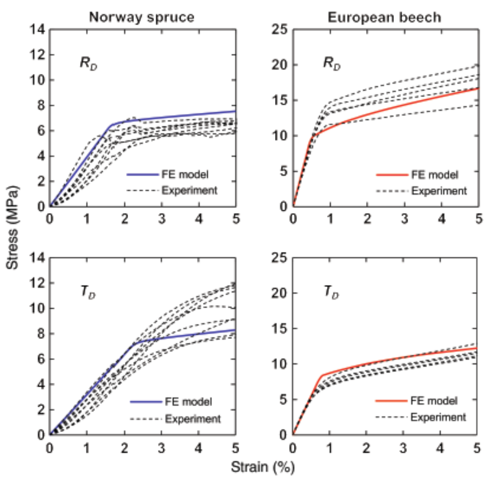

Fig. 2.7 Stress-strain curves of compression perpendicular to the grain [24]; The blue and red curves represent FE predictions of elasto-plastic deformation behavior. Symbols R_D and T_D represent the loading in the radial and tangential directions, respectively

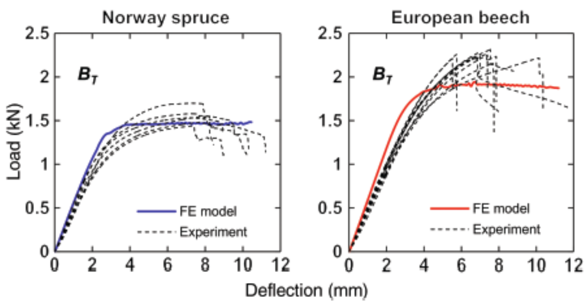

Fig. 2.8 Experimental and numerical (FE) prediction of wood behavior in bending based on force-deflection curves [24]; Symbol B_T represents the tangential load direction.

2.3.4 Summary and discussions

In this literature review of previous work regarding constitutive modelling for wood, the key literature, institutes, and authors in this field have been investigated. By comparing the load-deflection curves, the stress strain relationships, and the amplitude of *MOE*/*MOR*, previous models have been verified, respectively. It should be noted that the key work on constitutive modelling for wood is not limited to what is provided here, however the essential articles have been deliberately chosen.

To study how failure happens within *E. nitens* timber, one of the questions needed to be asked is: What is the material constitutive law of *E. nitens* timber? To answer this question, the mechanical behaviour of *E. nitens* timber should be known. Previous studies of *E. nitens* timber will be reviewed in section 2.4.

2.4 MECHANICAL PROPERTIES OF *EUCALYPTUS NITENS* TIMBER

For practical use, two measures are of particular interest in Timber Engineering: Modulus of Elasticity, also called Young's Modulus, and strength [3, 5] [53]. Modulus of Elasticity is a measure of resistance to loading [54, 55] and strength shows the maximum load carrying capacity of the timber [10]. In this Section, previous experimental studies of stiffness and strength for *E. nitens* timber will be discussed.

2.4.1 Modulus of Elasticity

Depending on the testing method, the Modulus of Elasticity or Young's Modulus can be defined as Dynamic Modulus of Elasticity (MOE) and Static MOE. Dynamic MOE can be calculated from the resonant frequency of the sample, its length and its density [56]. Dynamic MOE is an alternative to static MOE, which is the standard measurement technique defining wood stiffness in Australian and in international Standards [10, 57]. Static MOE is determined using a three-point/four-point bending test, in which a small clear wood beam with a cross-sectional area of 25 mm × 25 mm is supported near both ends and loaded at the mid-point or at one third points along the beam [57]. The load and deflection curve at mid-point in bending is measured as the sample deflects over a short distance, and static MOE is calculated from the dimensions, load and deflection [5, 6].

In the research of Harwood et al (*2005*) [58], the dynamic Young's Modulus (MOE) was measured from two types of samples resourced from *Eucalyptus nitens* and *Eucalyptus globulus* plantations; one type was green wood and the other was air-dried wood. Green Modulus of Elasticity (Dynamic MOE) was measured on freshly thawed samples. The samples were then air dried in a humidity-controlled room to 12% moisture content and the stiffness then re-measured. A linear regression between the green MOE and the air-dried MOE of plantation-grown Eucalyptus was found (*Fig. 2.9*). The MOE for the air-dried samples was found to be about 10% greater than for the green samples. This differed from the results found in studies using different species and sample sizes.

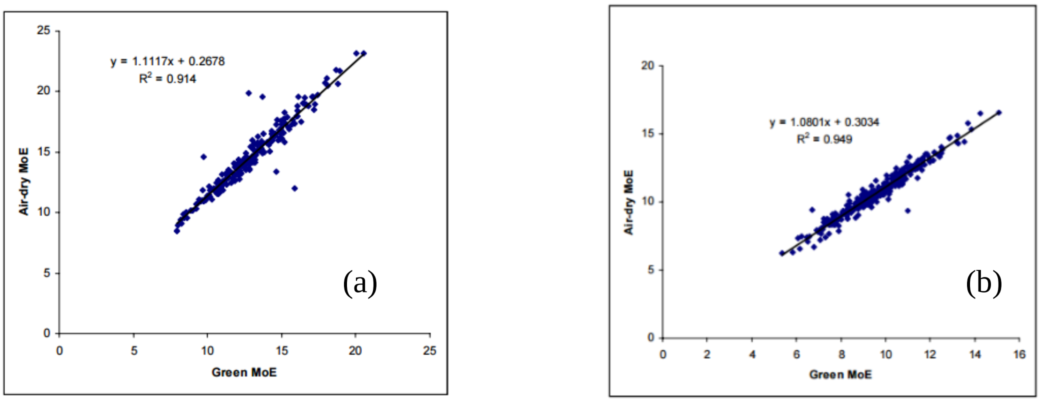

Fig. 2.9 Linear regression of air-dry MOE versus green MOE (GPa) for non-deflective samples of Eucalyptus studies [58]. (a), *E. globulus*; (b), *E. nitens*

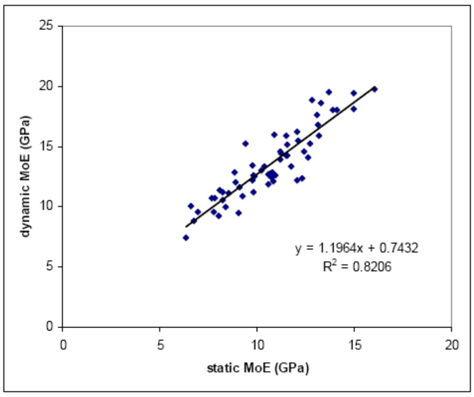

Fig. 2.10 Relationship between dynamic and static MOE, for 60 fixed-height samples (one sample per tree from each tree study [58]).

The relationship between MOE as determined by harmonic methods (dynamic MOE) and bending methods (static MOE) was also investigated using linear regression (*Fig. 2.10*). It was found that dynamic MOE was normally 20% higher than static MOE.

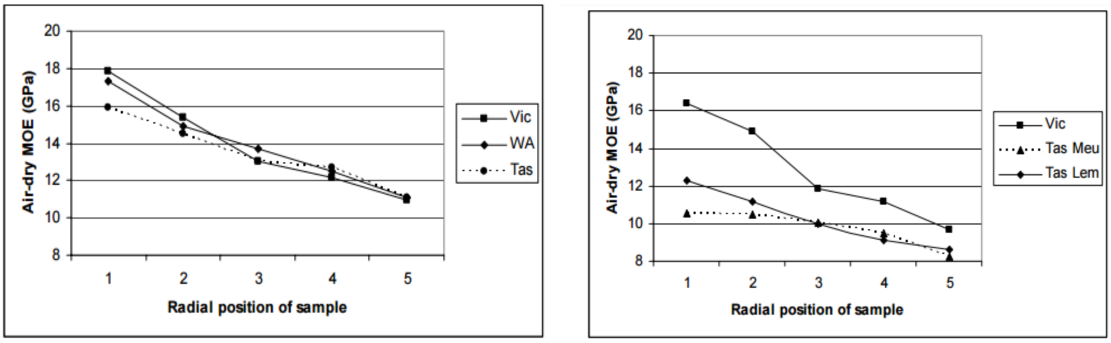

a *b*

Fig. 2.11. Mean air-dry MOE plotted against radial position of defect-free samples for Eucalyptus at the three sites [58]. a, *E. globulus*; b, *E. nitens*

Fig. 2.11 displays the variation in MOE for defect-free samples according to their radial position, with position 1 closest to the bark and position 5 closest to the pith. It was clear that radial position had a strong influence on air-dried MOE for all the defect-free data sets. On average, the samples from the outer part of the tree were stiffer than those from close to the pith. Linear regressions of air-dried MOE versus radial position were found.

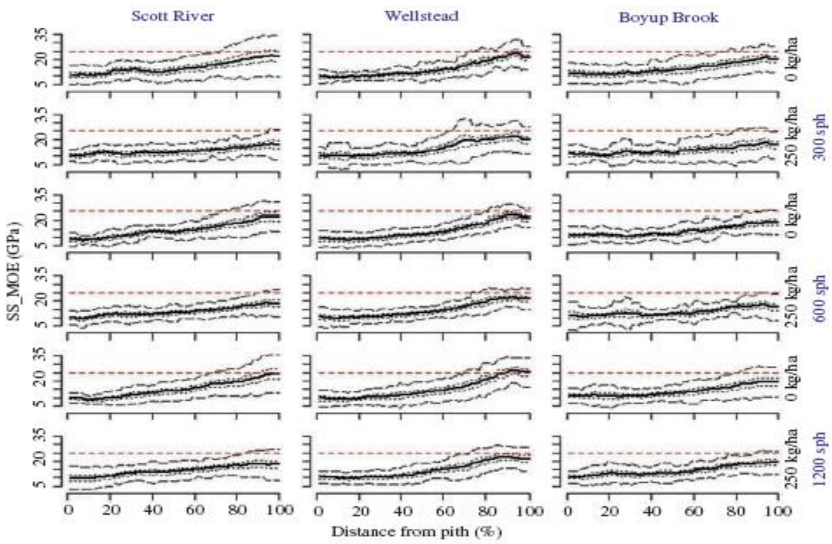

Fig. 2.12 Radial variation patterns in MOE, as predicted using SilviScan [59]. The inner band of dotted lines shows standard errors of the mean for each radial position; the outer band shows standard deviations [60]

These findings have been confirmed by other scholars [19, 61] for different species. Although there were some fluctuations in MOE with an increase in radius, generally the MOE increased as the radius increased, see *Fig. 2.12*.

2.4.2 Strength

To use *E. nitens* timber as a new structural material, relevant strength groups are needed to be established. The available information on *E. nitens* to date is limited to a few basic mechanical properties such the compressive stiffness and strength under short-term loading conditions [5, 62]. For example, for dry small clear *E. nitens* samples, variation in radial compressive strength was relatively higher than for axial compressive strength, and the compressive strength parallel to the long axis was more correlated with density than in the radial direction [3]. Functions of strengths related to the characteristics of plantation site, tree age and applied forestry management regimes [18, 19] or the microstructure of wood [71], eg. microfibril angle. The experimental data showed that the mean microfibril angle was negatively correlated to the stiffness (R=-0.67, see *Fig 2.13*) and the compressive strength [71] (R=-0.52, see *Fig 2.14*).

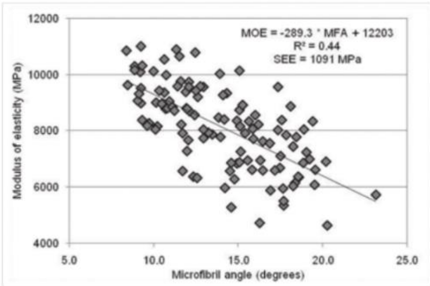

Fig. 2.13 Relationship between wood stiffness and microfibril angle in Eucalyptus wood [63], *E. globulus* at *MC*=11%

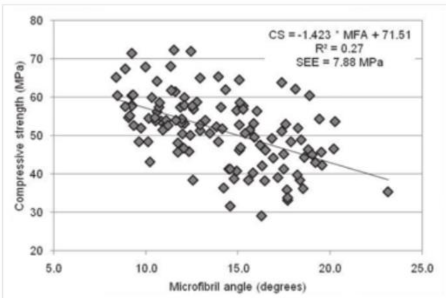

Fig. 2.14 Relationship between wood compressive strength and microfibril angle in Eucalyptus wood [63], *E. globulus* at *MC*=11%

The correlation between compressive stiffness and strength was studied, and a linear positive relation between the compressive stiffness and strength was found, see *Fig. 2.15*, where compressive stiffness could explain more than 22 % of the variations in the strength values of the samples. Similarly, findings can be obtained for the correlation between bending stiffness and strength by analysing data from Farrell, et al., [62] for *E. nitens*, see *Fig. 2.16*.

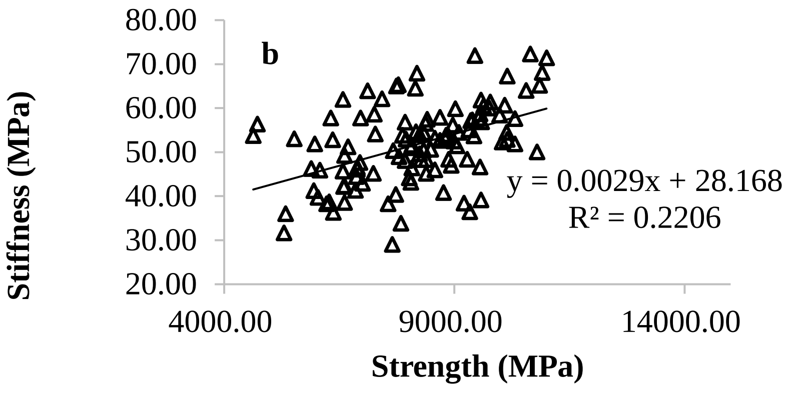

Fig. 2.15 The relationship between compressive stiffness and strength for *E. globulus* at 11% moisture content (data obtained from *Hein & Lima* [71])

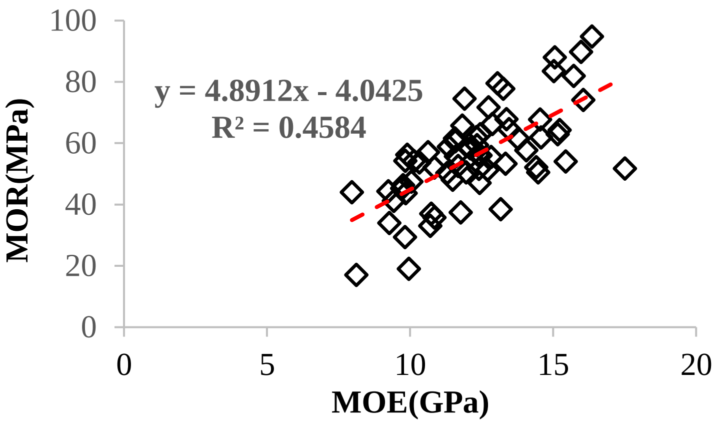

Fig. 2.16 The relationship between bending *MOE* and *MOR* for *E. nitens* (data obtained from *Farrell, et al*, [62])

2.4.3 Summary and discussions

The experimental findings for the wood properties of Eucalyptus were presented in this Section. It was found that the stiffness (*MOE*) within the tree increases with an increase in the distance from the centre. A linear relationship between the *MOR* and the *MOE* was identified.

However, information on the constitutive modelling of *E. nitens* timber with validation and calibration is missing. Wood is a three dimensional, orthotropic elastoplastic, viscoelastic, mechano-sorptive, creep material [23, 42-44]. Therefore, a comprehensive examination of stress-strain relationships at different load-to-grain angles and load-to-annual growth ring orientations is required.

What's more, the examination of the mechanical properties of *E. nitens*, such as compressive stiffness and strength, for structural applications was primarily on dried wood with low moisture content [3, 5, 6]. The safety and serviceability of timber structures are paramount in the building industry, and how these change as moisture content increases above fibre saturation point (*FSP*) needs to be addressed [9, 64]. For example, when timber members are soaked for a long time, water can be drawn into the wood by capillary action which leads to moisture contents above *FSP* [65, 66] and this can occur in compression members of bridges and piers when submerged in water, in wood piling foundations of buildings in the coast zone, in timber piles immersed in soil near the river but above the water table, and in houses in a flood zone. Therefore, the effect of moisture on the mechanical properties of *E. nitens* timber should be examined, and especially the mechanical properties of *E. nitens* above its *FSP* (fibre saturation point). This is the Objective One and Two of the current study, provided in Chapter 3 and 4, respectively. The work will be carried out with small defect-free (clear) specimens to meet the current design code for timber structures (AS/NZS 4063 2010 [45]; ASTM D2899 2012 [46]).

Previously, a relationship between moisture content and the mechanical properties of other timber species was found [9, 10, 56]. This work will be reviewed in section 2.5.

2.5 MOISTURE ADJUSTMENT MODELS

In this Section, the relationship between wood properties and moisture content is provided by what is called moisture adjustment modelling. Moisture adjustment modelling is an important step in establishing the actual mechanical properties of timber according to its moisture content. In past decades, much research has been undertaken and mostly it addressed variations in moisture content within the hygroscopic range [67-72], i.e., below fibre saturation (since the usual moisture content of wood is below 30 % [9, 73]). Fibre saturation is defined as the cell walls are saturated with chemically and physically bound water and there is no free water in the cell lumina [9, 10]. It should be noted that fibre saturation is not a discrete point but depends on species, age, local soil, moisture content, etc. [71].

2.5.1 Moisture adjustment models below fibre saturation point

Moisture adjustment models below fibre saturation point are based on examples with moisture content below 30% [74]. Generally, there are five types of moisture adjustment models and for each type of model, several variations are produced by making different assumptions concerning the form of the analytical expression or by using various subsets of the data [74]. The five basic models are:

- the zero-adjustment model,
- the constant percentage model,
- the strength ratio model,
- the Weibull model, and
- the surface model.

The Zero Adjustment Model is the simplest model in which properties are not adjusted to changes in moisture content.

The Constant Percentage Model adjusts a given property by a constant percentage regardless of grade or size when the moisture content changes from one level to another.

Perhaps, the first attempt to examine changes to the properties of structural timbers, according to moisture content, was the constant percentage model undertaken by Wilson in 1931 [74]. Wilson investigated the influence of moisture content on the physical properties of wood such as clear longleaf pine, and proposed an exponential formula [74], see Eq (2.1)

$$\mathrm{P} = P_1\left(\frac{P_1}{P_2}\right)^{-\left(\frac{M_1-12}{M_2-12}\right)} \tag{2.1}$$

where, P, P_1 and P_2 are property values at a moisture content of 12%, M_1 and M_2, respectively.

In contrast to this exponential model, the edition of ASTM Standards (*ASTM D 1990-02, 1990 [75]*) simplified the complicated set of adjustment procedures and gave the linear form shown in Eq (2.2).

$$F = (\alpha\text{-}\beta M_2)/(\alpha\text{-}\beta M_1) \tag{2.2}$$

Where, F is moisture content adjustment factor, M_1 and M_2 are two values of moisture content. α = 1.44 for *MOR* and 1.75 for modulus of elasticity (*MOE*), whilst, ß = 0.02 for *MOR* and 0.0333 for *MOE*.

Quadratic forms have also been used as presented in Eq (2.3) [74].

$$F = (a+bM_2+cM_2^2)/(a+bM_1+cM_1^2) \tag{2.3}$$

The regression coefficients, a, b, and c were estimated using data.

Strength Ratio Models assume that the moisture content adjustment factor (F) depends on the moisture content at which property changes (due to drying) are first observed via the strength ratio (SR) as a percentage, for the individual piece of wood.

Gerhards [76] investigated the seasoning effect on *MOR* and *MOE*, using 55 matched pairs of 4” × 8” southern pine beams. For each pair, one beam was tested green and the other beam was tested after it was seasoned to 12% moisture content. Gerhards concluded that the effect of moisture content on the *MOE* was independent of the strength ratio (*SR*). In contrast, the effect of seasoning on the *MOR* was dependent upon the *SR*. The relationship between F (called the “seasoning factor” by Gerhards) and strength ratio was expressed as:

Gerhards’ model:

$$F = 0.994 + 0.00503(SR) + 0.0104(SR_{dry} - SR_{green}) \tag{2.4}$$

Where, $SR_{dry} - SR_{green}$ is the difference in the strength ratio of the matched specimens as tested, dry and green. By assuming that the difference is zero, we can use Eq (2.4) to predict *F* for materials of different strength ratios when conditioned from green to a moisture content of 12% (*Fig. 2.17*).

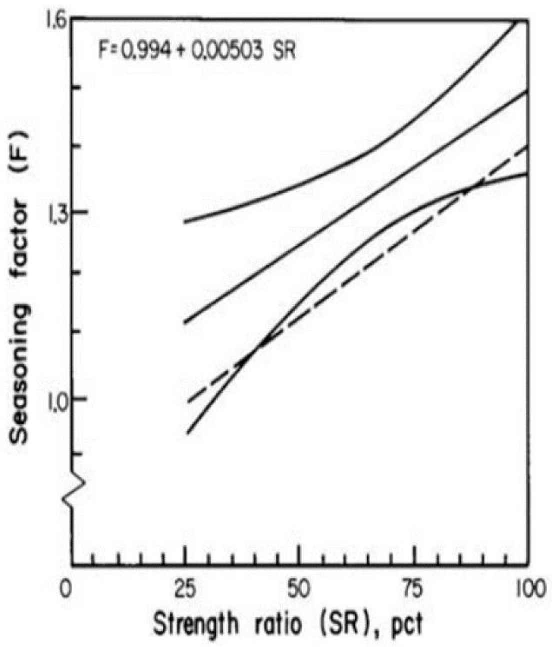

Fig. 2.17 Dependence of the seasoning factor of modulus of rupture on strength ratio for 4-inch-thick southern pine beams. The solid lines are the mean trend and the 95% confidence limits for the seasoning factor obtained by Gerhards [76]. The dashed line is the mean trend predicted by model No 7 in Green's study [77].

Hoffmeyer [67] noted a dependence between the moisture content adjustment factor and the strength level for *European spruce*. Trends in the moisture content effect for European spruce generally parallel those found by Madsen [78] for *Douglas-fir* (*Fig. 2.18*).

The Weibull model is the fourth type of model. This is able to fit the moisture content data for each grade size into to a Weibull distribution [79] with the parameters as functions of moisture content, see Eq (2.5).

$$P_2 = \omega_2(((P_1 - l_1)/\omega_1)^{m_1/m_2}) + l_2 \tag{2.5}$$

Where, m_i, ω_i, and l_i (i=1,2) are the Weibull shape parameter, scale parameter and location parameter at two moisture contents at state one (i=1) and state two (i=2), respectively.

In Eq (2.5), it is assumed that if a property is the *p*-th percentile in the distribution for moisture contents at state one, it would also be the *p*-th percentile in the distribution for moisture contents at state two. By this assumption, property P_2 is related to property P_1.

Although there are three parameters in Eq (2.5), McLain et al. [79] found that both the two- and the three-parameter distributions fitted their data reasonably well. The variations in the Weibull model were the result of different ways of modelling the Weibull parameters as a function of moisture content. For many studies into the reliability of timber structures, the Weibull model may be preferred because the Weibull distribution is being used extensively elsewhere in reliability analysis [80]. However, the Weibull model is not recommended for general use because of the difficulty in applying the model to grades and sizes which were not tested in the study [77].

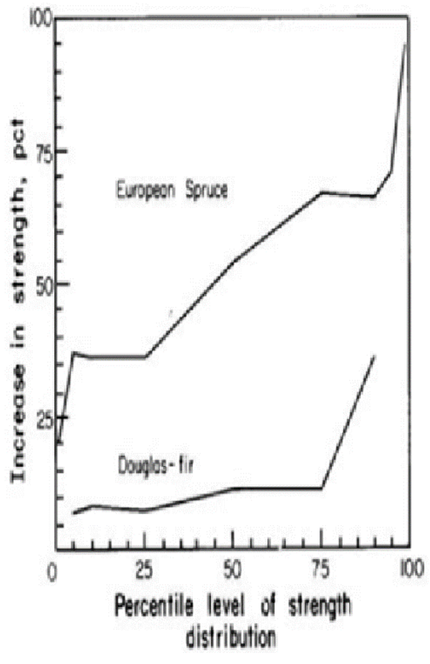

Fig. 2.18 Effect of strength level on the increase in bending strength due to drying (adopted from [67, 78])

Finally, the Surface Model, which is defined by contour lines fitting surfaces to the relationship between mechanical properties and moisture content, i.e., along the surface, properties move adjusting from one moisture content to another [77], see *Fig. 2.19* and *Fig. 2.20.* In other words, a contour is found which goes through a given property value P_1 at moisture content M_1, then property value P_2 at moisture content M_2 is the value of this contour at M_2.

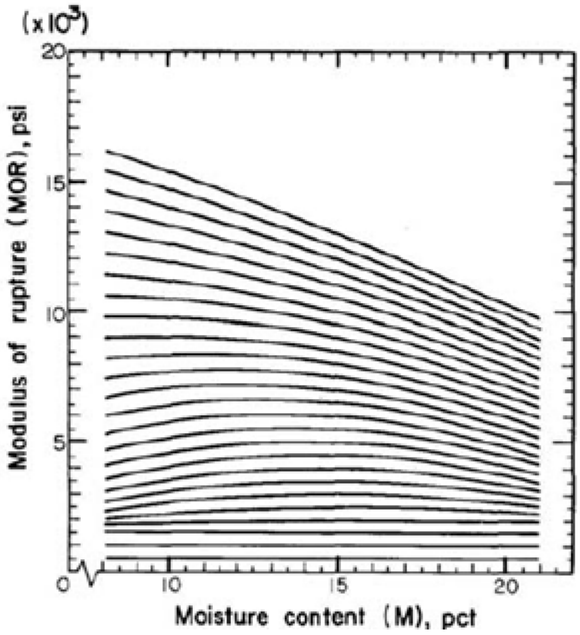

Fig. 2.19 Predicted modulus of rupture (*MOR*) using the quadratic surface model [77]

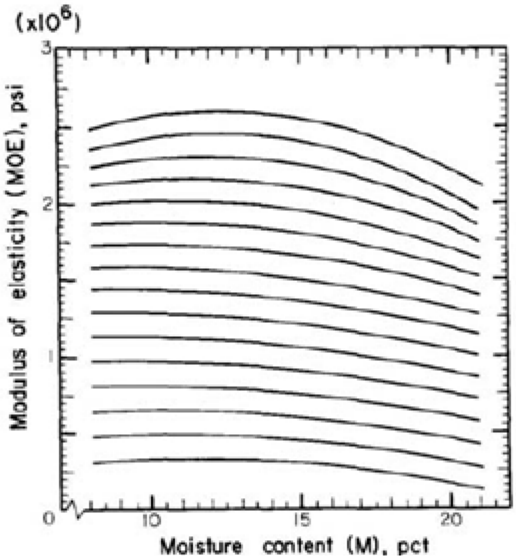

Fig. 2.20 Predicted modulus of elasticity (*MOE*) using the quadratic surface model [77]

In order to define contours, 21 percentiles (2nd, 5th, 10th, …, 90th, 95th, 98th) from each grade-size moisture-content combination were used in the light of the same underlying idea of the Weibull models, i.e., contours are defined by connecting like percentiles across moisture content. The surface models were fitted to each grade-size combination individually, as well as to the pooled data.

For example, two variations of the surface model were obtained by modelling the contours as either a linear or a quadratic function of moisture content. The coefficients of these contours were then modelled as a linear (linear contours) or a cubic (quadratic contours) function of the estimated property value at 15% moisture content. The choice of 15% moisture content was arbitrary; any other value could have been chosen [77].

In 1986, Green et al. [77] evaluated the performance of these five types of moisture adjustment models. They found that although the later four models offer a significant improvement in accuracy over the zero-adjustment model, the quadratic surface model is one of the more accurate models with the results independent of grade and size. The Weibull model based on a two-parameter Weibull distribution is as accurate as the quadratic surface model, but it is difficult to apply as the grades and sizes are not tested. Neither the constant percentage adjustment model nor the strength ratio model (*SR* model) produces a small average maximum absolute difference as do the Weibull or quadratic surface models. Meanwhile, the strength ratio model does not work due to the poor correlation between *MOR* and *SR* as well as that between *MOE* and *SR*. Therefore, Green et al. [77] suggested using a quadratic surface for the mechanical property and moisture content relationship to adjust in-grade data to a constant moisture content level.

Green et al., [77] also recommended that, if a relatively simple model is needed for general design use, the linear constant percentage adjustment model is appropriate for *MOE* or flexural stiffness (*EI*).

Currently, the most widely accepted model to adjust *MOE* for *MC* below the *FSP* is the linear constant percentage adjustment model, which is relatively simple to apply [77]. For example, this model is currently being used in the American Standard (*ASTM D1990 [75]*) for adjustment of allowable properties for dimensional lumber [69].

Perhaps, the most recent paper in this field was undertaken by Arnold [81]. Arnold studied the moisture-mechanical property relationships of untreated and thermally modified beech and spruce. In this study, bilinear dependency of the material properties varying with moisture content was used (*Fig. 2.21*). An acceptable agreement between measured stiffnesses (*MOE*s) or strengths (*MOR*s) and model predictions was found in varying treatments. This model could be considered to adopt in research from now on as it is simple to use for structural applications.

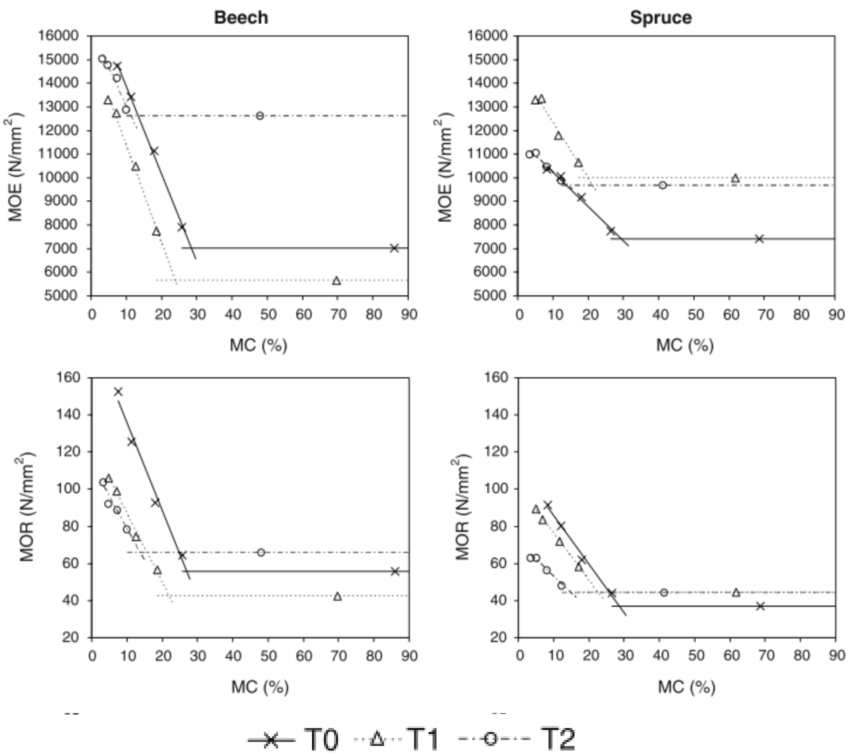

Fig. 2.21 Dependence of bending properties (*MOE* modulus of elasticity, *MOR* modulus of rupture) from wood moisture content (*MC*) at different treatment levels: T1, T2 and T3 [81]

2.5.2 Moisture adjustment models above fibre saturation point

Based on pioneering investigations into *European spruce* and *fir wood* [9] performed in the middle of the 20th century, *Fig. 2.22* shows the experimental relationship between compressive strength parallel to the fibre and the moisture content, from oven-dry timber (10%) to high degrees of moisture content above fibre saturation (60 %), without consideration of the effect of wood density and specimen size on strength and stiffness [9]. With reference to the studies provided in *Fig. 2.22*, the best approximation was given by the exponential function [9].

$$f_{c,0,mean}(u) = A \cdot e^{-Bu} + C \tag{2.6}$$

where, $f_{c,0,mean}(u)$ is the absolute strength at mean level, u is the moisture content, A, B, and C are constants and can be obtained by the least square approximation of the experiment data.

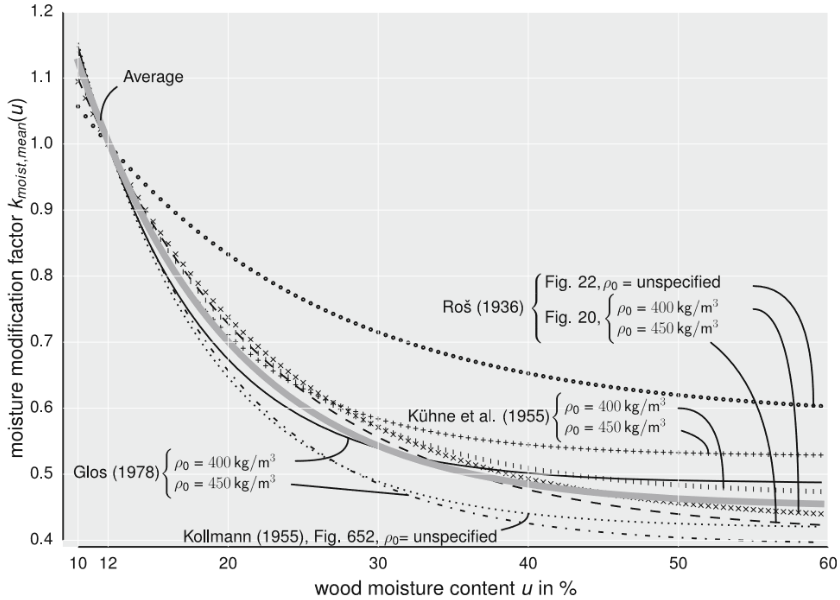

Fig. 2.22 Curves for a moisture modification factor for compression strength parallel to the fiber of *European spruce* (*Picea abies*) and *fir* (*Abies alba*) derived from literature data and equations [9]

For moisture modification factor, $F_{moist,mean}(u)$, the ratio between the moisture on a certain value for the mean compressive strength and a reference condition at a moisture content of 12%, is defined as

$$F_{\text{moist},mean}(u) = \frac{f_{c,0,mean}(u)}{f_{c,0,mean,dry}} = a \cdot e^{-bu} + c \tag{2.7}$$

Where the parameters, a, b, c are derived by the least square approximation of the testing data.

Using the assumption that the flexural rigidity (EI) doesn't change when varying moisture contents , Barrett and Hong [70] examined the variation in the flexural modulus of elasticity (*MOE*) of spruce-pine-fir lumber (known as SPF) in order to determine corresponding moisture adjustment factors below and above *FSP* for *MOE* (*Fig. 2.23*) [70].

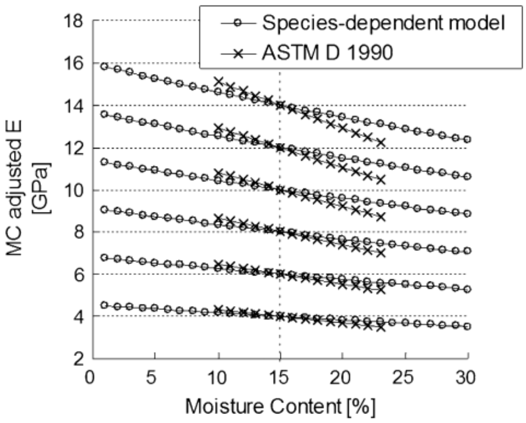

Fig. 2.23 Comparisons between predictions of the *MC* adjustment model in *ASTM D 1990[75]* and the species dependent *MC* adjustment model [70]

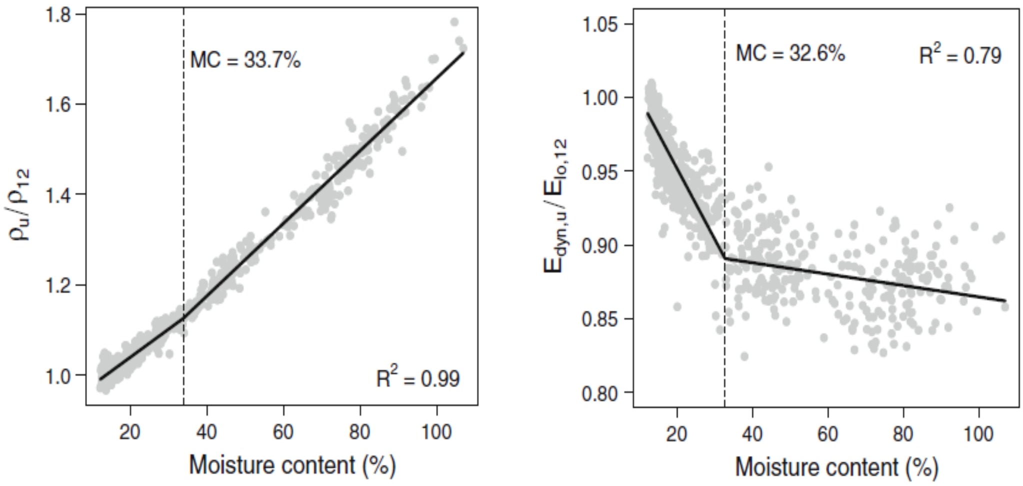

Fig. 2.24 Relationship between moisture content, relative density (sx) and dynamic modulus of elasticity (dx). Pu: density at *MC* = u; p12: density at *MC* u=12% N=750 [56]

While the research above *FSP* was for a limited number of species, including *Spruce/Pine/Fir, s*everal new studies showed an increasing interest in Chestnut and examined the moisture and property relationship in this timber [56]. For example, Nocetti et al. [56] investigated the effect of moisture content on its flexural properties and dynamic *MOE*. The experiment was conducted on 200 ungraded pieces with a cross section of 80mm by 80mm. It was found that for densities below fibre saturation point (*FSP*), the adjustment suggested by the European Standard EN 384 [82] was appropriate however, a more suitable equation was needed above *FSP* (*Fig. 2.24*). Nocetti et al. [56] therefore suggested an appropriate adjustment equation for Chestnut timber for structural applications (see *Fig. 2.25*). This adjustment equation is similar to the bilinear model used in [81], see *Fig. 2.21*.

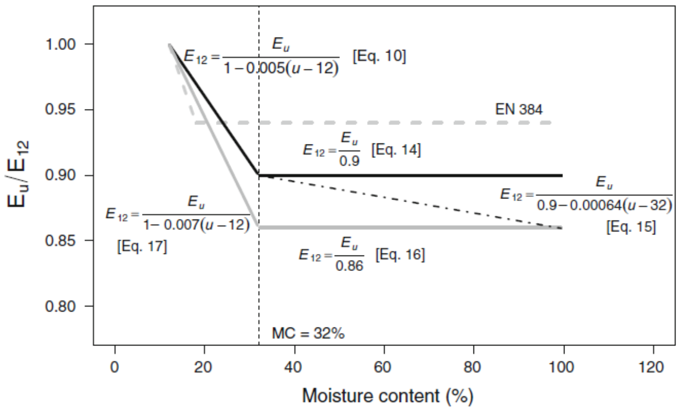

Fig. 2.25 Comparison between theoretical (gray lines) and observed (black lines) average adjustment equations [56]

2.5.3 Limitations and discussions

In Section 2.5, a literature review on moisture adjustment studies from oven-dry timber to high moisture content above fibre saturation point (*FSP*) was undertaken. Generally, it is well known that a reduction in strength and stiffness in timber occurs with moisture content increases below *FSP* and no significant changes occur above *FSP* [10]. However, the relationship between moisture content and mechanical properties was reported for only some wood species [69, 82], and these did not include Eucalyptus wood. The effects of high moisture content (*MC* above *FSP*) on Eucalyptus, especially regarding its mechanical properties, such as bending and compressive characteristics, have not yet been investigated. To overcome this limitation, one of the aims in this study is to examine the short-term response of *Eucalyptus nitens* under compression and bending below and above fibre saturation point. This work is mainly discussed in Chapters 3 and 4.

As Eucalyptus wood is recognised as a potential resource for structural use [4, 6, 22, 33] and there is still a significant lack of knowledge around its failure mechanism when moisture changes, numerical modelling will be done in Chapters 6 and 7 to provide an insight into the factors which affect failure in *E. nitens* timber below about 15%, and above fibre saturation.

2.6 SUMMARY

This chapter introduced the background information for this research project. The material characteristics of timber have been explored, previous constitutive modelling for wood material have been discussed, and the limitations of previous attempts at moisture adjustment models have been explained. Research gaps in the literature have been identified.

One challenge has been to provide substantiated information on the mechanical properties of *Eucalyptus nitens* wood such as strength and stiffness, in both dry and high moisture conditions, i.e., covering the moisture content below and above fibre saturation point. Another important challenge has been to model the anisotropic plasticity behaviour of *E. nitens* wood, including the moisture content effect. The third challenge has been to apply such a model to fast growing plantation Eucalyptus timber to help in understanding its use as a structural building material.

Chapter 3

3 COMPRESSIVE EXPERIMENT OF *EUCALYPTUS NITENS (E. NITENS)* TIMBER

3.1 INTRODUCTION

In this Chapter, the Objective One, which is to determine the short-term response of Eucalyptus *nitens* under compression with both dry and high moisture content, is met. *E. nitens*, was selected as it is a main commercial plantation Eucalyptus species in Australia and show an excellent potential to be used as a structural material [3]. In the following Sections, the anisotropic behaviour of *E. nitens* under compression with both dry and high moisture content was examined experimentally. Section 3.2 outlines the testing series and methods. In Section 3.3 and 3.4, the results and discussion are presented, respectively, and it is followed by the summary at the end. In this Chapter, compressive stress-strain curves and load-deflection curves of fibre managed *E. nitens* timber were determined, whilst compressive stiffness and compressive strength both parallel to and perpendicular to the grain were obtained. The simplified Hill strength theory is used to describe the failure envelope of *E. nitens* in compression both dry and high moisture content

3.2 TEST SERIES AND METHODS

3.2.1 Sample preparation

At a first stage to study this problem, the experiment focused on the ideal feature (i.e., the defect-free) of E. *nitens* wood material. The specimens were cut from well-defined tangential, radial and transverse faces of Eucalyptus (*E. nitens*) boards recovered from a 16-year-old *E. nitens* plantation resource, grown in the Woolnorth region in NE Tasmania, Australia, which has a maximum altitude of 190 m. A local trader supplied the boards. The boards were randomly selected to ensure a good range of variations in density values, and were also relatively free of gum veins, resin pockets and knots. Two group of samples were used in this study: Group I was standard small clear samples with dimension of 100 mm (in length) ×50 mm (in width) ×35 mm (in depth) and Group II was small clear block samples with the dimension of 35 mm (in length) ×50 mm (in width) ×35 mm (in depth), see *Fig. 3.1*. It should be noted that initially, samples were cut at larger dimensions: 200 mm (*L*) × 35 mm (*W*) × 50 mm (*D*) for Group I and 50 mm (L) × 35 mm (W) × 50 mm (D) for Group II. Samples were cut to the final size just before compression testing when high moisture content samples were just removed from water and to measure its moisture content.

For Group I, a total of 200 dry specimens and 200 wet samples have been prepared. 200 test pairs were selected; each pair has similar annual ring angle and has the similar material properties (*Fig. 3.2*).

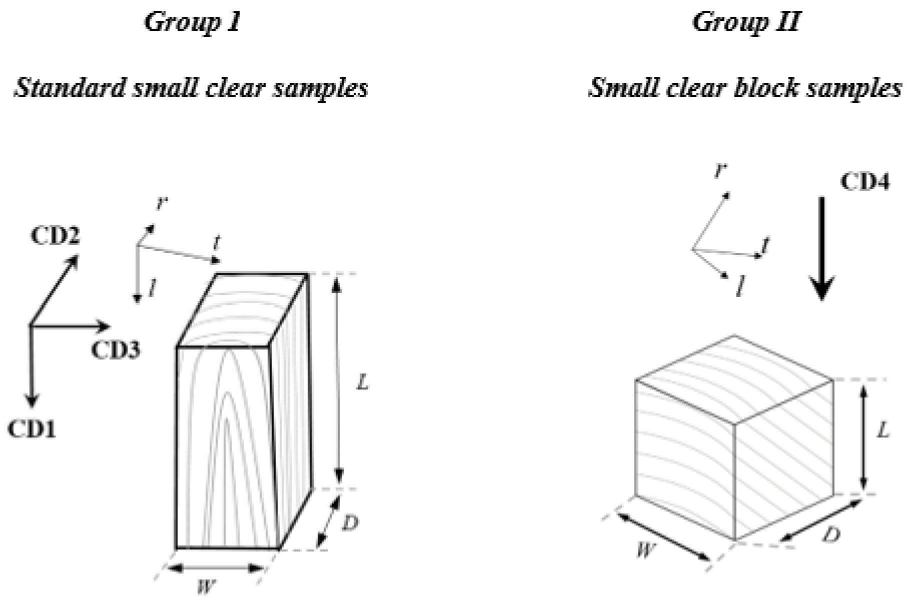

Fig. 3.1 Diagram showing compression test samples.

The length (L), width (W) and depth (D) = 150, 35, 50 mm and 35, 35, 50 mm for Group I and II, respectively. The radial directions of the wood fibre are longitudinal (l), tangential (t) and radial (r). In Group I samples, CD1, CD2 and CD3 represent the loading direction: compression parallel to the long axis, the wider cross section dimension, and the narrower cross section dimension, respectively. In Group II, CD4 represents compression with an angle to the grain for the small clear block samples.

For Group II, 100 specimens were prepared from boards relatively free of cracks and knots. For each grain angle, ten dry and ten wet samples were paired for examination. Each pair was cut from the same board and the samples were adjacent to each other to ensure similar material properties.

The dry samples were from the boards dried in an industrial hardwood kiln, while the wet samples were soaked in water for six months after kiln drying at 15 - 20 °C to ensure they were fully saturated. The annual ring angle and grain angle were measured using a protractor. The grain angle was defined as the angle between the wood fibres and the longitudinal axis of the sample, which was measured before testing and rechecked after failure.

Fig. 3.2 Typical cross section of the compression tests specimens for loading at the top, defined according to wood handbook [10]

3.2.2 Method of data analysis

Compressive strength and stiffness

The compressive strain was controlled by a moveable crosshead and calculated in the load direction from the relative position of the compression plates in relation to the original dimension of the sample. All deformations were measured from the point of crosshead travel relative to the value at which the load first developed.

In this study, the compressive strength parallel and perpendicular to the grain were derived using AS/NZS 4063:2010 [83]. Different evaluation methods are used to meet different testing standards [47, 84].

For Group I, the compressive strengths ($\sigma_{i,com}$, *i*=1,2,3) were calculated as:

$$
\begin{aligned}
\sigma_{1,com} &= \frac{f_{c1}}{W \cdot D} \\
\sigma_{2,com} &= \frac{f_{c2}}{W \cdot T} \\
\sigma_{3,com} &= \frac{f_{c3}}{T \cdot D}
\end{aligned}
\tag{3.1}
$$

where, f_{ci} is defined as ultimate loading force (kN). *W* (mm) and *D* (mm) are the width and thickness of the sample, respectively, and *T* (= 50 mm) is the width of the rectangular metal bearing (*Fig 3.3*). It should be noted that f_{c1} is the maximum loading force (kN) for CD1; f_{c2} and f_{c3} are the loading forces (kN) for CD2 and 3 at the deformation of 0.1h, respectively, where h is the original sample dimension in the load direction.

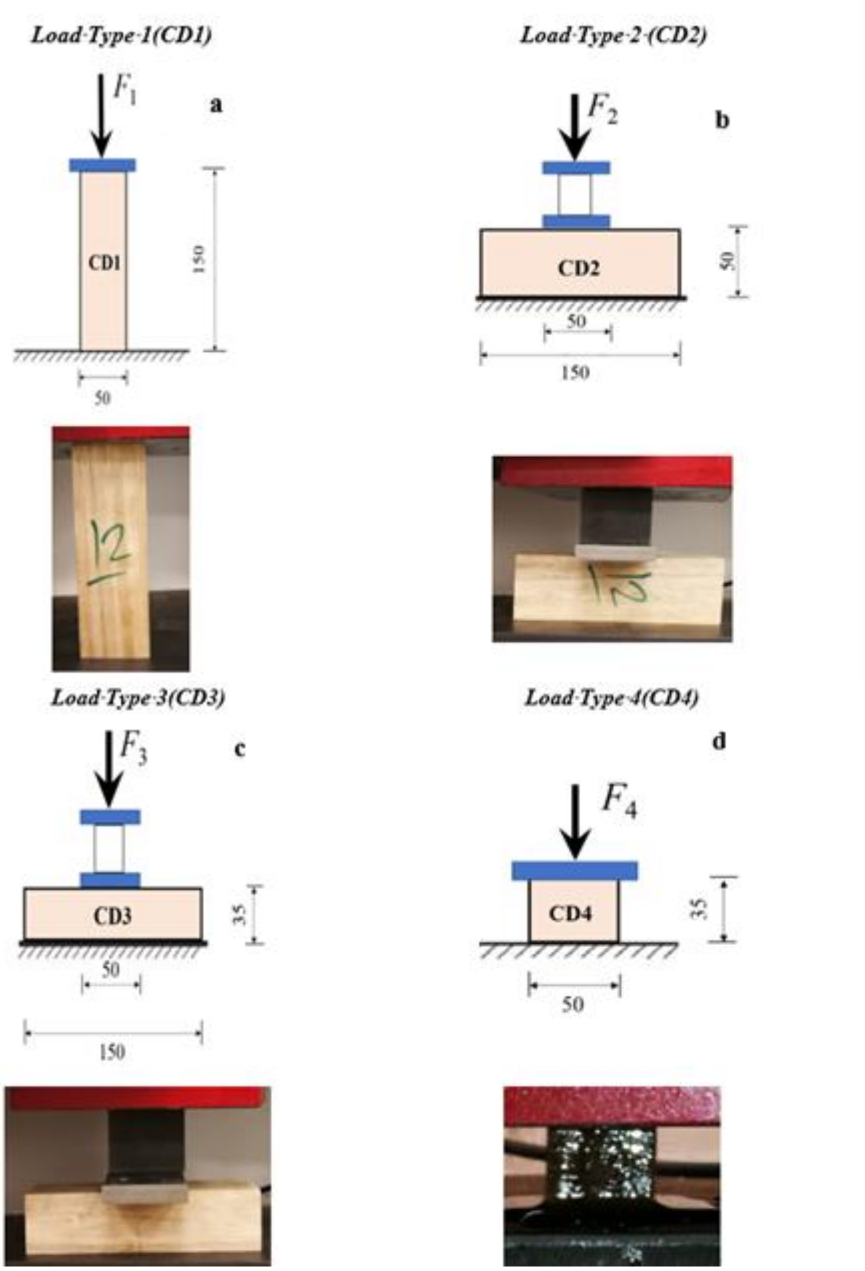

Fig. 3.3 Test setup for *E. nitens* compression; In Group I samples, CD1 (a), CD2 (b) and CD3 (c) represent the loading direction: compression parallel to the long axis, the wider cross section dimension, and the narrower cross section dimension, respectively. In Group II, CD4 (d) represents compression with an angle to the grain for the small clear block samples.

And the normal elastic modulus, also called compressive stiffness in this paper, was calculated as the slope of the line between approximately 10 % and 40 % of the ultimate loading force [24]. The compressive stiffnesses ($E_{i,com}$, *i*=1, 2, 3) were calculated as:

$$E_{1,com} = \frac{(f_{c1,40} - f_{c1,10}) \cdot L}{W \cdot D \cdot (u_{c1,40} - u_{c1,10})}$$
$$E_{2,com} = \frac{(f_{c2,40} - f_{c2,10}) \cdot D}{W \cdot T \cdot (u_{c2,40} - u_{c2,10})} \quad (3.2)$$
$$E_{3,com} = \frac{(f_{c3,40} - f_{c3,10}) \cdot W}{T \cdot D \cdot (u_{c3,40} - u_{c3,10})}$$

where, $f_{ci,40}$ and $f_{ci,10}$ are the forces at the 40% and 10% levels of the loading force of f_{ci} (*i*=1, 2, 3), $u_{ci,40}$ and $u_{ci,10}$ are the deformations (mm) at $f_{ci,40}$ and $f_{ci,10}$, respectively.

For Group II, the evaluation method is similar. The equations are:

$$\sigma_{4,com} = \frac{f_{c4}}{W \cdot D}$$
$$E_{4,com} = \frac{(f_{c4,40} - f_{c4,10}) \cdot L}{W \cdot D \cdot (u_{c4,40} - u_{c4,10})} \quad (3.3)$$

And the transform equations are:

$$\sigma_l = cos^2\alpha \cdot \sigma_4$$
$$\sigma_r = sin^2\alpha \cdot \sigma_4 \quad (3.4)$$
$$\tau_{lr} = -cos\alpha \cdot sin\alpha \cdot \sigma_4$$

where α is the grain angle, and σ_l and σ_r are the axial and radial direction, respectively; σ_4 is the stress at the load direction and τ_{lr} is the shear stress along the grain direction.

Moisture content and basic density

The moisture content (*MC*) of the samples was calculated according to AS/NZS 1080.1 [85]. Basic density (ρ_b) was calculated as [3]:

$$\rho_b = \frac{100M}{(100 + MC)V} \quad (3.5)$$

where, ρ_b is basic density (kg m^{-3}); M is the mass (kg) after oven drying, V is the volume (m^3) before oven drying, and MC is moisture content (%).

Moisture modification factor

Moisture modification factor, R_{MC}, is defined as the ratio between the strength at wet state to that at dry condition (MC = 12%) [9].

Hankinson's formula

Hankinson's formula was used to examine the relationship between strength or stiffness against grain angle [13, 86]. It is expressed as:

$$P_\alpha = \frac{P_0 P_{90}}{P_0 \, sin^2 \, \alpha + P_{90} \, cos^2 \, \alpha} \tag{3.6}$$

where, P_α is the predicted compressive strength/stiffness at grain angle α, P_0 is the CPA sample strength or stiffness as appropriate, P_{90} is the CPE sample strength or stiffness.

Failure modes

Compression failure modes of wood, crushing, compression and shearing, and end rolling and splitting, were classified according to their shape (see ASTM D 143 [57]). Failure modes were observed from the deformed samples and determined directly during the test.

Failure envelopes

The Hill criterion [87], that assumes the same strengths in tension and compression for anisotropic material, was used to describe the state of anisotropic failure in the tested samples.

If isotropic behaviour is assumed in the radial and tangential directions, then, in a plane stress field with the two principal directions, radial and longitudinal, the Hill criterion reduces to:

$$f^*_{Hill}(\sigma_i) = \frac{\sigma_l^2}{Y_l^2} + \frac{\sigma_r^2}{Y_r^2} - \frac{\sigma_l \cdot \sigma_r}{Y_l^2} - \frac{\sigma_l \cdot \sigma_r}{Y_r^2} + \frac{\sigma_l \cdot \sigma_r}{Y_t^2} + \frac{\tau_{lr}^2}{Y_{lr}^2} = 1 \tag{3.7}$$

where, Y_j ($j = l, r, t$) are the absolute values of compressive strength in the grain, radial, and tangential directions, respectively. Y_{lr} is the shear strength along the grain. Using the different pairs of mean strengths in the grain and radial directions obtained from compression testing at both low and high moisture contents, the Hill criteria at both low and high moisture contents can be determined.

Design characteristic value

Design characteristic values of *E. nitens* samples for dry and wet conditions were estimated at 5% percentile strength with 95% confidence [88].

Compression parallel to the grain is of importance in compression members, such as piles. The design strength of dry or fully water-saturated plantation-grown *E. nitens* column in compression, F_c, was calculated as [89]:

$$F_c = f_{c05} C_{dol} C_{hv} C_d C_g \tag{3.8}$$

where f_{c05} is the strength (characteristic value) of small clear wood samples at 5 % quantile of the normal distribution; the *C* values are adjustment factors: C_{dol} (=1/1.9) for duration of load and safety, C_{hv} (=1.05 for hardwood) for height and reduced variability, C_d for density (softwoods only), and C_g is for grade characteristic. If we assume that C_d=1 for *E. nitens*, the design characteristic values (allowable stress values) of full-sized *E. nitens* columns for both dry and water saturated conditions can be determined. It should be noted that a further experiment on full-sized dry and water saturated *E. nitens* columns is needed to check the value of C_d, however, in this paper it is the first development to show the method to determine the allowable stress values of full-sized water saturated clear *E. nitens* piles.

Data analysis

Statistical analyses were undertaken using Matlab (version R2019a, Natick, Massachusetts: The MathWorks Inc.). Linear regression statistics were used to calculate the correlation between the compressive stiffness and strength of dry and wet samples for CPA, and the coefficient of determination (R^2) was used to evaluate their significance. To determine the design characteristic value of small clear wood samples, a normal distribution model was adopted to fit cumulative probability distributions of compressive strength.

3.3 RESULTS

3.3.1 Testing procedures

Prior to testing, all specimens were weighed, and their *L*, *W* and *D* measured. A universal testing machine (capacity 200 kN) was used to apply the compression load (see AS/NZS 4063:2010 [83]). A data acquisition board connected to a computer with LabVIEW 2012 software was used to record, process, and analyse the data. The temperature and relative humidity during the tests were 15- 20 °C and 50 to 70 %, respectively.

Refs	Samples Size	MC[c]	Code	Load Direction	N[d]
ASTM D143–09 [a]	Group 1 150 (L) ×35 (W) ×50(D)	<15%	CPA-DRY	0	100
			CPE-DRY	90	50
					50
		>30%	CPA-WET	0	100
			CPE-WET	90	50
					50
RS 01[b]	Group 2 35(L) ×50(W) ×35(D)	<15%	C0-DRY	0	10
			C30-DRY	30	10
			C45-DRY	45	10
			C60-DRY	60	10
			C90-DRY	90	10
		>30%	C0-WET	0	10
			C30-WET	30	10
			C45-WET	45	10
			C60-WET	60	10
			C90-WET	90	10

[a] ASTM D143–09 [57].

[b] RS01, Reiterer & Stanzl-Tschegg, 2001[51].

[c] MC, moisture content.

[d] Number of replicate samples.

Table 3.1 Summary of experiments for standard clear *E. nitens* samples and clear block *E. nitens* samples in compression.

Compression was performed with displacement-control and at a constant loading rate for each testing (specified in *Table 3.1*) and discontinued when several drops were observed in the load-deflection curves or until a strain of approximately 10 % was reached. For CPA loading, the specimens were also fully supported at the base and fully loaded at the top surface (*Fig 3.3a*). For CPE loading, the base of the samples was fully supported underneath (*Fig 3.3b, c*). The loading plate, which was wider than the specimen, was carefully aligned to be parallel to this base support. The load was applied over the full 50 mm of the specimen's length. The force and the deformation between the loaded steel plate and the support were measured in the axis of loading. Immediately after testing, a small piece from each specimen was cut and oven dried for 72 h for determination of moisture content and dry density. The moisture content (*MC*) of the samples was calculated according to AS/NZS 1080.1 [85].

3.3.2 Load- deformation curves and stress-strain curves

Group I

For the dry wood samples, as the load under compression increased, deformation increased linearly up to the serviceability limit load, f_{cy}, the point where the relationship became visually non-linear or deformation functionally unacceptable [47]; this was 70 - 90 kN for CPA and 10 - 30 kN for CPE samples, respectively (*Fig.3.4*). Beyond f_{cy}, the ultimate loading force, f_c is reached. Progressive nonlinearity occurred throughout the loading period and can be easily observed; f_c, was close to f_{cy} for CPA and around 20–40 kN for CPE. No obvious differences in either CPA or CPE were found for the three annual growth ring orientations tested (0º, 45º and 90º).

For the stress-strain curves under compression, for both CPA and CPE at all annual ring directions, the linear range extended further for the dry than wet samples; the range of the wet samples ended at about 40 to 60 % of the serviceability limit load, f_{cy}, for the dry samples (*Fig. 3.5*). Beyond f_{cy}, more ductile stress-strain behaviour was found in wet than dry samples (*Fig. 3.5b* and *Fig. 3.5d*). The effect of ring orientation was not significant.

Group II

For load parallel to the grain (grain angle 0º), as the strain increased, there was at first a linear elastic range until a peak level of stress was observed. This is equal to the maximum stress of the sample; the linear range extended further for the dry than wet samples (*Fig. 3.6a, b*).

The stress level then dropped with further increases in strain, indicating an unstable "softening" behaviour associated with buckling of internal wood fibres [51]. However, the patterns of and rate of decrease varied between the five samples, showing at least one increase in stress following the first decrease indicating a period of stable "hardening" behaviour (*Fig. 3.6a*). For the wet samples, after the stress had dropped about 20–25% from the peak, a plateau was reached (*Fig. 3.6b*).

For load with an angle to the grain of 30º, for both dry and wet samples, the linear elastic range was less than for the 0º angle (*Fig. 3.6c, d*). After the maximum stress was reached, for the dry samples, as the strain increased, the stress dropped and then remained nearly constant before another drop; this process was repeated several times, indicating alternating periods of softening and hardening (*Fig. 3.6c*). For the wet samples, the stress remained constant for a period after the first drop (*Fig. 3.6d*).

For load with an angle to the grain at 45º, the elastic range was less again (*Fig. 3.6e, f*). For the dry samples, two types of strain-stress curves were observed: 1) after a first abrupt drop, the stress remained nearly constant until further drops, like the dry samples at a grain angle of 30º; and 2) a plateau region followed the maximum stress level. For all wet samples, a plateau was observed after the peak stress was reached (*Fig. 3.6f*); these samples could also be tested to a much higher strain (for example 50%) before total failure and exhibited more ductility than the dry samples (*Fig. 3.6e, f*).

For load with an angle to the grain of 60º, the linear range was short and after the peak all samples indicated a hardening behaviour; the stress level at which this occurred was about 40% lower in the wet than dry samples (*Fig. 3.6g, h*).

Load perpendicular to grain (grain angle 90º) was associated with lower maximum stress levels, followed by hardening (*Fig. 3.6i* and *Fig. 3.6j*). Similar strain stress curves were found for both dry and wet samples (*Fig. 3.6i* and *Fig. 3.6j*).

For samples from same board compression in radial direction, both dry and wet, strength and stiffness depended on boundary conditions (CD2 to CD4), maintaining an order of $E_{3,com} \approx E_{2,com} > E_{4,com}$ and $\sigma_{3,com} > \sigma_{2,com} > \sigma_{4,com}$. An increase in moisture content did not change this order (*Fig. 3.7*).

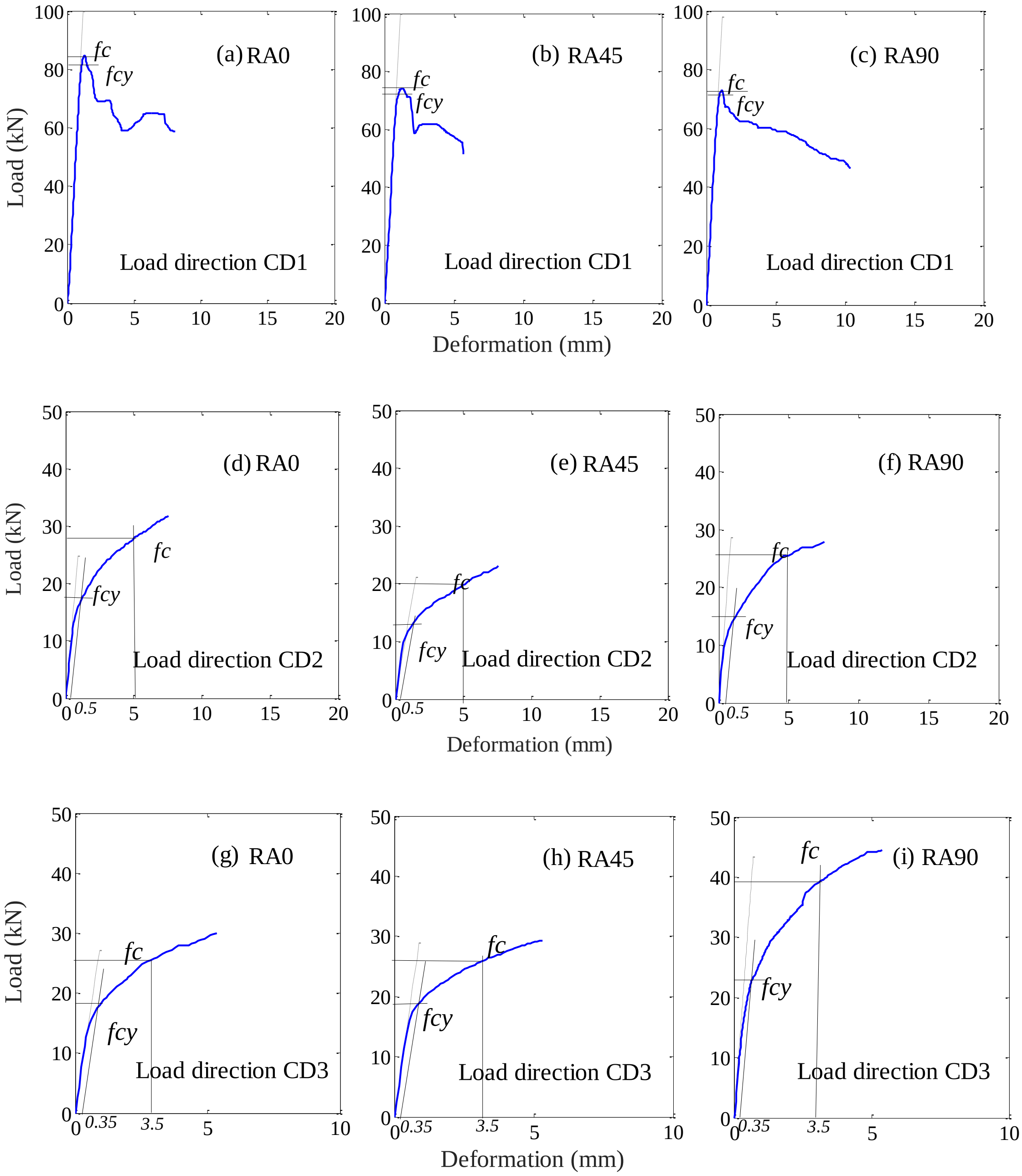

Fig. 3.4 The relationship between Load (kN) and Deformation (mm) of dry *E. nitens* wood samples: compression parallel to the grain, CPA and load direction CD1 (a, b, c) and compression perpendicular to the grain, CPE and either CD2 (d, e, f) or CD3 (g, h, i) for three annual growth ring orientations, RA = 0° (a, d, g), 45° (b, e, h) and 90° (c, f, i). The solid line is the measured curve, and the dashed line is the linear fit to the first part of the relationship; f_c and f_{cy} are the Ultimate loading force and Serviceability limit load, respectively. For the CPE tests, the fibres do not buckle at the yield point, so the linear fit (dashed line in Fig 3) is offset by a strain of 1% (solid straight line) and the Serviceability limit load (f_{cy}) is defined as the intersection of this offset with the measured load-deformation curve [47].

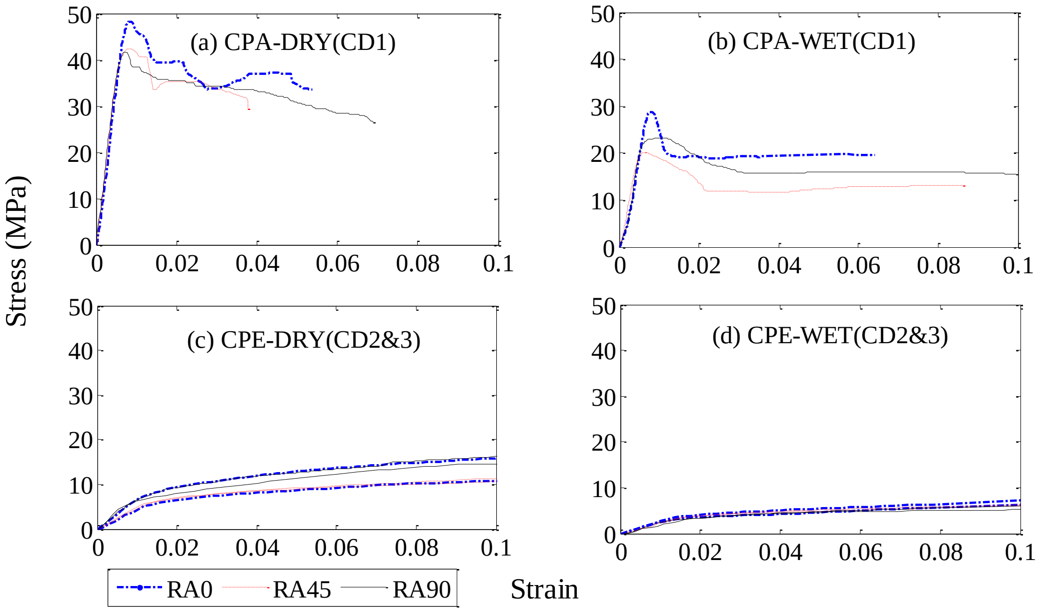

Fig. 3.5 The relationship between Stress (MPa) and Strain for compression tests on Group I standard small clear samples: Left: dry samples (a, c); right: wet samples (b, d); top row: compression parallel to the grain, CPA (a, b); bottom row: compression perpendicular to the grain, CPE (c, d).

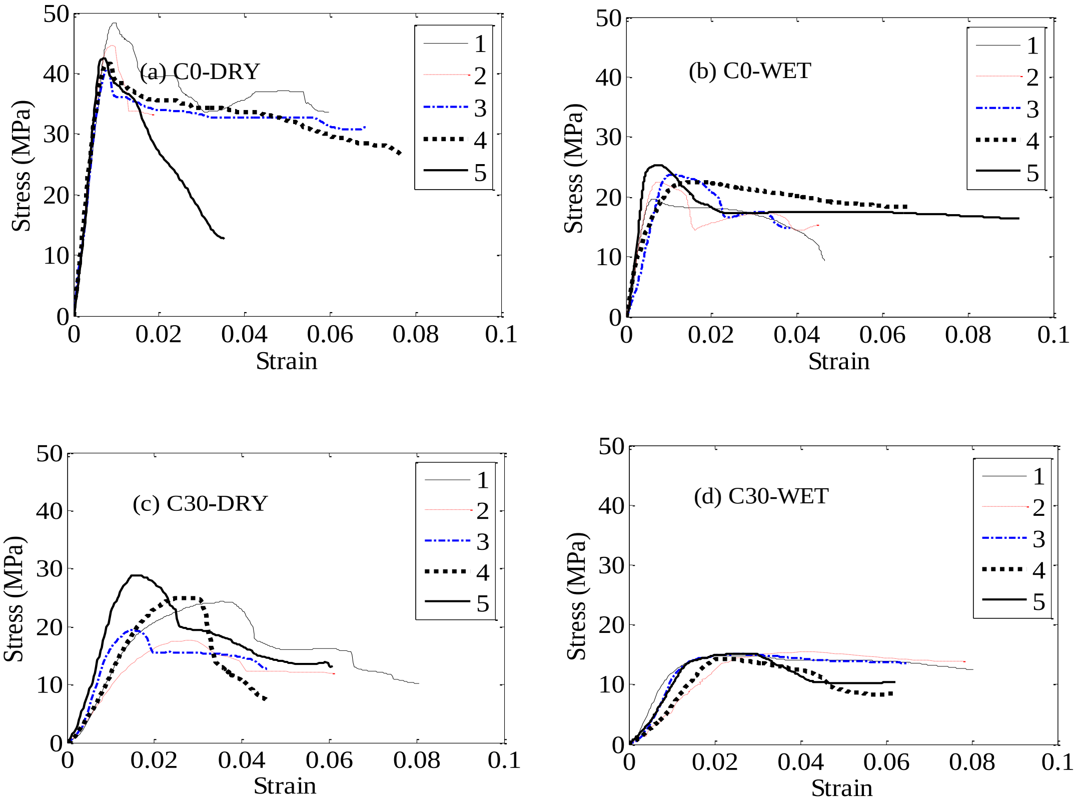

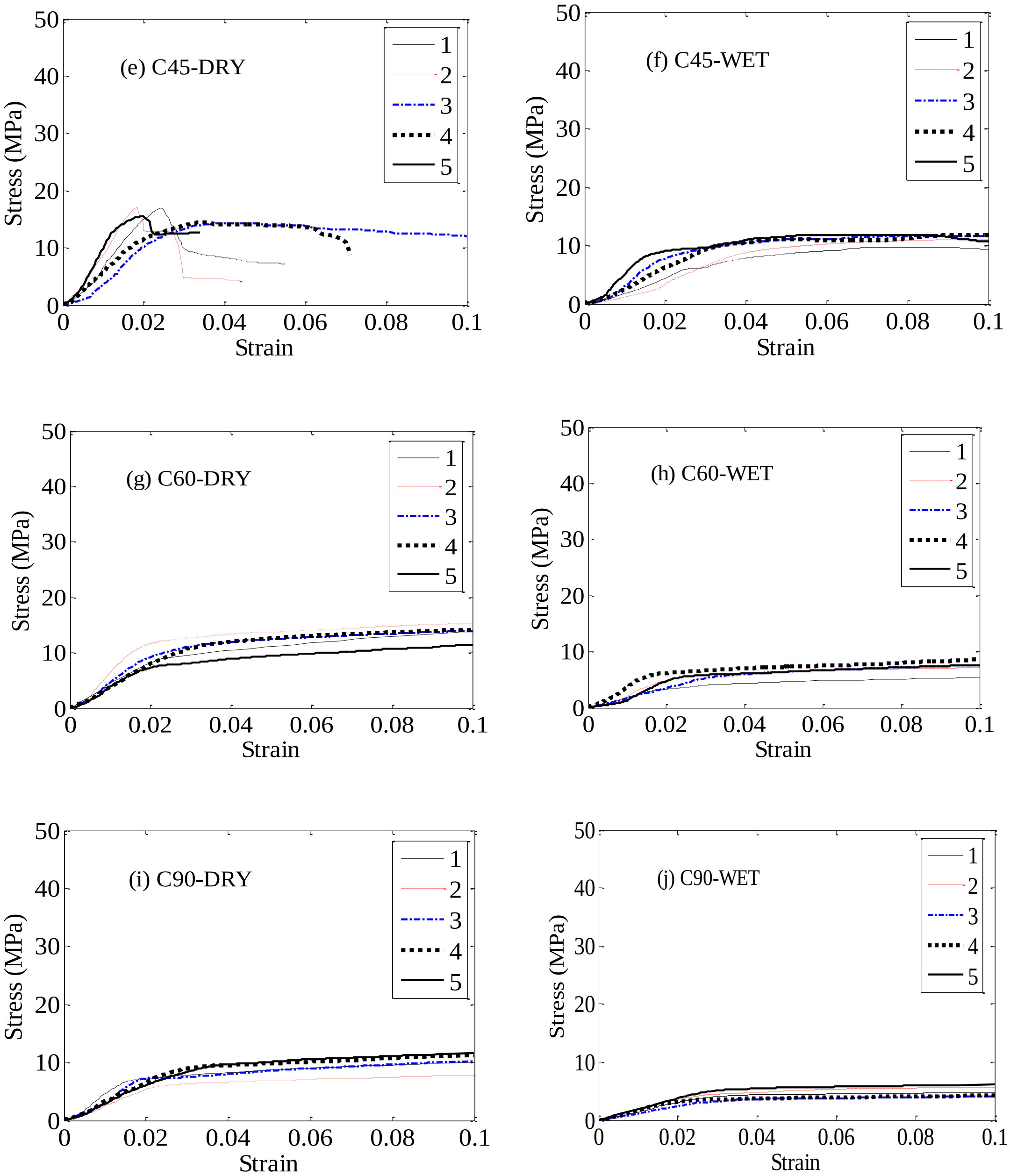

Fig. 3.6 The relationship between Stress (MPa) and Strain for compression tests on Group II small block samples: left: dry samples; right: wet samples, for five grain angles, α=0° (a, b), 30° (c, d), 45° (e, f), 60° (g, h), and 90° (i, j); the different lines in each Figure represent five replicate tests.

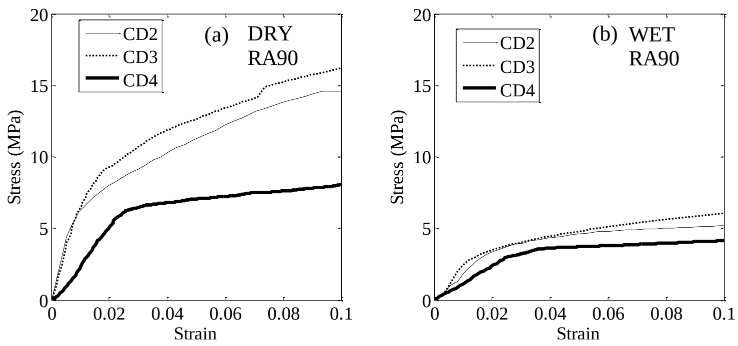

Fig. 3.7 The relationship between Stress (MPa) and Strain for compression in the radial direction for three boundary conditions (CD2, CD3 and CD4): left: dry samples; right: wet samples.

3.3.3 Compressive stiffness and strength

Group I

The mean basic density (ρ_b) and moisture content (*MC*) of the Group I dry and wet samples were 521.8 kg/m^3 and 11.9 %, and 484.5 kg/m^3 and 66.9 %, respectively, with COV values of 7.4% and 2.6 % for dry samples, and 10.2% and 19.3 % for wet samples, respectively, see *Table 3.2*.

For the CPA tests, the compressive stiffness (Young's modulus, MPa) of dry samples ranged from 5,320 to 10,580 MPa and the corresponding strength from 35.2 to 59.7 MPa; the mean values were 7,970 MPa and 47.8 MPa, respectively. The compressive stiffness of wet samples varied from 2,420 to 6,147 MPa and corresponding strength from 19.6 to 35.3 MPa; the mean values were 4,674 MPa and 28.7 MPa, respectively.

For CPE tests, the compressive stiffness and strength of dry samples ranged from 367 to 792 MPa, and the corresponding strength from 5.5 to 16.2 MPa; the mean values were 550 MPa and 10.6 MPa, respectively. The average value of compressive stiffness and strength for wet samples were 323 MPa and 5.7 MPa respectively, whilst the corresponding range were 146 - 457 MPa and 3.6 - 7.3 MPa, respectively.

Physical property	Statistical quantity	Dry CPA[b]	Dry CPE[c]	Wet CPA	Wet CPE	D19[d] CPA	D19[d] CPE	H12[e] CPA
Moisture content (%)	Mean (COV[a] %)	11.9 (2.6)		66.9 (19.3)		8.7 (2.3)	9.1 (6.6)	11
	Max	12.8		109.4		9.1	10.3	-
	Min	10.9		37.5		8.5	8.3	-
Young's modulus (MPa)	Mean (COV %)	7,970 (13.5)	550 (14.4)	4674 (15.2)	323 (18.1)			8,096 (17.9)
	Max	10,580	792	6,147	457			11,025
	Min	5,320	367	2,420	146			4648
Strength (MPa)	Mean (COV. %)	47.8 (10.5[I])	10.6 (20.1[II])	28.7 (12.3[I])	5.7 (13.9[II])	42.8 (11.4)	4.1 (24.4)	51.17 (18.0)
	Max	59.7	16.2	35.3	7.3	54.2	5.8	72.30
	Min	35.2	5.5	19.6	3.6	34.3	2.6	29.06
Basic density (kg/m^3)	Mean (COV. %)	521.8 (7.4)		484.5 (10.2)		508.5 (13.1)	527.4 (8.5)	
	Max	624.7		617.7		652.3	626.1	
	Min	408.4		387.8		429.3	480.5	

Table 3.2 Physical properties of Group I *E. nitens* dry and wet samples in compression; D19 [3] (for plantation *E. nitens*) and H12 [90] (for other plantation eucalypt species) refer to values found in other studies. [a] COV, coefficient of variation; [b] CPA, compression parallel to the grain; [c] CPE, compression perpendicular to the grain; [d] D19, Derikvand et al., 2019 [3]; [e] H12, Hein & Lima, 2012 [90]; [I, II] The suggested COV values by Wood Handbook [10]: I 18% and II 28%.

Group II

There was a decrease in compressive stiffness and strength with increase in grain angle that was consistent with Hankinson's formula [13, 86] (*Fig. 3.8*). Additional check has been undertaken using Orthotropic Tensor model [12] as it better fit the stiffness at the grain angle between 0° and 20°. An acceptable agreement also well confirmed the relationship between stiffness and grain angle (*Fig. 3.8a*).

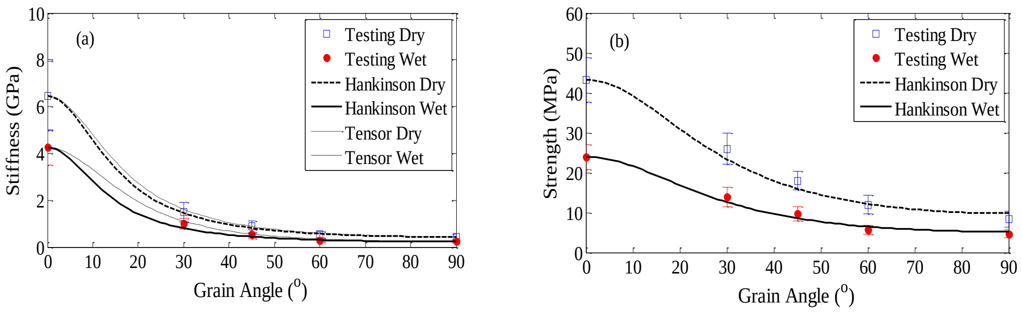

Fig. 3.8 The relationship between Stiffness (GPa)/ Strength (MPa) and Grain angle (°) for compression tests on Group II small block samples: top: stiffness (a); bottom: strength (b). Error Bars mean the standard deviations.

In general, the rate of decrease in compressive stiffness and strength was greatest as grain angle increased from 0º to 15º. Between 15º and 45º, the decrease was gradually reduced. Above 45º, both levelled off with little additional decrease. The decline in strength of wet samples was about 50% of the dry samples (*Fig. 3.8b*).

3.3.4 Failure modes

Group I

For the dry samples, crushing, compression and shearing, and end-rolling and splitting were observed for load parallel to the grain (CD1) (*Fig. 3.9a*). Compared with dry samples, wider kink bands and fewer cracks developed in the wet samples (*Fig. 3.9b*). In the compression zones of wet samples, the water was forced out.

Fig. 3.9 Deformation for compression tests on Group I standard small clear samples: Left: dry samples (a, c); right: wet samples (b, d); top row: compression parallel to the grain, CPA (a, b); bottom row: compression perpendicular to the grain, CPE (c, d).

Group II

Failure modes differed from those of Group I and were strongly dependent on the grain direction; and there were no obvious differences between the dry and wet samples for each load direction. The failure modes at a grain angle of 0º were mainly fibre buckling and wrinkling, at 30º fibre-layer slip delamination and some evidence of pure kink band formation, and at 45º and 60º also fibre-layer slip delamination and shear deformation (*Fig 3.10*). The failure of mode at 90º was crushing. In the deformed samples, cracks developed in bands associated with the annual growth rings or with radial and longitudinal planes (*Fig 3.10*).

Fig. 3.10 Deformation of *E. nitens* small block samples (Group II) in compression.

3.3.5 Failure envelopes

The failure envelope of the *E. nitens* in off-axis compression is a 1/4 elliptical arc from perpendicular to parallel to the grain, and the envelope enlarges as moisture content decreases (*Fig. 3.11*).

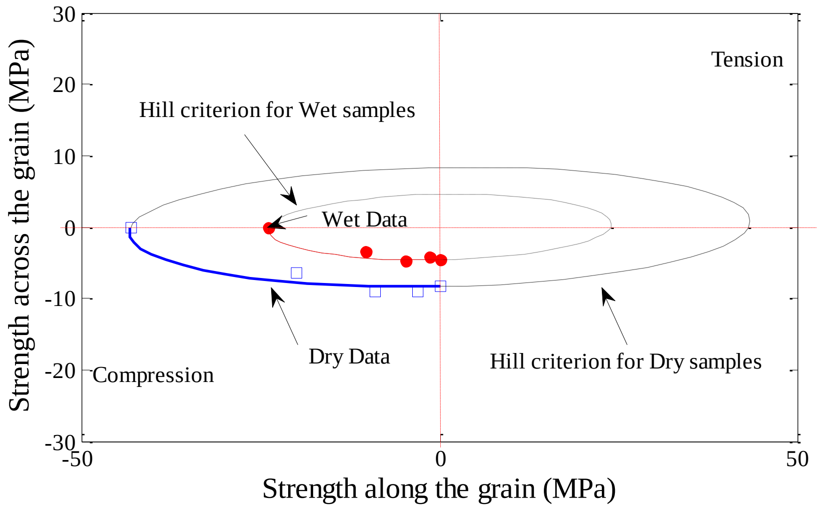

Fig. 3.11 Failure envelopes of *E. nitens* in the radial and longitudinal plane with low (average *MC* = 12 %) and high moisture content (average *MC* = 66.9 %) compared with Hill criteria [87]. Experimental data are mean values and are shown as points. The Hill criteria are shown as elliptical lines. The detailed equations for the Hill criteria are shown in Table 3.3 and use the absolute mean strengths from compression tests on Group II small block samples at grain angles of 0º, 45º and 90º.

Code	Formulae
Hill criterion of dry samples	$\frac{\sigma_l^2}{(43.2)^2}+\frac{\sigma_r^2}{(8.3)^2}-\frac{\sigma_l \cdot \sigma_r}{(43.2)^2}+\frac{\tau_{lr}^2}{(18.0)^2}=1$
Hill criterion of wet samples	$\frac{\sigma_l^2}{(23.9)^2}+\frac{\sigma_r^2}{(4.6)^2}-\frac{\sigma_l \cdot \sigma_r}{(23.9)^2}+\frac{\tau_{lr}^2}{(9.6)^2}=1$

Table 3.3 Hill criteria for experimental data in both dry and wet conditions. Absolute mean values of normal and shear compressive strengths and their standard deviations Y_l , Y_r and Y_{lr} = 43.2±5.5, 8.3±2.0, 18.0±2.4 MPa and 23.9±3.1, 4.6±1.0, 9.6±1.8 MPa for dry and wet Group II samples, respectively.

An acceptable agreement was found between the experimental results and the theoretical analysis based on the Hill criteria. The Hill criteria for experimental data in both dry and wet conditions were given in *Table 3.3*.

3.3.6 Linear regressions of stiffness and strength for CPA testing

Compressive stiffness was positively correlated with strength for both dry and wet samples. For dry samples, compressive stiffness explained > 42 % of the variation in compressive strength for load parallel to the grain (*Fig. 3.12b*), and for wet samples > 37% (*Fig. 3.12a*).

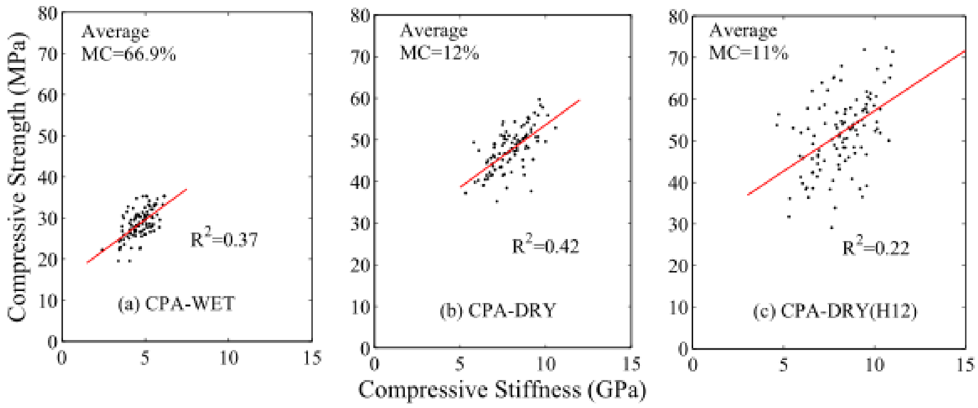

Fig. 3.12 Correlation between compressive stiffness and strength parallel to grain for (a) CPA-WET and (b) CPA-DRY in comparison to (c) load parallel to the grain for *E. grandis* at the moisture content of 11%. (Data for (c) were obtained from Hein & Lima [90].)

A higher coefficient of determination was found for dry (R^2 = 0.42) than wet (R^2 = 0.37) samples. A similarity between the linear regression models for both dry *E. nitens* and *E. grandis* samples was found (*Fig. 3.12b, c*).

3.3.7 Moisture modification factors and design characteristic values

For the CPA tests, theoretical normal probability distributions fitted the experimental compressive strength data for both dry and wet samples (*Fig. 3.13*). The distribution of compressive strength in absolute terms was narrower in the wet than dry samples, though similar when expressed as a proportion of the mean. Probability distributions of compressive strength for wet samples lied in a lower value region compared with dry samples, indicating that the design characteristic value of wet cases was lower than the dry cases. The moisture modification factor from dry (moisture content = 12 %) to fully water-saturated state (mean moisture content = 66.9 %) was 0.6 and 0.58 at the mean and the 5th percentile level, respectively (*Table 3.4*). Design characteristic values of small clear *E. nitens* samples for dry and wet conditions were 39.5 MPa and 22.9 MPa, respectively, while allowable stress values (design characteristic values) for dry and wet full-sized piles were 20.3 and 11.8 MPa, respectively (*Table 3.4*).

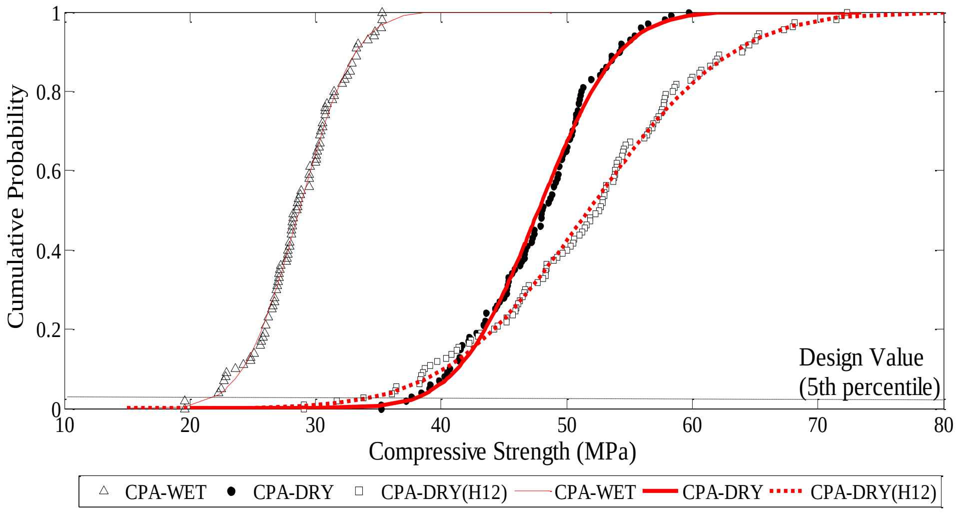

Fig. 3.13 Cumulative probability distributions of compressive strength parallel to grain of (a) CPA-WET and (b) CPA-DRY comparing with the data from the work of (c) *Hein & Lima, 2012* (H12)[90] at the moisture content of 11%. Experimental data are shown as points. The normal fit is shown as a line.

Parameters	Testing		
	Dry	Wet	M. F.*
Mean (MPa)	47.8	28.7	0.60
Standard deviation (MPa)	5.1	3.5	-
Characteristic value, f_{05} (MPa) for small clear samples	39.5	22.9	0.58
Allowable stress values (characteristic values) for structural sized pile	20.3	11.8	0.58

Table 3.4 Characteristic values of *E. nitens* compressive strength parallel to grain. *M. F. means modification factor from fully water-saturated state (mean moisture content = 66.9 %) to dry (moisture content = 12 %)

3.4 DISCUSSION

The study in this Chapter has shown that high moisture contents compromise the compressive strength and stiffness of plantation-grown *E. nitens*, approximately between 40% and 60%. However, annual ring direction had no significant effect in both CPA and CPE testing and for both dry and wet samples. This discussion first considers these findings in the context of previous studies in order to develop a rationale for the anisotropic material behaviour of *E. nitens.* The effect of high moisture content on the compressive behaviour and potential structural applications of plantation-grown *E. nitens* is then considered.

3.4.1 Basic density, moisture content and compression testing

For the dry samples, there was acceptable agreement with values of basic density (ρ_b) reported previously for plantation *E. nitens* by Derikvand et al [3]. Their mean ρ_b was around 520 kg/m^3. This is substantially lower than found for *E. nitens* in harvested timber from native forests (670 kg/m^3) [91], but this timber was much older and ρ_b increases with age [18, 19]. The coefficients of variation (COV) of ρ_b were lower than stated in the Wood Handbook [10], this difference may be linked to non-uniformities in the wood used to determine the values provided in the Wood Handbook [10]. The greater COV of the ρ_b and *MC* of the wet than dry samples was because the former covered a broader range of *MC*.

For the CPA testing, the mean values of strength and stiffness of the dry samples were within the range found previously for plantation eucalypts [3, 90]. However, for the CPE testing, the mean values of strength of the dry samples were around 2.5× higher than those found for *E. nitens* by Derikvand et al [3]. These authors used the 0.01*h* offset method [47] to obtain the compressive strength at the serviceability limit load (f_{cy}); in this study the 0.1*h* deformation method [83] was used to get compressive strength at ultimate loading force (f_c), which is up to 2× higher than *f*cy. Derikvand et al also used different test configurations, and a systematic differences are commonly found when two test configurations are applied to the same sample [47]. Therefore, the results of this study and Derikvand et al [3] were comparable. For the samples from a same board, the stresses for CD4 were lower than the corresponding CD2&3 stresses at the same strain for both wet and dry. As the testing method of CD2 and CD3 according to ASTM D143 and the uniform compression test (CD4) are different, therefore they have different results. For CD2&CD3, the neighbouring fibres are supporting the fibres directly loaded therefore the result of 7.0MPa is higher than the mean compression strength of 2.8MPa obtained using the uniform compression test (CD4) [47]. The COVs of strength were less than found by Derikvand et al [3] and as stated in the Wood Handbook [10]

(Table 2). This may also be because this study used uniform and defect-free samples from the same boards.

Thus, the experimental variables measured in this study appear reasonable and repeatable for plantation-grown *E. nitens*.

3.4.2 Anisotropic material behaviours

The compression behaviour of *E. nitens* was strongly dependent on the grain direction. These findings are consistent with previous studies on dry wood of other hardwood and also softwood species [13, 51, 52]. The present work extends this to wet samples of *E. nitens* and found that their compressive strength and stiffness were similarly sensitive to grain direction as well as moisture content.

The failure behaviour of both dry and wet samples consisted of four stages. The first, an elastic linear section, indicates that neither the compressive stress nor strain is larger than its serviceability limit value and there is full recovery from deformation. The second, a non-linear section, signals the beginning of an irreversible deformation caused by the folding and/or buckling of internal wood fibres [92]; this is accompanied by an audible sound during the test. In the third stage, a possible softening (load drop) or hardening (a plateau with increasing load) occurred, and the deformation was highly visible with increasing applied displacement. Rupture or strong hardening in the final stage meant that the wood was now functionally unacceptable. This four-stage behaviour, which was reversible only in the first stage, is characteristic of ductile failure of many engineering materials, and now describes the ductile compression behaviour of plantation-grown *E. nitens* in both dry and wet conditions.

The failure behaviour of both dry and wet samples was strongly dependent on the grain direction. The wood samples were much stiffer in compression parallel (grain angle 0º) compared to perpendicular (grain angle 90º) to the grain and the decrease in compressive strength and stiffness was rapid between 0º and 15º, and more gradual between 15º and 45º; above 45º, little additional decrease was found [14]. Thus, a grain angle of 45º represents the transition from an unstable "softening" type behaviour when loaded parallel to grain to a more stable "hardening" type behaviour when loaded perpendicular to grain. This is because the long and narrow cells of the wood microstructure act like columns in the longitudinal direction [17], and why failure behaviour changes from buckling of the cell walls for compression parallel to grain to crushing perpendicular to grain [10, 17]; it also accounts for the diversity of failure modes as grain angle increases for dry samples [51]; similar failure modes for wet samples were found in this study. Shear failures at the borders of the annual rings of dry wood samples are typically found at the boundary between late and early wood [51]; in this study the shear failures were similar for wet samples. The failure envelope of plantation-grown *E. nitens* in compression was 1/4 elliptical arc with a short axis in the radial direction and a long axis in the grain direction, since the strength parallel to the grain is much higher than perpendicular to the grain [36]. Thus, compressive behaviour of plantation *E. nitens* is highly anisotropic for a broad *MC* range above and below the *FSP* and is strongly dependent on the grain direction.

Not only grain direction and but also *MC* significantly influenced the compressive behaviours of the *E. nitens* samples. Load and deformation are generally more consistent among the wet than dry samples [9], and at a given angle, this was similarly observed in this study. Compressive strength increased and the failure envelope enlarged with decreasing moisture content [14]. Failure envelopes of dry compressive samples were 1/4 elliptical arc [36], and similar to the failure envelope for wet samples found in this study. Failure envelopes are of interest in timber engineering because stress limits can be established within these failure curves and used for structural sizing [87, 93]. Compressive strength increased with a decrease in moisture content, showing a moisture content sensitivity in compression behaviour of *E. nitens* experimentally and theoretically with diversity in grain direction.

3.4.3 Potential structural applications for plantation-grown *E. nitens* in a completely water-saturated state

High moisture contents reduced roughly 40% the CPA strength of *E. nitens* with a mean moisture modification factor of completely water-saturated state to dry at 0.6. Although similar observations have been reported in earlier studies for coniferous species [9], where the corresponding mean moisture modification factor was around 0.5 [9], the mean moisture modification factor of *E. nitens* was relevantly higher. Mean moisture modification factor of green to dry for other hardwood species, such as Mora (*Mo-*

ra spp.), and native eucalyptus forest, for example, Karri (*Eucalyptus diversicolor*), were 0.54 and 0.50, respectively [10]. The moisture modification factor of such *E. nitens* timber was relevantly higher than coniferous species [9], other hardwood species and native eucalypt [10]. These results have demonstrated that fast-grown plantation *E. nitens* shows promise as a structural material to be used as pier piles, bridge poles and building foundations piling which are vulnerable to water, as it has a lower strength reduction above *FSP* than those of coniferous species, other hardwood species and native eucalypt.

The positive correlations between CPA stiffnesses and strengths allowed estimates of CPA strengths for both low and high moisture samples. In timber engineering, it is usual to cut the timber so that the grain is parallel to the longitudinal axis of the beam [14] because this is the only way to produce a long beam from a log. Fortunately, that also produces a parallel to grain orientation that is conducive to strength since the strength parallel to the grain is much higher than perpendicular to the grain. Compression parallel to the grain is more important in compression members (such as columns or piles) as this exploits the highest compressive strength [9]. Correlation between strength and stiffness is of particular interest in timber engineering, since stiffness is frequently used as an indicative property for mechanical performance and predicting ultimate strength [53] (e.g. in machine strength grading). A positive linear-regression model for the relationship between CPA stiffness and strength for dry samples was found.–Although the coefficient of determination (R^2) was < 0.5, it is higher other similar measures on dry eucalypt samples, for example *E. grandis* (0.37 in [94]). A linear-regression model was developed for wet samples in the study using CPA stiffness as the single regressor in predicting strength, and a positive correlation was found between CPA stiffness and strength. This showed a practical application of *E. nitens* to the construction industry for below and above the *FSP*, as stiffness can be obtained from non-destructive testing, providing a method to evaluate the strength and assess structural safety and serviceability at low and high moisture content. An investigation using real structural elements is needed to confirm these linear-regression models as the presence of defects (knots, timber) decreases performance. The similarity between the regression models for the dry and wet cases in CPA testing indicates that the strength can be predicted from stiffness of *E. nitens* below and above the *FSP*.

A design value of 11.8 MPa for fully water-saturated plantation-grown *E. nitens* piles in compression is suggested. In this study, without consideration of the size effect, defect and knots, the suggested allowable stress values of dry and fully water-saturated plantation-grown *E. nitens* piles in compression are 20.3 and 11.8 MPa, respectively. These values are close to those for structural sized spruce pile specimens in axial compression in a dry, 20.3 MPa, and wet (water saturated) state, 13.4 MPa [9]. The results showed that *E. nitens* shows potential as a material for structural use, and can meet the requirements for compression members, such as columns and piles. Because defects and variability can be present in structural-sized material, their characteristics may differ from those found with small clear samples in this study; full-size testing is required to resolve whether this is the case. A further experiment on full-sized water saturated *E. nitens* piles is also needed to check the value of C_d as it is currently defined for softwoods only [89]. As this was the first study on the allowable stress values of full-sized water-saturated *E. nitens* piles, the focus was on small clear samples as these currently meet the design code for timber structures [11].

3.5 SUMMARY

In this Chapter, the first objective was achieved. The goal of this study was to characterize the anisotropic mechanical compressive properties of plantation *Eucalyptus nitens* in both high moisture content state, above the *FSP*, and the low moisture condition, and to explore the application in normal and a complete water saturated state. The compressive properties of *E. nitens* samples at both low and high moisture content states were determined. The samples were obtained from a 16-year-old fibre managed *E. nitens* resource in Tasmania, Australia. The moisture content sensitivity and anisotropic behaviour of the *E. nitens* timber were studied.

Findings could be summarised as follows.

- Load and deflection curves as well as the failure mode of the *E. nitens* specimens in compression were obtained, which could be used to validate the FE modelling of *E. nitens* timber in compression.
- Anisotropic properties of *E nitens* in both low and high moisture contents were examined. The experimental data in the research showed that compres-

sion behaviour of *E. nitens* was more dependent on the grain direction than the annual ring direction. The spatial yield surface of *E. nitens* was established by the simplified Hill strength theory and the elliptical surfaces were proved and showed moisture content sensitivity. The deformation of the specimen transformed from the unsteady-state “softening” at compression parallel to the grain, to steady-state “hardening” at compression perpendicular to the grain.

- Compressive stiffness and strength increase as grain angle decreases. That our findings and Hankinson’s formula largely agree, implies a validation of our research. Variation in the experimental data is because the specimens are from different boards with other material properties which are not consistent due to the influence of non-uniformities in the wood, such as early or later wood.

- It was also found that the compressive behaviour is dependent on the moisture content. The compressive strength is greatly affected by the moisture content and the loading direction, while the failure mode depends mainly on the load direction.

- Failure mode of *E. nitens* in different directions is mainly due to the mechanisms of fibre buckling and wrinkling when the grain angle is less than 30°. When the loading direction between 30° to 60°, the failure of material is mainly by fibre-layer slip delamination and shear deformation. When the loading direction is larger than 60°, crushing and failure is dominant initially, followed by a densification stage.

- The suggested design characteristic values of dry and fully water-saturated plantation-grown *E. nitens* piles in compression are 20.3 and 11.8 MPa, respectively. These values closed to the testing result from structural sized spruce pile specimens in axial compression at dry, 20.3 MPa, and wet (water saturated) state, 13.4 MPa [9], implying *E. nitens* shows potential as a material for structural use, and can meet the requirements for compression members, such as columns and piles

As plantation *Eucalyptus nitens* is a promising resource for structural use [5, 95], this research could be used for basic data to assess the structural performance of *E. nitens* columns or pile for both normal and water saturated conditions in future research. However, there is still a significant lack of knowledge about other physical properties of *E. nitens* to use such timber for construction. These physical properties include tensile failure, shear failure, and flexural failure. Flexural failure is an important failure mechanism due to timber is widely used as bending members. The next Chapter is to determine flexural characteristics of plantation Eucalyptus *nitens* timber at low and high moisture conditions.

Chapter 4

4 FLEXURAL EXPERIMENT OF *E. NITENS* TIMBER

4.1 INTRODUCTION

This chapter examines the short-term response of Eucalyptus in bending at low and high moisture contents in order to achieve Objective Two. After this introduction, Section 4.2 outlines the materials and methods for experiments used in the examination of the *E. nitens* beam in bending. Experimental results and discussions are provided in Section 4.3. Section 4.4 presents the summary.

4.2 MATERIALS AND METHODS

An experimental investigation of *E. nitens* was undertaken to obtain load and deflection curves in four-point bending as a function of growth ring angle, and at low and high moisture contents. Here, low moisture content means the moisture content (*MC*) is round 12% and high means the *MC* is above fibre saturation point (*FSP*). Bending stiffness (*MOE*) and strength (also called Modulus of Rupture, *MOR*) at high and low moisture contents were also determined from these load-deflection curves. The test series, methods, and test parameters used are summarised in *Table 4.1*. *MC* for the "low" and "high" *E. nitens* samples tested in the present study were in the range from 9.7 % to 12.6% for low moisture content samples and from 57. 9 % to 124. 3% for high moisture content samples, with mean (COV) values of 12 % (5.4 %) and 86 % (16.7 %), respectively (*Table 4.3*).

Code	moisture content (*MC*)	Specimens Size	loading rate (mm/min)	Number of replicate samples
4P-DRY	12%	410 (L)×25 (W)×25(D)	2.5	65
4P-WET	>30%	410 (L)×25 (W)×25(D)	2.5	65

Table 4.1 Summary of experiments for small clear *E. nitens* samples in bending.

4.2.1 Samples preparation

The dimensions of the 130 test samples were 410 mm (in length) × 25 mm (in width) × 25 mm (in depth) in accordance with ASTM D143-09 [98]. The samples were straight-grain and cut from well-defined tangential, radial, and transverse faces of *E. nitens* boards. The boards were randomly selected from different logs at a local mill, and were originally from a 16-year-old *E. nitens* fibre managed plantation located in the Woolnorth region of NE Tasmania, Australia, which has a maximum altitude of 190 m.

In total, 130 small clear *E. nitens* samples were used in the four-point bending tests. Half of them had a low moisture content (65 dry samples) with mean value of 12 % and the other half had a high moisture content (65 wet samples), ie., *MC* is above *FSP*. Each pair of samples (i.e. one dry and one wet) was cut from the same board and adjacent to each other, so that, excluding the moisture content, they had similar material properties. The dry samples were from boards dried in an industrial hardwood kiln, while the wet samples were soaked in water for three months to make sure they were fully saturated - they were then tested within two days after removal from the water to make sure wet samples were in a broad *MC* value above *FSP*.

The cross sections of the dry samples are illustrated in *Fig. 4.1*, showing the variation of annual growth ring angles of 0, 30, 45, 60, 90 degrees, respectively, while the corresponding wet samples have essentially the same ring angles. There were 26 samples each annual growth ring angle. Half is the dry samples, and the other half is fully saturated. The annual ring angles were measured before testing using a protractor and measured again after failure. Half of each was dry samples, and the other half was wet samples.

Fig. 4.1 Typical examples of cross section of the four-point bending *E. nitens* specimens

4.2.2 Testing facilities and procedures

A schematic diagram of the test setup for the Four-Point Bending Test with test photos is provided in *Fig. 4.2*. These tests were performed on a Universal Testing Machine (Hounsfield H50KM 50kN, serial number H50KM/669). The support frame consisted of a four-point bending test frame with 3 spans of 120 mm each (*Fig. 4.2*a). The loads and displacements were measured in the axis of loading (*Fig. 4.2*b).

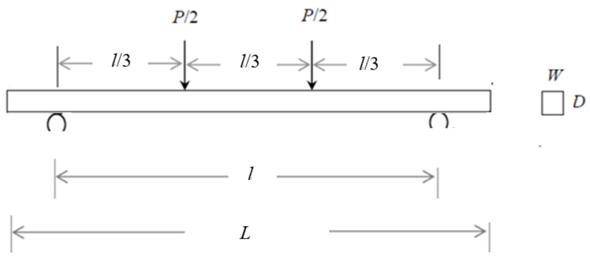

Please note the working span between two supporting points l=360 mm, the span between two loading points l/3=120mm. Dimensions of the specimens: 410 mm (L) × 25 mm (W) × 25 mm (D).

(a)

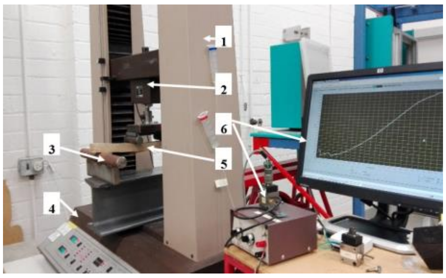

1 Universal Testing Machine 2 Loading element

3 Supporting frame 4 Bottom deck

5 Specimens 6 Data acquisition system

(b)

Fig. 4.2 Scheme diagram of four-points bending; (a) test schematic (b) test setup

Prior to testing, the weights and dimensions of the specimens were measured to determine their densities and volumes at testing time. The tests were conducted at roughly 20 ^{0}C; and the relative humidity (rh) was in the range of 50% to 70%. Immediately after testing, small pieces from each specimen were cut and oven dried for 72 hours to determine moisture content and basic density according to AS/NZS 1080.1 [85].

4.2.3 Data analysis

MOE and *MOR*

For determining the material properties of timber in bending, such as *MOE* and *MOR*, different evaluation methods were used according to the different testing standards. *MOE* and *MOR* were calculated according to the equations below:

$$MOE = \frac{23P_{pl}L^3}{108WD^3\delta_{\frac{1}{2},pl}} \tag{4.1}$$

where, L is working span (mm), i.e., the span between supports, W is beam width (mm), D is beam depth (mm), P_{pl} is the force (N) in the elastic region and its corresponding deflection at mid-span, $\delta_{\frac{1}{2},\mathrm{pl}}$ (mm).

In the elastic region, the deflections at mid-span and one-third span, $\delta_{\frac{1}{3},\mathrm{pl}}$ (m), can be calculated via Eq. (4.2), and the derivation is referred to Cheng et al. [65].

$$\delta_{\frac{1}{2},pl} = \frac{23\delta_{\frac{1}{3},pl}}{20} \tag{4.2}$$

$$MOE = \frac{5P_{pl}L^3}{27WD^3\delta_{\frac{1}{3},pl}} \tag{4.3}$$

The *MOR* was calculated from the ultimate load (N), P_{ult}, and was given by:

$$MOR = \frac{P_{ult}L}{WD^2} \tag{4.4}$$

Moisture content and basic density

The moisture content (*MC*) of the samples was calculated according to AS/NZS 1080.1 [85]. *Basic density* is calculated using the formula (3.5) provided in Chapter 3.

Moisture adjustment factor

A moisture adjustment factor [56], *F*(*MC*), is defined as showing the relative influence of moisture on *MOR* compared with a reference *MC*, usually at 12%. Linear functions [56] were applied to obtain moisture modification factors, below and above *FSP*, in this study and these are given by:

$$F(MC) = \frac{MOR_{MC}}{MOR_{12}} = a(MC - 12) + b \; (MC \leq FSP) \tag{4.5}$$

$$F(MC) = \frac{MOR_{MC}}{MOR_{12}} = c \; (MC > FSP) \tag{4.6}$$

where, a, b, and c are constants depending on experimental results.

Segmented regression analysis was undertaken to examine the relationship of *MOR*–*MC* and moisture modification factor.

Statistical analyses

To determine the load ΔP_e and the displacement, $\Delta\delta_{1/3}$, a linear relationship was fitted through the linear elastic range of the load and displacement curves. Statistical analyses were undertaken using Matlab (version R2019a, Natick, Massachusetts: The Math-Works Inc.). The theoretical probability functions of the normal distribution and the lognormal distribution were applied to fit probability distributions of *MOR* for dry and wet samples. A Kolmogorov–Smirnov test (K–S test) is applied to evaluate the fit between the theoretical probability distribution and the empirical probability distribution obtained from the experimental data, as it is sensitive to differences in both location and shape of the probability distribution functions [96]. The formula for the K–S test can be expressed as follows:

$$D_{bn} = \max_x \left| F_{bn}(x) - F_b(x) \right| \tag{4.7}$$

where, $\max_x |\ |$ is the maximum absolute distance; $F_{bn}(x)$ and $F_b(x)$ represent the empirical probability distribution function and the theoretical probability distribution function, respectively. $D_n(x)$ is the maximum absolute difference between $F_{bn}(x)$ and $F_b(x)$.

At the 0.05 level of significance, $D_{0.05} = K/\sqrt{n}$, where, K is Kurtosis and n is the number of samples. If D_{bn} is smaller than $D_{0.05}$, the theoretical probability distribution provides a good fit to the empirical probability distribution obtained from the test data, otherwise, the fit is unacceptable.

4.3 RESULTS AND DISCUSSIONS

4.3.1 Failure modes

According to ASTM D 143- 09 [57], failures in static bending include tension, compression and shear (*Table 4.2*). Among tension failures, there are four types of failure called simple tension, cross-grain tension, splintering tension and brash tension. Consistent with Derikvand et al [3], two types of failure were observed, namely, grain tension failure with combined compression, and bending tension failure (*Fig. 4.3*).

Types of Failure in Static Bending		**Photos of Failures**
Tension Failure	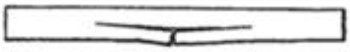 (a) Simple Tension. (Side View)	Simple tension 
	 (b) Cross-Grain Tension.* (Side View)	Cross grain tension 
	 (c) Splintering Tension. (View of Tension Surface)	Splintering tension
	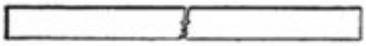 (d) Brash Tension. (View of Tension Surface)	
Compression Failure	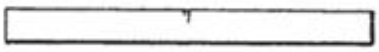 (e) Compression. (Side View)	
Shear Failure	 (f) Horizontal Shear. (Side View)	N/A

Table 4.2 Types of failure in static bending.

The term “cross grain” shall be considered to include all deviations of grain from the direction of the longitudinal axis or longitudinal edges of the specimen. It should be noted that spiral grain may be present even to a serious extent without being evident from a casual observation. The presence of cross grain having a slope that deviates more than 1 in 20 from the longitudinal edges of the specimen shall be cause for culling the test (ASTM D 143-09 [57])

Grain tension failure and combined compression

One of the failure types observed in the test is combined compression and tension failure. The load-deflection curves and the corresponding photo of the deformed samples are shown in *Fig. 4.3a, b*. The three stages of specimens in bending are shown in *Fig. 4.4*: these are linear displacement, compression failure appearance, and tension failure appearance with crack initiation. A yield curve was found after a relatively linear response during the elastic range of flexural deflection.

Types of Failure	**Cross grain tension failure**	**Simple tension failure**
Tension failure with combined compression	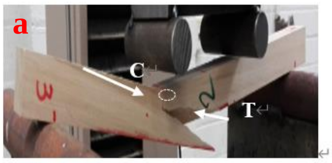 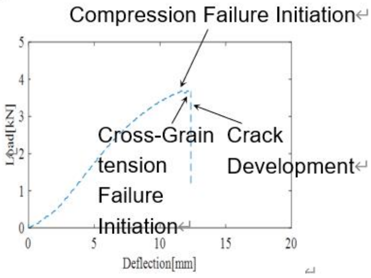	 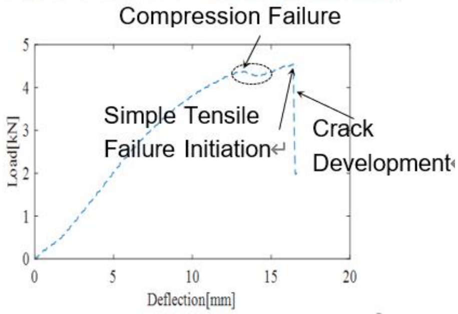
Tension failure only	 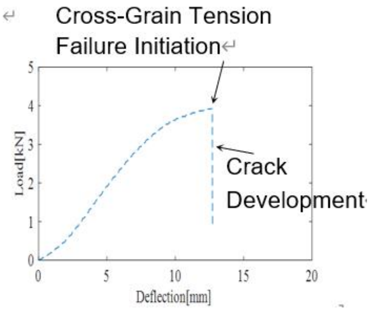	 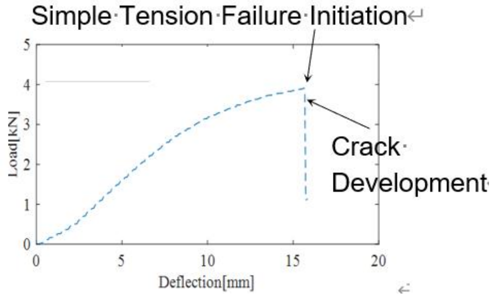

Fig. 4.3 Bending response and failure mode for dry *E. nitens* samples. Top row: Tension failure with combined compression (a, b); bottom row: Bending tension failure only (c, d); Left: Cross grain tension failure (a, c); right: Simple tension failure (b, d)

The yield curves indicate that the timber had reached its compression failure (*Fig. 4.3a, b*). The progress of the bending after the compression failure led to tension failure and crack initiation. At this time, cracks appeared in the tension side of the timber and developed upward, such that the neutral axis shifted toward the compression side. This type of tension failure is related to the ring angle as well as to the grain angle. When neither the ring angle nor the grain angle is equal to zero, there is normally cross grain tension failure. When both angles are equal to zero, a simple tension failure occurred, and the bending strength reached its maximum for this set of tests.

Overall, compared with other failure types, the combined compression and tension failure linked with higher bending strength as compression failure is generally found in good pieces where tensile capacity is higher than compression.

Fig. 4.4 Bending and failure of each stage for combined compression and tension failure *E. nitens* samples; (a) linear displacement, (b) compression failure appearance and (c) tension failure appearance with crack initiation

Bending tension failure

Another failure type in the tests was bending failure in tension alone, which includes simple tension and cross grain tension. The shapes of the load-deflection curves for this type of failure are consistent. After a relatively linear relationship, nonlinearity was observed. Failure occurred at or close to the mid-span on the tension side, starting on that face and developing to follow the fibre direction towards the compression side.

The failure was initiated in different areas in various specimens. This variation in locations is due to timber is a natural material with anisotropic non-uniformities, i.e., along or across the fibres, as well as earlywood or latewood. As a result, these differences in the material may undoubtedly cause deflection and failure from one board slightly varied from others originally from the same resource. Comparing wet and dry cases, more nonlinearity was observed in wet samples, while brittle behaviour dominated the failure for dry samples (*Fig. 4.5*).

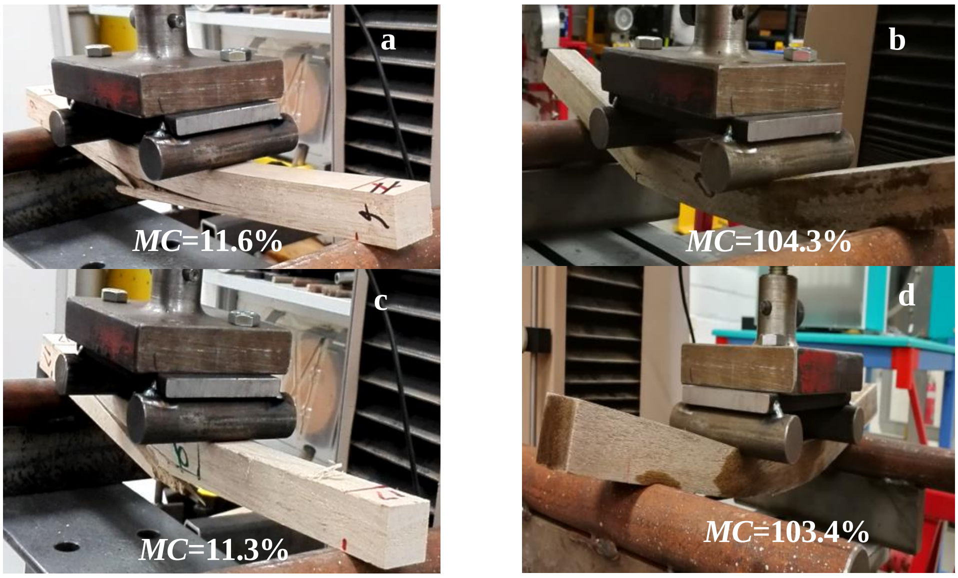

Fig. 4.5 Failure modes of the four-point bending *E. nitens* samples. Left: dry samples (a, c); right: wet samples (b, d); top row: grain tension failure with combined compression (a, b); bottom row: bending tension failure (c, d).

All dry samples (overall) showed a sudden tensile rupture in the timber in this set of tests at *MC* less than 15 % (*Fig. 4.5a, c*), which is consistent with previous findings [3, 4, 10, 57]. It seems that in the dry samples, once a rupture occurs it propagates rapidly throughout the material. In contrast, ductile failure behaviour was observed in wet samples, and the cracks remain localized (*Fig. 4.5b, d*). This may be because the water existing in the wet samples provided lubrication between the grain fibres allowing them to slide easily from one state to another at a microscopic level, while undergoing shear deformation - allowing a redistribution of local stresses.

4.3.2 Load-deflection curves

Fig. 4.6 represents the load-displacement behaviour for small clear *E. nitens* specimens at the loading point, i.e., one-third point. A brittle fracture is observed for clear timber beams at dry condition and a relatively linear response was observed when the deflection was roughly below 8 mm and 4 mm (see dash lines in *Fig. 4.6*) for wet samples, respectively. This is the elastic range of the load and deflection curve for *Eucalyptus nitens* beams in bending for this set of tests.

The dry samples exhibited a more extensive linear phase in the load-displacement curve, relating to a higher ultimate load with sudden brittle ruptures compared with wet samples.

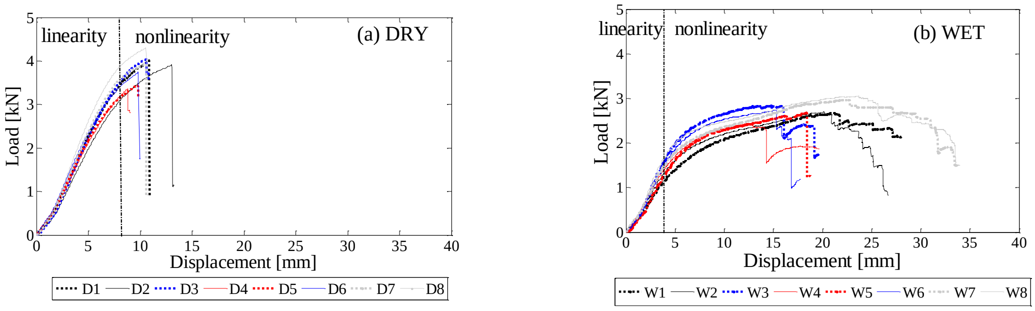

Fig. 4.6 Load-deflection curves of *E. nitens* in bending; (a) dry specimens and (b) wet specimens.

Conversely, a distinctly different ductile bending behaviour in wet samples was observed in the load–deflection curves. The wet samples exhibited considerably larger displacements at lower maximum loads, while the dry samples showed quite abrupt failures at relatively small displacements just beyond the proportional limit, connected with somewhat higher maximum loads. The wet samples showed abrupt drops, like the dry samples, but with a subsequent recovery of load, reaching a new lower plateau, often occurring several times (*Fig. 4.6b*). No obvious difference in load- displacement curves between the 0º, 30º, 45º, 60º and 90º annual growth ring orientations was found in this study.

4.3.3 Bending strength (*MOR*) and modulus of elasticity (*MOE*)

There was acceptable agreement with values of basic density measured with previous studies [3, 62]. The average values of the basic density from both dry and wet plantation *E. nitens* samples were 520.4 kg/m^3 and 496.9 kg/m^3, respectively (*Table 4.3*). It also found that the mean values for basic density were close to that reported by Farrell, et al. [62] for wet samples and Derikvand et al [3] for dry samples, with the difference less than 5%.

Another important measure, *MOE,* varied from 10.0 to 13.2 GPa for dry samples and from 6.4 to 11.6 GPa for wet samples, with mean values of 11.8 GPa and 9.5 GPa, respectively (*Fig. 4.7* and *Table 4.3*). *MOR* lies in the range of 62.2 MPa to 100.3 MPa for dry samples and 23.9 MPa to 87.7 MPa for wet samples, with mean values of 80.7 MPa and 59.0 MPa, respectively. These lie in the range of those of Farrell, et al., 2008

[62] and Heid & Brancheriau, 2018 [8] for high moisture samples and for low moisture samples, respectively (*Fig. 4.7*).

Physical property		Testing		Other Studies	
		Dry-E	Wet-E	Dry-E(H18) *	Wet-E(F08) **
MC (%)	Mean (*COV* %)	11.6 (5.4)	86.4 (16.7)	14 -	100.1 (20.5)
MOE (GPa)	Mean (*COV* %)	11.8 (6.8 I)	9.5 (12.0)	12.5 (18.9)	10.6 (21.1)
MOR (MPa)	Mean (*COV* %)	80.7 (9.0 II)	59.0 (19.8)	76.8 (20.5)	51.9 (30.0)
Basic Density (kg/m^3)	Mean (*COV* %)	520.4 (8.7)	496.9 (7.8)	517.7 (11.6)	479.8 (7.8)

*H18 [97] (for other plantation eucalypt species at low moisture condition) and **F08 [62] (for plantation *E. nitens* at high moisture condition) refer to values given in other scholars; I and II The suggested COV values by Wood Handbook [10]: I 22% and II 16%.

Table 4.3 Physical properties of *E. nitens* samples in four point bending;

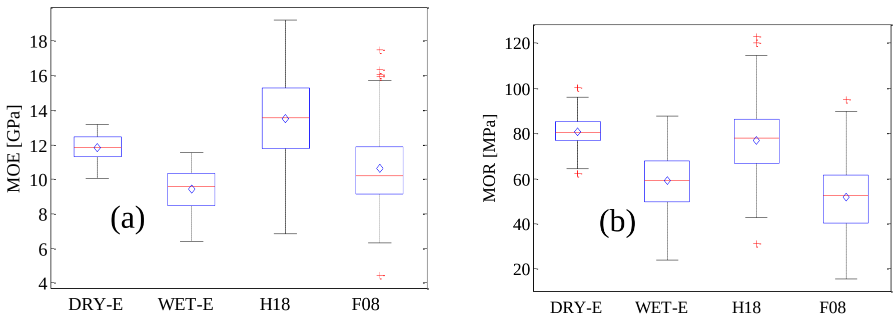

Fig. 4.7 Boxplot of *MOE* and *MOR* for *E. nitens* samples compared with other studies on plantation eucalypt species [62, 97]. (a) *MOE*; (b) *MOR*

The coefficients of variation (*COV*) for *MOE* and *MOR* in both dry and wet samples were also examined. The *COV*s of *MOR* and *MOE* for dry samples were lower than the corresponding cases provided by the Wood Handbook [10] and Heid & Brancheriau, 2018 [8] (*Table 4.3*). These lower *COV*s were due to the samples being cut from the same boards and being defect-free, with clear samples being selected to avoid the influences of non-uniformities in the wood samples as studied in the Wood Handbook [10], Farrell, et al., 2008 [62] and Heid & Brancheriau, 2018 [8]. *COV*s of *MOR* and *MOE* for wet samples were higher than the ones for dry samples due to the wet samples covering a broad moisture range.

Therefore, this study is shown to be reasonable and repeatable data for plantation-grown *E. nitens.*

4.3.4 Probability distribution of *MOR*

The empirical probability distributions of *MOR* of *E. nitens* in both dry and wet states were determined from the test data to assess its suitability for use in building structures. *Fig. 4.8* presents histograms of the *MOR* of dry and wet samples - fitted by lognormal and normal probability distribution functions.

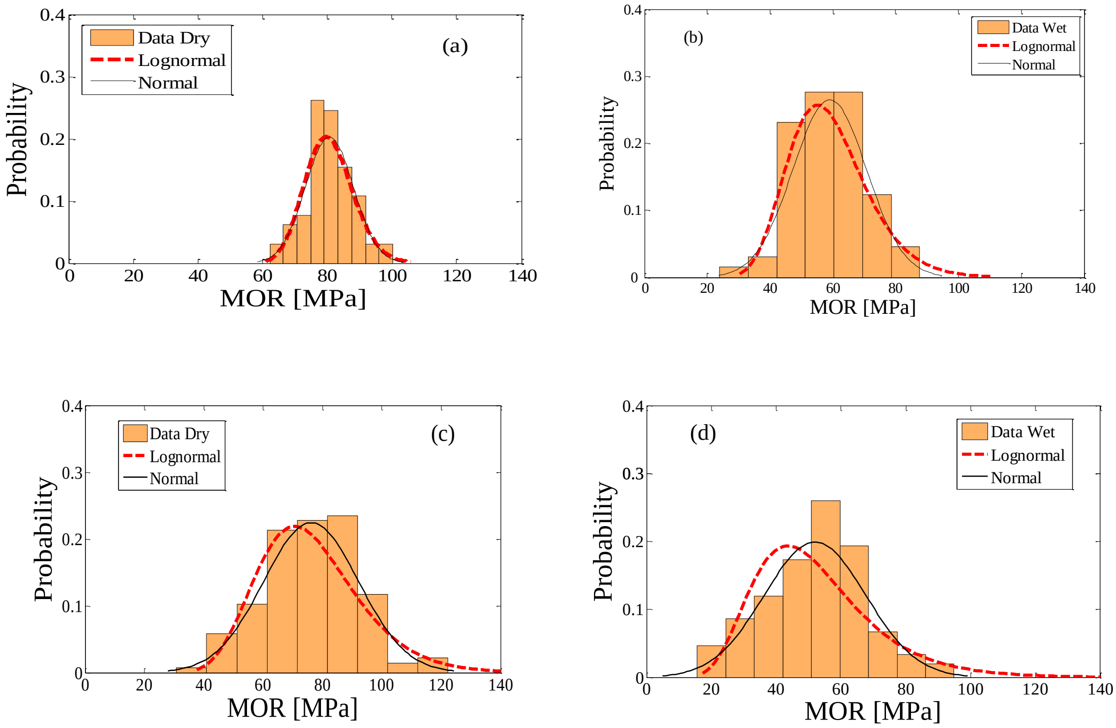

Fig. 4.8 Probability distribution of *MOR*. Left: dry samples (a, c); right: wet samples (b, d); top row: histograms of the *MOR* from authors' testing (a, b); bottom row: histograms of the *MOR* from values given in other research [8] [62] (c, d).

Code		Maximum absolute difference (D_{bn})		Critical Value ($D_{0.05}$)
		Lognormal	Normal	
Testing	Dry-E	0.0730	0.0644	0.1657
	Wet-E	0.0756	0.0592	0.1657
Other	Dry-E(H18) *	0.0908	0.0550	0.1152
Studies	Wet-E(F08) **	0.1268	0.0599	0.1097

Table 4.4 The maximum absolute difference between the experimental cumulative distribution and theoretical distribution using K-S testing. *Heid & Brancheriau, 2018 [8]. **Farrell, et al., 2008 [62].

The results of the K–S test were presented in *Table 4.4*, in which different data sets had different critical ($D_{0.05}$) and maximum absolute difference (D_{bn}) values.

Except Wet-E (F08), which showed only the normal probability distribution fitted the testing data, both theoretical probability distributions fitted the experimental data, however, the normal probability distribution showed a better fit as it had smaller maximum absolute difference, where a smaller value indicated a better fit. This was particularly evident in the left region for each case, where the normal distribution followed the testing data more accurately. This finding was consistent with previous research [83].

4.3.5 Design characteristic values

According to the design codes for timber structures (ASTMD2899 [89] and AS1720 [11]), design characteristic values can be still based on small clear sample testing. For US standards, design value of a structural beam element can be estimated from a strength characteristic value of small clear wood samples at 5% percentile strength with 95% confidence according to the ASTM standard (ASTMD2899 [89]). For Australian Standards, the design value, eg. F-grade, can be obtained from the small clear samples based on AS 2878 [98] and applied though the visual grading standards (AS 2082 [91]). These design values can be used to assess the allowance stress of the timber structural member in accordance with the current design standards, such as AS1720 [11].

Basic fitted parameters and the characteristic values of lognormal distribution and normal distribution is shown in *Table 4.5*. For the better fit probability distribution, i.e., normal distribution, suggested design characteristic values of plantation-grown small clear *E. nitens* samples for dry and wet conditions were 68.5 MPa and 39.8 MPa, respectively.

The moisture reduction factor of *E. nitens* in this study was at 0.55 at a 5% percentile level and at 0.7 at mean level, respectively. The moisture reduction factor of such *E. nitens* timber at the mean level was relevantly higher than for other commercial timber species, for example, Pinus, *radiata* (0.52 at mean level) and Spruce (more than 0.53 at mean level) [10], implying a potential use of *E. nitens* by the building industry, especially where the timber is vulnerable to be fully saturated.

Theoretical distribution		Testing		Other Studies	
		Dry-E	Wet-E	Dry-H18*	Wet-F08**
Lognormal distribution	Mean (MPa)	4.4	4.06	4.31	3.90
	S.D.* (MPa)	0.09	0.21	0.22	0.35
	characteristic value, f_r (MPa)	70.3	41.1	51.9	27.8
Normal distribution	Mean (MPa)	80.7	59.0	76.8	51.9
	S.D. (MPa)	7.4	11.7	15.8	15.6
	characteristic value, f_n (MPa)	68.5	39.8	50.9	26.3

Table 4.5 Fitting parameters and characteristic values of theoretical probability distribution functions. *S.D., standard deviation

4.4 SUMMARY

This Chapter determined the mechanical bending characteristic of plantation Eucalyptus *nitens* (*E. nitens*) samples at both low and high moisture contents in order to examine its suitability for use as a structural material. The samples were from a 16-year-old pulpwood *E. nitens* sourced from Tasmania, Australia. The bending strength values were obtained by performing four-point bending tests with a Universal Testing Machine, and second objective has been fulfilled.

The findings can be summarised as follows.

- Two types of failure modes, which are combined compression with tension failure and bending tension failure, were found for both dry and wet samples.
- Load and displacement curves for the *E. nitens* samples in bending were determined. Dry samples in general, failed by brittle fracture with a sudden tensile rupture in the timber, while wet samples featured larger displacements at

lower maximum loads and failed by ductile failure with several drops in load-displacement curves, indicating alternating periods of rupture and hardening.

- The mean and variation in material properties such as basic density, *MOE* and *MOR* at both low and high moisture contents were determined. The agreement between the data in this study and findings reported by other research [8, 62] on Eucalyptus timber for low or high moisture content showed that the results in these tests are reasonable for both low and high moisture content states.
- The bending strength probability distributions of *E. nitens* at both low and high moisture contents were estimated. The normal distribution showed a better fit and was selected to determine design characteristic values presented in this study. The design characteristic values for small clear *E. nitens* samples with low and high moisture contents were 68.5 MPa and 39.8 MPa, respectively.
- The test results for small clear *E. nitens* wood in four-point bending provided a moisture reduction factor at 0.55 and 0.7 at the 5th percentile and mean strength level, respectively. The results showed that *E. nitens* was promise as a material to be used in the construction industry for bending members especially in water saturated condition as the moisture modification factors of *E. nitens timber* at mean level were higher than those of *Pinus, radiata* (0.52) and Spruce (0.53).

In this Chapter, Eucalyptus plantation wood, *E. nitens*, is proved to be a potential resource for structural use as a bending member, especially when exposed to water. This research provides basis for *E. nitens* in structural applications. Further work could establish relevant design codes to facilitate using this resource for building and structural applications. These properties could also be used in the further research for finite element analysis of the structural performance of any potential timber product from such a plantation source. As the FEA together with constitutive modelling overcomes the limitations of the experiments due to the non-uniformity in *E. nitens* samples leading to a large variation in measured values and can give an insight into the underlying failure mechanism of *E. nitens*, the next Chapter will introduce a new constitutive modelling for *E. nitens* wood.

Chapter 5

5 A NEW MOISTURE-DEPENDENT MODEL OF TIMBER MATERIAL

5.1 INTRODUCTION

In order to achieve the third objective of this study, namely, to describe the short time behaviour of timber more realistically and efficiently including the effect of moisture, hence, the aim of this chapter is the development of a moisture-dependent anisotropic elasto-plasticity model for wood. After this introduction, Section 5.2 provides the background of the existing constitutive modelling for wood. Constitutive modelling of timber materials is outlined in Section 5.3. The method of identifying the plastic material parameters used in the proposed constitutive model is briefly outlined in Section 5.4. Section 5.5 presents a numerical implementation. Section 5.6 provides numerical examples for validation of this new constitutive model. Afterwards, a discussion highlighted the new features of this constitutive model is provided. Section 5.8 presents summary.

5.2 EXISTING CONSTITUTIVE MODELS FOR WOOD

In order to understanding the underlying failure mechanism of *E. nitens,* sophisticated methods are needed. The merit of such method is to overcome the limitations of the experiments as mechanical properties of *E. nitens* timber are very difficult to examine separately using an experimental approach due to the heterogeneity behaviour of natural wood, together with its nonlinear material characteristics. In other words, the experimental results are empirical and only tell us the phenomenon. Constitutive modelling handed with FEM technique appeared as an effective tool to do numerically reflect the realistic stress state within timber structures and predict their possible failure.

Several types of constitutive models have been proposed to describe the mechanical behaviour of wood at a macroscopic level [23, 99-101] [102] [46]. For example, Patton-Mallory (1997) used a tri-linear constitutive relationship incorporated into an orthotropic elastic material to model wooden bolted connections [102]. Tabiei and Wu (2000) developed an orthotropic model using an incremental-iterative secant stiffness approach [46]. Their model agreed well with experimental shear and compression data within the elastic range for the given species of wooden specimens. The ultimate compressive strength of wood is not accurately predicted by this model: numerical models such as this need to include inelastic behaviour, so as to model hardening behaviour accurately.

Hong et al (2015) studied Douglas fir in compression [27]. They developed a numerical model which incorporated Hill's anisotropic plasticity theory based on a bi-linear stress-strain constitutive relationship. The results of their numerical modelling agreed closely with their experimental results. Milch, et al [24] studied damage to Norway spruce and European beech both numerically and experimentally. They applied an elas-toplastic material model with nonlinear isotropic hardening and a Hill yield criterion. The results of their numerical modelling agreed acceptably with experimental data ob-tained from mechanical testing with loads applied at 90 degrees to the grain. However, when it comes to stress and strain along wood fibre, the hardening law is not always appropriate. The compression behaviour of wood in the longitudinal direction and both anatomical directions is different: the stress-strain curve changes from "softening" to "hardening" from the longitudinal direction to that perpendicular to the grain [51, 52]. These phenomena have also been observed in *E. nitens* timber both below and above *FSP*, which is provided in Chapter 3. In order to numerically model load carrying ca-pacity of *E. nitens* timber more correctly, the elastoplastic anisotropy in wood need to be included.

A change in moisture content significantly affects the strength of timber structures. For example, important wood species, such as Douglas fir, show a significant reduction in strength in high moisture situations [68]. Generally, the decrease in strength and stiff-ness in timber occurs when moisture content increase while staying below the Fibre saturation point (*FSP*) and no significant changes occur above *FSP* [10]. *FSP* is defined when there is an absence of any free water in the cell lumina, and the cell walls are sat-urated with chemically and physically bound water [9, 10]. As noted above, being a hy-groscopic material and being an anisotropic, biological, cellular structure, the compres-sive and flexural strengths of *E. nitens* timber also depend on its moisture content. This feature of *E. nitens* timber has been found experimentally and presented in Chapter 3 and 4. In compression members of bridges and piers when submerged in water, in tim-ber piles immersed in soil near the river but above the water table, and in houses in a flood zone when the timber members are soaked for a long time, water can be drawn into the wood by capillary action and lead to moisture contents above *FSP* [65, 66]. Re-assessment of the safety of timber structures when moisture content increases above its fibre saturation point (*FSP*) is of interest to many present-day workers [9]. To safely use

E. nitens by the building industry, especially where these members are vulnerable to water, the moisture dependent effect should be included in structural design, so as to predict a more accurate ultimate load/stress capacity in compressive or flexural *E. nitens* timber members exposed to water. The variation of material properties of *E. nitens* with moisture content can be found in Chapter 3 and 4.

To capture the consequences of the mechanical behaviours of *E. nitens* wood, a new moisture-dependent anisotropic elasto-plasticity model is introduced to indicate anisotropic material behaviour of wood for short time response when moisture content changes. The details are listed in the following section.

5.3 MOISTURE-DEPENDENT ANISOTROPIC ELASTO-PLASTICITY MODEL FOR TIMBER MATERIALS

As a consequence of the cellular structure of trees, wood is an anisotropic material [10]. A cut wood section is usually assumed to be a three-dimensional orthotropic material with three main directions that correspond to the natural arrangement of cells in tree stems. These directions are:

• Longitudinal, *L*, which is parallel to the mean fibre direction.

• Radial, *R*, which is perpendicular to the growth rings (in a plane perpendicular to the longitudinal direction).

• Tangential, *T*, which is tangential to the growth rings (in a plane perpendicular to the longitudinal direction).

The tangential and radial directions are generally perpendicular to each other. Therefore, the *L*, *R* and *T* directions form a local orthogonal system, superimposed on a cylindrical structure (*Fig 5.1*) Within a global cylindrical coordinate system, the orthogonal *LRT* coordinate sub-system is used to define properties. The cell wall structure consists of four layers built up mainly with fibril networks which contain hemicellulose and lignin (*Fig 5.2*) [17]. These cell wall structures deform when external force (s), e. g. gravity, wind loading or bending, act on them. Experiments find a permanent deformation in wood specimens when forces exceed the capacity of the wood fibres. This is a nonconservative and path-dependent elasto-plastic phenomenon [23, 24, 51].

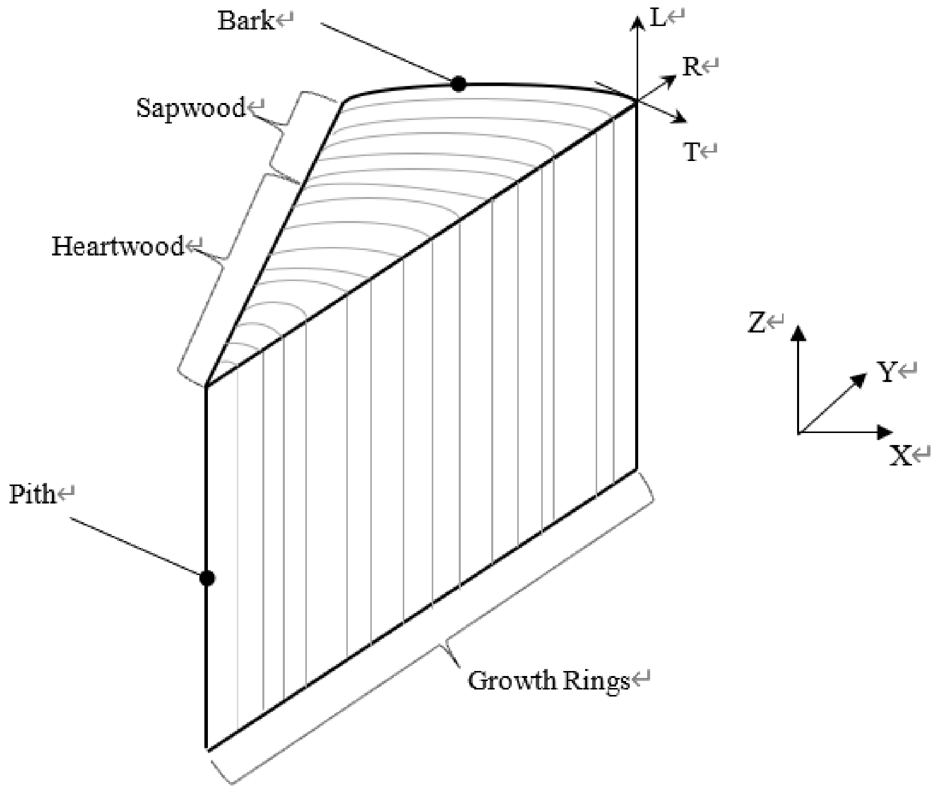

Fig. 5.1 Principal axes with respect to tree stem structure. Pith is heart in hardwood.

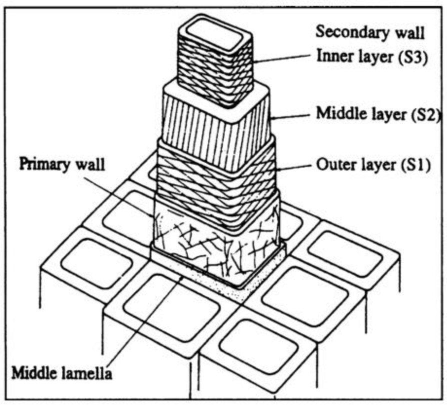

Fig. 5.2 Simplified structure of the cell wall [17]

Milch, et al [24] studied the damage of Norway spruce and European beech wood by static loading experiments. Ductile behaviour could be observed in compression perpendicular to grain. The failure behaviour of the tension and compression were also found to be different [36].

As mentioned previously, that as a hygroscopic material, the stiffness and strength of wood depend on the moisture content. For example, important hardwood species, such as European beech, show a large reduction in mechanical properties, strength in particular, at a high moisture content [23]. Hence to capture the consequences of the behaviour of wood in which the moisture content is very high - for example, in living trees, the effect of moisture should be included. For reliable predictions of this material behaviour, a new moisture dependent anisotropic plasticity is introduced in the next two sections to show the anisotropic material behaviour of wood varying according to moisture content. This model is a development from the one-parameter plasticity model for fibrous composites proposed by Wang et al [103, 104], which assumed the material was elastic in the fibre direction and transversely isotropic with a power law to model the isotropic hardening. A simple version of the effective stress was used [103, 104], which ignores the effect of the stress variables along the fibre. In the developed constitutive model for wood, Ramberg-Osgood hardening law was assumed as it was confirmed by experiments [14], and scalar function for plastic potential hardening is related to the i direction ($i = L, R, T$, where L is the longitudinal, R radial and T transverse direction). The plasticity along the grain for compression is included and loading-directional dependence on the plastic flow was considered [105]. Variation of material properties of timber with varying moisture contents is also included in a newly developed constitutive model, the values of these material properties could be identified from experimental data.

This constitutive model is orthotropic in elastic regions while anisotropic in plastic regions and can systematically study the path-dependent elasto-plastic phenomenon of wood at varying moisture contents and its different reactions to tension and compression. The principal axes of the constitutive model are presented in *Fig 5.1*. The theoretical backgrounds of this model are introduced in the following sections.

5.3.1 Elastic deformation

Before yielding, wood undergoes an elastic deformation, which implies a linear and fully recoverable material behaviour. The stress and strain relationship within the elastic range reads:

$$\boldsymbol{\sigma} = \boldsymbol{C_0} : \boldsymbol{\varepsilon}^e \tag{5.1}$$

where, $\boldsymbol{\varepsilon}^e$ is the elastic strain tensor, $\boldsymbol{\sigma}$ is the stress tensor. For orthotropic material, elastic compliance $\boldsymbol{C_0^{-1}}$ consists of 9 independent material variables, and details shown in Eq (5.2).

$$\boldsymbol{C_0^{-1}} = \begin{bmatrix} \begin{matrix} \frac{1}{E_{LL}} & \frac{-u_{RL}}{E_{RR}} & \frac{-u_{TL}}{E_{TT}} \\ \frac{-u_{LR}}{E_{LL}} & \frac{1}{E_{RR}} & \frac{-u_{TR}}{E_{TT}} \\ \frac{-u_{LT}}{E_{LL}} & \frac{-u_{RT}}{E_{RR}} & \frac{1}{E_{TT}} \end{matrix} & \boldsymbol{0}_{3\times3} \\ \boldsymbol{0}_{3\times3} & \begin{matrix} \frac{1}{G_{LR}} & 0 & 0 \\ 0 & \frac{1}{G_{LT}} & 0 \\ 0 & 0 & \frac{1}{G_{RT}} \end{matrix} \end{bmatrix} \tag{5.2}$$

where, Young's modulus E_{ii}, shear modulus G_{ij}, and Poisson's ratio u_{ij} ($i, j = L, R, T$) refer to the principal material directions *L*, *R* & *T*. All material variables (P_{MC}), e.g. Young's modulus, shear modulus and Poisson's ratio, depend on the moisture level and follow the empirical model [10, 56], which has been grounded for *E. nitens* by experimental findings shown in Chapter 4.

$$\begin{aligned} &P_{MC} = F(MC)P_{12} = a(MC-12)P_{12} + bP_{12} \qquad (MC \le FSP) \\ &P_{MC} = F(MC)P_{12} = cP_{12} \quad (MC > FSP) \end{aligned} \tag{5.3}$$

where, P_{MC} and P_{12} are respectively the material variables at a moisture content of MC% and 12%. $F(MC)$ is the moisture content adjustment factor; *a*, *b*, and *c* are constants depending on experimental results. *FSP* is fibre saturation point, which varies between species but is typically in the moisture content range of 20 to 30% [9, 10, 73]. The material variables include elastic parameters in this sections, and plastic parameters, which are defined in the following section.

5.3.2 Plastic deformation

When wood fails under tensile or shear loading, localised brittle fracture is observed. However, under compression, pronounced inelastic behaviour occurs. Plastic hardening in different anatomical directions is orientation dependent due to the arrangement of cells in the wood. For a general 3D anisotropy material, a Hill yield function [87], a quadratic form in stresses, is usually used without consideration of hydrostatic pressure and is assumed to be as follows:

$$f_{Hill}^{*} = k_1(\sigma_{LL} - \sigma_{RR})^2 + k_2(\sigma_{RR} - \sigma_{TT})^2 + k_3(\sigma_{TT} - \sigma_{LL})^2 + 2k_4\sigma_{RT}^2 + 2k_5\sigma_{TL}^2 + 2k_6\sigma_{LR}^2 \qquad (5.4)$$

where the stresses σ_{ij} ($i, j = L, R, T$) refer to the principal directions L, R, T, respectively. The parameters k_1- k_6 are constants, which define the current state of anisotropy at a moisture content of *MC* %, and are given by:

$$k_1 = \frac{1}{2}\left\{\left(\frac{Y_L^T + Y_L^C}{2Y_L^T Y_L^C}\right)^2 + \left(\frac{Y_R^T + Y_R^C}{2Y_R^T Y_R^C}\right)^2 - \left(\frac{Y_T^T + Y_T^C}{2Y_T^T Y_T^C}\right)^2\right\}$$

$$\begin{aligned}
k_2 &= \frac{1}{2}\left\{\left(\frac{Y_R^T + Y_R^C}{2Y_R^T Y_R^C}\right)^2 + \left(\frac{Y_T^T + Y_T^C}{2Y_T^T Y_T^C}\right)^2 - \left(\frac{Y_L^T + Y_L^C}{2Y_L^T Y_L^C}\right)^2\right\} \\
k_3 &= \frac{1}{2}\left\{\left(\frac{Y_T^T + Y_T^C}{2Y_T^T Y_T^C}\right)^2 + \left(\frac{Y_L^T + Y_L^C}{2Y_L^T Y_L^C}\right)^2 - \left(\frac{Y_R^T + Y_R^C}{2Y_R^T Y_R^C}\right)^2\right\} \qquad (5.5) \\
k_4 &= \frac{1}{2(Y_{RT}^S)^2}, \; k_5 = \frac{1}{2(Y_{TL}^S)^2}, \; k_6 = \frac{1}{2(Y_{LR}^S)^2}
\end{aligned}$$

where, Y_i^C, Y_i^T, Y_{ij}^S ($i, j = L, R, T$) are the absolute values of compressive, tensile, and shear yield strengths, respectively, in the principal stress space, and at a moisture content of *MC*%.

Similar to the Drucker–Prager yield criterion [106], a generalized Hill yield function is proposed for wood material by modifying the Hill yield function. This function is able to consider pressure-dependent criteria and is given by:

$$f_M^{*} = \sqrt{f_{Hill}^{*}} + k_7\sigma_{LL} + k_8\sigma_{RR} + k_9\sigma_{TT} \qquad (5.6)$$

where, f_M^* is modified Hill yield function which depends on hydrostatic pressure, f_{Hill}^* is the Hill yield function independent of hydrostatic pressure. The pressure-modified coefficients $k_7 - k_9$ are given by Eq (5.7) in the principal directions.

$$k_7 = \frac{Y_L^C - Y_L^T}{2Y_L^T Y_L^C},\ k_8 = \frac{Y_R^C - Y_R^T}{2Y_R^T Y_R^C},\ k_9 = \frac{Y_T^C - Y_T^T}{2Y_T^T Y_T^C}. \tag{5.7}$$

A schematic for anisotropic elasto-plastic behaviour of this constitutive model is shown in *Fig. 5.3*. The initial yield surface of this constitutive model is a tapered elliptical cylinder surface in principal stress space, and the projection in "π" plane is elliptical (*Fig. 5.3a, b*). Meanwhile, the elliptical initial yield surface enlarges as moisture content decreases from *FSP* to dry state (*Fig. 5.3c*). This is because the strength in the longitudinal direction is much higher than the strengths in the radial axis and the tangential axis.

The transition between elastic and inelastic domains in the stress space is proposed by Tsai and Wu (*1971*) [23, 107] as follows:

$$\begin{gathered} f_i(\boldsymbol{\sigma}, \alpha_i, MC) = \mathbf{A}_i(MC):\boldsymbol{\sigma} + \boldsymbol{\sigma}:\mathbf{B}_i(MC):\boldsymbol{\sigma} + q_i(\alpha_i, MC) - 1 \\ i = L, R, T \end{gathered} \tag{5.8}$$

where, the strain variable α_i, the strength tensor components $\mathbf{A}_i(MC)$ and $\mathbf{B}_i(MC)$, and the scalar function for plastic potential hardening $q_i(\alpha_i, MC)$ are related to the *i* direction (*i* = *L*, *R*, *T*). All relevant strength values and respective plasticity parameters are moisture dependent and can be known from experimental data.

The law of plastic potential hardening is assumed to follow the Ramberg-Osgood function, which is confirmed by experimental results from Beech wood [14]:

$$\varepsilon^p = (\sigma/K)^n \tag{5.9}$$

where, K and n are plasticity parameters and need to be evaluated from experimental results. The method to identify *K* and *n* is provided in Section 5.4.

The incremental plastic strains $d\varepsilon_{ij}^p$ ($i, j = L, R, T$) can be presented based on associated flow rule [108], and is given by:

$$d\varepsilon_{ij}^{p} = \frac{\partial f^{*}}{\partial \sigma_{ij}} d\lambda \tag{5.10}$$

where, the superscript p denotes plasticity, f^{*} is plastic potential and $d\lambda$ is a proportionality factor.

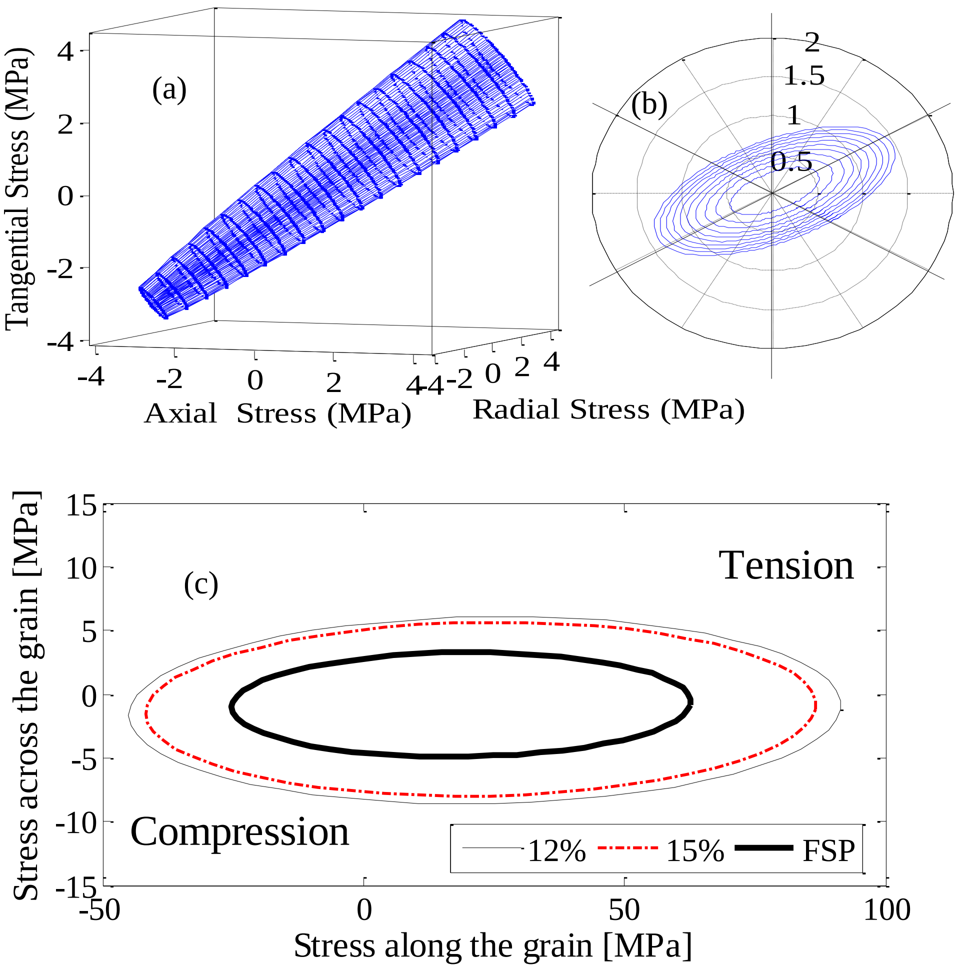

Fig. 5.3 A schematic of anisotropic elasto-plastic behaviour for moisture-dependent anisotropic elasto-plasticity model; (a) Initial yield surface in principal stress space (b) Initial yield surface in "π" plane (c) moisture sensitivity for yield surface

If the effective stress is defined as Eq (5.11) [105], the increment of plastic work per unit volume (dW^{P}), can be expressed by Eq (5.12):

$$\bar{\sigma} = \sqrt{\frac{3}{2}\{(\sigma_{RR}-\sigma_{TT})^2 + [2A\sigma_{RT}^2 + 2B(\sigma_{TL}^2+\sigma_{LR}^2)]\} + C^2\sigma_{LL}^2} + C(\sigma_{LL}+\sigma_{RR}+\sigma_{TT}) \tag{5.11}$$

$$dW^p = \boldsymbol{\sigma} d\boldsymbol{\varepsilon}^p = \bar{\sigma} d\bar{\varepsilon}^p = f^* d\lambda \tag{5.12}$$

where, $d\bar{\varepsilon}^p$ is effective plastic strain, new parameters, *A*, *B*, *C* describing the state of anisotropy of wood material and given by Eq (5.13).

$$A = \frac{(Y_R^T)^2}{2(Y_{RT}^S)^2},\; B = \frac{(Y_R^T)^2}{2(Y_{LR}^S)^2},$$
$$C = \frac{(Y_R^T)^2}{2}\left\{\left(\frac{Y_L^T + Y_L^C}{2Y_L^T Y_L^C}\right)^2 + \left(\frac{Y_R^T + Y_R^C}{2Y_R^T Y_R^C}\right)^2 - \left(\frac{Y_T^T + Y_T^C}{2Y_T^T Y_T^C}\right)^2\right\} \tag{5.13}$$

Then, the relation between plastic strain and increment of effective plastic strain is:

$$d\varepsilon_{ij}^p = \frac{\partial\bar{\sigma}}{\partial\sigma_{ij}} d\bar{\varepsilon}^p\,. \tag{5.14}$$

Then, assuming the wood material model to be transversely isotropic, the incremental plastic strain can be calculated by substituting Eq (5.11) with Eq (5.14) and is given by:

$$\begin{Bmatrix} d\varepsilon_{LL}^p \\ d\varepsilon_{RR}^p \\ d\varepsilon_{TT}^p \\ d\varepsilon_{RT}^p \\ d\varepsilon_{TL}^p \\ d\varepsilon_{LR}^p \end{Bmatrix} = \begin{Bmatrix} \dfrac{\sigma_{LL}}{\tilde{\sigma}} \\ \dfrac{3(\sigma_{RR}-\sigma_{TT})}{2\tilde{\sigma}} \\ \dfrac{3(\sigma_{TT}-\sigma_{RR})}{2\tilde{\sigma}} \\ \dfrac{6\sigma_{RT}}{\tilde{\sigma}} \\ \dfrac{3B\sigma_{TL}}{\tilde{\sigma}} \\ \dfrac{3B\sigma_{LR}}{\tilde{\sigma}} \end{Bmatrix} \times d\bar{\varepsilon}^p \tag{5.15}$$

where, $\tilde{\sigma} = \sqrt{\frac{3}{2}[4\sigma_{RT}^2 + (\sigma_{RR}-\sigma_{TT})^2 + 2B(\sigma_{LR}^2+\sigma_{TL}^2)] + \sigma_{LL}^2}$

5.3.3 Elastic-plastic compliance matrix

In the light of the hardening law, Eq (5.9), the instantaneous plastic modulus can be obtained:

$$H_p = \frac{d\bar{\sigma}}{d\bar{\varepsilon}^p} = \frac{K^n}{n\bar{\sigma}^{n-1}} \tag{5.16}$$

The total strain is split into elastic and plastic parts, as:

$$d\varepsilon_{ij} = d\varepsilon_{ij}^e + d\varepsilon_{ij}^p = S_{ijkl}^{\mathrm{e}}\, d\sigma_{kl} + S_{ijkl}^p\, d\sigma_{kl} = S_{ijkl}^{\mathrm{e}p} d\sigma_{kl}\,,\ (i,j,k,l = L,R,T) \tag{5.17}$$

in which ε_{ij}^e, ε_{ij}^p are elastic and plastic strains, and S_{ijkl}^{e}, S_{ijkl}^p and $S_{ijkl}^{\mathrm{e}p}$ are elastic, elastic–plastic, and plastic compliance matrices, respectively.

Plastic compliance matrices are given by combining (5.16) and (5.17):

$$S_{ijkl}^p = \frac{d\varepsilon_{ij}^p}{d\sigma_{kl}} = \frac{d\varepsilon_{ij}^p}{d\bar{\varepsilon}^p}\frac{d\bar{\varepsilon}^p}{d\bar{\sigma}}\frac{d\bar{\sigma}}{d\sigma_{kl}} = \frac{d\varepsilon_{ij}^p}{d\bar{\varepsilon}^p}\frac{1}{H_p}\frac{d\bar{\sigma}}{d\sigma_{kl}}\,. \tag{5.18}$$

The increment of the three-dimensional constitutive model proposed in this Chapter can be obtained by combining Equations (5.1), (5.8) , (5.15), (5.18), and is shown below:

$$\begin{Bmatrix} d\varepsilon_{LL} \\ d\varepsilon_{RR} \\ d\varepsilon_{TT} \\ d\varepsilon_{RT} \\ d\varepsilon_{TL} \\ d\varepsilon_{LR} \end{Bmatrix} = \begin{bmatrix} S_{LLLL} & S_{LLRR} & S_{LLTT} & S_{LLRT} & S_{LLTL} & S_{LLLR} \\ S_{RRLL} & S_{RRRR} & S_{RRTT} & S_{RRRT} & S_{RRTL} & S_{RRLR} \\ S_{TTLL} & S_{TTRR} & S_{TTTT} & S_{TTRT} & S_{TTTL} & S_{TTLR} \\ S_{RTLL} & S_{RTRR} & S_{RTTT} & S_{RTRT} & S_{RTTL} & S_{RTLR} \\ S_{TLLL} & S_{TLRR} & S_{TLTT} & S_{TLRT} & S_{TLTL} & S_{TLLR} \\ S_{LRLL} & S_{LRRR} & S_{LRTT} & S_{LRRT} & S_{LRTL} & S_{LRLR} \end{bmatrix}^{ep} \times \begin{Bmatrix} d\sigma_{LL} \\ d\sigma_{RR} \\ d\sigma_{TT} \\ d\sigma_{RT} \\ d\sigma_{TL} \\ d\sigma_{LR} \end{Bmatrix} \tag{5.19}$$

where, S_{ijkl} (i, j, k, l =L, R, T) is the elastic–plastic compliance matrix, and the details were provided in Appendix 1.

Inversing the elastic–plastic compliance matrix, the Jacobian matrix can be obtained and given by Eq (5.20).

$$J_{ep} = \left[S_{ijkl}^{ep} \right]^{-1}. \tag{5.20}$$

5.4 METHOD FOR IDENTIFYING THE PLASTIC HARDENING PARAMETERS

This study adopted and improved the approach proposed by Wang et al [109] to identify the plastic hardening parameters of the moisture dependent anisotropic plasticity model. Hardening parameters can be obtained from off-axis compression testing on wood specimens at a known moisture content, *MC*. If we know the experimental stress-strain curves, the plastic strain in the loading direction can be obtained via the measured strain minus its elastic part. Then, the effective plastic strain, $\bar{\varepsilon}^p(MC)$, and the effective stress, $\bar{\sigma}(MC)$, can be obtained according to the coordinate transformation, $h(\varphi, MC)$, of the stress and plastic strain curve from the off-axis testing:

$$\bar{\varepsilon}^p(MC) = \varepsilon_c^p(MC)/h(\varphi, MC) \tag{5.21}$$

$$\bar{\sigma}(MC) = h(\varphi, MC)\sigma_c(MC). \tag{5.22}$$

where, $\varepsilon_c^p(MC)$ and $\sigma_c(MC)$ represent plastic strain and stress along the loading direction at *MC*, respectively. $h(\varphi, MC)$ is the transform function at *MC*, and φ is the angle between the loading direction and the wood fibre.

For off-axis compression in L-R plane, (i.e., in a plane parallel to the fibres and perpendicular to the growth rings), the transform function can be simplified and is given by:

$$h(\varphi, MC) = \sqrt{\frac{3}{2}(sin^4\varphi + 2B(MC)sin^2\varphi cos^2\varphi) + C(MC)cos^4\varphi} \tag{5.23}$$

where, *B*(*MC*) and *C*(*MC*) are the anisotropy parameter at a given *MC* and is defined by Eq (5.13), and φ is the angle between the loading direction and the wood fibre.

In the constitutive model, a Ramberg-Osgood function approximately describes the relationship between the effective stress $\bar{\sigma}$ and plastic strain $\bar{\varepsilon}^p$ in the plastic range, Eq (5.9).

Combining Eq (5.9), (5.21), and (5.22), we obtain:

$$\varepsilon_C^p(MC)/h(\varphi, MC) = [h(\varphi, MC)\sigma_C(MC)/K]^n \tag{5.24}$$

$$ln[(\varepsilon_C^p(MC)/h(\varphi,MC)] = ln[(h(\varphi,MC)\sigma_C(MC)]n + ln(1/K^n) \tag{5.25}$$

Plasticity parameters K and n can be determined based on the least square optimal fit to the experimental effective stress and effective plastic strain relationship according to Eq (5.25), and an example is shown in *Fig 5.4*, where the original experimental data is provided in *Fig 5.5a*. The procedure to determine the effective stress and effective plastic strain from the experimental data is shown in *Fig 5.5* with description as follows.

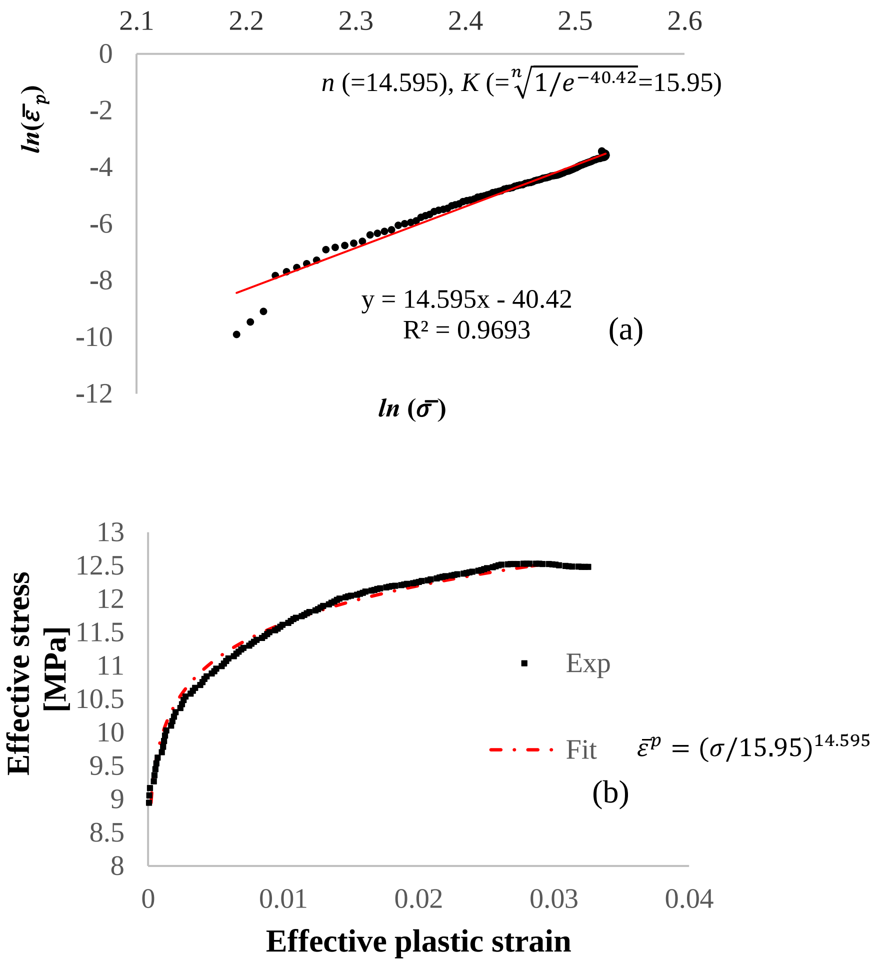

Fig. 5.4 An example for parameter identification on K and n at grain angle $\varphi = 45°$ and MC>FSP. (a) A least square optimal for identification on n (=14.595) and K (=$\sqrt[n]{1/e^{-40.42}}$=15.95); (b) Comparison between experimental data and the fitting hardening law.

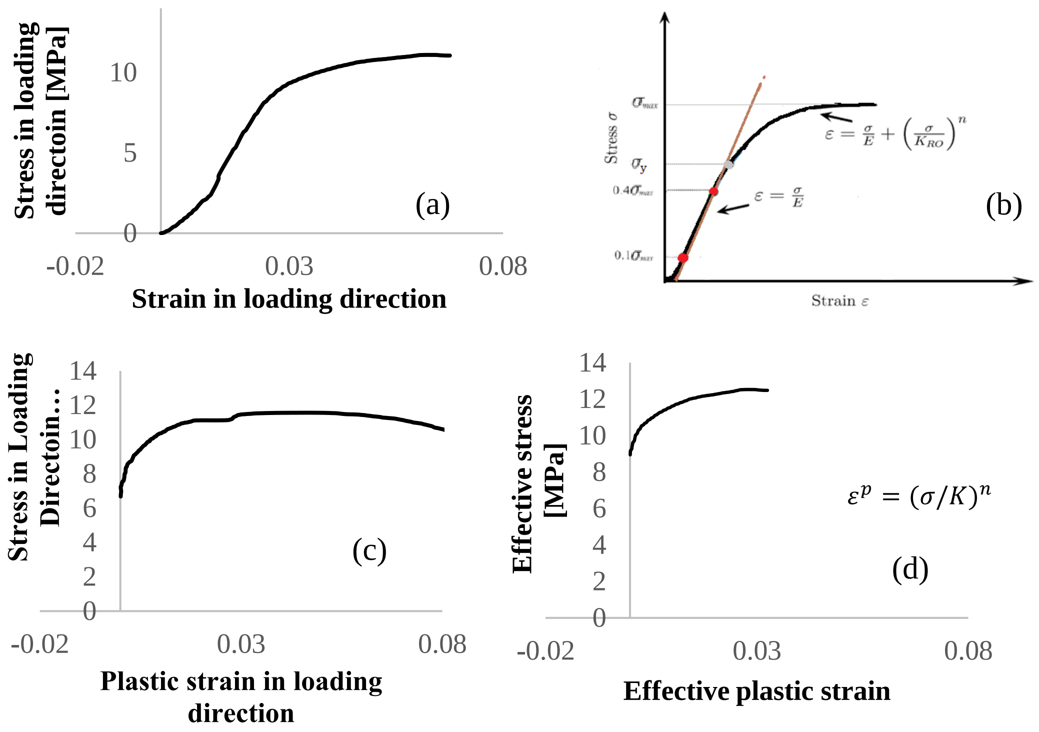

Fig 5.5 An example for obtaining the plastic strain from experimental strain and stress (MPa) curve: (a) experimental strain and stress (MPa) curve in loading direction, (b) method to obtain plastic strain from measured stress strain curve, (c) the relationship between plastic strain and stress (MPa) in loading direction, (d) effective plastic strain and effective stress (MPa) curves

For an experimental stress-strain curve at a known *MC* and loading direction (φ is known), for example *Fig 5.5a*, stress and plastic strain curve can be obtained (*Fig 5.5c*) when measured strain minus its elastic part (*Fig 5.5b*). The effective plastic strain and effective stress were calculated from measured plastic strain and stress according to Eq (5.21) and Eq (5.22), respectively. Effective plastic strain and effective stress curve is also provided in *Fig 5.5d*. In this example, the original experimental data is from compression tests on wet small block *E. nitens* samples at grain angles of 45º shown in *Fig 3.6f* of Chapter 3. For this set of data, *MC>FSP*, *B* = 0.043 and *C* = 0.57. *B* and *C* are calculated based on Eq (5.13) using the strengths data given in *Table 5.5*.

5.5 NUMERICAL IMPLEMENTATION

The moisture dependent fibre plasticity model can be implemented by an FE simulation using an incremental, iterative numerical approach [104]. In this study, commercial FE software ABAQUS was adapted to implement the moisture dependent anisotropic plasticity model. A UMAT (User-defined mechanical material behaviour in Abaqus) subroutine in ABAQUS is applied to perform the capability of the proposed modified constitutive model. The procedure for the UMAT subroutine is illustrated in a flow chart (*Fig 5.6*).

The details are as follows:

Stage 1: Data initialization. Set all state variables to their corresponding values from the last converged iteration of the previous increment [104]. These include material properties, strain increments, solution-dependent state variables, and current stresses.

Stage 2: Elastic predictor. Obtain the trial stresses and trial effective stresses:

$$\sigma_{n_s+1}^{trial} = \sigma_{n_s} + \left[S_{ijkl}^{e}\right]^{-1} \Delta\varepsilon_{n_s+1} \tag{5.26}$$

subscripts $(\bullet)_{n_s}$ indicate a state at the current time step, while the subscript $(\bullet)_{n_s+1}$ represents the next time step with a time increment, $\Delta t = t_{n_s+1} - t_{n_s}$.

Stage 3: Stress state identification. In this step, determine whether the element is in tension or compression. A positive value of average three principal stresses indicates that the element is in tension, i.e., $\sigma_m \geq 0$; otherwise, it is subjected to compression.

$$\sigma_m = \frac{\sigma_{LL} + \sigma_{RR} + \sigma_{TT}}{3} \tag{5.27}$$

Stage 4: Yield state identification and plastic deformation check. In this step, examine the possibility of irrecoverable deformation of the element. The yield criterion is evaluated by trial and current effective stresses.

If $\Phi_{n_s} \leq 0, \Phi_{n_s+1}^{trial} \leq 0$, no initial yield occurs, and the wood undergoes a linear deformation.

If $\Phi_{n_s} \leq 0, \Phi_{n_s+1}^{trial} > 0$, initial yield occurs, and plastic strain of wood element appears at the next (n_s+1) increment.

If $\Phi_{n_s} > 0, \Phi_{n_s+1}^{trial} > 0$, plastic deformation appears, and strain hardening occurs at the next increment. The yield surface has changed with changes of the strain hardening variable (s).

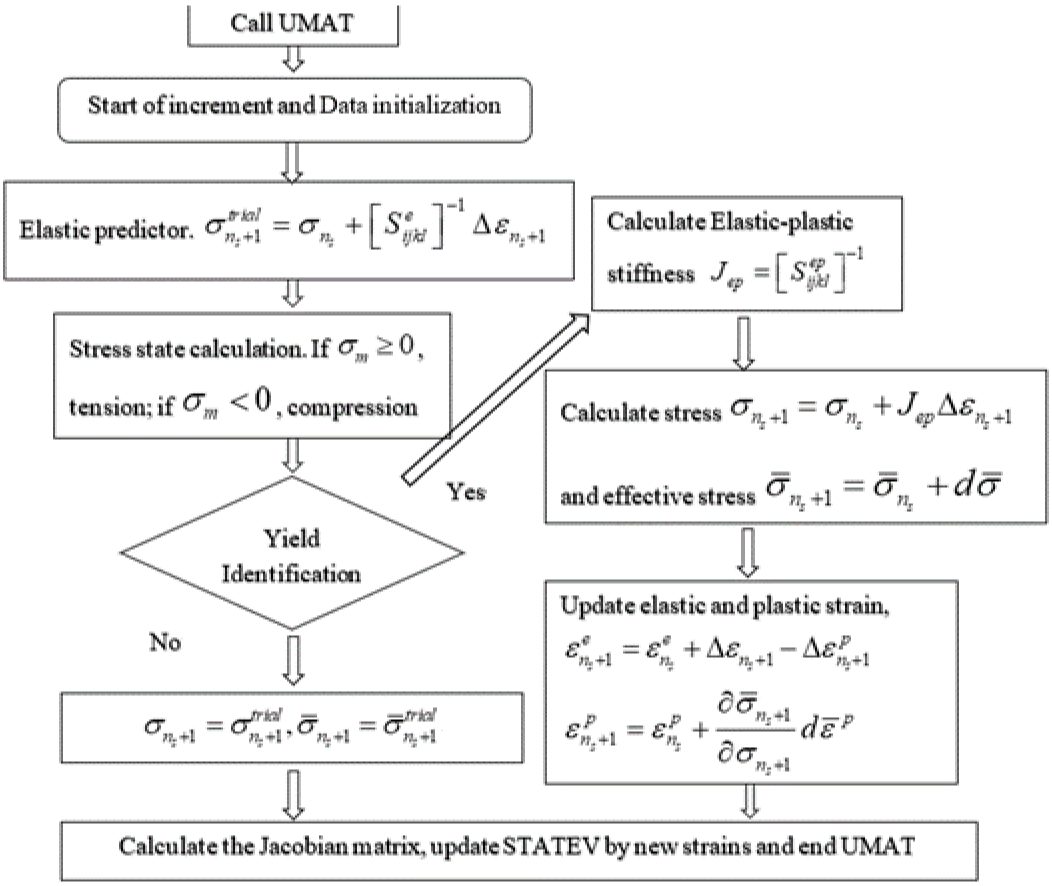

Fig. 5.6 Flow Chart of the Numerical implementation using UMAT

Stage 5: Stresses and strains update. Calculate the stress tensor and strain tensor at the current increment by Eq (5.28) for elastic deformation or by Eq (5.29) for plastic deformation.

If the trial state of stress remained in the elastic domain, the stress tensor and the total strain tensor at the end of the increment equals the elastic contribution as follows.

$$\begin{aligned} &\sigma_{n_s+1} = \sigma_{n_s+1}^{trial}, \bar{\sigma}_{n_s+1} = \bar{\sigma}_{n_s+1}^{trial} \\ &\varepsilon_{n_s+1}^{p} = \varepsilon_{n_s}^{p} = 0, \bar{\varepsilon}_{n_s+1}^{p} = \bar{\varepsilon}_{n_s}^{p} = 0, \end{aligned} \tag{5.28}$$

If plastic deformation occurs, then update the stresses and the state variables by Eq (5.29) based on the value of state variables from the previous increment.

$$\begin{aligned} &\sigma_{n_s+1} = \sigma_{n_s} + J_{ep}\Delta\varepsilon_{n_s+1} d\bar{\sigma} = \bar{\sigma}_{n_s+1} - \bar{\sigma}_{n_s} \\ &d\bar{\varepsilon}^{p} = \frac{d\bar{\sigma}}{Hp} \end{aligned} \tag{5.29}$$

$$\bar{\varepsilon}^{p}_{n_s+1} = \bar{\varepsilon}^{p}_{n_s} + d\bar{\varepsilon}^{p}$$

$$\varepsilon^{p}_{n_s+1} = \varepsilon^{p}_{n_s} + \frac{\partial \bar{\sigma}_{n_s+1}}{\partial \sigma_{n_s+1}} d\bar{\varepsilon}^{p}$$

$$\varepsilon^{e}_{n_s+1} = \varepsilon^{e}_{n_s} + \Delta\varepsilon_{n_s+1} - \Delta\varepsilon^{p}_{n_s+1}$$

Stage 6: State Variables Matrix (STATEV) update and UMAT end. Calculate the Jacobian matrix, update STATEV and exit UMAT. The updated state values stored in STATEV will be initial values for the next step.

5.6 VERIFICATION AND VALIDATION

This section verifies the functionality of the proposed 3D moisture dependent anisotropic plasticity model for accurately predicting the short-term responses. Example 1 is complemented with an experimental validation using testing data of beech wood [14, 24, 31] under moisture dependent compressions in order to compare the moisture dependent behaviours predicted by the proposed constitutive model. The material properties of Examples 1 are given in *Table 5.1* and *Table 5.2*. These parameters are obtained from experimental results using beech wood [14, 31]. Example 2 further extends the validation of the proposed constitutive model to compressive behaviours of *E. nitens* timber, both below and above *FSP* via FE methods.

5.6.1 Example 1 - Waisted specimens for beech wood in moisture dependent compression tests

This example shows the performance of proposed constitutive model for predicting moisture dependent mechanical behaviour for wood. Comparison between this constitutive model with experimental work of Hering et al [14, 31] is illustrated. The dimension of the model is 100 mm length (*L*) × 28 mm width (*W*) × 28 mm depth (*D*) with a cross-sectional area of 14 mm × 14 mm with a length of 11 mm, in the narrow part (*Fig 5.7*). The compression tests were carried out in standard climatic conditions, and the measured data is provided in *Table 5.1* and *Table 5.2*. Although these data are from different studies (See the reference resource shown in *Table 5.1* and *Table 5.2*, the values of the data are in the same range, this implies that the data we used is reproducibility and can be used for investigating moisture dependent mechanical behaviour of beech wood.

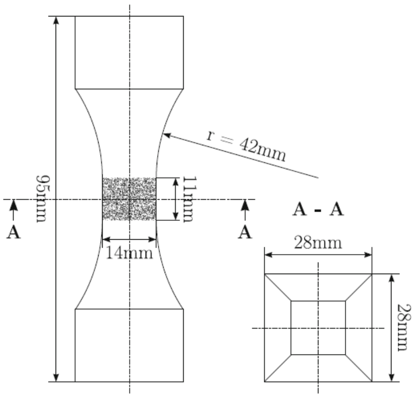

Fig. 5.7 Waisted specimens with random texture used for compression testing [31]

Resource	MC (%)	Density (kg/m³)			Young 's modules (Mpa)			Poisson Ratio					
		R	L	T	R	L	T	tr	tl	rl	rt	lr	lt
H11	8.7	724	705	621	1990	14400	679	0.65	0.26	0.31	0.29	0.09	0.1
	12.9	713	740	621	1900	13900	606	0.64	0.24	0.27	0.27	0.07	0.09
	16	726	716	626	1570	13200	505	0.64	0.18	0.24	0.27	0.06	0.06
	18	717	707	622	1430	11600	475	0.63	0.18	0.24	0.28	0.05	0.06
S33	10.5		745		2240	13700	1140	0.75	0.51	0.45	0.36	0.07	0.04
W66	8.2		-		2070	11100	1070	0.65	0.48	0.37	0.33	0.06	0.03
N98	12		-		1100	-	580	0.77	-	-	0.29	-	-

H11, Hering et al., 2011 [31]; S33, Stamer and Sieglerschmidt, 1933 [31]; W66, Wommelsdorf et al,1966 [31]; N98 Neumann et al, 1998 [31]

Table 5.1 Densities and Elastic material properties for beech wood under compression testing with different moistures

	MC (%)	Compressive Strength (MPa)			K		n	
		L	R	T	R	T	R	T
H12	8.7	73.4 (8.2)	15.9 (5.4)	6.9 (4.5)	20.4	11.9	17.1	8.3
	12.9	60.1 (11.2)	13.5 (5.6)	6.0 (3.1)	16.6	9.6	20.7	9.7
	16	48.0 (12.9)	10.9 (3.7)	5.0 (4.5)	12.8	7.5	26.6	7.5
	18	40.2 (15.6)	10.0 (6.5)	4.5 (3.2)	12	6.6	23.1	6.6
M16	15	47.5	9.49	8.1	-	-	-	-

H12, Hering et al., 2012 [14]; M16, Milch et al, 2016[24]

Table 5.2 Plastic material properties for beech wood under compression testing with different moistures

The data provided, except for some Poisson's ratios (e.g. u_{rt} and u_{tr}), show linear decreases of corresponding material parameters relative to an increase in moisture content in all material directions, see *Fig 5.8-Fig. 5.10* indicating that the empirical moisture adjustment model, Eq (5.3), used could be appropriate for our purpose when *MC* below *FSP*, which varies between species but is typically in the moisture content range from 20 to 30% [9, 10, 73].

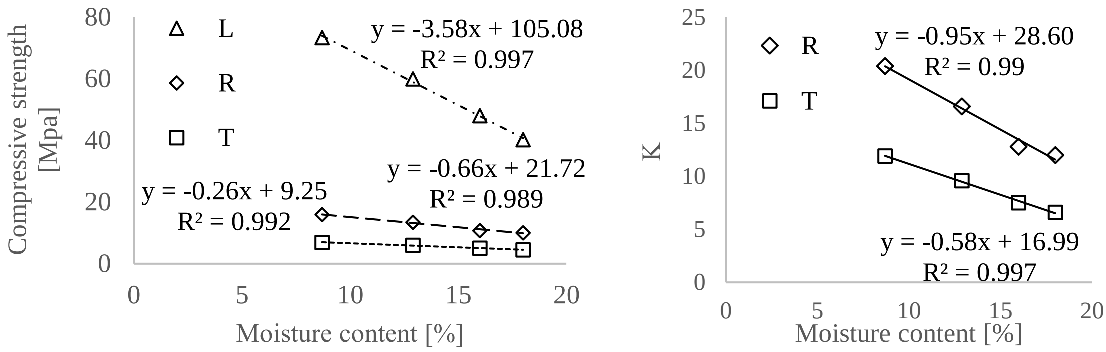

Fig. 5.8 The relationship between the plastic material properties and moisture content for beech wood in compression: a) compressive strength; b) plastic hardening parameter (Analysed data from the work of Hering et al [14, 31])

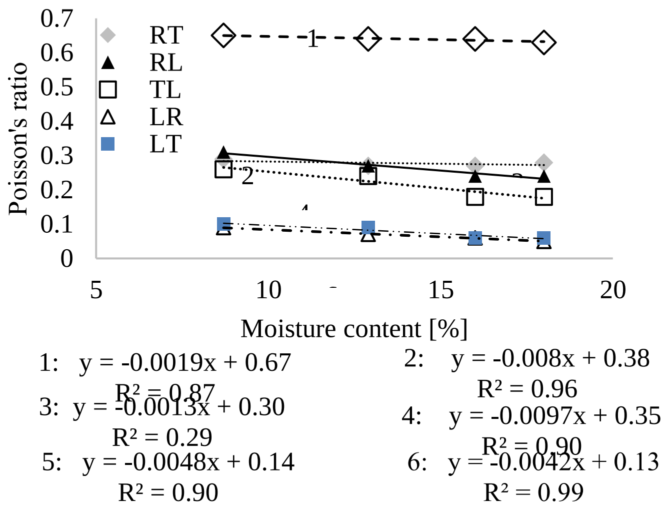

Fig. 5.9 The relationship between the measured Poisson's ratio and moisture content for beech wood in compression (Analysed data from the work of Hering et al [14, 31])

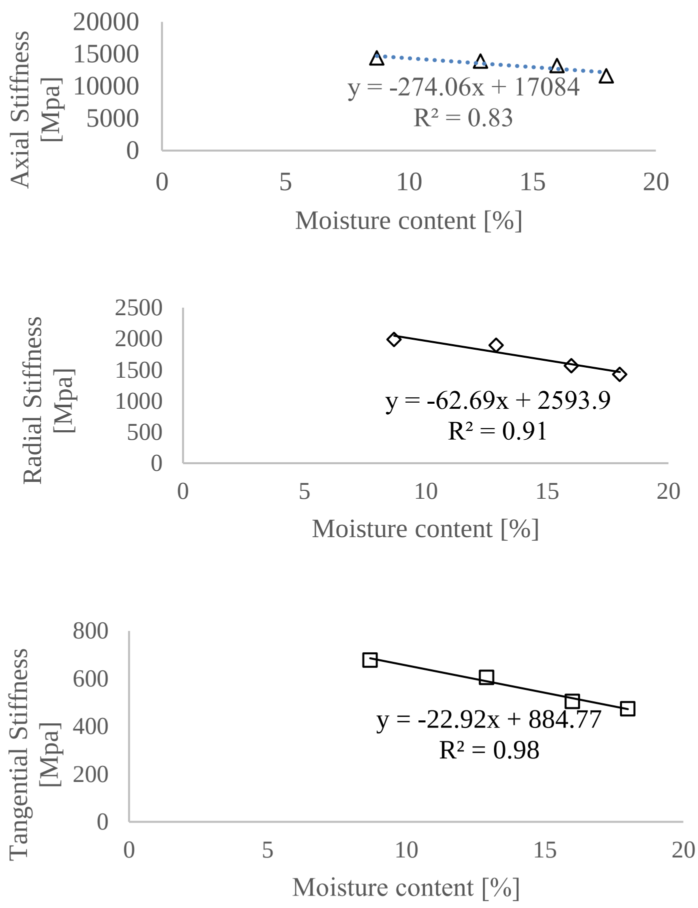

Fig. 5.10 The relationship between the measured stiffness and moisture content for beech wood in compression (Analysed data from the work of Hering et al [14, 31])

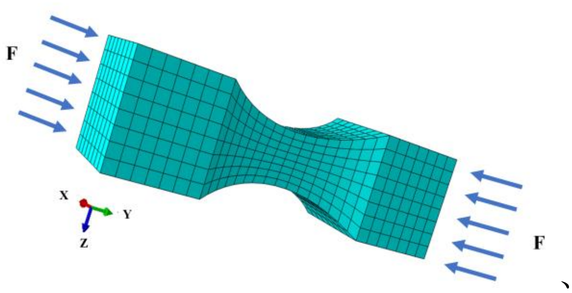

Fig. 5.11 Finite element model of waisted specimens for beech wood in moisture dependent compression tests

For the FEM, the model for compressive loads on the waisted beech wood specimens is given in *Fig 5.11*, which precisely reflected the experimental work, i.e., the dimensions, the applied load and the boundary conditions (BC): The geometry is discretised by 2511 general purpose linear brick elements (C3D8R). The forces are uniform surface loads acting on the top surface. The bottom surface of the model restricted any three-dimensional movement.

	MC	**Density**	**Poisson's ratio**			**shear moduli***			**shear yield stress***		
	(%)	**(kg/m³)**	u_{LR}	u_{LT}	u_{RT}	G_{LR} (MPa)	G_{LT} (MPa)	G_{LR} (MPa)	Y_{LR} (MPa)	Y_{LT} (MPa)	Y_{RT} (MPa)
Case 1	8.7	742.78	0.09	0.1	0.29	1608	1059	460	12.6	10.1	14.2
Case 2	12	780.52	0.07	0.09	0.27						
Case 3	16	799.64	0.06	0.06	0.27						
Case 4	18	804.76	0.05	0.06	0.28						

* means testing data for beech wood from Milch et al. 2016 [24].

Table 5.3 Other physical properties for beech wood used in Finite Element Model

The moisture dependent compressive behaviour of the waisted beech wood in radial and tangential directions was examined. For each anatomical direction, four cases at moisture contents of 8.7%, 12.6%, 16%, and 18%, respectively, were examined. The input parameters of the constitutive model for the corresponding moisture content are given in *Table 5.1* for densities and elastic moduli and *Table 5.2* for plastic hardening parameters in the directions *L*, *R*, *T*, respectively. These parameters were obtained from the same beech wood samples which resulted in the experimental stress-strain curves provided in *Fig 5.12*. As shear moduli and shear yield stresses have not been given in the same papers, the values from another paper for beech wood [24] were used in the simulation and were given in *Table 5.3*. Poisson's ratios, shear moduli and shear stresses do not significantly affect the compression perpendicular to the grain. Therefore, an assumption has been made that Poisson's ratios, shear moduli and shear stresses are constant when the moisture content changes during the simulation. The yield stresses in radial and tangential directions were optimized to obtain a minimal relative error in the numerical stress strain curve with respect to experimental data.

A comparison for stress-strain curves between the testing and the modelling of waisted beech wood specimens in compression with different moisture contents in both anatomical directions, e. g. radial and tangential directions, is presented in *Fig 5.12.* Apart from some minor deviations in the transition zone between linear and nonlinear behaviour, the numerical results well agree with the experimental data (i.e., error less than 5%). The match in elastic range and hardening implies that elastic deformations and the hardening law for plastic evolution under different moisture conditions for the proposed constitutive model were reasonable for beech wood including the moisture effect, however, some deviations were found in plastic flow. These differences may result from the assumption of ideal geometry and homogeneous material distribution in the numerical models while some natural factors, e.g., the material heterogeneity, which may contribute to the result, have not yet been considered in the proposed models.

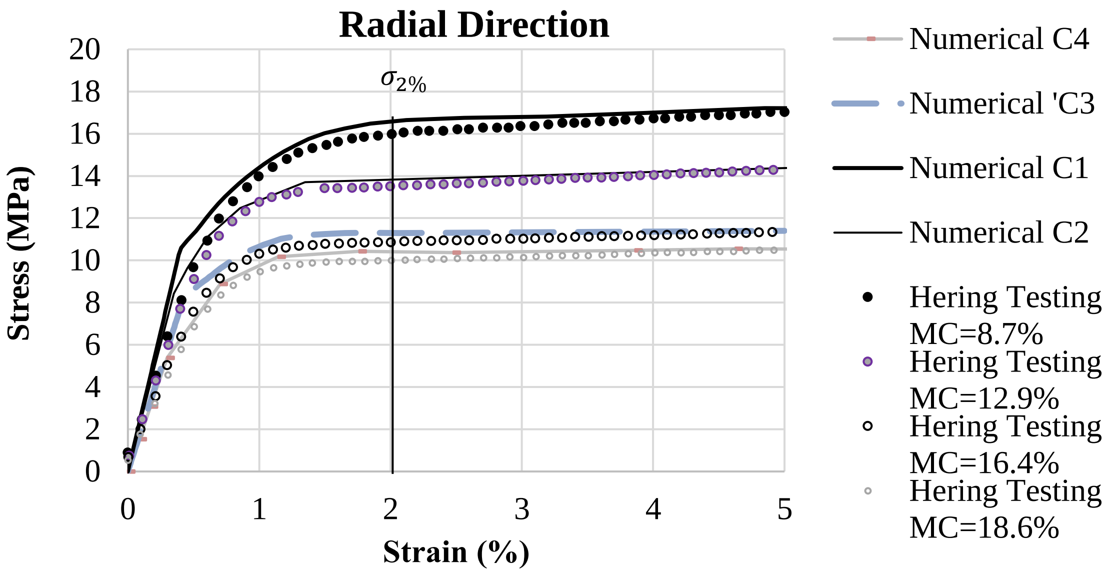

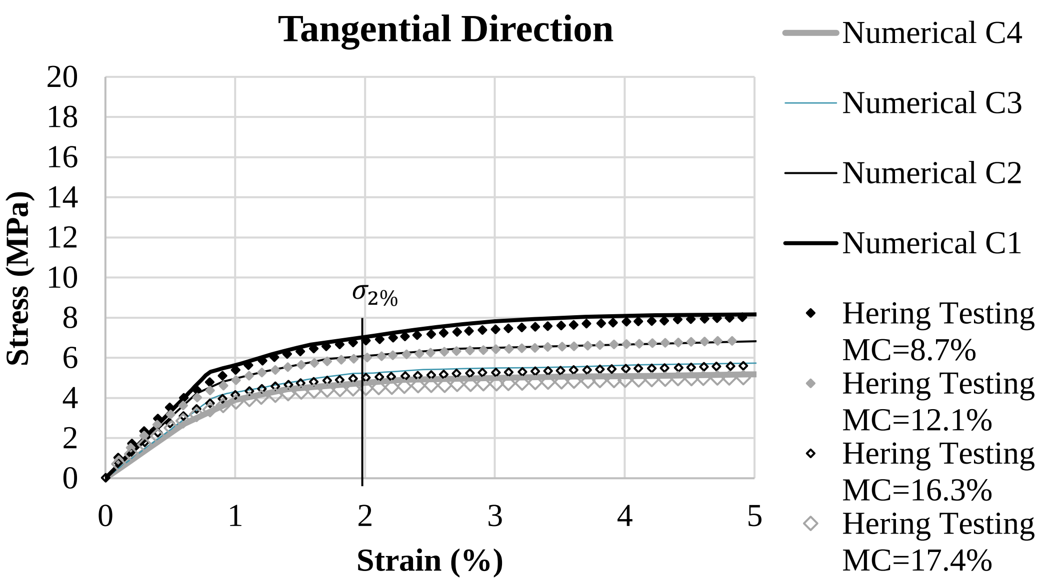

Fig. 5.12 Numerical result using moisture dependent anisotropic plasticity model comparing with measurements [14]. Compressive strength here is defined as the intersection of 2% strain line with the measured stress-strain curve according to Hering et al., 2012 [14]. The material parameters used for these simulations can be found in Table 5.1-5.3.

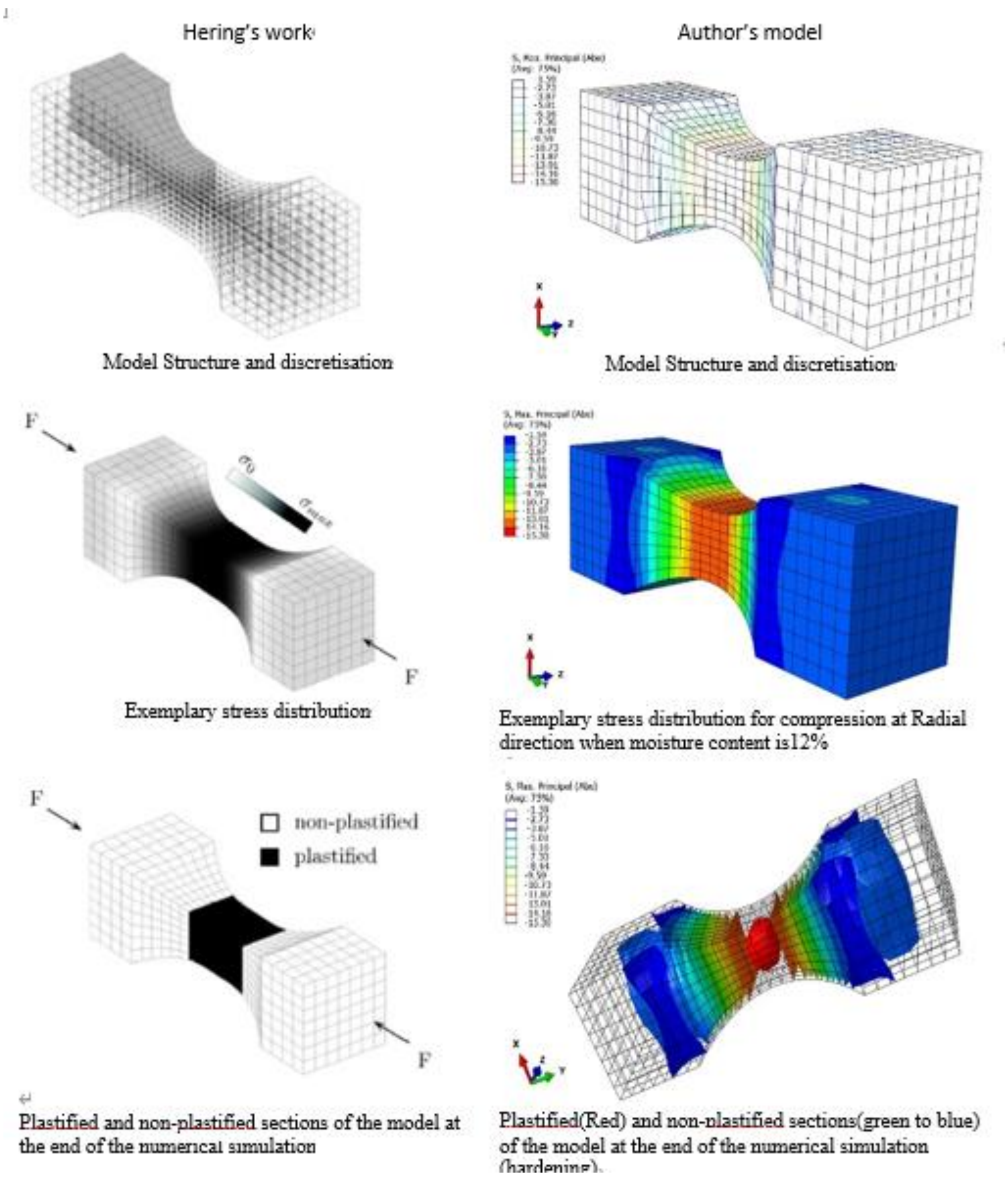

Fig. 5.13 Comparison between work of Hering et al., [14] and the numerical result using moisture dependent anisotropic plasticity model

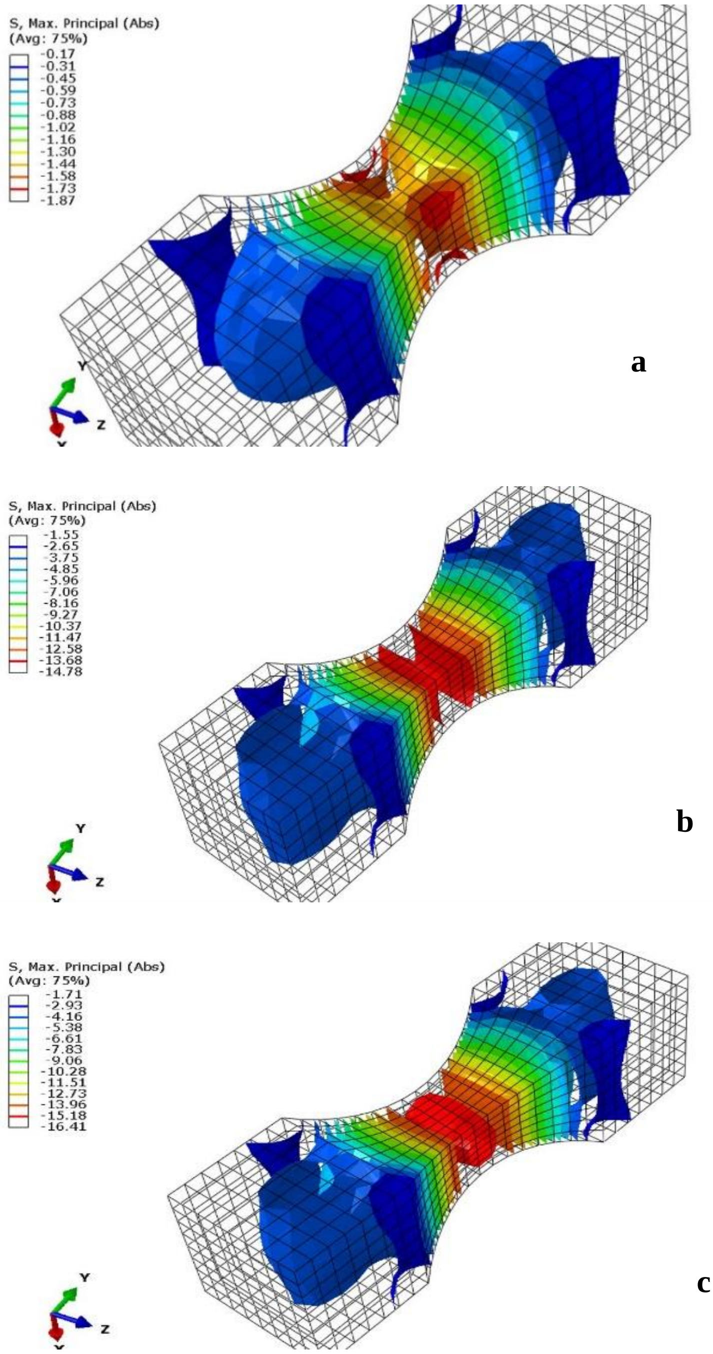

Fig. 5.14 Modelled stress distribution for compression at radial direction when moisture content is 8.7%: (a) elastic range, (b) nonlinear yielding with plastic flow, (c) hardening

A further comparison of stress distribution of simulation between the work of Hering et al [14] and numerical model at the strain of 1% (case 1 in radial direction) confirmed the good agreement, see *Fig 5.13*, and plastic sections were found in the narrow specimen section coinciding with the location of crushing in the experimental samples [14].

Stress and strain modelled result of moisture dependent compression perpendicular to the grain can be classified into 3 different regions: 1) the elastic range, 2) the nonlinear yielding with plastic flow and 3) hardening. See the modelled stress distributions presented in *Fig 5.14*. In the elastic range, a linear growing parallel isostress surface from side to centre along the compressive direction can be observed (*Fig 5.14a*), while stress nearer the surface is larger than the interior stress in the narrow specimen section due to the geometry of the specimen. It should be noted that, the deformation in the elastic range is recoverable when the load decreases.

The stress distribution of the model during yielding is given in *Fig 5.14b*, where internal wood fibres folded at the yield load and a permanent deformation occurs. Similar linear growing paralleled isostress surfaces are found in the thicker end parts, suggesting that stress there is within the elastic range, while a plastic deformation zone is formed in the centre of the narrow section coinciding with the location of crushing of the experimental samples [14].

The plastic region extends with an increase in load after yielding during the hardening phase, see *Fig 5.14c*, which implies the chosen hardening law was suitable as a model of the measurement data in the radial and tangential directions.

In conclusion, the results of the FE modelling confirm a marked influence of the moisture content on the stress-strain behaviour, not only in the elastic but also in the plastic domain. The proposed constitutive model is proved to be suitable as a description of the measurement data in the radial and tangential material directions. Comparisons between the model prediction and the work of Hering et al [14] found that stress–strain curves match well with experiments, which indicates that the UMAT subroutine is applicable to beech wood in moisture dependent compression tests and the UMAT program have been implemented correctly to provide an accurate prediction of stress–strain curves.

However, wood is a hygroscopic material and current validations only focus on the moisture content below Fibre Saturation Point (*FSP*) due to there being very few attempts to evaluate the mechanical behaviour of wood with moisture content above *FSP*, and quantitative experimental data for the moisture dependence of the elasto-plasticity behavior of wood is rather sparse. The next example uses this constitutive model to reproduce the experimental findings for the off-axis compression behaviours for *E. nitens* timber both below and above *FSP* to extend the usage of the proposed constitutive model.

5.6.2 Example 2 - Compressive testing on small block *E. nitens* samples below and above *FSP*

The second example uses the small standard *E. nitens* samples loaded by compression parallel and perpendicular to grain both at moisture content of 12% and above *FSP*. A small standard block model, which precisely reflects the experimental work, i.e., dimensions, applied load, and the boundary conditions (BC), was constructed using commercial software, ABAQUS (Version 2019, Dassault Systemes, France). The geometry of the model is 150 mm (in length) × 50 mm (in width) × 35 mm (in depth), see *Fig 5.15*.

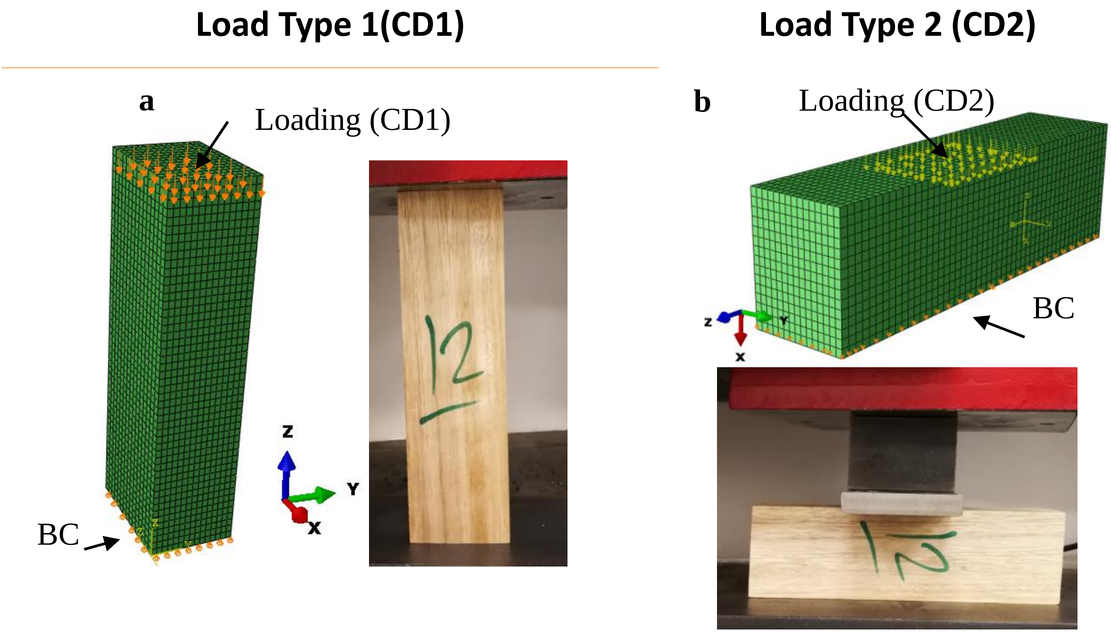

Fig. 5.15 FEM modelling for *E. nitens* samples in compression for CD1 (a) and CD2 (b) represent the loading direction: compression parallel to the long axis, and the wider cross section dimension, respectively. BC means the boundary condition.

The predominant load to model is labelled as follows: CD1, compression parallel to the longitude of the small standard model; and CD2, compression perpendicular to the longitude of the small standard model. The model has a uniform pressure loading on the loading surface. Loading surface is the whole top surface for CD1 (*Fig 5.15a*) and a 50mm wide surface for CD2 (*Fig 5.15b*). Opposed to the loading surface, three directional motions of the bottom surface are restricted, see *Fig 5.15* for boundary conditions. The model has longitudinal direction (axis L) in the Z-axis and a clockwise rotation at an angle (θ) around the Z-axis in the global coordinate system, when examining diverse load-to-annual growth ring compressive forces perpendicular to the grain. The model has been discretized by 11250 general purpose linear brick elements (C3D8R).

For simplicity, the FE models were simulated to show nonlinear compressive behaviour within its ultimate strength using the material nonlinear analysis without consideration of geometric nonlinearity, whilst the stress/strain curve for compression and tension is assumed to be the same since only compression is examined. The constitutive parameters in the FEM were given in *Table 6.1* and *Table 6.3* with the identification method provided.

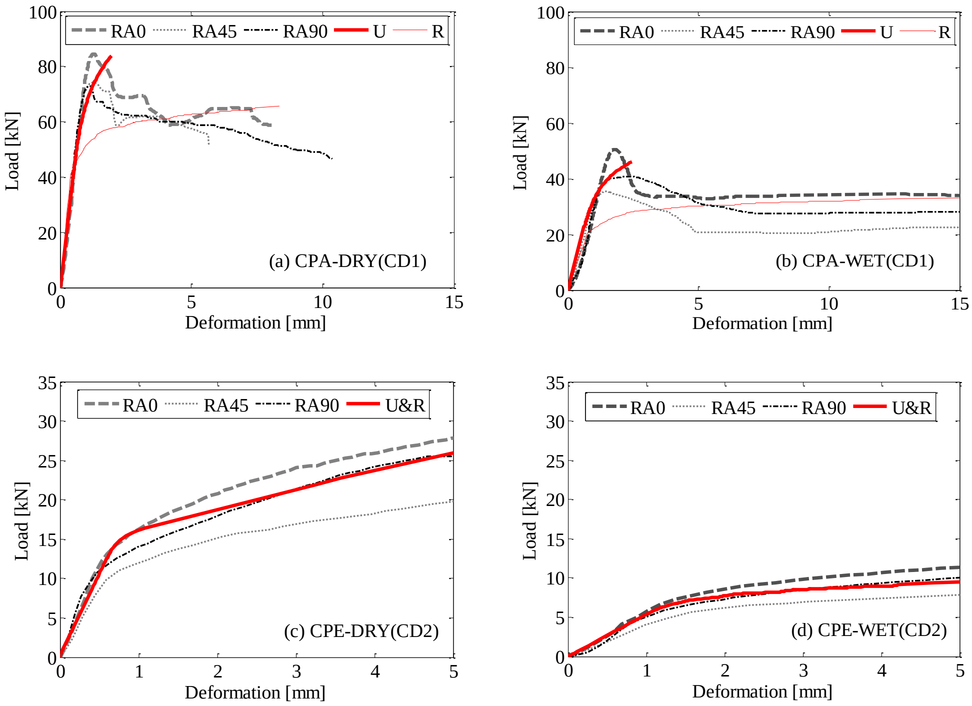

Fig. 5.16 The comparison between numerical result (red solid lines) and measured data (grey dash lines) for compression tests on Group I standard small clear samples. Left: dry cases (a, c); right: wet cases (b, d,f); top row: compression parallel to the grain, CPA (a, b); bottom rows: compression perpendicular to the grain, CPE (c, d). Dry cases mean *MC*=12% while wet cases mean *MC* above *FSP*.

Data		**Dry**			**Wet**		
		Test	FEA	Difference (%)	Test	FEA	Difference (%)
CPA(CD1)	Stiffness (MPa)	7341	7087	3.5	3277	3067	6.4
	Strength (MPa)	43.8	47.5	8.4	24.1	26.4	9.5
CPE(CD2)	Stiffness (MPa)	660	609	7.7	227	216	4.5
	Strength (MPa)	13.9	14.8	6.5	6.4	6.0	6.3

Table 5.4 The normal elastic moduli and ultimate strengths from the experimental and numerical tests. The values of the experimental results are obtained from Fig 5.16, and the mean values are used for comparison. The values of the numerical results are also obtained from Fig 5.16

Fig 5.16 illustrates the load deflection behaviour of FE models in compression at low and high moisture contents, both parallel and perpendicular to the grain, with a comparison of experimental data from *E. nitens* specimens. A good agreement (ie. error less than 10%) between the numerical prediction and the experimental data was found in the elastic range and the hardening stage for both low and high moisture content situations. This proved that the proposed material models were reasonable for *E. nitens* wood including the moisture effect for CPA (compression parallel to grain) and CPE (compression perpendicular to the grain). (*Table 5.4*).

5.7 NEW FEATURES AND DISCUSSIONS

In this section, the new features of the constitutive model are discussed. Comparing with other constitutive models for wood, the time dependent behaviour of wood is neglected to let this constitutive model be as simple as possible without losing its physical meaning, i.e., that is it is able to more realistically and accurately predict the anisotropic behaviour of wood with varying moisture contents until the wood reaches ultimate capacity in a short period loading condition. With wood being a hygroscopic material, its strength decreases significantly with an increase of the moisture content up to the fibre saturation point (*FSP*). For example, the decrease in strength can be up to 50% for both hardwood species, such as European beech, and softwood species, for example Pine, when the wood has a moisture content at or above *FSP* [10, 23]. This constitutive model is able to provide an efficient approach to include the effects of moisture content, covering the whole wood moisture content range from dry timber (*MC*<15%) to timber with a high degree of moisture content i.e., above fibre saturation (30 to 80 %) and difference in tension and compression on failure.

Failure envelops are very interesting in timber engineering since stress limits can be established and used for structural sizing using the envelope failure curves [87, 93]. In this section, this feature of the failure criterion in this constitutive model is explored further.

5.7.1 Initial yield surface

The non-dimensional initial yield surface of this constitutive model is presented in the principal stress space (*Fig 5.17*), by comparing the Von Mises, Hill, and Drucker–Prager criteria. The corresponding projection in the "π" plane is also shown in the right column. The "π" plane is defined by Eq (5.30), that is, the plane passing the coordinate origin and having an equipotential line with three equal principal stresses in the principal stress space.

$$\sigma_{LL} + \sigma_{RR} + \sigma_{TT} = 0 \tag{5.30}$$

In the principal stress space, the yield surface of this constitutive model is a tapered elliptical cylinder and an increase in *LRT* stresses with increasing hydrostatic pressure was observed *Fig 5.17a*).

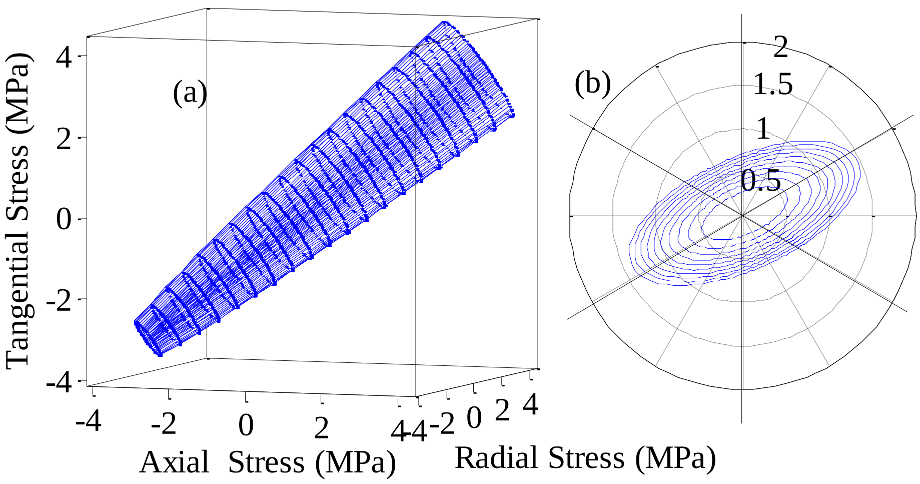

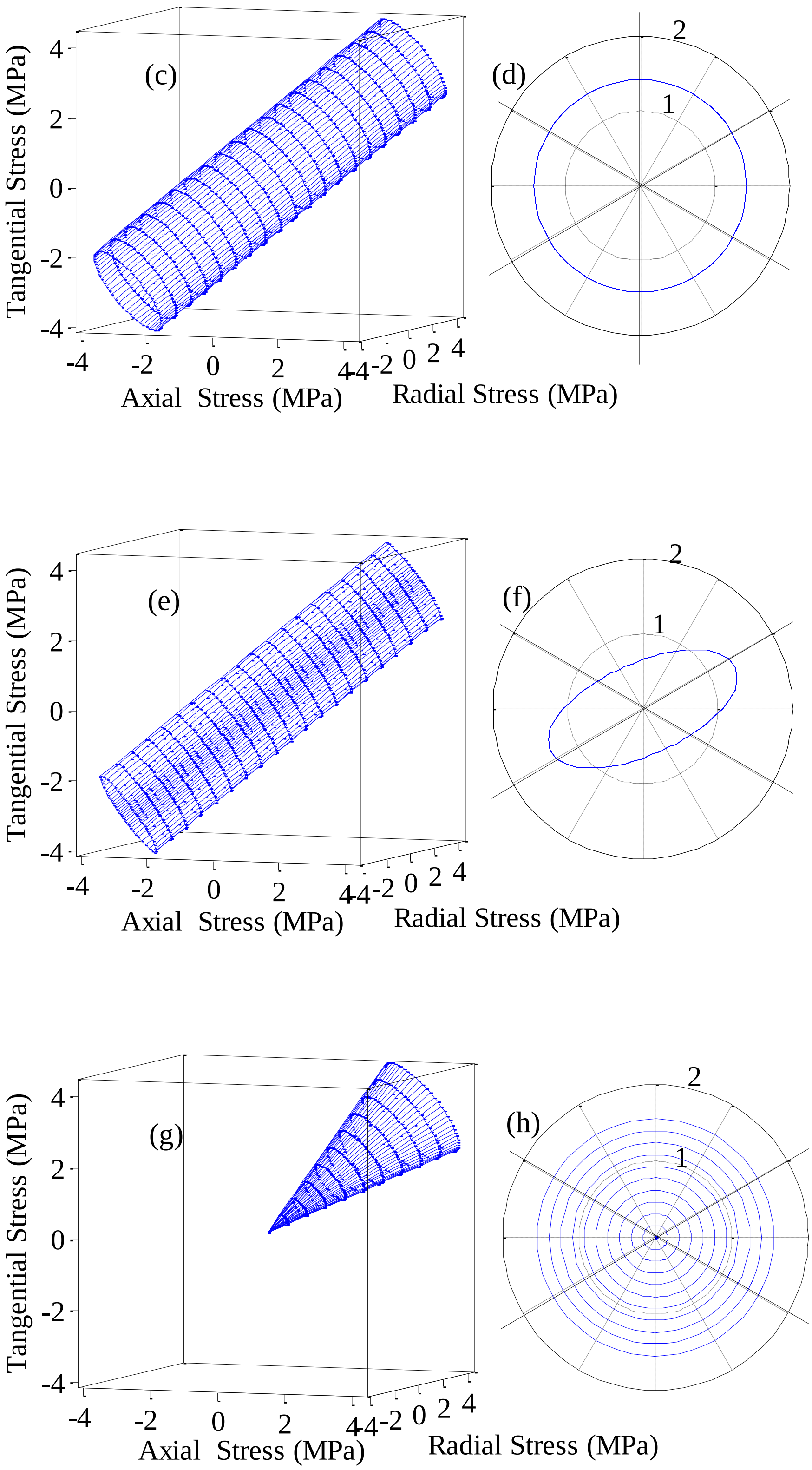

Fig. 5.17 3D initial yield surface of the proposed constitutive model (a, b) for wood comparing the typical Von Mises (c, d), Hill (e, f) and Drucker–Prager (g, h)criterions, left: in the principle stress space (a, c, e, g); right, in the "π" plane (b, d, f, h)

In contrast to a typical Von Mises criterion (*Fig 5.17c, d*), which is a circular cylinder, the strength of this constitutive model in the longitudinal direction is much higher than other two directions, i.e., the strengths in the radial and tangential axes. This is similar to a normal Hill criterion (*Fig 5.17e, f*). This implies that the yield surface of this constitutive model is able to reflect some wood anisotropic behaviour. Since the yield stress parallel to the grain is much higher than the one perpendicular to the grain [87], the long axis of the elliptical shape is along grain direction (*Fig 5.17f*). In the Hill criterion, it is assumed that tensile and compressive strength are the same, so the elliptical yield surface in the "π" plane shows constant varying hydrostatic pressure. The yield surface of this constitutive model is an extension of the Hill criterion, and the linear terms of the differences between tensile and compressive strengths are included. Therefore, opposite to the normal Hill criterion but similar to the Drucker–Prager criterion (*Fig 5.17 h*), the radius of the yield surface in the "π" plane increases with the increase of hydrostatic pressure due to the asymmetry between the tensile and compressive sides, which reflects the difference in the tensile and compressive strengths of the wood. In other words, the spatial yield surface is no longer a regular elliptical cylinder and the size of the projection in "π" plane changes (*Fig 5.17a, b*). The variation of yield strength with moisture content can be found in Eq (5.3).

5.7.2 Comparison with experimental data

Firstly, the initial failure surfaces of proposed constitutive model (GH), Eq (5.6), were compared with the experimental data obtained from off-axis compression and tension testing on *E. nitens* samples above and below *FSP*. The experimental work regarding the off-axis compression was provided in Chapter 3, while off-axis tension testing method is described in Appendix 2. The off-axis tension tests for *E. nitens* specimens were performed with displacement-control using Universal Testing Machine (Zwick Roell-Z100, capacity 100 kN) and discontinued when the rupture failure was observed in the load-deformation curves. Due to the availability of the measurements of the off-axial behaviours of *E. niten*, the analysis focused on experimental data in quadrant 1 and 3 only (the pure compression or tension side). Experimental data for dry and wet samples with loading at different grain angles and the corresponding failure surfaces are presented in *Fig 5.18*. The initial failure surface for GH model is determined according to the yield stresses given in the first and second column of *Table 5.5* for dry and wet cases, respectively. The same compressive values were used to determine a Hill yield surface. The root mean square error (RMSE) calculated using the Equation (5.31) was introduced to assess the difference between the model-predicted failure surfaces and the experimental data.

$$RMSE = \sqrt{\sum_{i=1}^{N} (Simulation_{(i)} - Experiment_{(i)})^2 / N} \tag{5.31}$$

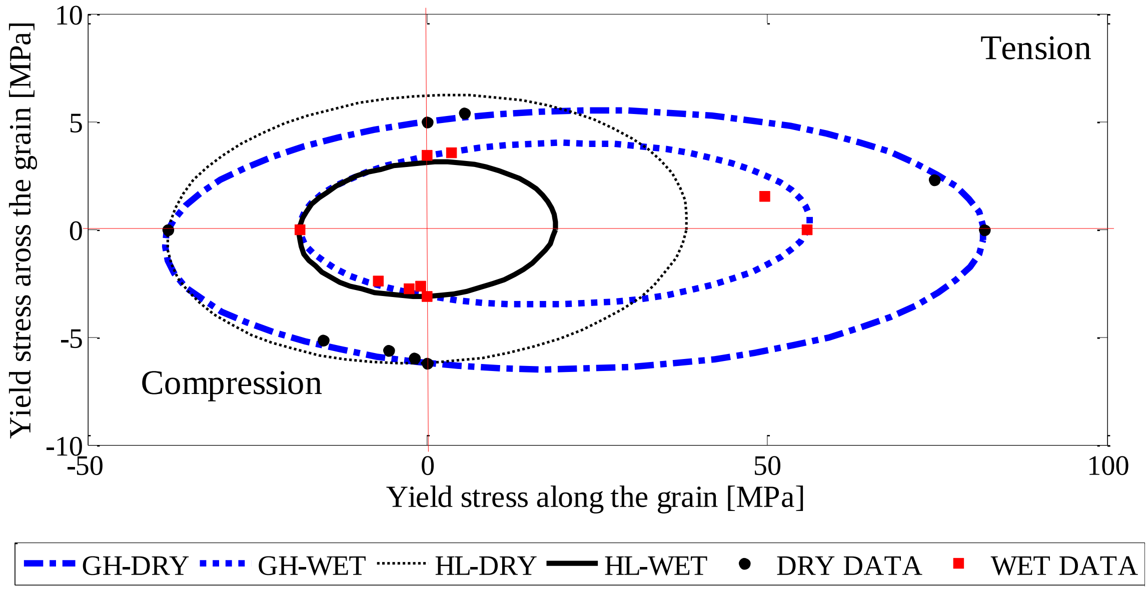

Fig. 5.18 The initial yield surfaces of the *E. nitens* timber at dry (*MC*=12%) and wet conditions (*MC*>*FSP*) predicted by proposed constitutive model comparing with experiments (introduced in Chapter 3 for compression and in Appendix 2 for tension) and Hill criterions. GH, yield criterion used in the proposed constitutive model; HL, Hill criterion; The parameters used for the HL and GH can be found in first two columns of Table 5.5.

A good agreement was found between the predictions of the GH model and the experimentally measured data, comparing with those predicted by Hill model (*Table 5.6*). A decrease in moisture content raised the value of the yield stresses and expanded the surfaces of the failure surface, while the different strengths under tension and compression were found (*Fig 5.18*).

Properties	***E. nitens***		***Spruce***
	Dry *(MC=12%)*	WET*(MC>FSP)*	Dry *(MC=12%)*
Tensile yield stress in longitudinal direction, $\boldsymbol{Y_L^T}$ (MPa)	82	56	55
Tensile yield stress in radial direction, $\boldsymbol{Y_R^T}$ (MPa)	5.0	3.4	5
Compressive yield stress in longitudinal direction, $\boldsymbol{Y_L^C}$ (MPa)	38.1	18.8	45
Compressive yield stress in radial direction, $\boldsymbol{Y_R^C}$ (MPa)	6.2	3.1	5
Shear yield stress in L-R plane, $\boldsymbol{Y_{LR}^S}$ (MPa)	18	9.6	8

Table 5.5 Values of yield stresses for Eucalyptus and Spruce [36] timber to determine the initial failure surface. The values of *E. nitens* are obtained from experimental results provided in Chapter 3 and 7

Code	**RMSE**	
	DRY	WET
Yield surface (HL)	>15%	>15%
Yield surface (GH)	<10%	<15%

Table 5.6 The root mean square error for each surface provided in Fig 5.18 calculated using Eq (5.31); HL, Hill model and GH, proposed constitutive model.

Therefore, compared with the Hill criterion, the yield criterion of the proposed constitutive model is more suitable for modelling of wood with asymmetry in tension and compression including the influence of the moisture content. This also demonstrates the suitability of the failure criterion of the developed constitutive model for application to wood material in this study, by coupling the Hill yield criterion with the Drucker–Prager yield criterion.

The failure surfaces kept an elliptical shape when the moisture content changed, and moisture content affected the lengths of the long and short axes in this elliptical failure envelope (*Fig 5.19*).

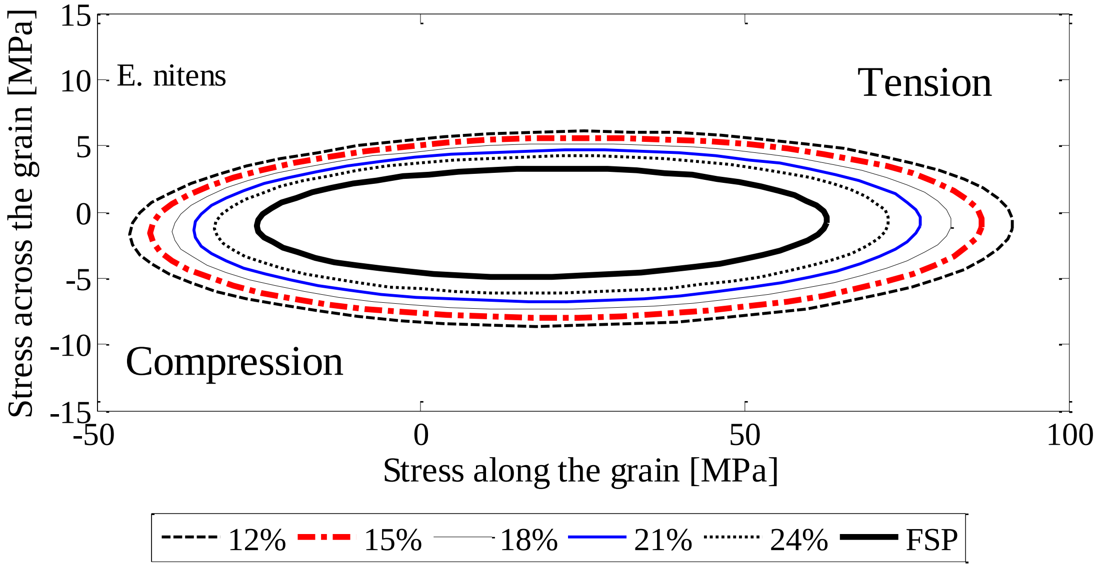

Fig. 5.19 Variation of the yield surface of *E. nitens* with moisture content using parameters in Table 5.5 calculated according to Equations (5.3) and (5.6); *FSP* is assumed to be 30% [65].

Finally, the GH model-predicted failure surface was compared with the data from biaxial tests on spruce specimens further evaluate the GH model. This is because the lack of the experimental facility in the University of Tasmania to undertake a precise measurement on the biaxial behaviours of *E. nitens.* While the results from biaxial tests are more suited for evaluating failure criterions than uniaxial tests since they reflect at least the two-dimensional load-carrying characteristics of the material behaviours. The comparison between the failure criterion of this constitutive model with the experimental data (black dots) is provided in *Fig 5.20*. These experimental points were obtained from loading that was predominantly parallel and perpendicular to the grain on clear Spruce wood samples at dry condition.

Wood has different post-failure mechanisms for tension and compression and for loads parallel to the grain or perpendicular to the grain [110]. For biaxial tests on spruce specimens, when wood fails under tensile loading, localised brittle fracture is observed. However, under compression, pronounced inelastic behaviour occurs [23]. Experiments on spruce wood show an elliptic yield surface before inelastic behaviour occurs [36, 110].

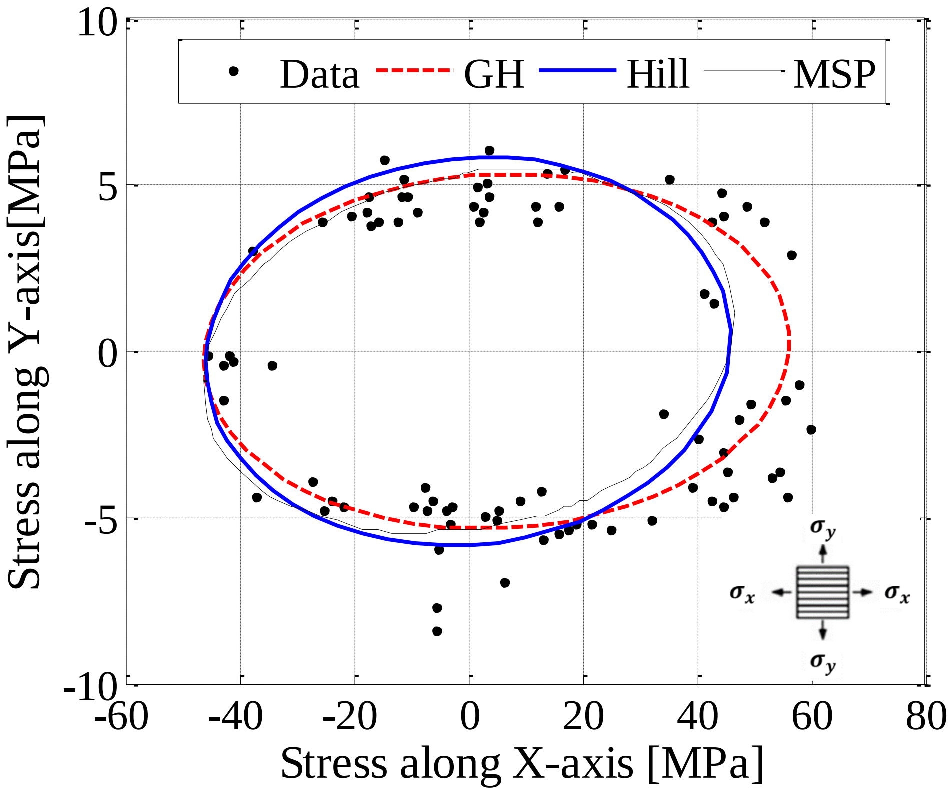

Fig. 5.20 Model-predicted failure surfaces and experimental results (black dots) [36] of biaxial tests on spruce wood. MSP, multi-surface plasticity failure surface criterion [36]. HILL, Hill criterion; GH, generalised Hill yield criterion used in the proposed constitutive model. The parameters used for the proposed constitutive model and Hill model can be found in Table 5.5.

A remarkable number of experimental points lay outside the predicted Hill criterion and the multi-surface plasticity failure surface (MSP) criterion based on De Borst et al.'s work [36]. The failure surfaces predicted by the proposed failure criterion (GH) according to the mean values of the tensile and compressive yield stresses given in the last column of *Table 5.5*, matched well with most of the experimental data (see black dots in *Fig 5.20*). An excellent agreement was found between the predictions of the GH model and the experimentally measured data (*Table 5.7*), while the differences between the three failure surfaces are within a range of 5%–25%. Compared with the multi-surface plasticity failure surface and the Hill criterion, the yield criterion of the proposed constitutive model is more suitable for describing the anisotropy of wood (e.g. Spruce) since the model predictions were more accurate, matching the difference between tensile and compressive experimental results (*Fig 5.20* and *Table 5.7*). This proved that the proposed material models were more reasonable for modelling Spruce wood in two-dimensional load cases, both for tension or compression only situations and for combined tension and compression states. It should be noted that multi-surface plasticity failure surface (MSP) criterion could also consider the difference between tension and compression, but it is more complicated.

Code	**RMSE**
MSP	>20%
HILL	>15% but <20%
GH	>5% but <10%

Table 5.7 The root mean square error (RMSE) for each surface provided in Fig 5.20 calculated using Eq (5.31)

In summary, a moisture dependent anisotropic plasticity model can accurately predict the two-dimensional load-carrying characteristics of wood, for example, Spruce. This constitutive model is orthotropic in the elastic region while anisotropic in the plastic region. A Hill yield criterion was combined with the Drucker–Prager yield criterion to produce an anisotropic yield criterion (GH), allowing a variation in tension and compression.

5.8 SUMMARY

The third objective of this study, proposing a moisture dependent anisotropic plasticity model for *E. nitens* timber, has been achieved in the present chapter. The theoretical backgrounds of this model were introduced with associated non-linear plasticity theory, ie, the definition of a yield surface and a plastic potential rule. A modified yield criterion was used by combining the Drucker–Prager yield criterion with the Hill yield criterion - allowing modelling of the anisotropic ultimate capacity of wood, with asymmetry in tension and compression. The plastic potential law was assumed to follow the Ramberg-Osgood function, which has been confirmed by previous experimental research. All model variables, eg. Young's moduli, yield stresses and hardening parameters, etc., considered changes in moisture level in order to study the effect of moisture content on the load carrying capacity of timber. Then, a Fortran program was coded using a

UMAT (user-material subroutine) via the commercial software ABAQUS to integrate the constitutive model into the three-dimensional finite element framework.

This constitutive model was validated and evaluated against previous studies [14, 38] and compression testing on *E. nitens* specimens. Firstly, the comparison between the current constitutive model with the experimental work of Hering et al [14, 31] was illustrated to validate moisture content dependency. Secondly, the proposed constitutive model was proved to be suitable as a description of the measurement data in the radial and longitudinal directions of *E. nitens* timber at *MC* = 12% and >*FSP*. This is a potential new building material and the target in this research. The results confirmed a marked influence of moisture content on the stress-strain behaviour of compression parallel and perpendicular to the grain, not only in the elastic but also in the plastic domain.

Then, new features of the constitutive model were discussed. The yield surfaces of this constitutive model were compared with biaxial testing results from clear spruce cruciform wood samples at dry condition [38]. The main advantage of this new constitutive model is that it can be used for the modelling of wood with asymmetry in tension and compression, and it has a simple single yield criterion that is able to accurately reproduce the plastic anisotropy of wood whilst using an associated flow rule. Yield surfaces kept an elliptical shape when the moisture changed, even though the failure strengths in tension and compression could be different.

Due to the normal non-uniformity of wood samples, it is hard to study the effect of each factor independently via testing. Since the numerical approach combined with constitutive modelling overcomes this limitation, the next chapter will develop numerical models using this constitutive model to examine the underlying anisotropic failure mechanism of *E. nitens* timber with low and high moisture contents. Parametric invesitagation will also be undertaken to numerically find the major factors.

Chapter 6

6 NUMERICAL MODELLING OF *E. NITENS* TIMBER UNDER COMPRESSION

6.1 INTRODUCTION

In order to show how the fourth objective of this study was achieved, Chapter 6 outlines a numerical modelling/numerical simulation of *E. nitens* timber with both low and high moisture contents. Aiming to understand the underlying failure mechanism of *E. nitens,* the short-term response and ultimate strength distribution of *E. nitens* timber under off-axis compression were examined using the Finite Element Method with a moisture content dependent anisotropic plasticity model. This method overcomes the limitations of experiments for practical applications since the mechanical properties of *E. nitens* timber are very difficult to examine separately using an experimental approach due to the heterogeneous behaviour of natural wood, together with its nonlinear material characteristics. After this introduction, the method of identifying the parameters used in the simulations in this chapter for the moisture dependent, anisotropic plasticity model is briefly outlined in Section 6.2. Section 6.3 introduces the setup for the numerical modelling. The numerical modelling of the load-deflection curves for *Eucalyptus* wood specimens is compared with the experimental findings in order to calibrate the numerical modelling parameters. In the following sections, the effect of grain angle on the stiffness and strength of the compressive models is explored. A parametric study into the sensitivity of stiffness and strength is also undertaken and a discussion section follows. Finally, summary is drawn.

6.2 IDENTIFICATION OF PARAMETERS

This Section briefly introduces how to identify the parameters of the proposed constitutive model described in Chapter 5 based on experimental data. There are 22 independent parameters in the constitutive model, including nine elastic parameters: 3 normal elastic moduli (E_{LL}, E_{RR}, E_{TT}), 3 shear moduli (G_{LR}, G_{RT}, G_{TL}), and 3 Poisson's ratios (u_{LR}, u_{LT}, u_{RT}); 13 plastic parameters: 3 tensile yield stresses (Y_L^T, Y_R^T, Y_T^T), 3 compressive yield stresses (Y_L^C, Y_R^C, Y_T^C), 3 shear yield strengths (Y_{LR}^S, Y_{RT}^S, Y_{LT}^S), 2 tensile hardening parameters (K^T, n^T) and 2 compressive hardening parameters (K^C, n^C). All parameters are defined as being moisture dependent according to Eq. (5.3). Principal material directions L, R, or T refer to Longitudinal, Radial, and Tangential directions of timber, respectively.

Compressive failure is most important at all contact points between structural elements in buildings, bridges and decks, particularly for members in compression, such as columns [9, 47, 111, 112]. To better understand such mechanical failure in timber, this Chapter focuses on numerical modelling of the compressive behaviour of *E. nitens* timber in the L-R plane, since the common structural usage of wood in timber engineering exploits the longitudinal direction where the highest strength values [12, 31] are found. Therefore, only 8 independent parameters need to be identified from compressive data for *E. nitens* timber at a given moisture content, since Poisson's ratio does not influence the compressive failure mechanism significantly [14, 31]. These parameters include three elastic parameters, (E_{LL}, E_{RR}, G_{LR}), compressive yield stresses (Y_L^C, Y_R^C, Y_{LR}^S) and compressive hardening parameters (K^C, n^C), in the constitutive model. The values of these parameters for the simulations at a moisture content of 12% are provided in *Table 6.1* with an assumption of transverse isotropy in the radial and tangential plane, and since compression and tension are assumed to have the same value since only compression is examined.

MC	**Material Properties**		
12%	E_{LL} = 7000 (MPa)	E_{RR}= E_{TT}=310 (MPa)	K = 12.1 (MPa)
	Y_L^C =38.1 (MPa)	G_{LR} = G_{RT}= G_{TL} =780 (MPa)	n = 17.4
	$Y_R^C = Y_T^C$=6.2 (Mpa)	$Y_{LR}^S = Y_{LT}^S = Y_{RT}^S =$ 12.4 (MPa)	

Table 6.1 Values of properties for the numerical simulation on *E. nitens* wood under compression at a moisture content of 12% using the proposed constitutive model. These parameters include three normal elastic moduli (E_{LL}, E_{RR}, E_{TT}), 3 shear moduli (G_{LR}, G_{RT}, G_{TL}), three compressive yield stresses (Y_L^C, Y_R^C, Y_T^C), 3 shear yield stresses (Y_{LR}^S, Y_{LT}^S, Y_{RT}^S) and compressive hardening parameters (K, n); Symbols *L*, *R*, or *T* represent the principal anatomical directions (*L*, Longitudinal, *R*, Radial and *T*, Tangential). The values of wet cases follow P_{12}c where c is given in Table 6.3.

Compressive normal and shear elastic moduli can be obtained from the compression tests on Group II small block samples at grain angles of 0º, 45º and 90º as presented in Chapter 3. These elastic moduli are calculated as the slope of the line between approximately 10% and 40% of the ultimate loading force [24] as shown in *Fig. 6.1*. The ultimate loading forces were obtained at the maximum loading force for softening behaviour or at the deformation of 0.1h for hardening behaviour, where and h is the original sample dimension in the load direction, as shown in *Fig. 6.1*. Yield stress is defined as the point the stress-strain curve first diverges from a line as shown in *Fig 6.2*. The mean values of the normal and shear elastic moduli and yield stress of measured data from Group II small block dry samples in compression at grain angles of 0º, 45º and 90º are used to determine the values of the parameters presented in *Table 6.1*.

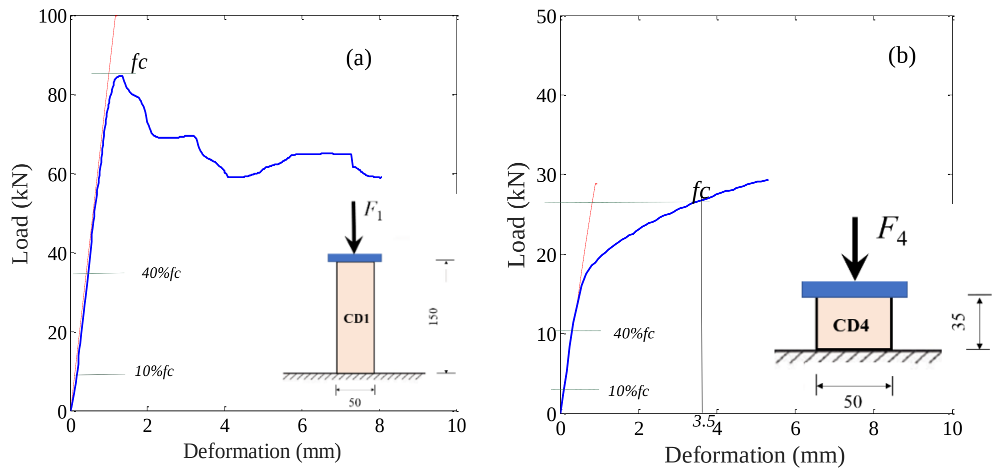

Fig. 6.1 Examples for determination of stiffnesses (a, b) and yield stresses (c, d). The solid blue line is the plot of measured data, and *fc* is the ultimate loading force at the maximum loading force for softening behaviour (a), or at the deformation of 0.1*h* for hardening behaviour (b), respectively. The red dashed line is the line of best fit between approximately 10% and 40% of ultimate loading force.

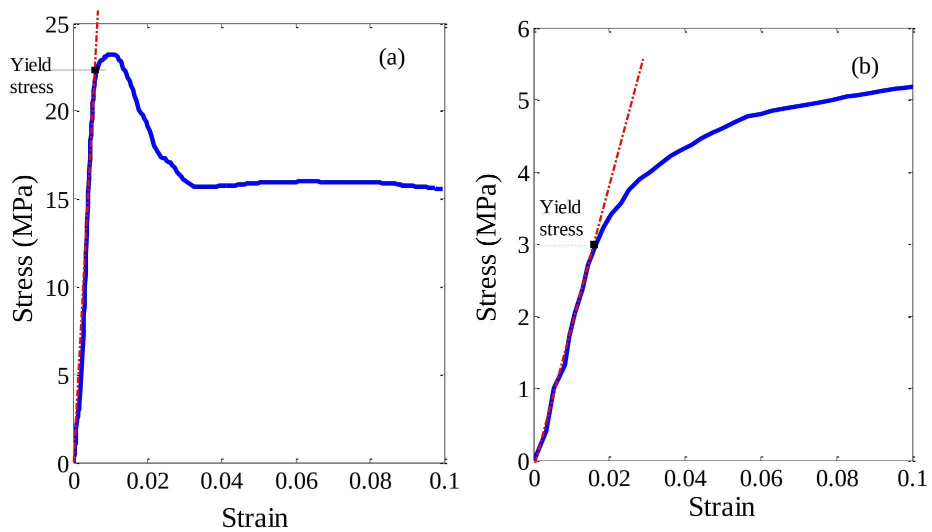

Fig. 6.2 Examples for the determination of yield stresses. The solid blue line is the measured curve for softening behaviour (a) or hardening behaviour (b), respectively. The red dashed line is the linear fit to the first part of the relationship.

Compressive hardening parameters were obtained using the method in Section 5.4, which was adopted and improved from the approach proposed by Wang et al [109]. Compression test data from small block Eucalyptus *nitens* samples in the L-R plane (defined in Chapter 3) with both low and high moisture contents, was used to determine B and C based on Eq (5.13) and to identify plasticity parameters K and n, respectively. According to the mean strengths given in Table 5.7, which were calculated from the experimental data of *E. nitens*, C = 0.35 (MC=12%), C = 0.57 (MC>FSP), B = 0.047 (MC=12%) and B = 0.043 (MC>FSP), n and K can be determined based on the least square optimal fit as shown in *Fig 5.4*. The ranges of plasticity parameters K and n are presented in *Table 6.2* with a known coordinate transformation, $h(\varphi, MC)$ at a given MC.

	Code		***K***	***n***
***E. nitens* Wood**	**DRY**	mean	62.50	18.79
		max	156.60	28.59
		min	36.50	12.03
	WET	mean	19.10	16.35
		max	21.30	24.36
		min	15.40	10.36

Table 6.2 The identified parameters (K and n) for *E. nitens* wood.

6.3 NUMERICAL MODELLING SETUP AND CALIBRATION

6.3.1 Numerical setup

This section attempts to reproduce the experimental behaviour for the load-deflection curves of *E. nitens* samples via FEM with the consititutive model proposed in Chapter 5. To undertake this numerical modelling, 3-dimensional finite element models are used to simulate the nonlinear compressive behaviour of *E. nitens* timber with both low and high moisture contents under off-axis compression in order to calibrate the parameters used in the numerical modelling. The dimensions of the model are 35 mm (long) × 50 mm (wide) × 35 mm (deep), and this has been discretised by 35568 general purpose linear brick elements (C3D8R), see *Fig 6.3*. The model has a uniform pressure loading over the whole top surface, while being restricted in the three directions opposed to the loading surface. The longitudinal direction of the wood fibre in the model corresponds to the X-axis in the global coordinate system when compression is at a grain angle of 0°. The local coordinate system will rotate clockwise around the Y-axis in the global coordinate system at angles (φ) of 30°, 45°, 60° and 90°, respectively to explore the effect of grain angle on compressive stiffness and strength. For simplicity, the FE models were simulated to show nonlinear compressive behaviour within its ultimate strength using material nonlinear analysis without consideration of geometric nonlinearity, whilst the stress/strain curve for compression and tension was assumed to be the same since only compression was examined. The standard mechanical parameters of the constitutive model are provided in *Table 6.1* for *MC* = 12% and were obtained from the off-axis compressive testing of *E. nitens* samples discussed in Chapter 3. The bilinear dependency of the material properties varying with moisture content, Eq (6.1) and Eq (6.2), were then applied to estimate the material properties of the FEM models for moisture contents above and below *FSP*. The coefficients for the varying moisture content properties of *E. nitens* are provided in *Table 6.3*.

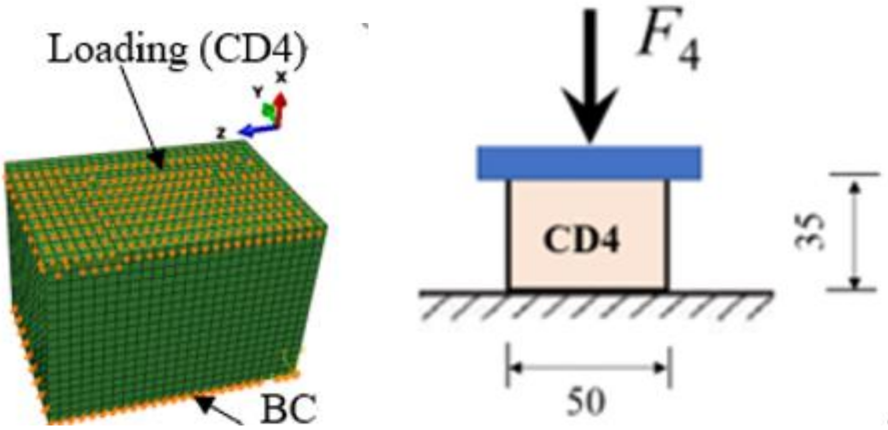

Fig. 6.3 FEM modelling for block *E. nitens* samples in compression; CD4 represents compression at an angle to the grain for the small clear block samples. BC means the boundary condition.

The longitudinal direction of the wood fibre in the model corresponds to the X-axis in the global coordinate system when compression is at a grain angle of 0°. The local coordinate system will rotate clockwise around the Y-axis in the global coordinate system at angles (φ) 30°, 45°, 60° and 90°, respectively to explore the grain angle effect on compressive stiffness and strength. For simplicity, the FE models were simulated to show nonlinear compressive behaviour within its ultimate strength using the material nonlinear analysis without consideration of geometric nonlinearity, whilst the stress/strain curve for compression and tension is assumed to be the same since only compression is examined. The standard mechanical parameters of the constitutive model were provided in *Table 6.1* for *MC* = 12% and were obtained from the off-axis compressive testing of *E. nitens* samples discussed in Chapter 3. Bilinear dependency of the material properties varying with moisture content, Eq (6.1) and Eq (6.2), were then applied to estimate the material properties of the saturated FEM models (*MC* below and above *FSP)*. The coefficients for the properties of *E. nitens* varying moisture content are provided in *Table 6.3*.

These coefficients are defined in Eq (5.3) of Chapter 5, and the Equations are also provided below:

$$P(MC) = P_{12}[a(MC - 12) + b]\ (MC < FSP) \tag{6.1}$$

$$P(MC) = P_{12}c\ (MC \geq FSP) \tag{6.2}$$

where, *P(MC)* and P_{12} are respectively the material variables at moisture contents of *MC*% and 12%; *a*, *b*, and *c* are constants depending on the experimental results with the assumption that the fibre saturation point (*FSP*) for *E. nitens* is 30% [113].

Density values used in the numerical models are real densities, which were obtained from the basic density (503 kg/m^3) and the corresponding moisture content according to Eq (6.3)

$$\rho_r = \rho_b \times \frac{100 + MC}{100} \tag{6.3}$$

where, ρ_{r} is the *real density value* used in the FEM model given that moisture content is *MC* (%) and ρ_b is the basic density in kilograms per cubic metre. The mean value of basic densities measured from the *E. nitens* Group I samples, shown in *Table 3.2*, is assumed to be the standard value, (521.8+484.5)/2= 503 kg/m^3. The Poisson's ratios are constant when the moisture content changes, as they do not significantly affect the off-axis compressive behaviour of *E. nitens* timber. The values of the Poisson's ratios are u_{LR}=0.1, u_{LT}=0.1, u_{RT}=0.29.

Material Properties	Coefficients			Material Properties	Coefficients		
	a	b	c		a	b	c
E_{LL}	-0.0228	1.2733	0.59	G_{LR}	-0.0283	1.34	0.49
E_{RR}	-0.0233	1.28	0.58	G_{LT}	-0.0283	1.34	0.49
E_{TT}	-0.0233	1.28	0.58	G_{RT}	-0.0283	1.34	0.49
Y_L^C	-0.0283	1.34	0.49	Y_{LR}^S	-0.0311	1.3733	0.44
Y_R^C	-0.03	1.36	0.46	Y_{LT}^S	-0.0311	1.3733	0.44
Y_T^C	-0.03	1.36	0.46	Y_{RT}^S	-0.0311	1.3733	0.44

Table 6.3 Values for coefficients of bilinear dependency of the material properties varying with moisture content. These material properties include three normal elastic moduli (E_{LL}, E_{RR}, E_{TT}), 3 shear moduli (G_{LR}, G_{RT}, G_{TL}), three compressive yield stresses (Y_L^C, Y_R^C, Y_T^C) and 3 shear yield stresses (Y_{LR}^S, Y_{LT}^S, Y_{RT}^S); Symbols *L*, *R*, or *T* represent the principal anatomical directions (*L*, Longitudinal; *R*, Radial and *T*, Tangential).

It should be noted that the hardening parameters and stiffness values of the wet cases were modified slightly to allow the simulated compressive strength to be close to the experimental data by using the minimal relative error optimisation method [114].

6.3.2 Calibration of load deflection curves

Fig. 6.4 illustrates the load deflection behaviour of FE models in compression at low and high moisture contents, at grain angles (φ) of 0°, 30°, 45°, 60°, and 90°, together with a comparison of experimental data from *E. nitens* specimens. The numerical compressive stiffnesses of dry and wet models were calculated by the slope of the line between approximately 10% and 40% of the ultimate loading force of the simulation curves. The numerical compressive strengths were obtained at 0.1*h* deformation (*h=35mm*) for φ> 45° or at the plastic strain of 0.02 for $\varphi \leq 45°$. The stiffness and the strength from the numerical simulation for each case were compared with the mean values of corresponding experimental data and are given in *Table 6.4*.

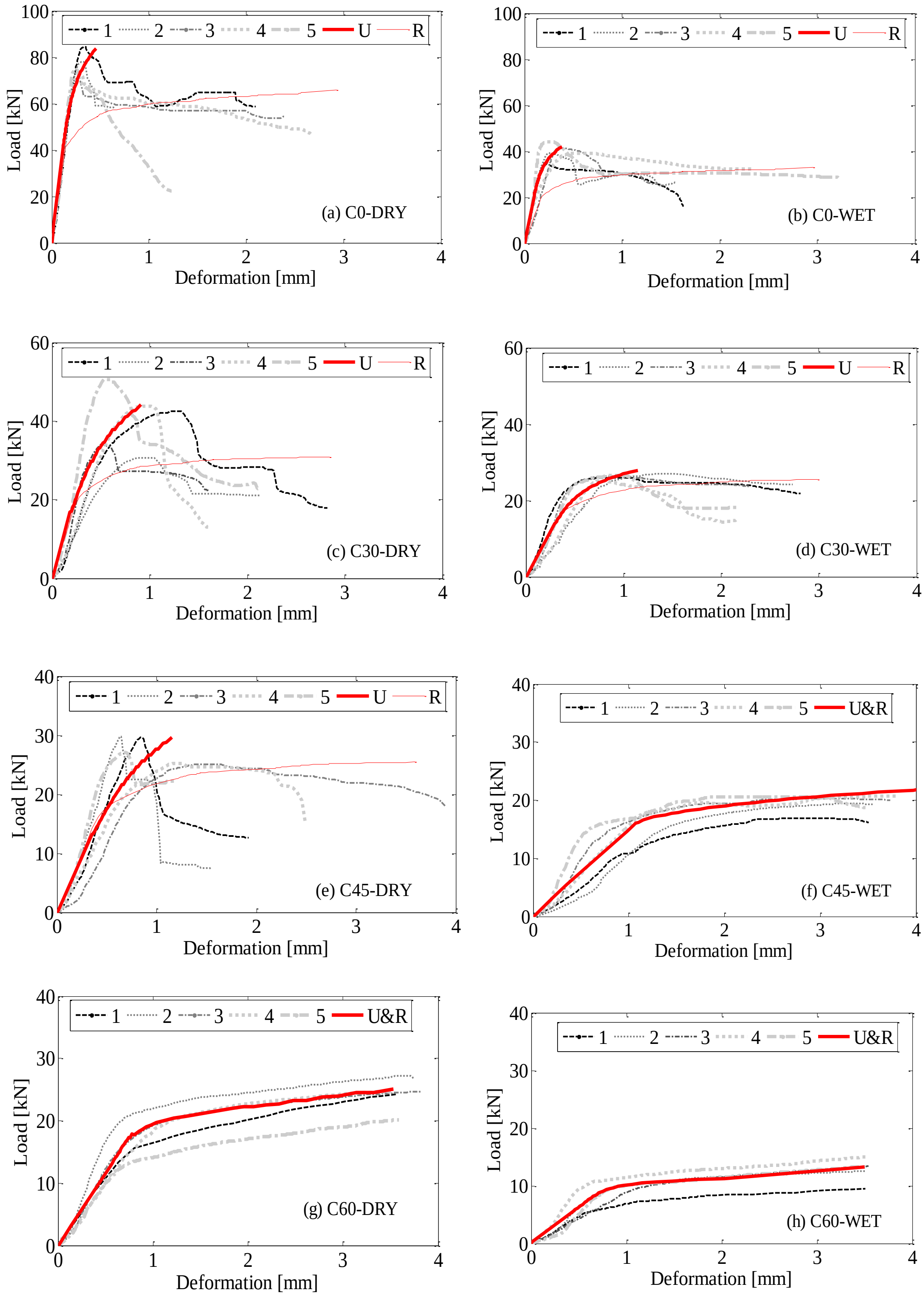

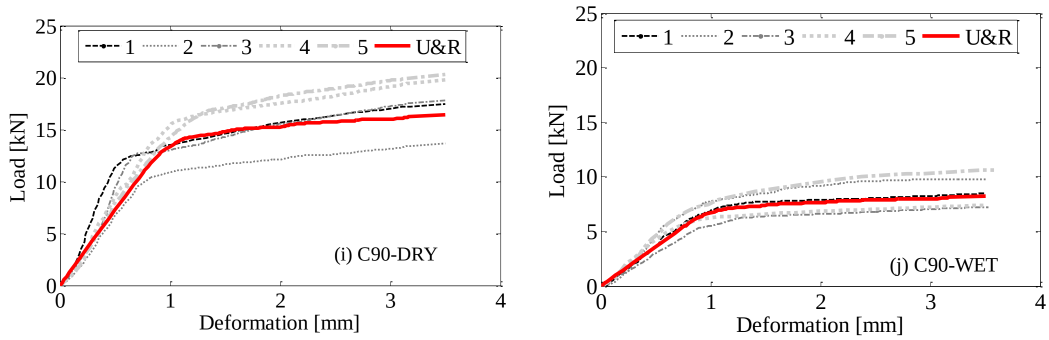

Fig. 6.4 The comparison between numerical results (solid lines) and measured data (dash lines) for compression tests on Group II small block samples: Left: dry samples; right: wet samples, for five grain angles, α=0° (a, b), 30° (c, d), 45° (e, f), 60° (g, h), and 90° (i, j). U means the numerical case for capturing the ultimate strength, R means the numerical result for reflecting the residual stress.

Code	Physical property	Dry			Wet		
		Test	FEA	Difference (%)	Test	FEA	Difference (%)
G0	Stiffness (MPa)	6453.5	6237.9	3.3	4260.9	3970.0	6.8
	Strength (MPa)	43.2	44.9	4.0	23.9	22.9	4.0
G30	Stiffness (MPa)	1494.1	1553.9	4.0	1005.5	988.8	1.7
	Strength (MPa)	26.0	26.9	3.3	13.8	14.0	1.3
G45	Stiffness (MPa)	886.1	800.0	9.7	559.5	514.0	8.1
	Strength (MPa)	18.0	17.7	1.9	9.6	9.0	6.1
G60	Stiffness (MPa)	531.9	551.0	3.6	274.4	292.0	6.4
	Strength (MPa)	12.0	12.5	4.0	5.7	6.0	5.5
G90	Stiffness (MPa)	437.3	401.0	8.3	235.0	240.5	2.3
	Strength (MPa)	8.3	8.6	3.6	4.6	4.3	5.2

Table 6.4 Mean values of normal elastic moduli and ultimate strengths from the experimental tests and numerical modelling. An example of their determination is shown in Fig 6.1, and the compressive strengths and stiffnesses were calculated using Eq (6.4).

The compressive strengths and stiffnesses were calculated as:

$$\sigma_{com} = \frac{f_c}{W \cdot D}$$

$$E_{com} = \frac{(f_{c,40} - f_{c,10}) \cdot L}{W \cdot D \cdot (u_{c,40} - u_{c,10})} \tag{6.4}$$

where, f_c is defined as ultimate force (kN); L (mm), W (mm) and D (mm) are the length, width and depth of the model, respectively; L, W and D = 35, 50 and 35 mm; $f_{c,40}$ and $f_{c,10}$ are the forces at the 40% and 10% levels of ultimate force, $u_{c,40}$ and $u_{c,10}$ are the deformations (mm) at $f_{c,40}$ and $f_{c,10}$, respectively.

A correlation between the numerical prediction and the experimental data was found in the elastic range (compressive stiffness) and the plastic stage (compressive strength) below and at the ultimate strengths for both low and high moisture content situations (*Table 6.4*). This demonstrated that the proposed constitutive model was reasonable for obtaining the ultimate strength distribution of *E. nitens* timber including the moisture effect for off-axis compression. It should be noted that, as the constitutive model does not include softening, post-yield behaviour for the numerical cases at grain angles below 45° was not a good fit with the experimental data, where "softening" behaviour was observed. Future work will include a study of softening in order to model the residual stress distribution within *E. nitens* timber after peak loading.

6.3.3 Validation based on stiffness and strength against grain angle.

Numerical values for compressive strength and stiffness as a function of grain angle are presented in *Fig 6.5*. The numerical values were obtained according to the off-axis numerical results presented in Section 6.3.2, i.e., the ultimate values and the slope of the elastic range of load-deformation curves were used to determine the numerical strength and stiffnesses. It was found that the numerical values of compressive stiffness and strength predicted by the FE model increased, as grain angle decreased. The values of compressive strength and stiffness for FEM modelling can be found in *Table 6.4*.

These findings agree well with Hankinson's equation, Eq (3.6), and the experimental results (provided in Chapter 3) and they are consistent with the results of previous orthotropic compressive stiffness and strength studies based on dry samples [12, 13, 115]. The present work extends this to wet samples and finds that compressive strength and stiffness of *E. nitens* are sensitive to moisture content and the grain angle below and above *FSP*.

In general, compressive stiffness and strength values decrease sharply with increasing grain angles up to 45°. Above this angle, compressive stiffness and strength level off and little additional decrease is found. This correlation further validated the numerical modelling.

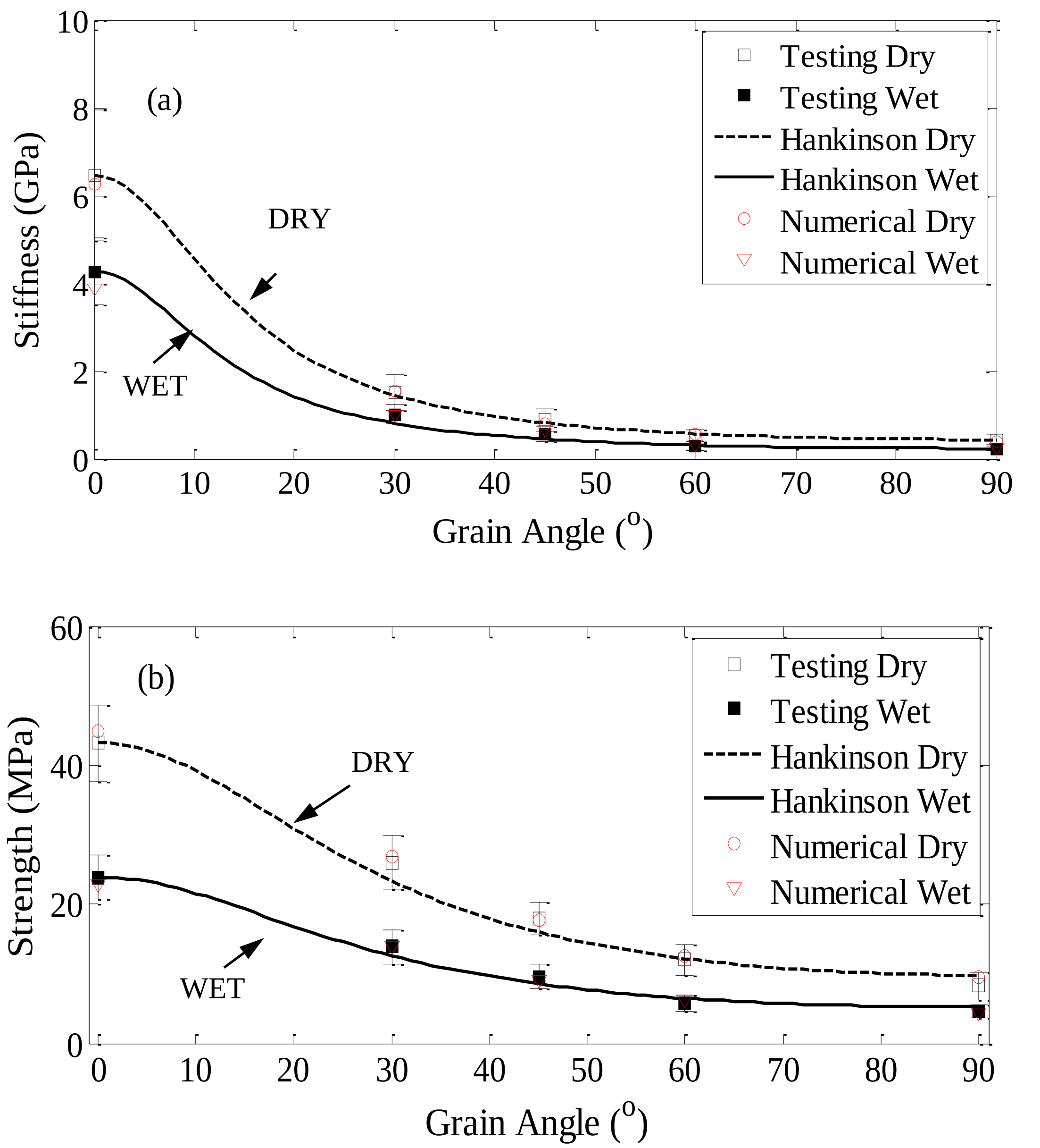

Fig. 6.5 The relationship between Stiffness (GPa) and Strength (MPa) to Grain angle (°) for numerical results compared with experimental data and Hankinson's formula [13, 86]: top chart (a): stiffness; bottom chart (b): strength.

6.4 FURTHER STUDY

6.4.1 Deformation shape and stress distribution

Fig. 6.6 presents the deformation shape and shear stress distributions of the numerical off-axis compression simulations at grain angles of 0°, 30°, 45°, 60° and 90°, respectively, with low moisture content.

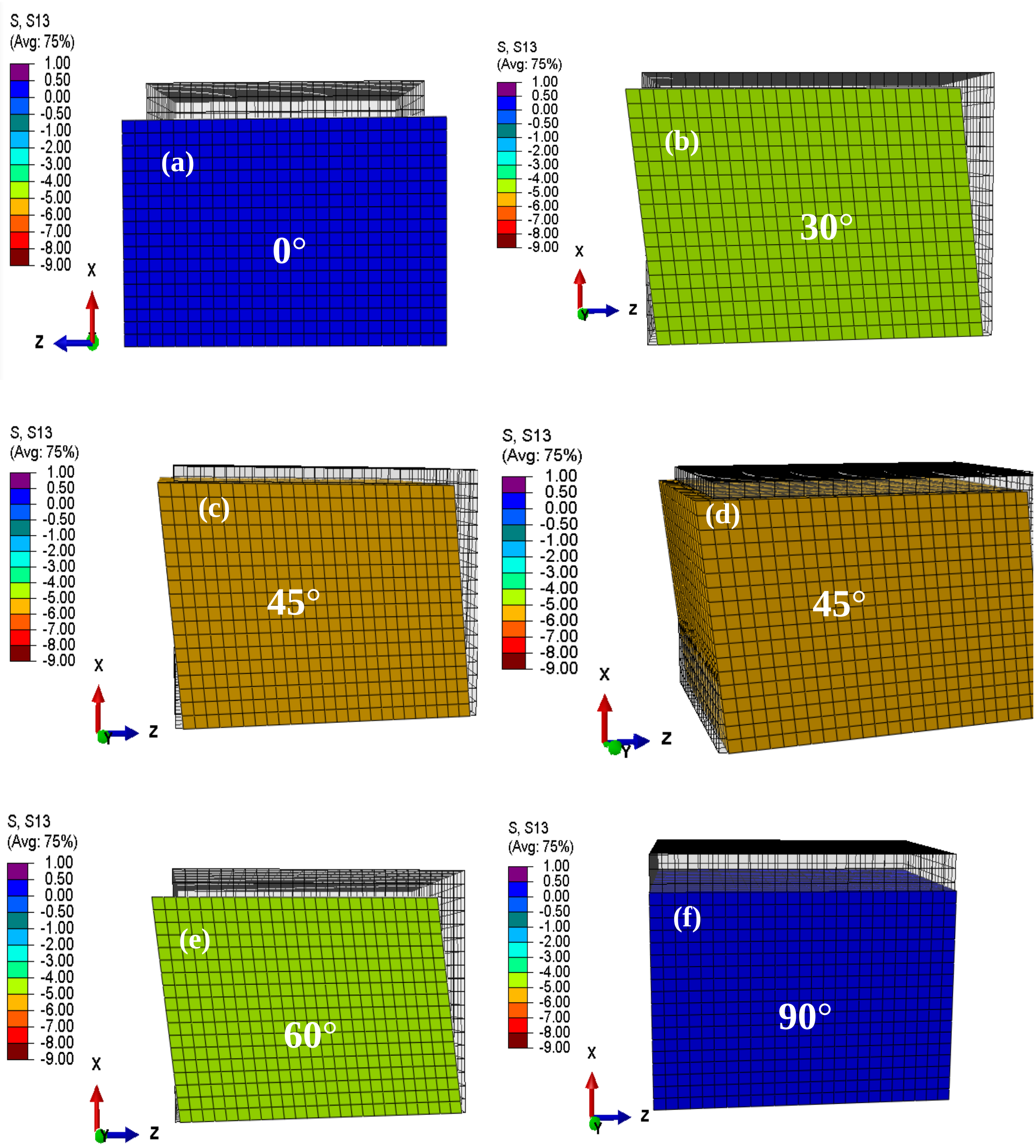

Fig. 6.6 Deformation shape and shear stress distribution (MPa) of numerical *E. nitens* block models at grain angles of (a) 0°, (b) 30°, (c, d) 45°, (e) 60° and (f) 90° with low moisture content at a compressive loading of 20 kN. S13 represents the shear stress along the grain in L-R plane (i.e., parallel to the fibres and perpendicular to the growth rings).

The numerical model, shown in *Fig 6.3*, modelled a uniform distributed compression loading of 20 kN on the top surface. It was found that the deformation shape links with the grain angle and a change in grain angle alters the deformation substantially. Extruded and vertically expanded for a grain angle of 0°, compressive and shear deformation for grain angles of 30°, 45° and 60°, and crush for a grain angle of 90°. The results are consistent with a previous experimental study [51] and the findings in Chapter 3 (*Fig 6.7*). Shear stresses appeared at grain angles of 30°, 45° and 60°, linking with shear deformations (*Fig 6.6* and *Fig 6.7*). A uniform shear stress distribution within the numerical models was found (*Fig. 6.6*). Comparing the numerical cases at grain angle of at 30°, 45° and 60°, the maximum shear stress occurred at 45°.

Fig. 6.7 Deformation of *E. nitens* block samples in compression (same as Fig 3.10)

6.4.2 Normal and shear stress components

Fig 6.8 presents the distributions of six stress components for the FEM models at a compressive loading of 14 kN for grain angles of 0°, 45°, and 90°, respectively. The compressive loading chosen here is within the linear range of dry specimens loaded perpendicular to the grain. A uniform stress distribution was found, and these stresses were mainly in the L-R plane where the compressive loading occurred. In the following discussion, only the stresses/strains in the L-R plane will be examined.

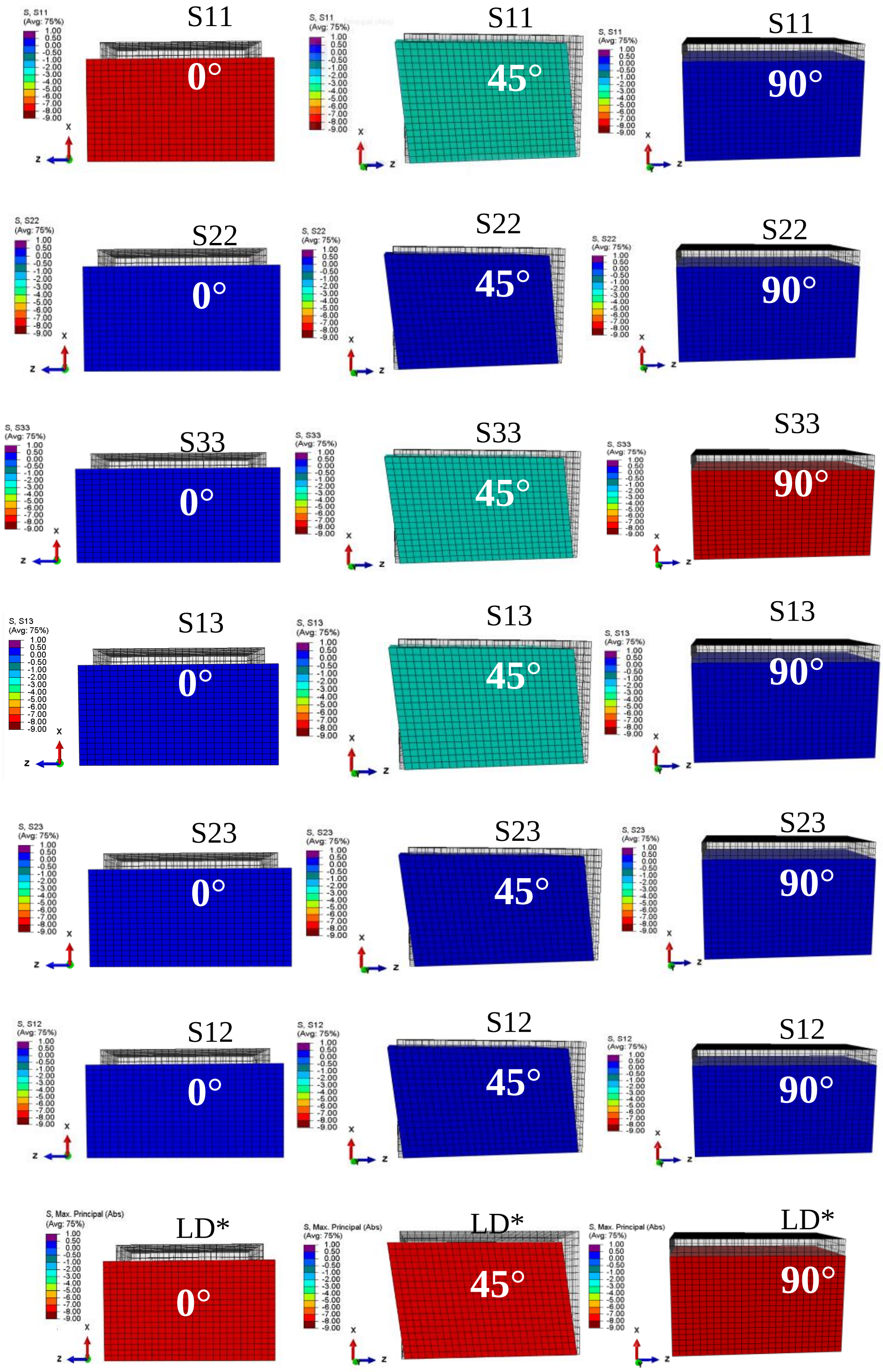

Fig. 6.8 Stress (MPa) component distribution of *E. nitens* small block models at grain angle of 0°, 45°and 90° in compression for low/high moisture contents at a compressive loading of 14 kN. *LD means the compressive loading direction. Symbols 1, 2, 3 represent the principal anatomical directions (*L*, *T*, or *R*).

6.4.3 Comparison with the isotropic von Mises and Hill models

The isotropic Hill criterion is widely used in timber engineering to describe wood anisotropy [24]. In this section, the load-deflection curves calculated via the proposed constitutive model (GH) in Chapter 5 were compared with those from the von Mises model (VM) and the Hill model (HL). The properties of the orthotropic von Mises and the Hill models for *E. nitens* timber used in the simulation are provided in *Table 6.5* and they are derived from *Table 6.1* and *6.3*.

Properties		**DRY**			**WET**		
Elastic	Normal elastic moduli (MPa)	*L*	*R*	*T*	*L*	*R*	*T*
		7000	310	310	4125	180	180
	Shear elastic moduli (MPa)	*LR*	*LT*	*RT*	*LR*	*LT*	*RT*
		780	600	600	380	200	200
	Poisson ratio	0.1	0.1	0.29	0.1	0.1	0.29
Plastic	Isotropic hardening (MPa)	$E_{tang} = 51.2$			$E_{tang} = 24.5$		
	Hill yield stress (MPa)	*L*	*R*	*T*	*L*	*R*	*T*
		38.2	6.8	6.8	18.8	3.1	3.1
		LR	*LT*	*RT*	*LR*	*LT*	*RT*
		12.4	10.2	10.2	5.5	4	4
	von Mises yield stress (MPa)	6.8			3.1		

Table 6.5 Standard material properties of *E. nitens* timber used in the von Mises model and the Hill model. Symbols *L*, *R*, *T* represent the principal anatomical directions: longitudinal, radial and tangential.

Before yield, the *E. nitens* timber with both low and high moisture content underwent an elastic deformation (*Fig 6.9*), which means a linear and fully recoverable material behaviour. The load and deformation curves for the three constitutive models were similar within this elastic range varying with the loading direction. As the grain angle increased, the slope of the stress-strain curve decreased, which implies that the compressive stiffness decreases with an increase in grain angle. This trend is consistent with the experimental data (*Fig 6.9*).

According to testing data for *E. nitens* timber both below and above *FSP*, an anisotropic hardening stress-strain curve in the plastic region was found. For compression at grain angles below 45°, the hardening law is not always appropriate as experimental load-deflections sometimes suddenly decrease after the peak (*Fig 6.9a, b, c, d and e*) due to the timber's brittle behaviour. Therefore, by including elastoplastic anisotropy in the proposed constitutive model, the load carrying capacity of *E. nitens* timber can be examined more accurately. However, the plastic hardening predicted by the von Mises and the Hill models was isotropic and were similar at grain angles of 0°, 30°, 45°, 60° and 90°. Compared with other loading directions, the results of the numerical modelling via the constitutive models (GH, HL, VM) agreed most closely with the experimental results with loads applied at a grain angle of 90° (*Fig 6.9i, j*), and reasonable agreement at a grain angle of 60º (*Fig 6.9g & h*).

It can be seen that grain angle had a stronger effect on the numerical load-deformation curves than moisture content (*Fig 6.10*). The moisture decreased modelled compressive yield stresses and modulus of elasticity (*Fig 6.10*), and this agreed with the experimental results (*Fig 6.9*). A more ductile failure was found in the wet cases compared with the dry cases (*Fig 6.9* and *Fig 6.10*) and this is because moisture makes the wood fibre's ductility increase [116].

The numerical modelling also proved that the von Mises model, was not suitable for modelling *E. nitens* wood in off-axis compression both below and above *FSP*, as it shows a constant yield stress (*Fig 6.10b, e*).

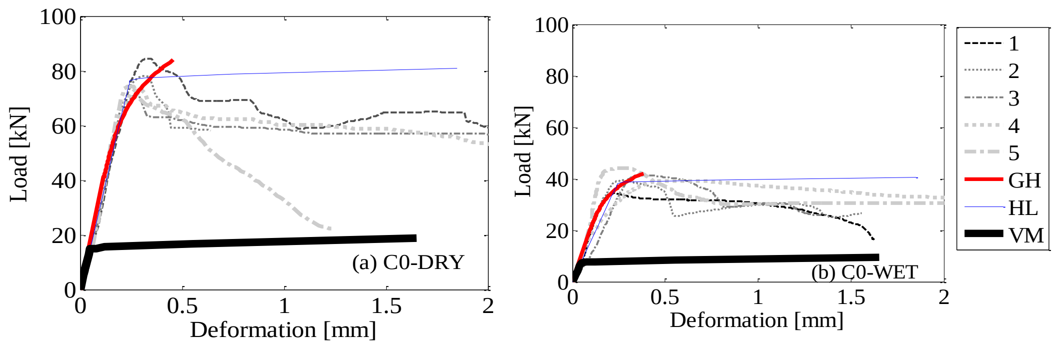

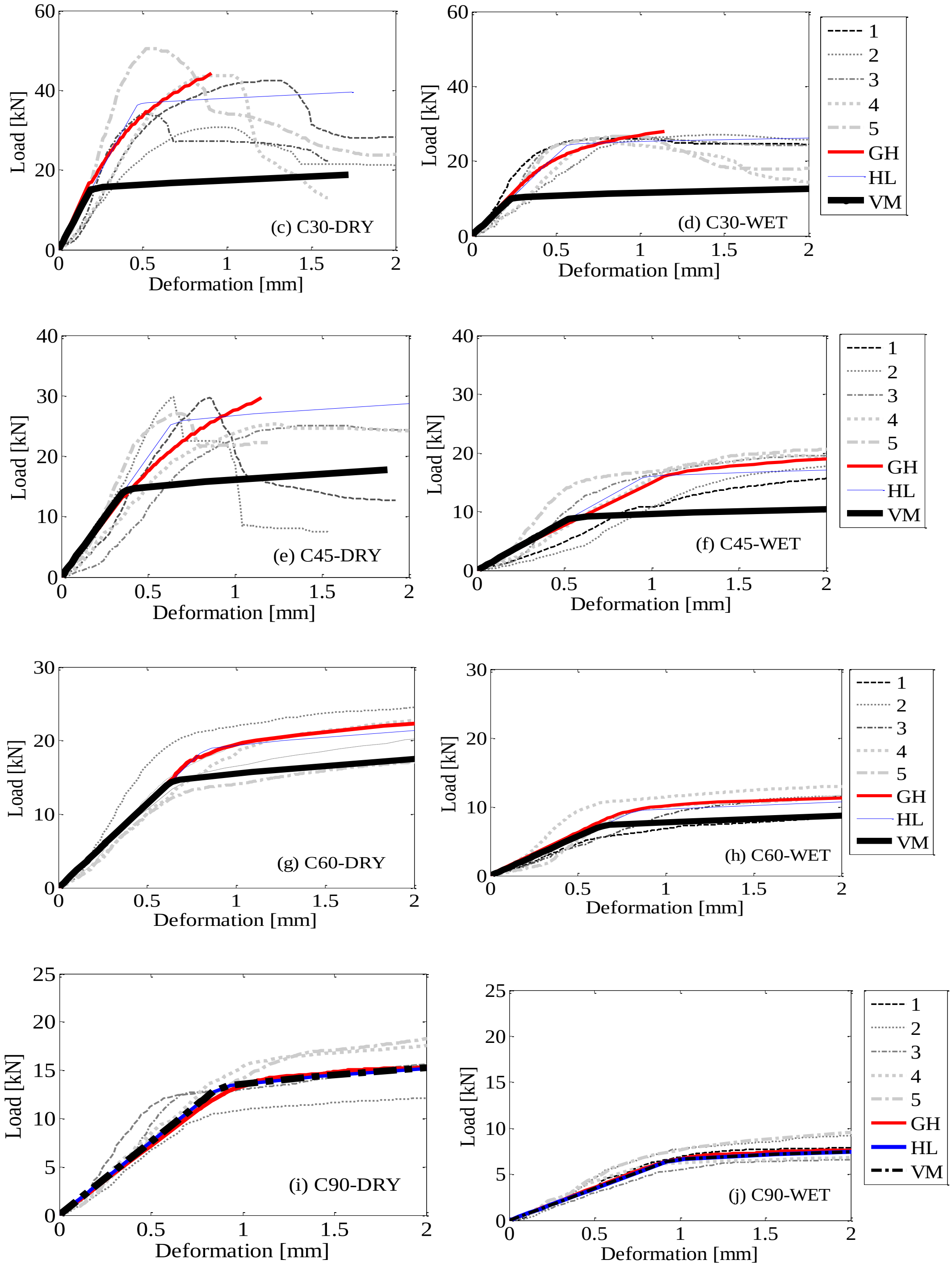

Fig. 6.9 Load-Deformation curves predicted by the three constitutive models (solid lines) and measured compressive data (grey dash/dotted lines) for five angles; (a, b), 0º; (c, d), 30º; (e, f), 45º; (g, h), 60º and (i, j), 90°. Left charts; dry cases, right charts; wet cases. GH is the proposed constitutive model in Chapter 5; HLis the Hill model; VM is the von Mises model.

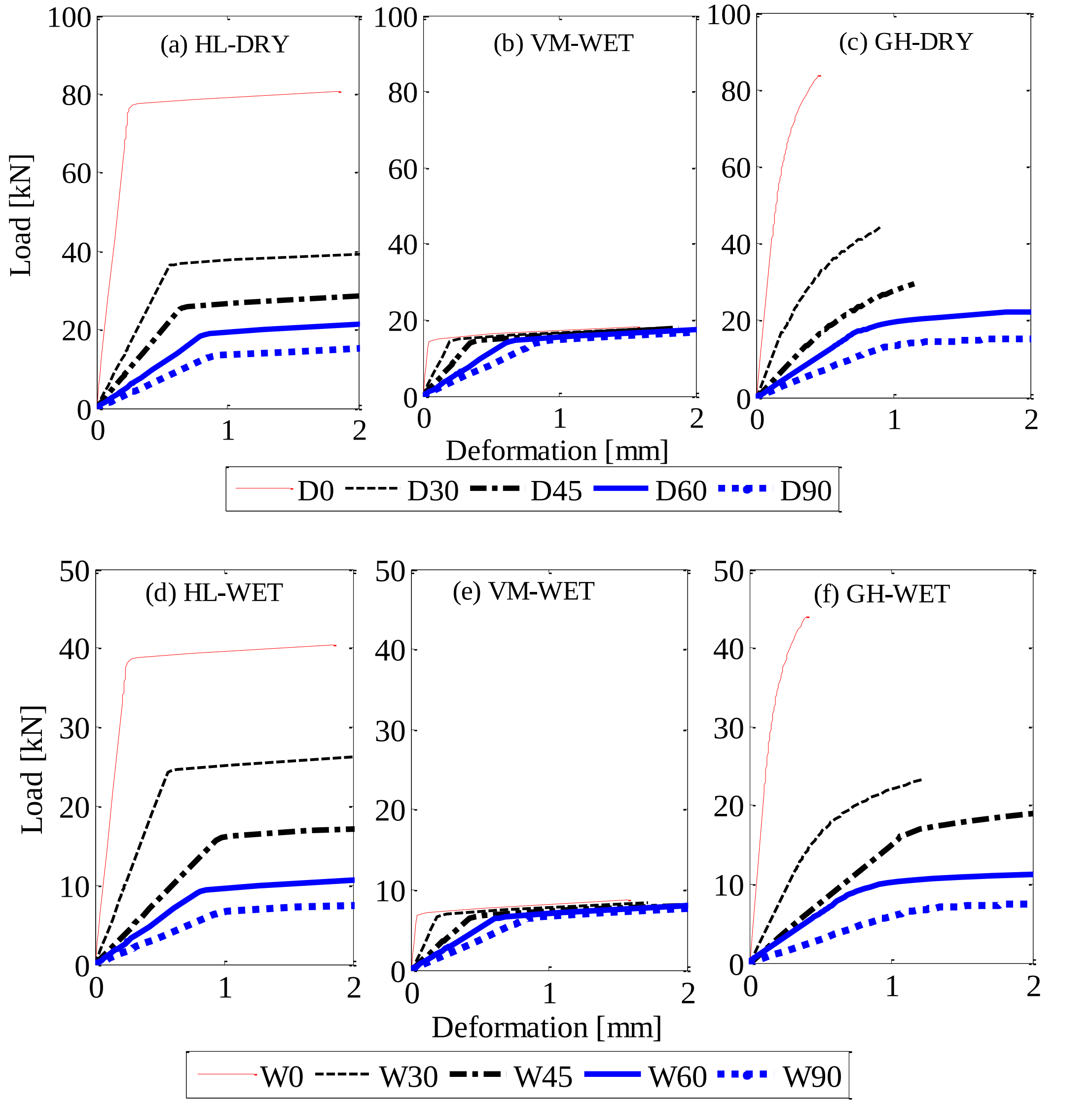

Fig. 6.10 Load-Deformation relationship varies with the loading direction for the three constitutive models: (a, d) HL, Hill model; (b, e) VM, von Mises model; (c, f) GH, proposed constitutive model in Chapter 5 for (a, b, c) dry and (d, e, f) wet conditions

The results were also compared with the values predicted by an orthotropic elastic (only) constitutive model (OE) and by an orthotropic model with perfect plasticity (PP) in dry conditions in order to further check the findings. The numerical stiffnesses of the five constitutive models were the same, while the post yield behaviours of the five constitutive models were different (*Fig 6.11*). The OE and the PP models were not suitable to describe the inelastic (i.e. post yield) compressive behaviour of *E. nitens*, as hardening was observed in experiments (*Fig 6.11*). The von Mises model was also not suitable as it could only accurately predict load-deformation for one loading direction (*Fig 6.10* and *Fig 6.11*).

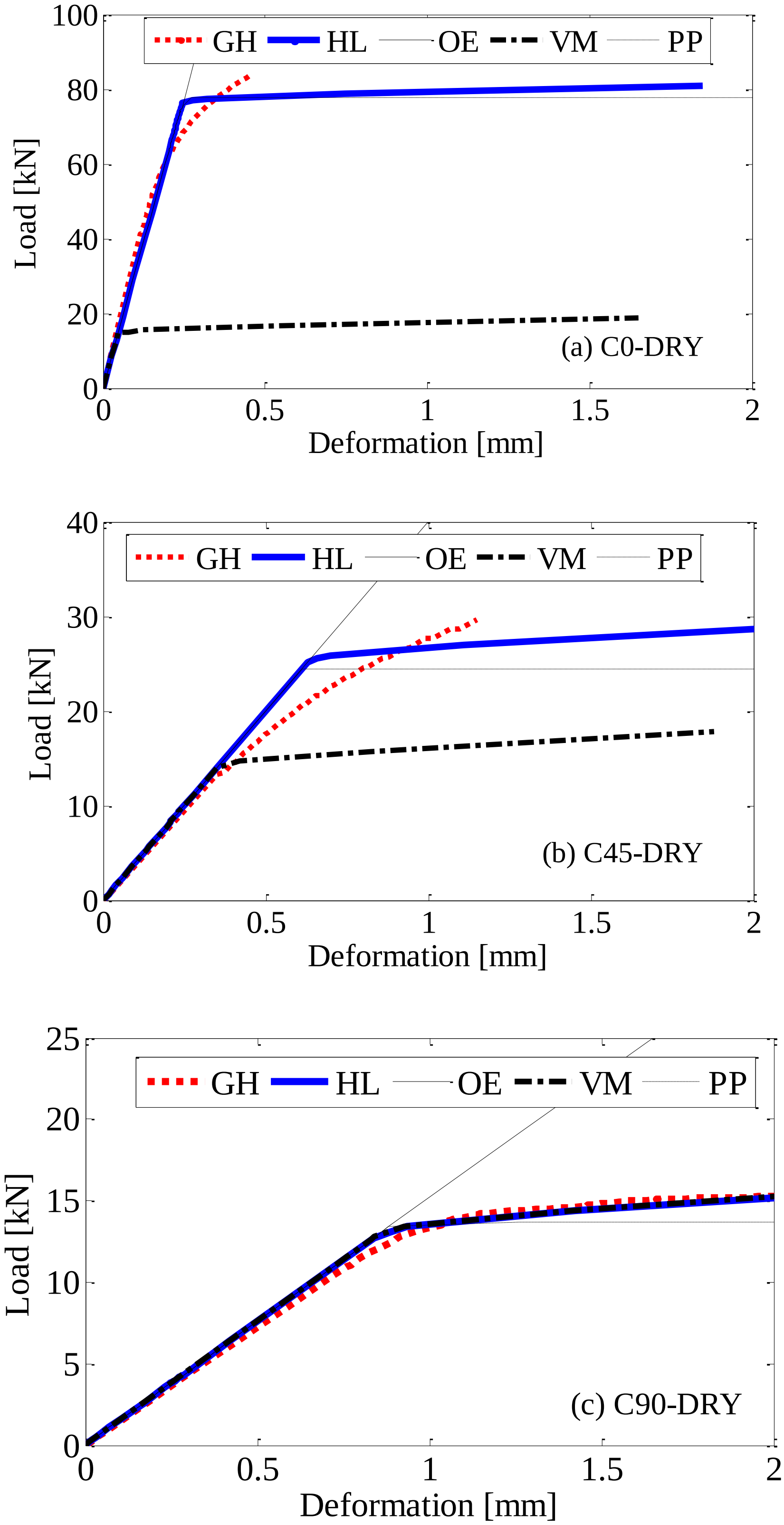

Fig. 6.11 The comparison between load-deformation curves predicted by five constitutive models for dry samples. HL, Hill model; OE, orthotropic elasticity only model; VM, von Mises model; PP orthotropic model with perfect plasticity; GH, proposed constitutive model in Chapter 5

The agreement between the model predictions and the experimental data shows that the proposed moisture-dependent anisotropic elasto-plasticity constitutive model can be utilised effectively in the investigation of the anisotropic compressive behaviours of *E. nitens* timber both below and above *FSP*.

6.4.4 Yield surfaces and Mohr's circle

When loaded in different grain directions, the vector components of compressive strength in the direction parallel to the grain and perpendicular to the grain are calculated by Formula (6.5). The transform equations are presented below.

$$
\begin{aligned}
\sigma_{\mathrm{LL}} &= \cos^2\varphi\sigma_{\mathrm{f}} \\
\sigma_{\mathrm{RR}} &= \sin^2\varphi\sigma_{\mathrm{f}} \\
\tau_{\mathrm{LR}} &= -\sin\varphi\cos\varphi\sigma_f
\end{aligned}
\tag{6.5}
$$

where, φ is the grain angle. σ_{LL} and σ_{RR} are the axial and radial normal stresses, respectively. σ_f is the stress in the load direction and τ_{LR} is shear stress along the grain direction in the L-R plane.

The failure surfaces in the L-R principal space for dry and wet conditions are shown in *Fig. 6.12* and in the third quadrant, the stress paths at grain angles of 0°, 30°, 45°, 60° and 90° calculated from FEM models are depicted under off-axis compression. The yield stress values of the Hill model and, of the GH model given in Eq (5.6), are defined by the values of the mechanical properties for *E. nitens* provided in *Table 6.6*. Compared with the Hill yield surface, the failure surfaces predicted by the GH model matched better with the experimental data, and in particular at grain angles of 30° and 45° (*Table 6.7* and *Fig 6.12*). This demonstrates the suitability of the failure criterion of the developed constitutive model (GH) of this study, which couples the Hill yield criterion with the Drucker–Prager yield criterion, for application to wood material (*Fig 6.12*).

The wet cases had lower yield stress compared with the dry cases covering all the grain angle situations, implying that moisture content affects the values of the yield stresses and of the yield surface. The anisotropy of *E. nitens* timber with moisture content sensitivity was, therefore, proven: sensitivity in the longitudinal direction is much higher than in the radial directions and the yield surface enlarges with a decrease in moisture content.

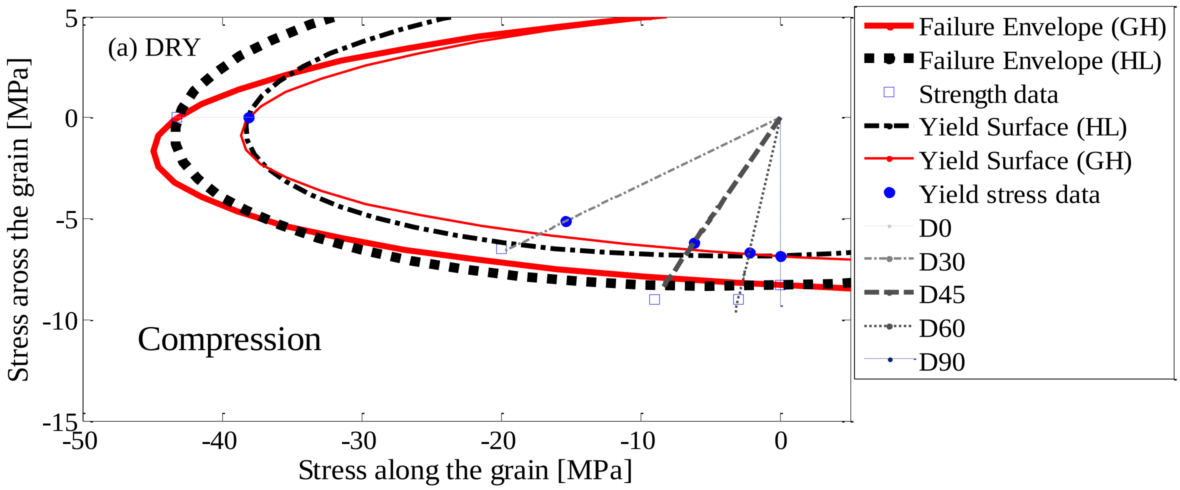

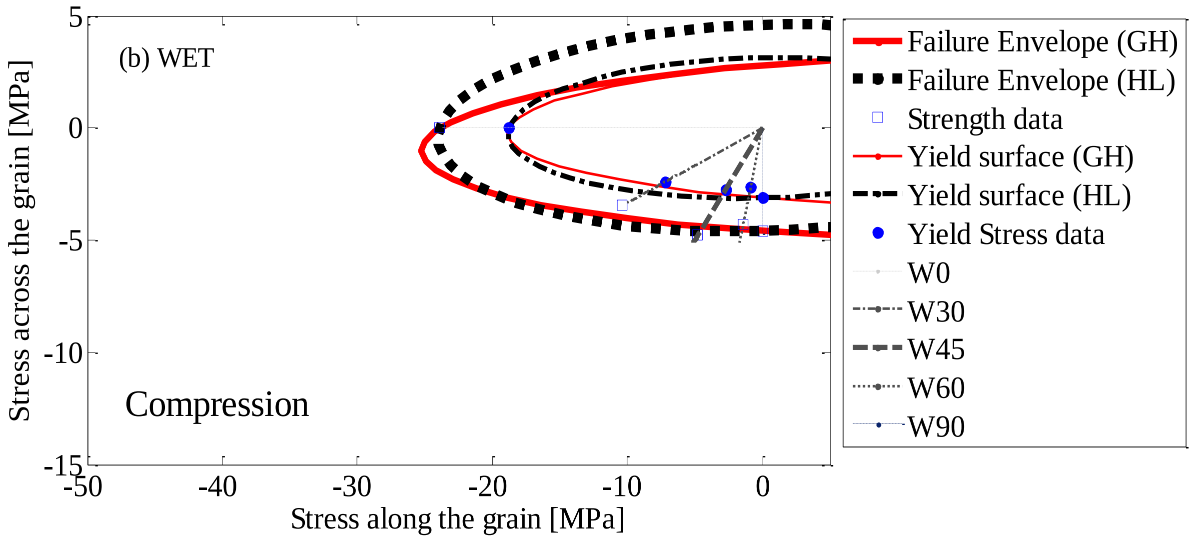

Fig. 6.12 Failure surfaces and 2-D normal stress paths and for off-axis compression on *E. nitens* block models at grain angles of 0°, 30°,45°, 60° and 90° with (a) low (dry) and (b) high (wet) moisture contents

Linear stress paths for each compressive loading direction were found both in the elastic and inelastic ranges (*Fig 6.12*). This indicated that the development of the yield surfaces for off-axis compression on *E. nitens* timber is not coupled with each other at the time plastic deformation starts. If plastic strains occur, the yield surface will change in size and shape as shown in *Fig 6.12*. Evolved failure envelopes for each individual stress path were also shown, and these correlated well with the experimental results (see squares and dots in *Fig. 6.12*).

Properties	**Initial yield surface**		**Failure envelope**	
	Dry (*MC*=12%)	WET(*MC*>*FSP*)	Dry (*MC*=12%)	WET(*MC*>*FSP*)
Tensile strength in longitudinal direction, $\boldsymbol{Y_L^T}$ (MPa)	81.9	56.0	91	62.2
Tensile strength in radial direction, $\boldsymbol{Y_R^T}$ (MPa)	5.0	3.4	5.5	3.8
Compressive strength in longitudinal direction, $\boldsymbol{Y_L^C}$ (MPa)	38.1	18.8	43.2	23.9
Compressive strength in radial direction, $\boldsymbol{Y_R^C}$ (MPa)	6.2	3.1	8.3	4.6
Shear strength in L-R plane, $\boldsymbol{Y_{LR}^S}$ (MPa)	12.4	5.5	18	9.6

Table 6.6 Values of mechanical properties for *E. nitens* to determine the initial yield surface and failure envelope for both dry and wet conditions. The shear and compressive yield stresses and strengths are determined from the experimental data provided in Chapter 3, while the yield stresses and strengths in tension are from the experiments discussed in Section 7.2.2 of Chapter 7.

Code	**RMSE**	
	DRY	WET
Yield surface (HL)	>20 %	>15%
Yield surface (GH)	<10%	<10%
Failure envelope (HL)	>15% but <20%	>10% but <15%
Failure envelope (GH)	<10%	<10%

Table 6.7 The root mean square error (RMSE) for each surface provided in Fig 6.12 calculated using Eq (5.31), for the Hill model (HL), and the proposed constitutive model (GH) in Chapter 5

Mohr circle is calculated from Eq (6.6) and shows the stresses in the *E. nitens* model when *E. nitens* yields under compression. It is shown that as the grain angle increased, the radius of the Mohr circle decreased. This implied that the resistance to loading for *E. nitens* declines from compression parallel to the grain to perpendicular to the grain both below and above *FSP*, thereby agreeing with the experimental results discussed in

Chapter 3.

$$\sigma_m = \frac{\sigma_{LL} + \sigma_{RR}}{2} + \frac{\sigma_{LL} - \sigma_{RR}}{2} cos2\alpha - \tau_{LR} sin2\alpha$$

$$\tau_m = \frac{\sigma_{LL} - \sigma_{RR}}{2} sin2\alpha + \tau_{LR} cos2\alpha \qquad (6.6)$$

$$tg2\alpha = -\frac{2\tau_{LR}}{\sigma_{LL} - \sigma_{RR}}$$

where, σ_{LL} and σ_{RR} are the axial and radial normal stresses, respectively; τ_{LR} is shear stress along the grain direction in L-R plane and σ_m and τ_m are the corresponding stress state in the Mohr circle, α is the grain angle, $tg2\alpha$ is the tangent of double angle value for the grain angle.

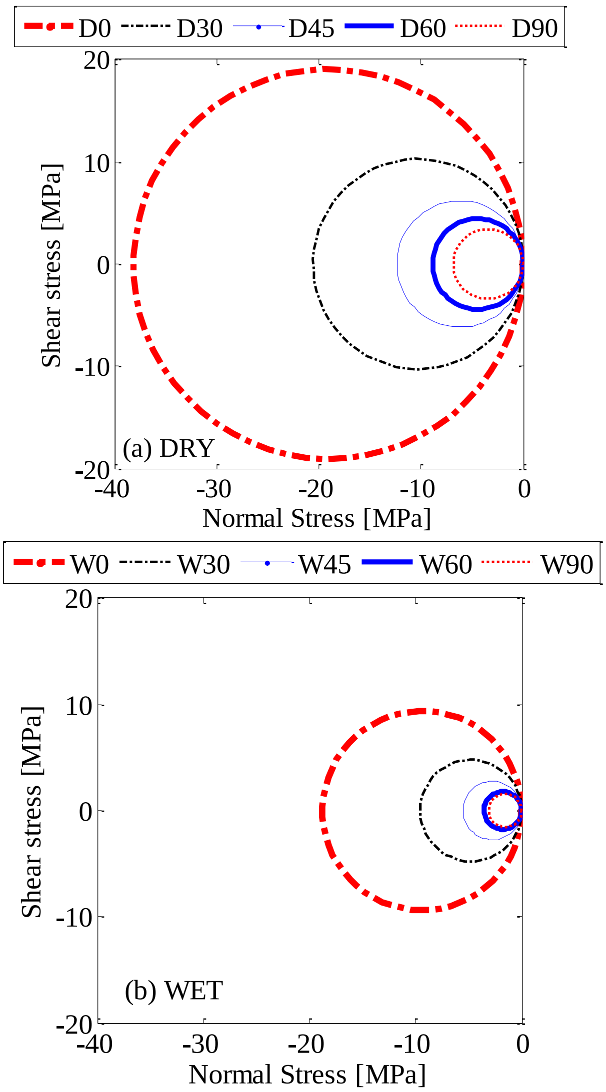

Fig. 6.13 Mohr circle for stress state regarding off-axis compression on small block models at grain angles of 0°, 30°,45°, 60° and 90° with (a) low and (b) high moisture contents. An example of the determination of the yield stresses is shown in Fig 6.2, and the mean values for the yield stresses from off-axis compression on small block samples to determine the Mohr circles, calculated using Eq (6.6), are given in Table 6.8.

At grain angles of 30°, 45°, and 60°, shear stress exists, and shear failure becomes dominant due to the corresponding normal stress being less than its failure value (*Fig 6.13*). This confirms the fundamental role of failure mechanism in wood fibre as the strength-determining component in wood. Compared with the dry cases, a lower resistance was found for wet cases at grain angles of 0°, 30°, 45°, 60° and 90°, implying an increase in the risk of *E. nitens* yielding above the *FSP*.

	Grain angle (°)	**0**	**30**	**45**	**60**	**90**
DRY (*MC*=12%)	Yield stress (MPa)	38.1	20.6	12.4	8.9	6.8
	Its longitudinal component, σ_{LL} (MPa)	38.1	15.4	6.2	2.2	0.0
	Its shear component, σ_{LR} , (MPa)	0.0	8.9	6.2	3.8	0.0
	Its radial component, σ_{RR}, (MPa)	0.0	5.1	6.2	6.7	6.8
WET (*MC*>*FSP*)	Yield stress (MPa)	18.8	9.6	5.5	3.5	3.1
	Its longitudinal component, σ_{LL} , (MPa)	18.8	7.2	2.8	0.9	0.0
	Its shear component, σ_{LR} ,(MPa)	0.0	4.1	2.8	1.5	0.0
	Its radial component, σ_{RR}, (MPa)	0.0	2.4	2.8	2.7	3.1

Table 6.8 The mean values and the components of the yield stresses from off-axis compression on small block samples at grain angles of 0°, 30°,45°, 60° and 90°.

The components of the stress variables against the grain angle with a compressive loading of 14 kN are presented in *Fig 6.14*.

Shear stress increases for grain angles from 0° to 45°, then, after shear stress reaches its peak at 45°, it decreases with further increases in grain angle (*Fig 6.14*). Normal stress along the grain decreases as the grain angle increases, while normal stress across the grain increases as the grain angle increases. The internal stress state within *E. nitens* timber links strongly with its failure mode. At grain angles of 0°, the normal stress along the grain is dominant compared with the corresponding shear stress and normal stress across the grain, which leads to fibre buckling. At loading directions of 30°, 45° and 60°, shear stress plays a significant role and therefore, the failure mode of *E. nitens* timber is mainly due to fibre-layer slip delamination and shear deformation. For grain angles of 90°, the effect of normal stress across the grain is significant, correlating with the crushing failure observed in the experiment presented in Chapter 3. This is why the compressive behaviour of *E. nitens* timber is significantly influenced by loading direction

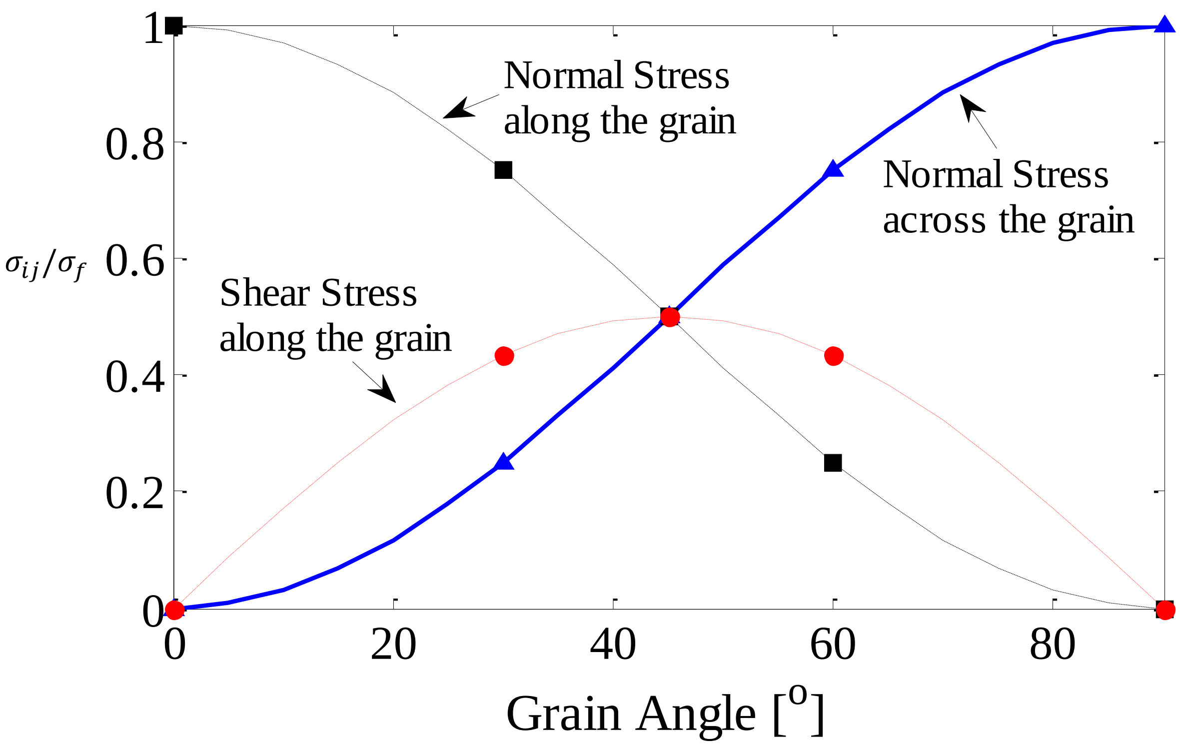

Fig. 6.14 The stress components (at compressive loadings of 14 kN) against grain angle. The numerical result is represented by dots and the analytical results as lines. σ_{ij} (i, j =L, R) and σ_f are the stress component and the stress in the load direction; Symbols L and R represent the principal anatomical directions: Longitudinal direction and Radial direction. The values of the numerical results are presented in Fig 6.8 and Table 6.9.

These findings were consistent with previous experimental studies on the dry wood of other species [51, 52, 92]. This section examined the normal and shear components in wet *E. nitens* timber and addressed the knowledge gap of previous studies on wood (usually on conifer species) below the *FSP*, where only loading to grain angles of 0° and 90° have been published. For its potential as a construction material, the underlying anisotropic failure mechanism of *E. nitens* timber both below and above *FSP* under off-axis compression has been here examined for the first time.

Grain angle (°)	Stress Value (MPa)			
	Longitudinal direction (σ_{LL})	Shear direction (σ_{LR})	Radial direction (σ_{RR})	Loading direction (σ_f)
0	7.986	0.001	0.002	7.986
30	5.998	3.462	1.999	7.995
45	3.999	3.999	3.999	7.997
60	1.996	3.457	5.989	7.985
90	0.001	0.000	7.997	7.997

Table 6.9 Stress (MPa) components of *E. nitens* small block FEM models at grain angle of 0°, 30°, 45°, 60 ° and 90° in compression for low moisture content (MC=12%) at a compressive loading of 14 kN.

6.5 PARAMETRIC INVESTIGATION

In this section, a sensitivity investigation in L-R plane (i.e., in a plane parallel to the fibres and perpendicular to the growth rings) is undertaken to examine how the parameters used affect the simulated outputs in the numerical model. The acute angle between the compressive direction and the longitudinal direction is defined as the grain angle, and 1134 numerical cases have been simulated. The sensitivity of compressive stiffness and of compressive strength to loading direction for 10% changes in the key elastic and plastic material parameters with varying grain angles is provided in *Table 6.10* and *Table 6.11*, respectively. This 10% change is used due to the minimum value of the COVs of the physical properties (ie., Young's modulus and strength) for the *E. nitens* testing samples below and above *FSP* being 10.5% (*Table 3.2*). Therefore, each key parameter has been varied by 10% to make sure the changes within the range of key parameters have physical meaning.

Grain Angle (°)	**% change in compressive stiffness in loading direction for a 10% change in constitutive model parameters (The value of the constitutive model parameters used are presented in Table 6.1 for dry and Table 6.5 for wet)**							
	10% decrease in constitutive model parameters				10% increase in constitutive model parameters			
	E_{LL}	E_{RR}	G_{LR}	Others	E_{LL}	E_{RR}	G_{LR}	Others
0	-10.0	-0	-0.0	-0.0	+10.0	+0.0	+0.0	+0.0
15	-5.2	-0.8	-6.0	-0.0	+3.6	+0.4	+4.4	+0.0
30	-1.2	-4.8	-6.0	-0.0	+0.8	+3.2	+4.8	+0.0
45	-0.0	-7.6	-4.1	-0.0	+0.0	+6.0	+2.4	+0.0
60	-0.0	-9.2	-2.0	-0.0	+0.0	+8.0	+1.2	+0.0
75	-0.0	-9.6	-0.4	-0.0	+0.0	+9.6	+0.4	+0.0
90	-0.0	-10.0	-0.0	-0.0	+0.0	+10.0	+0.0	+0.0

Table 6.10 Sensitivity of compressive stiffness in the L-R plane to changes in constitutive model parameters

In the simulations, both the dry and wet cases had the same result for sensitivity of compressive stiffness in the L-R plane. Variation in E_{LL} only significantly affected the compressive stiffness at grain angles between 0° and 15°, then gradually decreased and became insignificant in the range between 30° and 90° (see *Table 6.10*). G_{LR} produced an important change in compressive stiffness in the range 15° to 60°. In the range from 15° to 60°, the impact of G_{LR} increased and approached its peak at roughly 21°, and then it reduced gradually and could be neglected after 60°. E_{RR} had no significant effect in the range from 0° to 15°. It became stronger gradually and played a leading role for angles above 45°. After 45°, the influence of E_{RR} remained unchanged but it was the most significant factor compared with E_{LL} and G_{LR}. For other constitutive model parameters, there was no significant effect at grain angles between 0° and 90° in the L-R plane.

Radial Yield Stress ($Y_{\boldsymbol{R}}^{\boldsymbol{C}}$) had little effect on compressive strength at angles between 0° and 15° but after 15° the influence of $Y_{\boldsymbol{R}}^{\boldsymbol{C}}$ gradually appeared and increased from 8.5%

to 10 % as the angle increased (*Table 6.11*), i.e., 8.5 % at 30°, 9.8% at 60°, and 10% at 90°. Similar findings were found for the effect of a 10% decrease in Y_R^C on compressive strength.

Grain Angle (°)	**% change in compressive strength in loading direction for 10% change in constitutive model parameter (The value of the constitutive model parameters used are presented in Table 6.1)**											
	10% decrease in constitutive model parameters						10% increase in constitutive model parameters					
	Y_L^C	Y_R^C	Y_{LR}^S	K	n	Others	Y_L^C	Y_R^C	Y_{LR}^S	K	n	Others
0	-10.0	-0.0	-0.0	-0.0	-0.0	-0.0	+10.0	+0.0	+0.0	+0.0	+0.0	+0.0
15	-5.1	-5.5	-5.2	-0.2	-0.0	-0.0	+4.6	+5.0	+4.8	+0.1	+0.0	+0.0
30	-1.8	-8.5	-5.2	-0.9	-0.0	-0.0	+1.5	+8.2	+5.0	+0.6	+0.0	+0.0
45	-0.7	-9.4	-3.2	-1.3	-0.1	-0.0	+0.6	+9.3	+3.0	+1.0	+0.0	+0.0
60	-0.2	-9.8	-1.6	-1.9	-0.3	-0.0	+0.2	+9.8	+1.5	+1.4	+0.1	+0.0
75	-0.1	-10.0	-0.6	-2.8	-0.5	-0.0	+0.0	+10.0	+0.5	+2.0	+0.3	+0.0
90	-0.0	-10.0	-0.0	-3.0	-0.8	-0.0	+0.0	+10.0	+0.0	+2.4	+0.4	+0.0

Table 6.11 Sensitivity of compressive strength in the L-R plane to changes in constitutive model parameters

Longitudinal yield stress (Y_L^C) also affected the value of compressive strength. Variation in the longitudinal compressive yield stress affected the compressive strength most significantly at angles between 0° and 15°. However, the impact of Y_L^C reduced with an increase in grain angle, and after 30° its effect was negligible; for example, a 10% decrease in Y_L^C results in a 10% reduction of compressive strength in a loading direction of 0° to a 5.2% reduction at 15°, and a 1.2 % reduction at 30°. Similarly, for a 10% increase in Y_L^C, an increase in shear stress parallel to the grain (Y_{LR}^S) led to a rise in compressive strength in the range from 0° to 60°. The effect of Y_{LR}^S on compressive strength was most at grain angles ranged from 15° to 30°, then it gradually decreased to become insignificant after 50°. There was no significant effect of other parameters on compressive strength for grain angles from 0° to 90°.

6.6 DISCUSSION

The applicability of the moisture-dependent anisotropic elasto-plasticity model in this study was illustrated numerically by the compressive behaviour of *E. nitens* according to changes in moisture. The proposed anisotropic plasticity material model overcomes the limitations of previous studies that use either an orthotropic elastic model [15] or apply plasticity theory with nonlinear isotropic hardening [16, 17]. Examples of the latter include isotropic Hill and von Mises models, which are not always appropriate for stress and strain relationships with varying grain angle.

Results have indicated that the proposed constitutive model could predict the stiffness and strength of *E. nitens* in dry and wet conditions as a function of the inclined grain orientation with reasonable accuracy. The underlying anisotropic failure mechanism of *E. nitens* timber under off-axis compression was also explored. This showed the state of the internal stresses (normal stresses along and across the grain as well as the shear stress along the wood fibre) control the failure mechanism. The stress state varies with grain angle and the moisture content affects the values of the yield stresses. Therefore, as observed in experiments, the failure mode depends mainly on the load direction, while compressive strengths are affected by moisture content and loading direction.

Uniform stress distribution was found both below and above *FSP*. This means that, under off-axis pure compression, the stress at any location within the model is the same for both low and high moisture contents, assuming that wood is a homogeneous material. However, the specimens usually failed at the interface of latewood in an annual ring with the early wood of the next annual ring. This is because wood is not a homogeneous material: density and stiffness variation can be obtained by precise measurements, for example with SilviScan [60, 61]. Within an annual ring there is a gradual increase of density from the earlywood to the latewood region, whereas at the annual ring border a discrete drop in density from the latewood to the earlywood of the next annual ring occurs, showing that wood is a gradient material, i.e., properties vary gradually with dimensions [51]. As the stiffness of eucalypts is strongly related to density [19], mechanical properties such as elasticity and strength will change in the same way within an annual ring and at the ring border. Therefore, a further study on the effect of spatial distribution (heterogeneity) of material properties on the failure of *E. nitens* timber using numerical approach based on the newly developed constitutive model is suggested. Also, there is interaction effects between longitudinal shear stresses and normal stresses (tension and compression) on their strength properties. Therefore, further work should include such interaction effect in the proposed constitutive model.

6.7 SUMMARY

This chapter explored the underlying anisotropic failure mechanism of *E. nitens* timber under compression, fulfilling the fourth objective of the study. The numerical investigation into the short-term response of *E. nitens* under compression with varying grain angles and at low and high moisture contents, compared with the experimental data demonstrated acceptable agreement, showing that the constitutive model works well for *Eucalyptus* wood. The main findings of this Chapter can be summarised as follows:

- Compared with moisture content, grain angle had a stronger effect on the anisotropic compressive behaviour of *E. nitens* timber. The internal stresses within the *E. nitens* timber links strongly with its failure model. The normal stress along the grain is dominant at a grain angle of 0°, leading to fibre buckling, while crushing failure at compression perpendicular to the grain (90°) is found when normal stress across the grain is significant. Fibre-layer slip delamination and shear deformation are found when the loading directions are 30°, 45° and 60°, due to shear stress playing an important role.

- The anisotropy of *E. nitens* timber was proved numerically by an elliptical yield surface with moisture content sensitivity: the strength in the longitudinal direction is much higher than that in the radial axis, and the shape of the yield surface is enlarged when there is a decrease in moisture content. Lower moisture content also leads to lower plasticity, while the high moisture cases often showed more ductility. The numerical results confirm a marked influence from MC on the load-deflection behaviour, not only in the elastic but also in the plastic domain, showing acceptable agreement with the experimental data and demonstrating that the proposed constitutive model together with FEM can be used to examine the compressive elastic–plastic behaviour of *E. nitens* timber within a wide range of moisture contents.

- Compared with the isotropic and similar plastic hardening at grain angles of 0°, 30°, 45°, 60° and 90° as predicted by the von Mises and the Hill models, the proposed constitutive model is able to simulate the anisotropic hardening stress-strain curve in the plastic region, and this has also been observed in *E. nitens* timber both below and above *FSP* experimentally. Therefore, by including elastoplastic anisotropy in the proposed constitutive model, evolution of the yield surfaces for off-axis compression on *E. nitens* timber can be examined more correctly.

- A parametric investigation into the sensitivity of the compressive stiffness and strength to changes in the key material parameters of *E. nitens* timber was undertaken. There is no significant effect of Poisson's ratio on compressive stiffness and strength for grain angles from 0° to 90°. At grain angles between 0° and 15°, variation in the longitudinal Young's modulus (E_{LL}) and yield stress (Y_L^C) most significantly affect the compressive stiffness and strength, respectively. When the grain angle is ranged from 15° to 30°, changes in the shear modulus ($G_{L\mathrm{R}}$) and yield stress (Y_{LR}^{S}) result in the largest change in compressive stiffness and strength. After 30°, the radial Young's modulus (E_{RR}) and yield stress (Y_R^C) have dominant roles in compressive stiffness and strength, respectively, while the other parameters of the constitutive model have no obvious effect.

This chapter confirms that the proposed model could reasonably predict the anisotropic compressive behaviour of *E. nitens* timber in dry and wet conditions. Underlying factors as to why the failure mechanism of *E. nitens* timber was significantly influenced by the moisture content and the loading direction were found. However, there were still some limitations. The current study assumed an idealised homogeneous material feature for *E. nitens* timber, whereas the non-uniformity of wood leads to a large variation in failure behaviours in *E. nitens* samples, as has been observed in experiments. Further work could include the defects and knots group in the numerical model, and numerically examine the effect of such heterogeneity on the failure mechanism of *E. nitens* timber. Also, amongst other failure modes, such as tensile failure, shear failure, and flexural failure, flexural failure is an important failure mechanism [10] due to the ways in which timber is used as well as the behaviour of stands of trees in wind. The next step is to examine the flexural failure of *E. nitens* timber in low and high moisture conditions with an examination of the effect of high moisture content contributing to failure of *E. nitens* timber.

Chapter 7

7 NUMERICAL MODELLING OF *E. NITENS* TIMBER UNDER TENSION AND BENDING

7.1 INTRODUCTION

This chapter aims to address the fifth objective, ie., examining the damage to *E. nitens timber* in bending, during low and high moisture content conditions, with consideration of difference in tension and compression. Section 7.2 outlines a numerical simulation of off-axis tension for *E. nitens* timber during low and high moisture conditions using Finite Element Method with a moisture content dependent anisotropic elasto-plasticity model. The simulated results were then compared with the isotropic Hill model and von Mises model predictions. Section 7.3 presents numerical modelling of four-point bending in Eucalyptus specimens during low and high moisture content conditions, and this was compared with experimental data to further calibrate the FEM model. The effect of grain angle and moisture content on the strength of the bending models was then explored. Finally, summary based on the results are drawn.

7.2 OFF AXIS TENSION

The mechanical behaviour of a *E. nitens* tension sample was modelled using commercial software, ABAQUS (Version 2019, Dassault Systemes, France). Three-dimensional Finite Element Models were constructed to simulate the off-axis tension behaviour of *E. nitens* wood during low and high moisture conditions (*Fig 7.1*) to explore the application of proposed constitutive model to *E. nitens* wood in tension. The dimensions of the model were 600 mm (in length) × 50 mm (in width) × 10 mm (in depth) for tension perpendicular to the grain, see MODEL I (*Fig 7.1a*), and the same dimensions with a 100 mm long narrowing in the middle to 10 mm × 10 mm for tension with grain angles of 0° and 45°, see MODEL II (*Fig 7.1b*). These dimensions for the FEM models were chosen in accordance with the size of the corresponding experimental *E. nitens* tension samples (*Fig 7.1 c,d*). For the Finite Element models, MODEL I and II, the original longitudinal direction (fibre direction) is along the X-axis (*Fig 7.1a, b*).

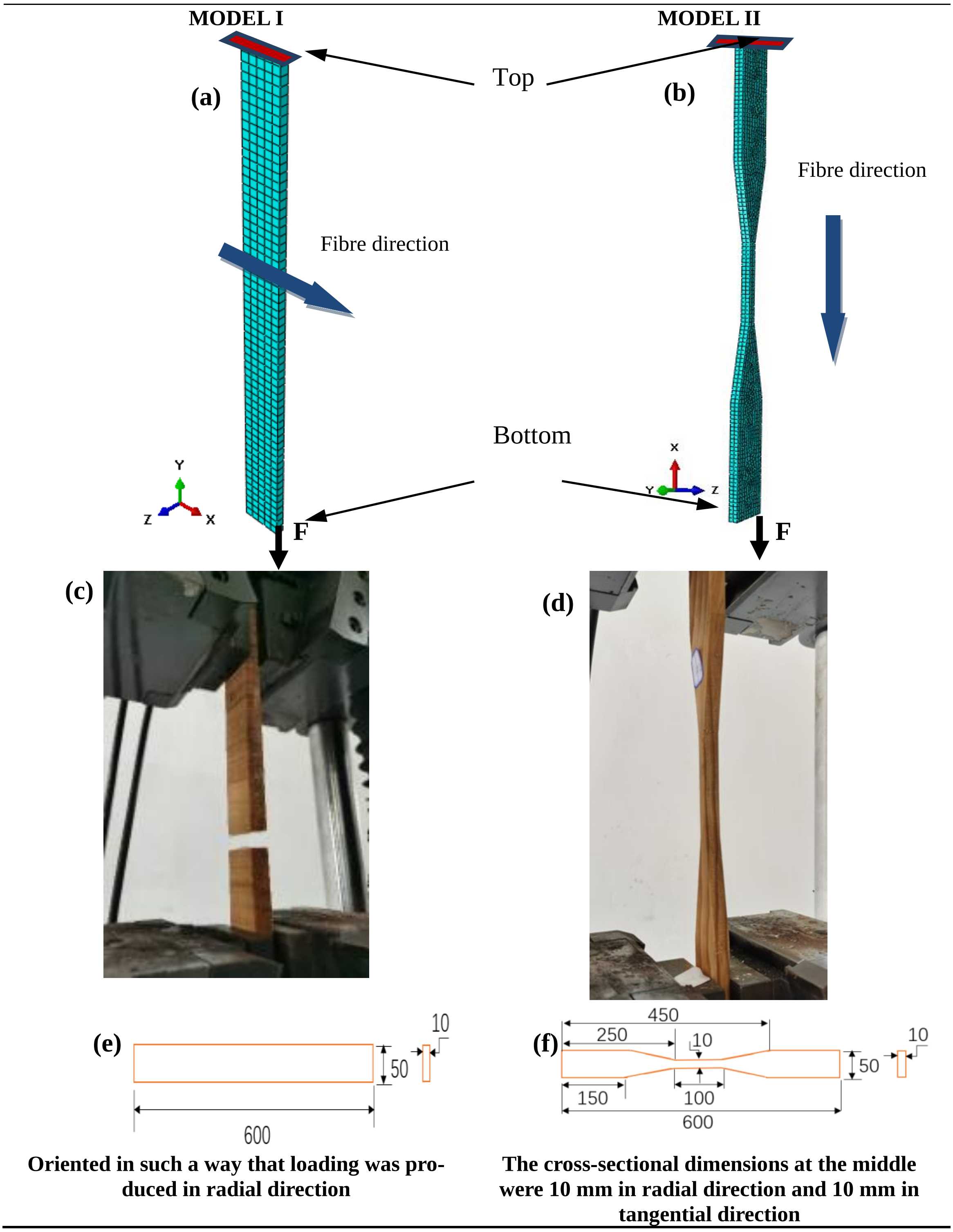

Fig. 7.1 Off-axis tension on *E. nitens* timber: (a, b) Finite element model of *E. nitens* sample for off-axis tension tests, (c, d) test photos (e, f) sample dimensions .

The local coordinate system of MODEL II will rotate clockwise around the Z-axis in the global coordinate system at an angle (φ) of 45° to explore the effect of grain angle on the tensile strength of the FEM model. Only the grain angle of 45° was chosen because of the availability of the experimental data. The bottoms of the model were constrained by moving boundaries to reflect the applied tension load parallel to the long axis of the samples, while the top surface was restrained to prevent three directional movement (*Fig 7.1a, b*), which reflected the experimental work described in Appendix 2.

MC	**Material Properties**	
	E_{LL} = 128000 (MPa)	E_{RR}= E_{TT}=100 (MPa)
12%	Y_L^T = 82.2 (MPa)	G_{LR} = G_{RT}= G_{TL} =160 (MPa)
	$Y_R^T = Y_T^T$=5.0 (MPa)	$Y_{LR}^S = Y_{LT}^S = Y_{RT}^S = 14.4$ (MPa)

Table 7.1 Material properties of dry (MC=12%) *E. nitens* wood used in Finite Element Model for off-axis tests with an assumption of transversely isotropic properties in the radial and tangential planes. These parameters include three normal elastic moduli (E_{LL}, E_{RR}, E_{TT}), 3 shear moduli (G_{LR}, G_{RT}, G_{TL}), three tensile yield stresses (Y_L^T, Y_R^T, Y_T^T), and 3 shear yield stresses (Y_{LR}^S, Y_{LT}^S, Y_{RT}^S); Symbols *L*, *R* and *T* represent the principal anatomical directions: Longitudinal, Radial and Tangential direction.

The tensile parameters of the moisture dependent anisotropic elastio-plastic model are given in *Table 7.1* for dry conditions (MC=12%) with the assumption that the values are similar for compression since only tension was examined in this section. Other parameters are the same as the compressive cases presented in Chapter 6. Then the bilinear moisture dependent material property model, Eq (6.1) and Eq (6.2), which were discussed in Chapter 6, was applied to estimate the material properties of the FEM models with *MC* below and above *FSP*. The values of wet cases follow the equation, $P_{12}c$. Coefficient, *c*, used in the FEM modelling is provided in *Table 7.2*.

Material Properties	**Coefficient, c**	**Material Properties**	**Coefficient, c**
$\boldsymbol{E_{LL}}$	0.8	Y_R^T/Y_T^T	0.69
$\boldsymbol{E_{RR}}$/ $\boldsymbol{E_{TT}}$	0.7	G_{LR}/ G_{LT}/ G_{RT}	0.75
$\boldsymbol{Y_L^T}$	0.68	$Y_{LR}^S/Y_{LT}^S/Y_{RT}^S$	0.69

Table 7.2 Values of coefficient, c, for bilinear dependency of the material properties above *FSP*. These material properties include three normal elastic moduli (E_{LL}, E_{RR}, E_{TT}), 3 shear moduli (G_{LR}, G_{RT}, G_{TL}), three tensile yield stresses (Y_L^T, Y_R^T, Y_T^T) and 3 shear yield stresses (Y_{LR}^S, Y_{LT}^S, Y_{RT}^S); Symbols *L*, *R*, or *T* represent the principal anatomical directions (*L*, Longitudinal; *R*, Radial and *T*, Tangential).

The isotropic Hill and von Mises models have the same parameter values for comparison.

7.2.1 Stress strain curves

Fig 7.2 presents the stress strain curves for tensile models at grain angles of 0°, 45° and 90° with low and high moisture contents in order to examine the anisotropic stress strain behaviour in tension for different grain orientations.

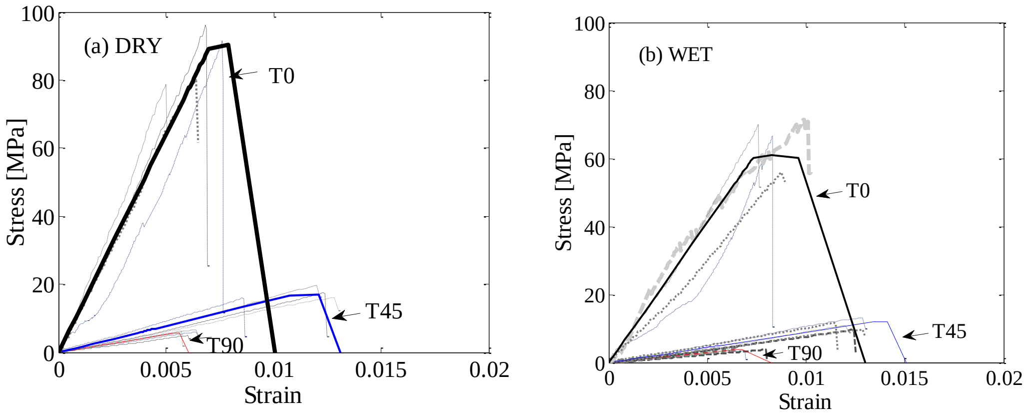

Fig. 7.2 Stress strain curves predicted by the constitutive model (solid lines) compared with measured tensile data (grey dash/dotted lines) of eucalyptus wood specimens for three angles α=0°, 45° and 90°; Left plot, dry cases, right plot, wet cases; T0, α=0°; T45, α=45°; T90, α=90°.

In the experimental results, after a relatively linear stress strain relationship, an abrupt brittle fracture is observed. As the grain angle increases, the slope of the stress-strain curve becomes less, which implies that the tensile stiffness decreases with an increase in grain angle. The experimental and numerical results in wet conditions show lower stress and more ductility compared with the corresponding dry cases covering the same three grain angle situations (*Fig 7.2*). The element deletion technique in Abaqus is adopted here to model the tension rupture by means of an option in VUMAT. This technique removes the contribution of the element to the overall structure when its ultimate strength is reached and decreases the stresses to zero. It is thus able to predict accurately the abrupt brittle fracture in tension for *E. nitens* compared to the model predicted stress strain curve without element deletion (*Fig 7.3*). A comparison between the experimental work and the numerical predictions confirmed reasonable agreement with the numerical curves for each case (*Fig 7.2*). A reduction in the tensile strength with an increase in grain angle was found both below and above *FSP*, which showed that the model presented high anisotropic behaviour in agreement with the experimental findings (*Fig 7.2*). It also proved that the von Mises model was not suitable for modelling *E. nitens* wood in off-axis tension both below and above *FSP*, as it showed a constant tensile strength (*Fig 7.3)*.

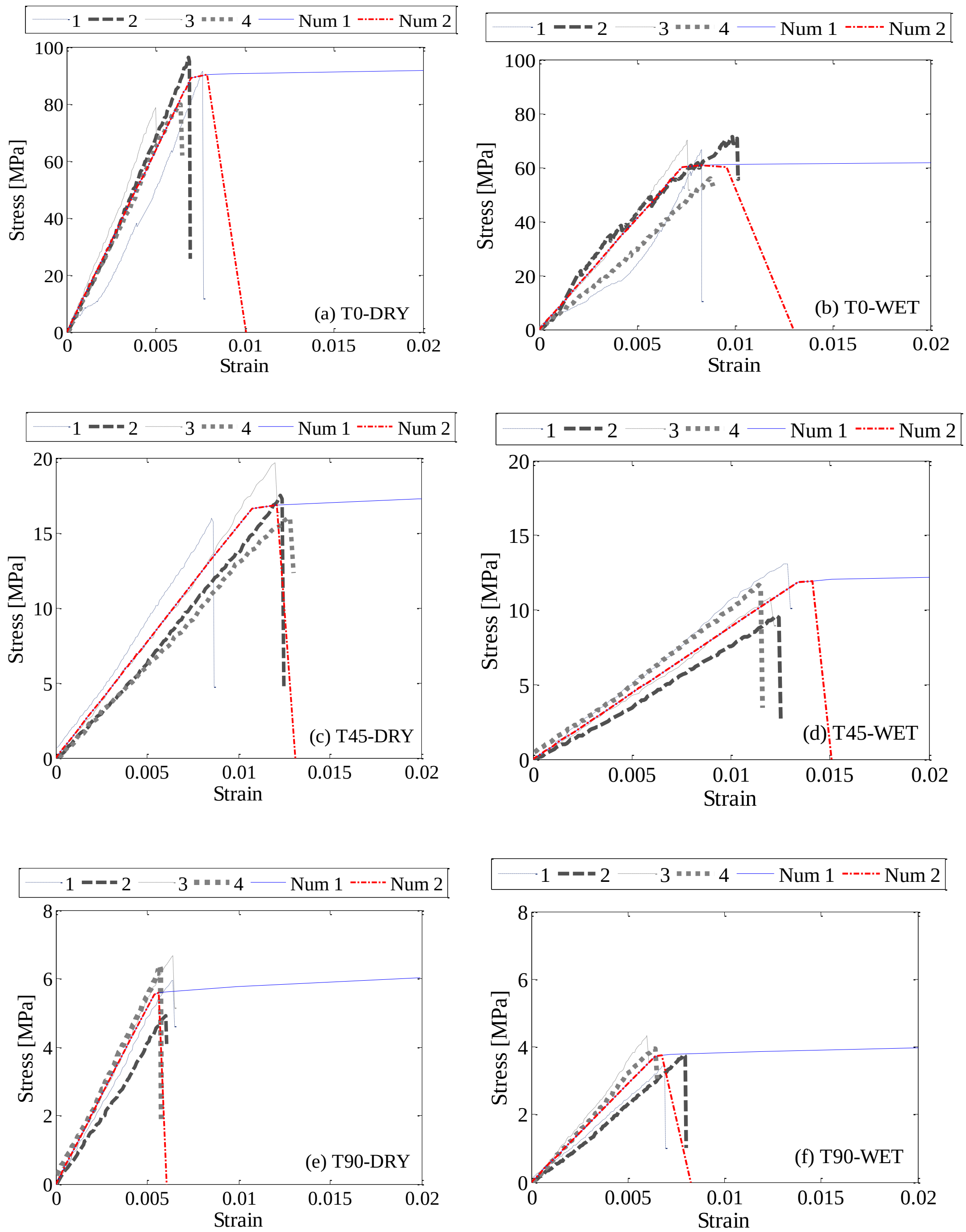

Fig. 7.3 Stress-strain curves predicted by constitutive model (solid lines) and measured tensile data (grey dash/dotted lines) for three angles, α=0° (a, b), 45° (c, d), and 90° (e, f). Left, dry cases, right, wet cases, Num 1, without element deletion, Num 2, with element deletion

7.2.2 Failure envelopes on tension side

For off-axis tension on *E. nitens* in dry and wet conditions, stress paths at grain angles of 0°, 10°, 45°, and 90° in the first quadrant of the L-R principal space are shown in *Fig. 7.4* with failure envelopes. Linear numerical stress paths for each tensile loading direction were found, whilst the wet cases had lower tensile strengths compared with the dry cases (*Fig 7.4*). These findings implied that moisture content affected the values of the tensile strengths both along and across the wood fibre. The failure envelopes of timber *E. nitens* timber on the tension side enlarged as the moisture content decreased.

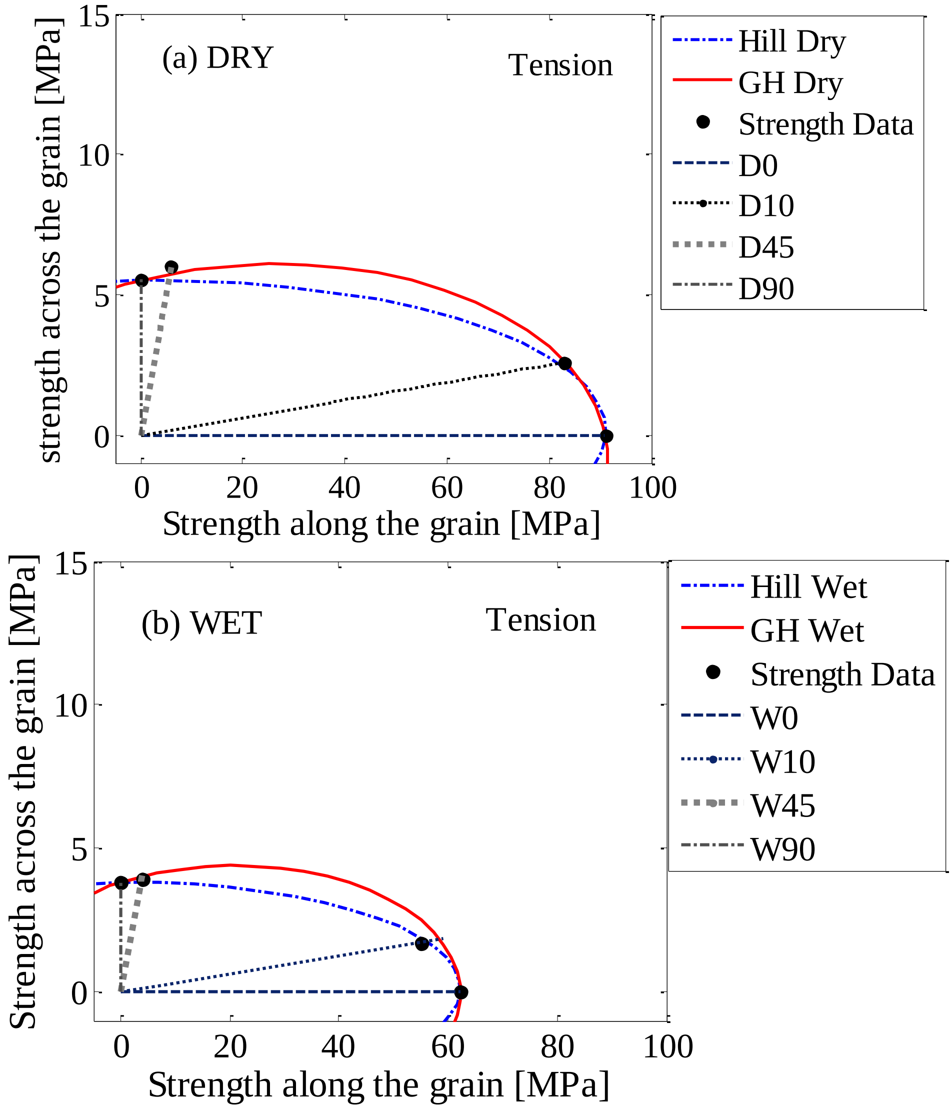

Fig. 7.4 Failure envelopes of *E. nitens* timber with (a) low and (b) high moisture contents in the first quadrant of the L-R principal space. The dots present the mean values of experimental data. The black lines present 2-D numerical stress paths for off-axis tension at grain angles of 0°, 10°,45°and 90°. Values of parameters to determine the failure envelopes are provided in the last two columns of Table 6.6. HILL, Hill criterion; GH, generalised Hill yield criterion used in the proposed constitutive model.

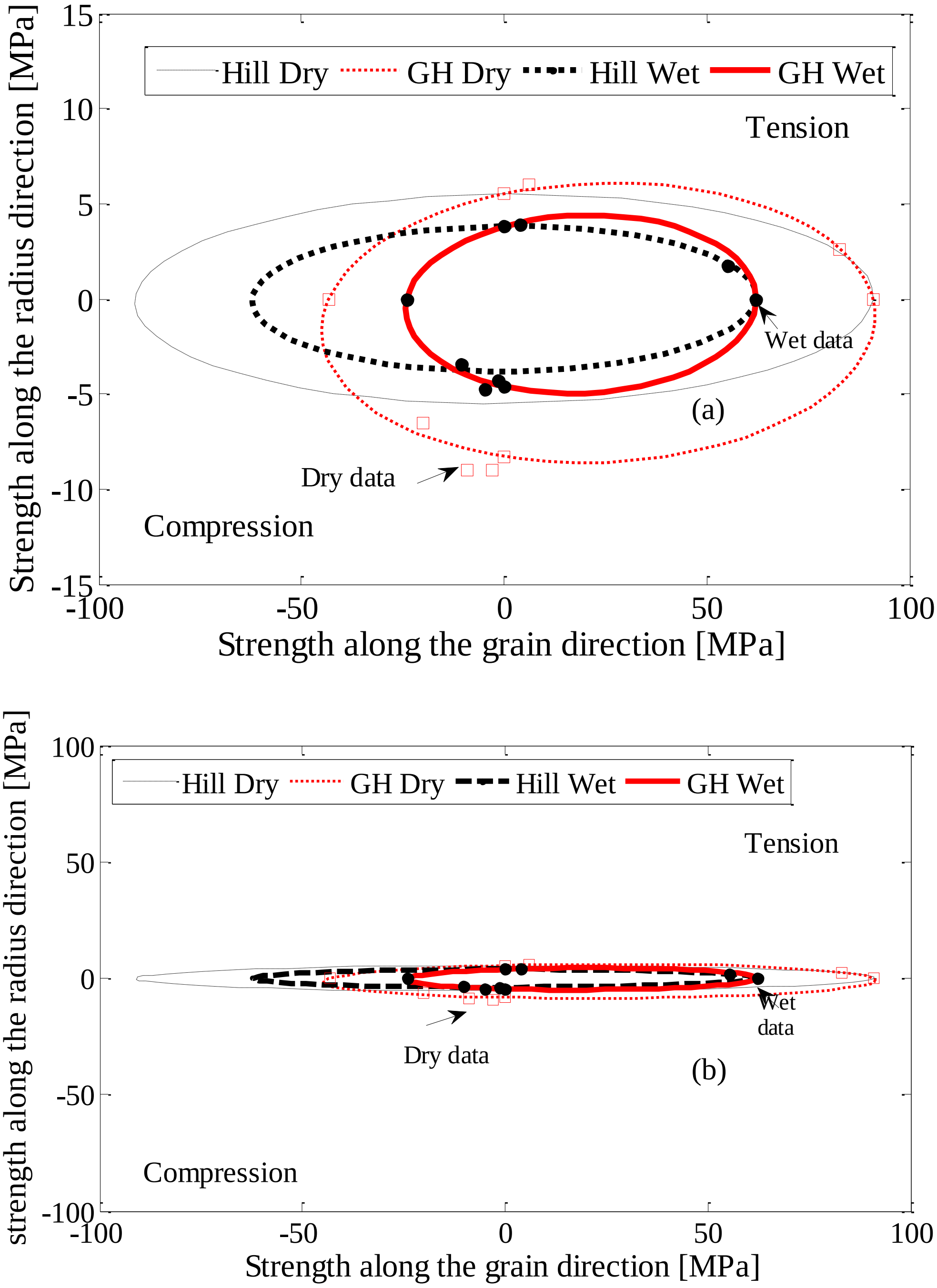

Fig. 7.5 Failure envelopes for *E. nitens* timber at dry (*MC*=12%) and wet (*MC*>*FSP*) conditions compared with experiments. HILL, Hill criterion; GH, generalised Hill yield criterion used in the proposed constitutive model. The dots present the mean values of experimental data for compression testing described in Chapter 3 and for tension testing described in Appendix 2.

Similar to the findings for compression, the failure envelopes predicted by the proposed failure criterion (GH), Eq (5.6), matched better with the experimental data than those predicated by the Hill model due to the tensile and compressive strengths of *E. nitens* timber being different (*Fig 7.5a*). This demonstrates that the developed constitutive model is more suitable to describe the anisotropic behaviour of *E. nitens* timber than the Hill model both above and below *FSP*. For tensile strength perpendicular to the grain, the failure strengths for both dry and wet conditions are closer to each other compared with those along the wood fibre (*Fig 7.5b*). This is because the tensile failure mode perpendicular to the grain differs from that parallel to the grain due to the microstructure of wood: ie. long and narrow cells are oriented in a longitudinal direction and act like columns of fibre.

7.2.3 Comparison with the simulation in compression

In this section, the stress-strain curves calculated using the proposed constitutive model (GH), with and without symmetry in tension and compression, were compared with those from the von Mises model (VM) and the Hill model (HL). The same parameters provided in *Table 6.1* were used. The moisture dependent anisotropic elastio-plastic model demonstrated more accuracy in modelling the anisotropic behaviour of *E. nitens* with comparison to the isotropic Hill and von Mises models as they assume the same strength values for tension and compression (*Fig 7.6a, b*), while different strengths in tension and compression were observed in experiments on *E. nitens* samples, see *Fig 7.5*. Therefore, the proposed constitutive model is an improvement on the von Mises and the Hills models for modelling anisotropic tensile and compressive behaviours both below and above *FSP* for *E. nitens.* It should be noted that the numerical examples presented herein are intended to demonstrate the features of the moisture dependent anisotropic elastio-plastic model, taking into account differences in tension and compression. Therefore, the softening and tensile rupture behaviours were not included. A ductile failure mechanism is found in compression experiments compared with the rupture failure behaviour in tension.

Table 7.3 shows the failure strengths of *E. nitens* timber for off-axis tension and off-axis compression in dry and wet conditions, respectively, at grain angles of 0°, 45° and 90°.For both tension and compression, as the grain angle increased, the failure strength decreased, implying the strengths of *E. nitens* timber were obviously dependent on grain direction, ie., the highest failure strengths were found parallel to the grain while the lowest strength values existed when the load was perpendicular to the grain for both tension and compression. A higher tensile failure strength along the grain than that under compression was found both above and below *FSP*. Compare with the dry cases, lower failure strengths were found for wet cases for the three grain angle situations, implying an increase in the risk of *E. nitens* failure with an increase in *MC*.

The present work found that the failure strengths and the mechanical behaviour of *E. nitens* timber in tension and compression were different above and below *FSP*. The correlation between the model predictions and the experimental data showed that the proposed constitutive model was more effective for modelling *E. nitens* wood for anisotropic tensile and compressive behaviours compared with the von Mises and Hill models because it took the asymmetry in tension and compression into account.

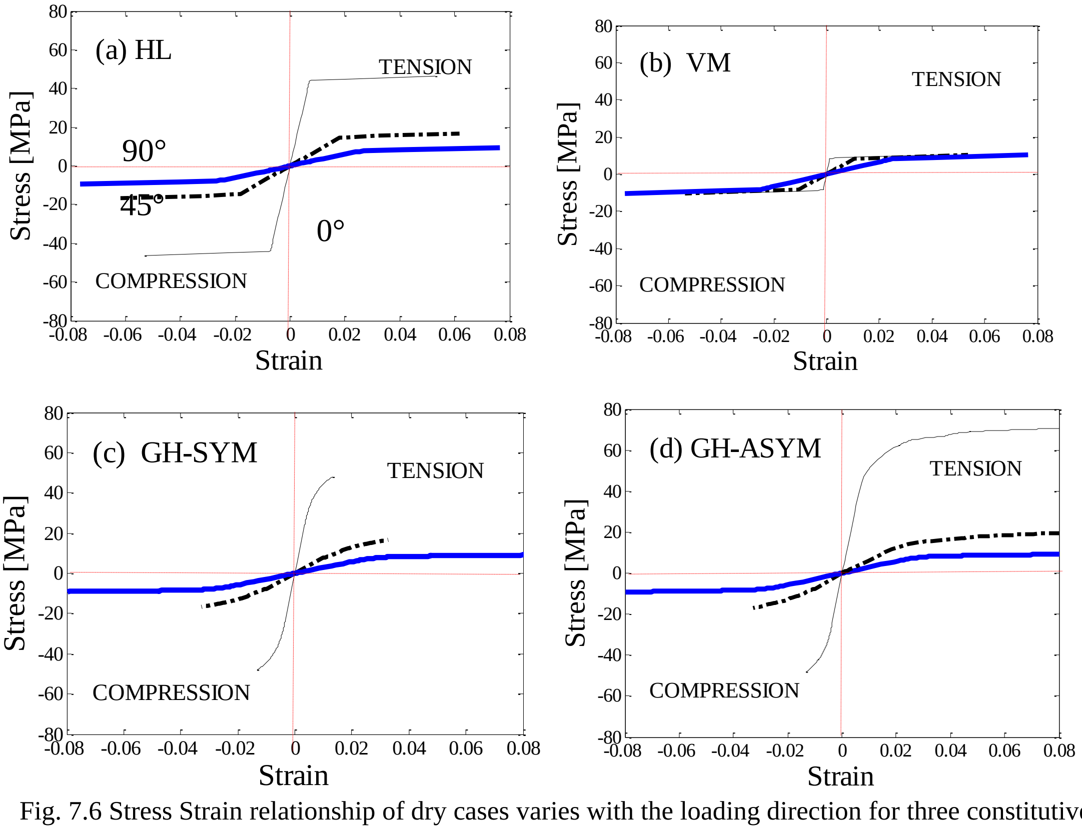

Fig. 7.6 Stress Strain relationship of dry cases varies with the loading direction for three constitutive models: (a) HL, Hill model, (b) VM, von Mises model, (c, d) GH, proposed constitutive model without (c) and with (d) difference in tension and compression

		Compression			**Tension**		
	Grain angle (°)	0	45	90	0	45	90
DRY (*MC*=12%)	Failure strength (MPa)	43.2	18	8.3	91	12	5.5
WET (*MC*>*FSP*)	Failure strength (MPa)	23.9	9.6	4.6	62.2	7.86	3.8

Table 7.3 The failure strengths from testing in off-axis tension/compression at grain angles of 0°, 45° and 90°. The compressive strengths are determined from the experimental data provided in Table 3.3, while the tensile strengths are from the experiments discussed in Fig 7.4

7.3 FLEXURAL NUMERICAL MODELLING

This section examines the nonlinear bending behaviour of *E. nitens* timber using the FEM approach with a moisture-dependent anisotropic elasto-plasticity model to give an insight into the failure mechanism of *E. nitens* in bending. Experimental load-deflection curves for *E. nitens* four point bending samples with low and high moisture content as shown in Chapter 4, were used for calibrating the parameters of the constititive models. Three-dimensional Finite Element Models were constructed, which precisely reflected the experimental work in the Chapter 4. See *Fig 7.7* for loading and boundary conditions. The working span was 360mm long divided into 3 spans of 120mm each (*Fig 7.7*). In detail, the model was loaded with two uniform pressure loadings acting at the one-third and two-third positions. The area of each loading surface was 250 mm^2 to avoid any stress concentration and the supporting points were restricted from any three-dimensional movement.

The dimensions of the model, 410mm (Length) × 25mm (Width) × 25mm (Depth), corresponded to the dimensions of the actual *E nitens* timber samples. The geometry in all the analyses was discretised by 54000 general purpose linear brick elements (C3D8R) with plasticity capabilities. The model has a longitudinal direction in the Z-axis and radial and tangential directions follow the X-axis and Y-axis in the global coordinate system, respectively. The local coordinate system will rotate clockwise around the Y-axis in the global coordinate system at an angle (φ) to explore the effect of the grain angle on bending behaviours of *E. nitens* beams.

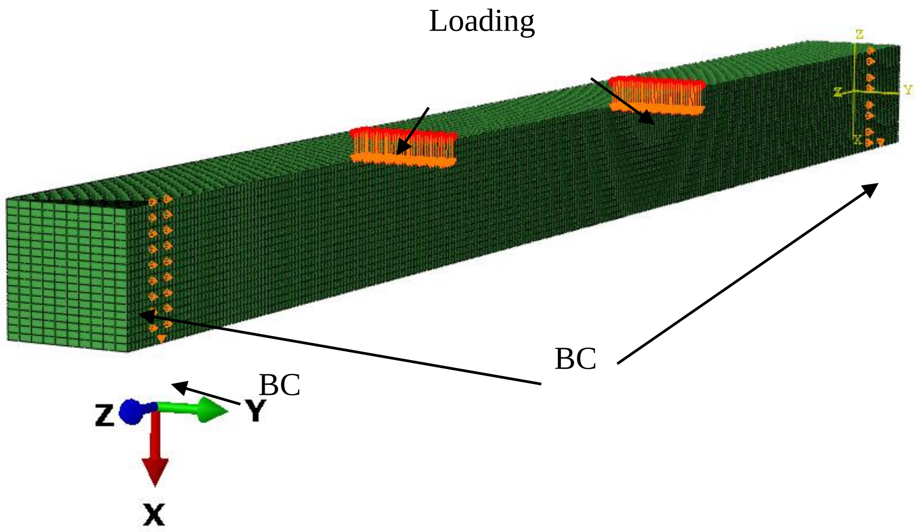

Fig. 7.7 FEM modelling for *E. nitens* samples in four-point bending; BC means boundary conditions.

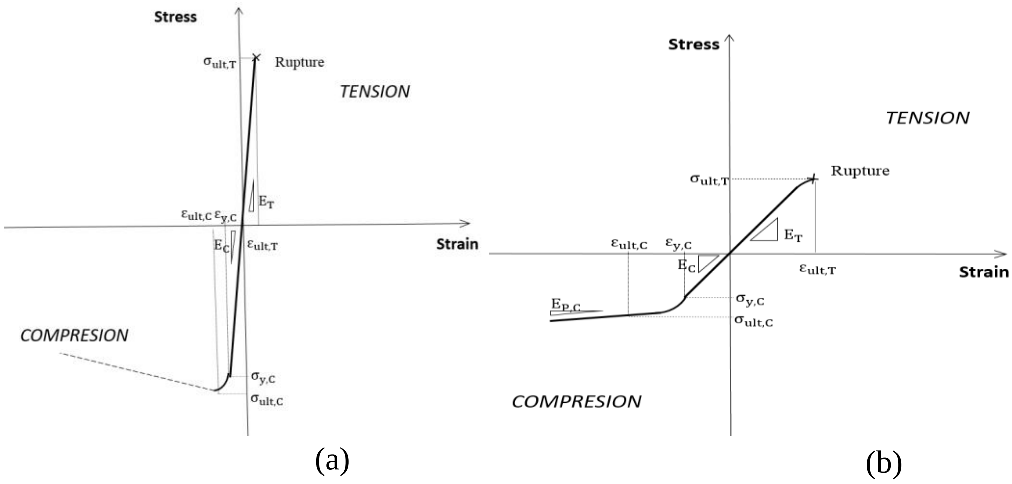

Fig. 7.8 A schematic of strain-stress behaviour for the moisture-dependent anisotropic elasto-plasticity model; (a) strain-stress curves for loading parallel to the grain; (b) strain-stress curves for loading perpendicular to the grain

E_c is compressive stiffness, $E_{p,c}$ *is* hardening compressive stiffness, E_T is tensile stiffness, $\sigma_{Ult,T}$ is ultimate tensile stress, $\varepsilon_{Ult,T}$ is ultimate tensile strain, $\sigma_{Ult,C}$ is ultimate compressive stress, $\varepsilon_{Ult,C}$ is ultimate compressive strain, $\sigma_{y,c}$ is yield compressive stress, $\varepsilon_{y,C}$ is yield compressive strain.

During the simulation, only material nonlinear analysis was used, for simplicity, without consideration of geometric nonlinearity. A schematic for a stress and strain curve of

E. nitens wood is provided in *Fig 7.8*. Experiments on *E. nitens* found tension occurred parallel and perpendicular to the grain, followed by an elastic relationship with rupture at the end of the curve [94], while compressive behaviour transformed from softening to hardening as the direction of loading changed from parallel to perpendicular to the grain, (see Chapter 3). Tension rupture was modelled using the element deletion technique in ABAQUS.

For the longitudinal direction, *MOE* (Moduli of elasticity) of 11.8GPa and 9.5GPa were used for dry and wet cases respectively, with a moisture modification factor at 0.8. The value of tensile strength for the dry case and the strength reduction factor for *MC*>*FSP* used in the simulation were 89.2 MPa and 0.7, respectively. These values were optimized to obtain the minimal relative error for the numerical load displacement curve compared with the mean curve for the experimental data. Other parameters of the moisture-dependent anisotropic elasto-plasticity model were provided in *Table 6.1* and *Table 6.3* with the assumption that they were the same. This assumption is reasonable for the transverse direction, as experiments on *E. nitens* specimens showed similar values (*Fig 7.5*).

7.3.1 Load-displacement curves compared with experimental results

For four-point bending modelling, the angle between the direction of the wood fibre and the longitude of the *E. nitens* beam is defined as the grain angle, θ . The term ASYM effect refers to the difference between tensile and compressive yield stresses. A parameter, α , shows the ratio between the tensile and compressive yield stresses used in the simulations, ie., when $\alpha=1$, it means the tensile and compressive yield stresses are the same, while $\alpha=2$ indicates that compressive tensile yield stresses are half the corresponding tensile yield stresses. In this model, for an ASYM effect case, the ratio between the tensile and compressive yield stress is 2. This means that the tensile strength is 2 times than the compressive strength.

Fig 7.9 represents the load-displacement curves for bending behaviour in *E. nitens* numerical models at the loading points, compared with the experimental data from *E. nitens* specimens. The wet cases exhibited more plastic deformation after the initial linear elastic phase and had considerably larger deflections at lower maximum loads.

Their correlation in the elastic range and nonlinear displacements implied that the elastic deformations and the hardening law for plastic evolution of the proposed constitutive model were reasonable for *E. nitens* including the effect of moisture content on bending.

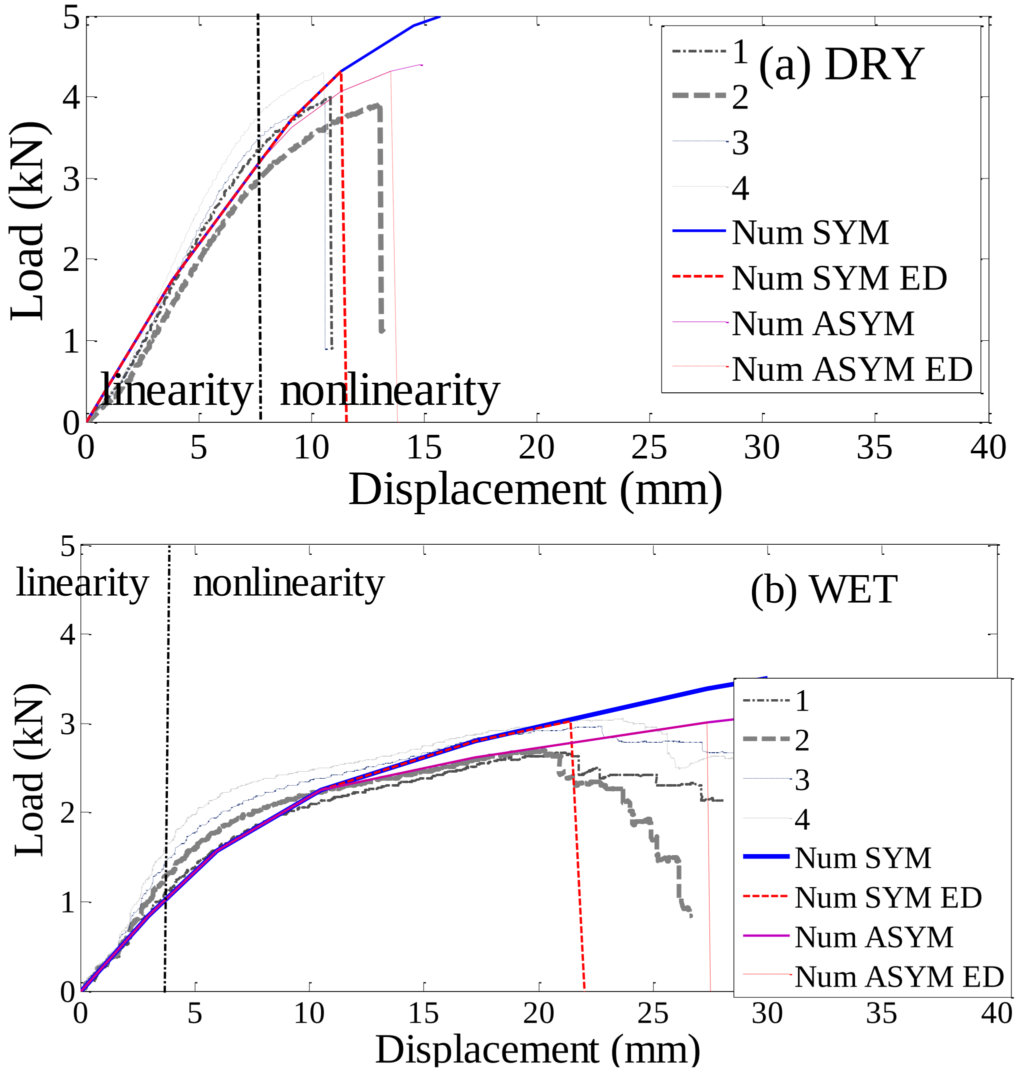

Fig. 7.9 Load-displacement behaviour for four point bending numerical analyses on small clear *E. nitens* models compared with the experimental data. (a) Dry cases and (b) Wet cases. Solid blue and purple lines show the numerical result (asym and sym means asymmetry and symmetry cases, ED means element deletion), grey lines show the experimental results.

The numerical predictions with element deletion in the tension side were more realistic for modelling the rupture in bending. While asymmetry case is more accurately to reflect the load-displacement curves of experiments compared with symmetry case. Therefore, differences in tension and compression should be considered in order to give more insight into the bending behaviour of *E. nitens* timber. It should be noted that, numerical bending behaviour in load-displacement curve for wet cases was not a good fit with the experimental data post the ultimate strength was reached. It is perhaps that the constitutive model does not include softening and the "softening" behaviour in compression parallel to the grain was obviously observed in the experiment for *E. nitens* timber. Future work will include softening behaviour to examine more deeply the failure behaviour of *E. nitens* in bending when the post ultimate strength stage is reached.

7.3.2 Effect of grain angle and moisture content

Fig 7.10 shows that the difference between the cases with and without the ASYM effect increased as the grain angle increased at the 1 kN loading for both dry and wet conditions.

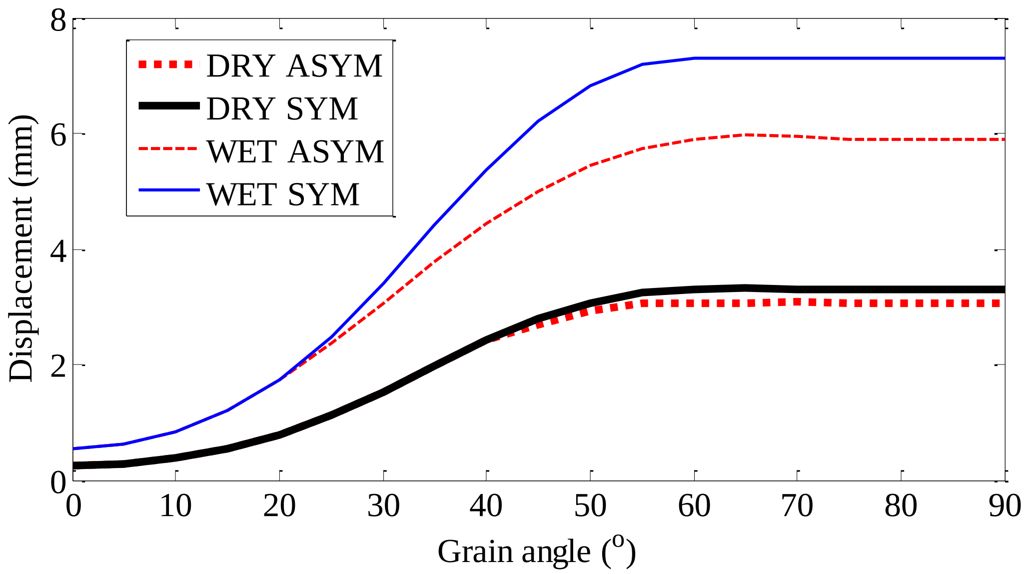

Fig. 7.10 Relationship between grain angle and displacement at mid-span of the *E. nitens* beam

As the fibre angle increased, the displacement of mid-span of the *E. nitens* beam at the 1 kN loading increased for both dry and wet cases. This was because the normal elastic modulus (E_{LL}) along the fibre is significantly higher than that across the fibre (E_{RR}), and therefore, the relationship between the mid-span displacement and the grain angle progressively increases.

Differences in mid-span displacement with and without ASYM effect progressively increased as the grain angle increased. For dry cases, below a fibre angle of 40°, the mid-span displacements at the 1 kN loading for the cases with and without ASYM effect matched very well, due to the beam staying in the elastic range. This implied the model was fully elastic and that the tensile /compressive yield stress was not reached below the grain angle of 40°. For grain angles between 40° and 90°, the mid-span displacement for the ASYM effect case is lower than the displacement without ASYM effect.

It was also found that a larger mid-span displacement correlated well with a higher *MC* (see *Fig 7.10*, in which solid lines plot data for *MC*=12%, while solid lines with circles plot data for *MC*>*FSP*). The correlation between the displacement at the mid-span and the moisture content is clearly visible.

7.4 SUMMARY

In this Chapter, the anisotropic effect on *E. nitens* timber failure was illustrated numerically by both off-axis tension and four-point static bending with different grain angles at low and high moisture contents. The validation of the numerical modelling was also demonstrated by comparisons with the experimental data below and above the *FSP*. Thus, the final Objective was achieved. The findings can be summarized as follows.

- The anisotropy of tensile strengths for *E. nitens* was found to affect by loading direction and moisture content. The wet cases had lower tensile strength along the wood fibre compared with the dry cases, however, when it came to tensile strength perpendicular to the grain, the failure tensile strengths for both dry and wet cases were similar.

- The moisture dependent anisotropic elastio-plastic model demonstrated with more accuracy the anisotropic behaviour of *E. nitens* compared to the isotropic Hill and von Mises models, including differences in tension and compression. The proposed constitutive model implemented by FEM has overcome the limitations in the analytical approach, eg. Hankinson's equation, which only takes account of the effect of normal stresses, and it can reproduce the anistropic behaviours of *E. nitens* timber more realistically.

- Moisture content was a key influence in the bending failure of the *E. nitens* beam, whilst grain angle also strongly affected failure.
- FEM techniques combined with the newly developed moisture dependent anisotropic elastio-plastic constitutive model in Chapter 5 provided a new approach to establishing design codes for *E. nitens* timber beams both for normal use and in water saturated applications.

Using the proposed constitutive model, the nonlinear bending behaviours of fibre managed plantation *E. nitens* timber were examined numerically based on the properties of small clear *E. nitens* samples. However, some strength properties of wood exhibits stressed volume dependency, which is known as size effects. This phenomenon exists in all the major strength properties and are more important is more important where actions result in tension strength perpendicular to the grain often associated with sloping grain. Therefore, further work could examine how size effects contribute to the variation in ultimate strength of structural sized *E. nitens* timber members using FEM based on the proposed constitutive model. The further research, could also establish relevant design codes via FE methods to facilitate using this resource for building and structural applications.

Chapter 8

8 CONCLUSIONS AND FUTURE WORK

8.1 INTRODUCTION

Current thinking has shown that fast growing plantation eucalypts have the potential for structural applications. This thesis aimed examine the suitability of *E. nitens* for use as a structural material and to provide an improved systematic understanding of the moisture dependent anisotropic mechanical behaviour of *E. nitens* timber during short duration loading.

To understand this behaviour, experimental, theoretical, and numerical approaches were combined. Firstly, compression and four-point bending experiments on *E. nitens* samples were carried out under low and high moisture conditions. Here, low means the moisture content (*MC*) was round 12% and high means the moisture content was above the *FSP*. The moisture content sensitivity and anisotropic behaviour of *E. nitens* timber were studied using an experimental approach. Secondly, a 3D moisture dependent anisotropic plasticity model for *E. nitens* timber was proposed for the first time to predict a more accurate ultimate capacity for such timber. In this model, the Drucker–Prager yield criterion was combined with the Hill yield criterion to create a generalized yield criterion where each material constant was defined as a function of moisture content. The model was then implemented with a stress update scheme based on the framework of the finite element method (FEM). Experimental data for other species with varying loading directions or varying moisture content, and for *E. nitens* timber in compression below and above its *FSP*, were used in order to validate and calibrate the numerical work. Thirdly, numerical modelling on *E. nitens* timber was undertaken, and the underlying anisotropic failure mechanism of *E. nitens* timber explored. Those numerical studies overcame the limitations of previous attempts based on experiments or theoretical work only, as moisture dependent material properties are very difficult to measure and examine separately using an experimental approach, due to the heterogeneous behaviour of natural wood, and no analytical solutions existed due to wood's nonlinear material characteristics.

8.2 CONCLUDING REMARKS

In Chapter 3 and Chapter 4, Objective One and Two, to quantify the short-term response of Eucalyptus wood under compression and bending during low and high moisture conditions were attained**.** The goal of this study was to characterize the mechanical properties of plantation *Eucalyptus nitens* in a high moisture content state, above the *FSP*, in comparison to a low moisture condition, and to explore construction applications in a completely water saturated state. In this study, compression and four-point bending experiments on small clear *E. nitens* samples were carried out using a Universal Testing Machine. The samples were obtained from a 16-year-old plantation *E. nitens* resource in Tasmania, Australia. The moisture content sensitivity and its effect on mechanical behaviour of *E. nitens* in compression and bending were studied.

Key findings can be summarised as follows.

<u>Mechanical compressive properties in Chapter 3:</u>

- Load and deflection curves as well as the failure mode of the *E. nitens* specimens in compression, which can be used to verify modelling of the mechanical failure behaviour of Eucalyptus wood in compression using FEM, were obtained from experiments.

- Compressive stiffness and strength increase with a decrease in grain angle. These findings agree with the experimental data and Hankinson's formula, and they imply a validation of our research.

- The failure behaviour of both dry and wet samples was strongly dependent on grain direction. The wood samples were much stiffer in compression parallel to the grain (grain angle 0º) compared to perpendicular (grain angle 90º), and the decrease in compressive strength and stiffness was rapid between 0º and 15º, and more gradual between 15º and 45º; above 45º, little additional decrease was found. A grain angle of 45º represents the transition from an unstable "softening" type of behaviour when loaded parallel to the grain to a more stable "hardening" type behaviour when loaded perpendicular to the grain.

- The failure envelope of plantation-grown *E. nitens* in compression is a 1/4 elliptical arc with the short axis in the radial direction and the long axis in the grain direction since the strength parallel to the grain is much higher than perpendicular to the grain. Compressive behaviour of plantation *E. nitens* is highly anisotropic for a broad *MC* range above and below the *FSP* and is sensitive to moisture content.

- The suggested design characteristic values of dry and fully water-saturated plantation-grown *E. nitens* piles in compression are 20.3 and 11.8 MPa, respectively. These values are close to the testing results from structural sized spruce pile specimens in axial compression in a dry state, 20.3 MPa, and in a wet (water saturated) state, 13.4 MPa [9], showing *E. nitens* can be a material for structural use, and can meet the requirements for compression members, such as columns and piles.

<u>Mechanical flexural properties in Chapter 4:</u>

- The high (*MC*) samples exhibited larger displacements at low ultimate loads, while the low *MC* samples showed quite abrupt failures at relatively small displacements with high ultimate loads.

- A linear-regression model was developed in the study using bending stiffness as the single regressor in predicting the bending strength of the beam. The correlation between bending stiffness and strength was also sufficiently close to allow estimates of *MOR*, by adjusting the *MOE*.

- A normal distribution better fitted the experimental data than a lognormal distribution. The design characteristic values for *E. nitens* with low and high *MC* were 68.5 MPa and 39.8 MPa, respectively.

- The moisture modification factor was 0.55 at a 5% percentile level and 0.7 at mean level, respectively, demonstrating that *MC* significantly affects the *MOR*. The moisture modification factors of *E. nitens* timber at mean level are higher than those of traditional construction materials, such as *Pinus radiata* (0.52), implying that *E. nitens* is promising as a material to be used in the construction industry for bending members especially in water saturated conditions.

The mechanical compressive and flexural properties of *E. nitens* timber below and above *FSP* have been determined in this thesis. This is because apart from those for fully immersed piles [64, 117, 118], few design standards provide strength and stiffness values for round wood at *FSP* and above. Those that do are for coniferous species only [9, 64, 117] and it is now necessary to develop the same standards for plantation eucalypts in order to use this resource for structural application. Experimental studies showed that *E. nitens* has anisotropic mechanical properties. This research on design values will provide basic data for *E. nitens* in structural applications, especially when exposed to water. However, the heterogeneous nature of natural wood introduces variations to experimental results, and these variations cannot easily be separated by experimental approach. In other words, the experimental results are empirical and only tell us the phenomenon. In order to understand the underlying failure mechanism of *E. nitens*, constitutive modelling with FEM technique was used to do numerical modelling for reflecting the stress state within timber structures and predicting their possible failure more realistically.

With the aim of achieving the Objective Three of the research, Chapter 5 proposed a moisture-dependent anisotropic elasto-plasticity model to display more realistically the short-term mechanical response in *E. nitens* timber with different moisture contents. This constitutive model is orthotropic in the elastic region while anisotropic in the plastic region and can systematically study the path-dependent elasto-plastic phenomenon of *E. nitens* timber with differences in tensile and compressive strength. In this constitutive model, a generalized Hill yield criterion was proposed combining the Drucker–Prager yield criterion with the Hill yield criterion to include asymmetry in tension and compression. All model variables depend on the moisture content and are obtained from corresponding experimental results.

Using a numerical approach, a UMAT subroutine within the commercial software ABAQUS was coded to model complex material behaviour according to the proposed moisture-dependent anisotropic elasto-plasticity model. The simulated yield surface, the stress strain curves and the load-displacement relationship agreed with the data from mechanical testing of wood, and compared favourably with the work of De Borst et al. [36], Hering et al. [14] and the experimental data from *E. nitens* samples. This showed that the proposed constitutive model can be used for timber with various moisture contents and in different load to grain orientations. Results indicate that the proposed constitutive model could predict the stiffness and strength of *E. nitens* in dry and wet conditions as a function of inclined grain orientation with reasonable accuracy, showing that the material model can be utilised for Eucalyptus wood. The yield stress of the *E. nitens* timber in the longitudinal direction was much higher than in the other two directions, i.e., the radial axis and the tangential axis. This implies that *E. nitens* timber was anisotropic in contrast to a typical Von Mises criterion, which is a circular cylinder. Also, the radius of the yield surface in the "π" plane increased with a decrease of hydrostatic pressure, ie. opposite to the normal Hill criterion, but like the Drucker–Prager criterion, due to asymmetry between the tensile and compressive sides.

The constitutive model was a breakthrough in the constitutive modelling of wood, providing results for a comprehensive study of anisotropic plastic constitutive behaviour incorporating anisotropic and moisture effects. This is because previous studies applied plasticity theory with a nonlinear isotropic hardening response [24, 30], for example for Norway spruce and European beech wood. However, when modelling the anisotropic mechanical behaviour of *E. nitens* timber, the isotropic hardening law is not always appropriate. The compressive behaviour of wood in the longitudinal direction and the radial direction is different: the stress-strain curve changes from "softening" to "hardening" from the longitudinal direction to that perpendicular to the grain [51, 52]. Including elastoplastic anisotropy in the proposed constitutive model, the load carrying capacity of *E. nitens* timber can be examined more accurately, compared with the isotropic Hill criterion, which is widely used in timber engineering to describe wood anisotropy [24]. It should be noted that the moisture dependent anisotropic elastio-plastic model did not include softening. Future work could include softening in order to deeply examine the residual stress distribution within the *E. nitens* timber after failure.

As the last two Objectives in the research project, the underlying anisotropic behaviour of *E. nitens* timber was examined numerically with the aid of the ABAQUS software in Chapter 6 and Chapter 7.

Findings can be summarised as follows.

<u>Anisotropic compressive behaviours in Chapter 6:</u>

- Anisotropic inelastic behaviour was detected numerically for *E. nitens* timber under compression, both below and above *FSP*, the stress along the loading direction not only increased as the strain increased but also rose with a decrease in grain angle. Numerical compressive stiffness and strength values decreased sharply with increasing grain angles up to 45° and levelled off above 45° for dry and wet cases.

- Grain angle had a stronger effect on anisotropy compressive behaviour of *E. nitens* timber compared with moisture content. Shear stress increased with an increase in grain angle at the beginning, then after shear stress reach its peak, it decreased with further increases in grain angle and became zero at a grain angle of 90°. At loading directions of 30°, 45° and 60°, shear stress played a leading role and therefore, failure mode of the *E. nitens* timber is mainly due to fibre-layer slip delamination and shear deformation, which is observed in the experiment presented in Chapter 3. Fibre buckling is found at a grain angle of 0° since the normal stress along the grain is dominant, whilst normal stress across the grain is significant at compression perpendicular to the grain (90°), correlating to the crushing failure.

- The shape of the initial yield surface enlarged with a decrease in moisture content, showing that the yield stress of the *E. nitens* timber is sensitive to moisture content. For both dry and wet, before yield, the *E. nitens* wood presents an elastic deformation, which means a linear and fully recoverable material behaviour. The stress paths were within the initial yield surface. Post yield, the elliptical shape of the evolved yield surface changed, and both the long axis (longitudinal direction) and the short axis (radial axis direction) enlarges.

- Using FEM, a uniform stress distribution during a pure compression test on *E. nitens* specimens was found both below and above *FSP*. This means that, for a homogeneous material, the stress at any location within the specimen with low and high moisture content under compression is the same. A progressive change in displacement along the compression at a central area of the samples could be also distinctly observed.

- According to parametric investigation in the L-R plane (i.e., in a plane parallel to the fibres and perpendicular to the growth rings), there was no significant effect of Poisson's ratios on compressive stiffness and strength during grain angles from 0° to 90°. For other parameters, the compressive stiffness at loading direction (responding compressive stiffness) mainly depended on elastic parameters (normal moduli and shear moduli), while the plastic parameters played an important role on the compressive strength at loading direction.

Anisotropic failure mechanism of *E. nitens* timber in Chapter 7

- The anisotropy of *E. nitens* timber in tension was also proved together with moisture content sensitivity, but few developments of the failure surfaces were found at a given *MC* as there were no plastic deformations in tension.
- The wet cases had lower tensile strength along the wood fibre compared with the dry cases, however, when it comes to tensile strength perpendicular to the grain, the failure strength for both dry and wet were similar.
- A moisture dependent anisotropic elastio-plastic model demonstrated with more accuracy the anisotropic behaviour of *E. nitens* in comparison to the isotropic Hill and von Mises models, including differences in tension and compression.
- The numerical tensile strength values against grain angle are consistent with the results of experimental data, and broadly agree with Hankinson's equation whereby the largest difference is in the range between grain angles of 10° and 45°, where shear stresses exist. The proposed constitutive model implemented by FEM has overcome the limitations in the analytical approach, eg. Hankinson's equation, which only takes account of the effect of normal stresses, and it can reproduce the anistropic tension behaviours for *E. nitens* timber more realistically.
- Moisture content and grain angle were key influences in the bending failure of the *E. nitens* beam, whilst differences in tension and compression also affected load displacement curves of *E. nitens* timber in bending.

In Chapter 6 and 7, the underlying anisotropic failure mechanism of *E. nitens* timber was explored. The inherent stresses within *E. nitens* timber link strongly with its failure mode. However, the current study assumed an idealised homogeneous material feature for *E. nitens* timber, whereas the non-uniformity of wood leads to a large variation in failure behaviours in *E. nitens* samples, as has been observed in experiments. Further work is required to examine the effect of size effect on the failure mechanism of structural sized *E. nitens* timber members with numerical modelling the heterogeneity of wood material. Also, although the prediction of anisotropic plasticity behaviour for *E. nitens* timber using the proposed constitutive model for low and high moisture contents agreed with experiments on defect free samples, coupled effects between shear stresses and normal stresses has not been included in the newly developed constitutive model. Therefore, a further study on such effect on the failure of structural sized *E. nitens* timber members using numerical approach based on a constitutive model with such coupled effects is also required. Moreover, this model focused on idealised (i.e., defect-free) wood in short term loading scenarios, whereas the influence of long-term loading leads to creep in *E. nitens* timber, and this has not been taken into account in this study. Further study could include long term properties in the moisture dependent anisotropic elasto-plasticity model in order to extend the use of this constitutive model, and its application to *E. nitens* as a new structural material.

In summary, one of the main contributions of this study was to examine the suitability of *E. nitens* as a new construction material and in this context compressive and flexure mechanical properties below and above *FSP* were discussed. *E. nitens* is promise as a material to be used in the construction industry for compressive or bending members, especially in water saturated condition. The results provide the basis for design codes for using *E. nitens* wood in dry and water-saturated applications. *E. nitens* has anisotropic mechanical characterization and its strength shows moisture content sensitivity. The second main contribution was to introduce a moisture dependent anisotropic plasticity model for wood, in particular for *E. nitens*. This creates a tool to predict the ultimate strength of *E. nitens* more accurately at various moisture contents and with different load directions.

8.3 SUGGESTED FUTURE WORK

This research is the first generation for the development of a moisture dependent anisotropic plasticity model for *E. nitens* wood as well as for use plantation E. *nitens* as a new structural material in compression and bending for both dry and water saturated states. This research has laid the groundwork to establish relevant design codes and specifications for using *E. nitens*. At the same time, the moisture dependent anisotropic plasticity model is not limited to the species examined in this thesis. Subject to the availability of experimental data to validate modelling, the model can be used for other wood species or material which has similar features.

Potential future work could:

- Model softening and crack development during damage to *E. nitens* structural members combined with cohesive interface elements to predict the initiation and propagation of interfacial cracks. This is because FE modelling work combined with a moisture dependent anisotropic plasticity model could predict compression and bending behaviours of *E. nitens* in dry and wet conditions with reasonable accuracy, and this can be considered as a suitable basis for fracture mechanical analyses.
- Include quantification of the contribution of knot groups to the mechanical compressive and flexure properties of *E. nitens* to create a predictive model for strength and performance of structurally sized *E. nitens* members with knots.
- Address the effect of varying moisture contents on the mechanical behaviour of structurally sized *E. nitens* timber members in compression and bending experimentally in order to better understand how structural *E. nitens* members respond under static loading with different moisture conditions.
- Etc. Further work could be risk assessment of *E. nitens* structural members especially when exposed to water**,** based on finite element analysis or using the design data in this research.

9 BIBLIOGRAPHIES

1. Pagel, C.L., R. Lenner, and C.B. Wessels, *Investigation into material resistance factors and properties of young, engineered Eucalyptus grandis timber.* Construction and Building Materials, 2020. **230**: p. 117059.
2. Šubic, B., G. Fajdiga, and J. Lopatič, *Bending Stiffness, Load-Bearing Capacity and Flexural Rigidity of Slender Hybrid Wood-Based Beams.* Forests, 2018. **9**(11): p. 703.
3. Derikvand, M., et al., *Characterisation of Physical and Mechanical Properties of Unthinned and Unpruned Plantation-Grown Eucalyptus nitens H.Deane & Maiden Lumber.* Forests, 2019. **10**(2): p. 194.
4. Bal, B.C. and İ. Bektaş, *The effects of some factors on the impact bending strength of laminated veneer lumber.* BioResources, 2012. **7**(4): p. 5855-5863.
5. Derikvand, M., et al., *Short-term and long-term bending properties of nail-laminated timber constructed of fast-grown plantation eucalypt.* Construction and Building Materials, 2019. **211**: p. 952-964.
6. Derikvand, M., et al., *Bending performance of nail-laminated timber constructed of fast-grown plantation eucalypt.* European Journal of Wood and Wood Products, 2019. **77**(3): p. 421-437.
7. Bailleres, H., G. Hopewell, and G. Boughton, *MOE and MOR assessment technologies for improving graded recovery of exotic pines in Australia, 2009.* Forest & Wood Products Australia (FWPA): Victoria, Australia.
8. Hein, P.R.G. and L. Brancheriau, *Comparison between three-point and four-point flexural tests to determine wood strength of Eucalyptus specimens.* Maderas. Ciencia y tecnología, 2018(ahead): p. 0-0.
9. Aicher, S. and G. Stapf, *Compressive strength parallel to the fiber of spruce with high moisture content.* European Journal of Wood and Wood Products, 2016. **74**(4): p. 527-542.
10. Ross, R.J., *Wood handbook: wood as an engineering material.* USDA Forest Service, Forest Products Laboratory, General Technical Report FPL-GTR-190, 2010: 509 p. 1 v., 2010. **190**.
11. AS1720, *Timber Structures Part 1: Design Methods.* Standards Australia, 2010. **Sydney, Australia**.
12. Lang, E.M., et al., *Orthotropic strength and elasticity of hardwoods in relation to composite manufacture part iii: orthotropic elasticity of structural veneers.* Wood and fiber science, 2007. **35**(2): p. 308-320.
13. Lang, E.M., et al., *Orthotropic strength and elasticity of hardwoods in relation to composite manufacture. Part II. Orthotropy of compression strength and elasticity.* Wood and fiber science, 2007. **34**(2): p. 350-365.
14. Hering, S., et al., *Characterisation of moisture-dependent plasticity of beech wood and its application to a multi-surface plasticity model.* Holzforschung, 2012. **66**(3).
15. Johnson, N.L., S. Kotz, and N. Balakrishnan, *Continuous Univariate Distributions, Vol. 1 (Wiley Series in Probability and Statistics).*
16. Bodig, J. and B.A. Jayne, *Mechanics of wood and wood composites*. Vol. 712. 1982: Van Nostrand Reinhold New York.
17. Polyanin, A.D. and A.D. Manzhirov, *Timber: its nature and behaviour*. 2000: CRC Press.
18. Yang, J. and R. Evans, *Prediction of MOE of eucalypt wood from microfibril angle and density.* Holz als Roh-und Werkstoff, 2003. **61**(6): p. 449-452.

19. Medhurst, J., et al., *Intra-specific competition and the radial development of wood density, microfibril angle and modulus of elasticity in plantation-grown Eucalyptus nitens.* Trees, 2012. **26**(6): p. 1771-1780.
20. Lara-Bocanegra, A.J., et al., *Finger-jointed Eucalyptus globulus with 1C-PUR adhesive for high performance engineered laminated products.* Construction and Building Materials, 2017. **135**: p. 529-537.
21. Gilbert, B.P., et al., *Veneer based composite hollow utility poles manufactured from hardwood plantation thinned trees.* Construction and Building Materials, 2014. **66**: p. 458-466.
22. Derikvand, M., et al., *What to Do with Structurally Low-Grade Wood from Australia's Plantation Eucalyptus; Building Application?* BioResources, 2016. **12**(1): p. 4-7.
23. Hassani, M.M., et al., *Rheological model for wood.* Computer Methods in Applied Mechanics and Engineering, 2015. **283**: p. 1032-1060.
24. Milch, J., et al., *Determination of the elasto-plastic material characteristics of Norway spruce and European beech wood by experimental and numerical analyses.* Holzforschung, 2016. **70**(11): p. 1081-1092.
25. Mackerle, J., *Finite element analyses in wood research: a bibliography.* Wood Science and Technology, 2005. **39**(7): p. 579-600.
26. Oudjene, M. and M. Khelifa, *Elasto-plastic constitutive law for wood behaviour under compressive loadings.* Construction and Building Materials, 2009. **23**(11): p. 3359-3366.
27. Hong, J.-P., J.D. Barrett, and F. Lam, *Three-dimensional finite element analysis of the Japanese traditional post-and-beam connection.* Journal of Wood Science, 2011. **57**(2): p. 119-125.
28. Clouston, P.L. and F. Lam, *A stochastic plasticity approach to strength modeling of strand-based wood composites.* Composites Science and Technology, 2002. **62**(10-11): p. 1381-1395.
29. Clouston, P.L. and F. Lam, *Computational modeling of strand-based wood composites.* Journal of engineering mechanics, 2001. **127**(8): p. 844-851.
30. Hering, S. and P. Niemz, *Moisture-dependent, viscoelastic creep of European beech wood in longitudinal direction.* European Journal of Wood and Wood Products, 2012. **70**(5): p. 667-670.
31. Hering, S., D. Keunecke, and P. Niemz, *Moisture-dependent orthotropic elasticity of beech wood.* Wood Science and Technology, 2011. **46**(5): p. 927-938.
32. Cheng, Y., et al., *Anisotropic material behaviour under compression of Eucalyptus nitens with high moisture content.* Construction and Building Materials, 2022. **314**.
33. Crafford, P.L. and C.B. Wessels, *The potential of young, green finger-jointed Eucalyptus grandis lumber for roof truss manufacturing.* Southern Forests: a Journal of Forest Science, 2016. **78**(1): p. 61-71.
34. Gilbert, B.P., et al., *Strength modelling of laminated veneer lumber (LVL) beams.* Construction and Building Materials, 2017. **149**: p. 763-777.
35. Gilbert, B.P., et al., *Mechanical properties of rotary veneers recovered from early to midrotation subtropical-hardwood plantation logs for veneer-based composite applications.* Journal of Materials in Civil Engineering, 2017. **29**(10): p. 04017194.
36. de Borst, K., et al., *Mechanical characterization of wood: An integrative approach ranging from nanoscale to structure.* Computers & Structures, 2013. **127**: p. 53-67.
37. Bader, T.K., et al., *Poromechanical scale transitions of failure stresses in wood: from the lignin to the spruce level.* 2010. **90**: p. 750-767.
38. Eberhardsteiner, J., *Biaxial testing of orthotropic materials using electronic speckle pattern interferometry.* Measurement, 1995. **16**(3): p. 139-148.

39. Fournier, M., et al., *Growth stress patterns in tree stems.* Wood Science and Technology, 1990. **24**(2): p. 131-142.
40. Gril, J., et al., *Tree growth stress and related problems.* Journal of Wood Science, 2017.
41. Hart, J.F., *A review of the effects of silviculture on wood quality.* 2010.
42. Chassagne, P., et al., *Three Dimensional Creep Model for Wood Under Variable Humidity-Numerical Analyses at Different Material Scales.* Mechanics of Time-Dependent Materials, 2005. **9**(4): p. 1-21.
43. Leicester, R.H., *A rheological model for mechano-sorptive deflections of beams.* Wood Science and Technology, 1971. **5**(3): p. 211-220.
44. Toratti, T., *Creep of timber beams in a variable environment*. 1992: na.
45. Patton-Mallory, M., *The three-dimensional mechanics and failure of single bolt wood connections*. 1996.
46. Tabiei, A. and J. Wu, *Three-dimensional nonlinear orthotropic finite element material model for wood.* Composite Structures, 2000. **50**: p. 143-149.
47. Leijten, A.J.M., H.J. Larsen, and T.A.C.M. Van der Put, *Structural design for compression strength perpendicular to the grain of timber beams.* Construction and Building Materials, 2010. **24**(3): p. 252-257.
48. Tsai, S.W. and E.M. Wu, *A General Theory of Strength for Anisotropic Materials.* 1971. **5**(1): p. 58-80.
49. Hill, R., *Theoretical plasticity of textured aggregates.* Mathematical Proceedings of the Cambridge Philosophical Society, 1979. **85**(1): p. 179-191.
50. Kazimi, S.M.A., *Solid mechanics*. 1984, New Delhi: Tata McGraw-Hill.
51. Reiterer, A. and S.E. Stanzl-Tschegg, *Compressive behaviour of softwood under uniaxial loading at different orientations to the grain.* Mechanics of materials, 2001. **33**(12): p. 705-715.
52. Franke, S. and P. Quenneville. *The Material Behaviour of Radiata Pine under Compression*. in *WCTE 2010 World Conference on Timber Engineering, Riva del Garda, Italy*. 2010.
53. Kovryga, A., J.O. Chuquin Gamarra, and J.W.G. van de Kuilen, *Strength and stiffness predictions with focus on different acoustic measurement methods.* European Journal of Wood and Wood Products, 2020. **78**(5): p. 941-949.
54. Baker, C.J., *The Development of a Theoretical Model for the Windthrow of Plants.* J. theor. Biol., 1995. **175**: p. 355–372.
55. A.H. ENGLAND, C.J. BAKER, and S.E.T. SAUNDERSON, *A dynamic analysis of windthrow of trees.* FORESTRY, 2000. **73**(2): p. 225-237.
56. Nocetti, M., M. Brunetti, and M. Bacher, *Effect of moisture content on the flexural properties and dynamic modulus of elasticity of dimension chestnut timber.* European Journal of Wood and Wood Products, 2014. **73**(1): p. 51-60.
57. ASTMD143–09, *standard test methods for small clear specimens of timber.* ASTM International, 2009. **West Conshohocken, PA, USA**.
58. Harwood, C., et al., *Patterns of variation in wood stiffness of plantation-grown Eucalyptus globulus and E. nitens.* CRC for Sustainable Production Forestry, 2005.
59. R, E., *Wood stiffness by X-ray diffractometry', In: Characterisation of the Cellulosic Cell Wall.* 11: Proceedings of the workshop 25-27 August 2003, Grand Lake, Colorado, USA. Southern Research Station, University of Iowa and the Society of Wood Science and Technology, Stokke D, Groom L (eds), Blackwell Publishing, 2006.
60. Downes, G., et al., *Wood properties of Eucalyptus globulus at three sites in Western Australia: Effects of fertiliser and plantation stocking.* Australian Forestry, 2014. **77**.
61. Downes, G.M., et al., *Measuring and modelling stem growth and wood formation: An overview.* Dendrochronologia, 2009. **27**(2): p. 147-157.

62. R. Farrell, T. Innes, and G. Nolan, *Sorting plantation Eucalyptus nitens logs with acoustic wave velocity.* Forest & Wood Products Australia (FWPA): Victoria, Australia, 2008.
63. Gherardi Hein, P.R. and J. Tarcísio Lima, *Relationships between microfibril angle, modulus of elasticity and compressive strength in Eucalyptus wood.* Maderas. Ciencia y tecnología, 2012(ahead): p. 0-0.
64. NEN-EN1995-1-1NB, *National annex to NEN-EN 1995-1-1. Eurocode 5: design of timber structures —part 1-1: General—common rules and rules for buildings (includes C1:2006 and A1:2008).* Netherlands Standardisation Institute (NEN), 2011. **Delft, Netherlands**.
65. Cheng, Y., et al., *Flexural characteristics of Eucalyptus nitens timber with high moisture content.* BioResources, 2021. **16**(2): p. 2921-2936.
66. Wang, C.-H. and X. Wang, *Vulnerability of timber in ground contact to fungal decay under climate change.* Climatic Change, 2012. **115**.
67. Hoffmeyer, P. *Moisture content-strength relationship for spruce lumber subjected to bending, compression and tension along the grain*. in *Proceedings, IUFRO wood engineering group meeting, Vancouver, BC*. 1978.
68. Aplin, E.N., D. Green, and J. Barrett, *The influence of moisture content on the flexural properties of Douglas fir dimension lumber.* Research paper FPL-United States Department of Agriculture, Forest Service, Forest Products Laboratory (USA), 1986.
69. Green, D.W. and J.W. Evans, *Evolution of standardized procedures for adjusting lumber properties for change in moisture content.* Gen. Tech. Rep. FPL-GTR-127. Madison, WI: US Department of Agriculture, Forest Service, Forest Products Laboratory. 50 p., 2001. **127**.
70. Barrett, J.D. and J.-P. Hong, *Moisture content adjustments for dynamic modulus of elasticity of wood members.* Wood Science and Technology, 2009. **44**(3): p. 485-495.
71. Glass, S.V. and S.L. Zelinka, *Moisture relations and physical properties of wood.* Wood handbook: wood as an engineering material: chapter 4. Centennial ed. General technical report FPL; GTR-190. Madison, WI: US Dept. of Agriculture, Forest Service, Forest Products Laboratory, 2010: p. 4.1-4.19., 2010. **190**: p. 4.1-4.19.
72. Haibin Zhou1, H.R., Jianxiong Lv1, Jinghui Jiang1, Xunshun Wang2, *BENDING STRENGTH ADJUSTMENTS FOR MOISTURE CONTENT FOR CHINESE FIR STRUCTURAL LUMBER.* World Conference on Timber Science, 2010.
73. Dieste, A., K. Rodríguez, and V. Baño, *Wood–water relations of chestnut wood used for structural purposes.* European Journal of Wood and Wood Products, 2013. **71**(1): p. 133-134.
74. Green, D.W., *Moisture Content and the Shrinkage of Lumber.*
75. ASTMD1990, *Standard methods for establishing allowable properties for visually graded dimension lumber from In-Grade tests of full-size specimens.* ASTM International, 2000. **West Conshohocken, PA, USA**.
76. Gerhards, C.C., *Effect of moisture content and temperature on the mechanical properties of wood: an analysis of immediate effects.* Wood and Fiber Science, 1980. **14**(1): p. 4-36.
77. Green, D.W., et al., *Predicting the effect of moisture content on the flexural properties of southern pine dimension lumber.* Wood and Fiber Science, 1986. **18**(1): p. 134-156.
78. Madsen, B., *Moisture content–strength relationship for lumber subjected to bending.* Canadian Journal of Civil Engineering, 1975. **2**(4): p. 466-473.
79. McLain, T.E., *The influence of moisture content on the flexural properties of southern pine dimension lumber [microform] / T.E. McLain ... [et. al.]*. Research paper FPL ; 447.,

ed. L. Forest Products. 1984, Madison, Wis: U.S. Dept. of Agriculture, Forest Service, Forest Products Laboratory.

80. Thoft-Christensen, P. and M.J. Baker, *Structural reliability theory and its applications*. 1982, Berlin; New York: Springer.

81. Arnold, M., *Effect of moisture on the bending properties of thermally modified beech and spruce.* Journal of Materials Science, 2009. **45**(3): p. 669.

82. EN384, *Structural timber—determination of characteristic values of mechanical properties and density.* European Committee for Standardization, Brussels, 2010.

83. AS/NZS4063.1, *Characterization of structural timber Part 1: Test method.* Standards Australia, 2010. **Sydney, Australia**.

84. Wang, C., R.H. Leicester, and M.N. Nguyen, *Probabilistic procedure for design of untreated timber poles in-ground under attack of decay fungi.* Reliability Engineering & System Safety, 2008. **93**(3): p. 476-481.

85. AS/NZS1080.1, *Timber—Methods of Test—Moisture Content.* Standards Australia, 2012. **Sydney, Australia**.

86. Hankinson, R., *Investigation of crushing strength of spruce at varying angles of grain.* Air service information circular, 1921. **3**(259): p. 130.

87. Mascia, N.T. and R.A. Simoni, *Analysis of failure criteria applied to wood.* Engineering Failure Analysis, 2013. **35**: p. 703-712.

88. AS/NZS4063.2, *Structural timber-Characteristic values of strength graded timber.* Standards Australia, 2010. **Sydney, Australia**.

89. ASTMD2899, *Standard practice for establishing allowable stresses for round timber piles.* ASTM International, 2012. **West Conshohocken, PA, USA**.

90. Gherardi Hein, P.R. and J. Tarcísio Lima, *Relationships between microfibril angle, modulus of elasticity and compressive strength in Eucalyptus wood.* Maderas. Ciencia y tecnología, 2012. **14**(3): p. 267-274.

91. AS2082, *Timber - Hardwood - Visually stress graded for structural purposes.* Standards Australia, 2007. **Sydney, Australia**.

92. Gibson, L.J. and M.F. Ashby, *Cellular solids: structure and properties*. 1999: Cambridge university press.

93. Mascia, N.T. and E.A. Nicolas, *Evaluation of Tsai–Wu criterion and Hankinson's formula for a Brazilian wood species by comparison with experimental off-axis strength tests.* Wood Material Science and Engineering, 2012. **7**(1): p. 49-58.

94. Crespo, J., et al., *Mechanical Properties of Small Clear Specimens of Eucalyptus globulus Labill.* Materials (Basel), 2020. **13**(4): p. 906.

95. Lahr, F.A.R., et al., *WOOD UTILIZATION OF Eucalyptus grandis IN STRUCTURAL ELEMENTS: DENSITIES AND MECHANICAL PROPERTIES.* Engenharia Agrícola, 2018. **38**(5): p. 642-647.

96. Bryc, W., *The normal distribution: characterizations with applications*. Vol. 100. 2012: Springer Science & Business Media.

97. Gherardi Hein, P.R. and L. Brancheriau, *Comparison between three-point and four-point flexural tests to determine wood strength of Eucalyptus specimens.* Maderas: Ciencia y Tecnología, 2018. **20**.

98. AS2878, *Timber – Classification into strength groups.* Standards Australia, 2000. **Sydney, Australia**.

99. Toson, B., P. Viot, and J.J. Pesqué, *Finite element modeling of Balsa wood structures under severe loadings.* Engineering Structures, 2014. **70**: p. 36-52.

100. Moses, D.M. and H.G. Prion, *Anisotropic plasticity and failure prediction in wood composites.* Ansys. net (online), 2002.

101. Tabarsa, T., *Compression perpendicular-to-grain behaviour of wood*. 1999.

102. Patton-Mallory, M., *The three-dimensional mechanics and failure of single bolt wood connections.* 1997.
103. Wang, J. and Y. Xiao, *Some improvements on Sun–Chen's one-parameter plasticity model for fibrous composites – Part I: Constitutive modelling for tension–compression asymmetry response.* Journal of Composite Materials, 2016. **51**(3): p. 405-418.
104. Wang, J. and Y. Xiao, *Some improvements on Sun-Chen's one-parameter plasticity model for fibrous composites (Part II: Finite element method implementation and applications).* Journal of Composite Materials, 2016. **51**(4): p. 533-545.
105. Yokozeki, T., et al., *Simple constitutive model for nonlinear response of fiber-reinforced composites with loading-directional dependence.* Composites Science and Technology, 2007. **67**(1): p. 111-118.
106. Drucker, D.C. and W. Prager, *Soil mechanics and plastic analysis or limit design.* Quarterly of applied mathematics, 1952. **10**(2): p. 157-165.
107. Tsai, S.W. and E.M. Wu, *A General Theory of Strength for Anisotropic Materials.* Journal of Composite Materials, 1971. **5**(1): p. 58-80.
108. Lubliner, J., *Plasticity Theory*. 2008: Dover Publications.
109. Wang, J., Y. Xiao, and M. Kawai, *Parameter identification problem in one-parameter plasticity model for fibrous composites.* Advanced Composite Materials, 2018: p. 1-23.
110. Mackenzie-Helnwein, P., J. Eberhardsteiner, and H.A. Mang, *A multi-surface plasticity model for clear wood and its application to the finite element analysis of structural details.* Computational Mechanics, 2003. **31**: p. 204-218.
111. Neumann, M., et al., *Compressive behaviour of axially loaded spruce wood under large deformations at different strain rates.* European Journal of Wood and Wood Products, 2010. **69**(3): p. 345-357.
112. Leijten, A.J.M., A.J.M. Jorissen, and B.J.C. de Leijer, *The local bearing capacity perpendicular to grain of structural timber elements.* Construction and Building Materials, 2012. **27**(1): p. 54-59.
113. Dawson, B.S.W., et al., *Effect of supercritical CO2 treatment and kiln drying on collapse in Eucalyptus nitens wood.* European Journal of Wood and Wood Products, 2020. **78**(2): p. 209-217.
114. Resch, E. and M. Kaliske, *Three-dimensional numerical analyses of load-bearing behavior and failure of multiple double-shear dowel-type connections in timber engineering.* Computers & Structures, 2010. **88**(3): p. 165-177.
115. Lang, E.M., et al., *Orthotropic strength and elasticity of hardwoods in relation to composite manufacture. Part I. Orthotropy of shear strength.* Wood and fiber science, 2007. **32**(4): p. 502-519.
116. Báder, M. and R. Németh, *Moisture-dependent mechanical properties of longitudinally compressed wood.* European Journal of Wood and Wood Products, 2019. **77**(6): p. 1009-1019.
117. NEN5491, *Quality requirements for timber—piles—coniferous timber.* Netherlands Standardisation Institute (NEN), 1999. **Delft, Netherlands**.
118. DIN1052-1, *Timber structures; design and construction.* German Institute for Standardization (DIN), 1988. **Berlin, Germany**.

APPENDICES

Appendix 1

S_{ijkl} ($i, j, k, l = L, R, T$) is the item of elastic–plastic compliance matrix, S_{ijkl}^{ep}, which reads:

$$S_{LLLL} = \frac{1}{E_{LL}} + \frac{1}{H_p}[\frac{\sigma_{LL}}{\tilde{\sigma}}]^2,$$

$$S_{LLRR} = S_{LLTT} = -\frac{\upsilon_{LR}}{E_{LL}},$$

$$S_{LLRT} = S_{LLTL} = S_{LLLR} = 0$$

$$S_{RRRR} = \frac{1}{E_{RR}} + \frac{1}{H_p}[\frac{3(\sigma_{RR} - \sigma_{TT})}{2\tilde{\sigma}} + \sqrt{\frac{3}{2}}(V-1)]^2,$$

$$S_{RRTT} = -\frac{\upsilon_{RT}}{E_{RR}} + \frac{1}{H_p}[\frac{3(\sigma_{RR} - \sigma_{TT})}{2\tilde{\sigma}} + \sqrt{\frac{3}{2}}(V-1)][\frac{3(\sigma_{TT} - \sigma_{RR})}{2\tilde{\sigma}} + \sqrt{\frac{3}{2}}(V-1)],$$

$$S_{RRRT} = \frac{6\sigma_{RT}}{H_p\tilde{\sigma}}[\frac{3(\sigma_{RR} - \sigma_{TT})}{2\tilde{\sigma}} + \sqrt{\frac{3}{2}}(V-1)],$$

$$S_{RRTL} = \frac{3BV^2\sigma_{TL}}{H_p\tilde{\sigma}}[\frac{3(\sigma_{RR} - \sigma_{TT})}{2\tilde{\sigma}} + \sqrt{\frac{3}{2}}(V-1)],$$

$$S_{RRLR} = \frac{3BV^2\sigma_{LR}}{H_p\tilde{\sigma}}[\frac{3(\sigma_{RR} - \sigma_{TT})}{2\tilde{\sigma}} + \sqrt{\frac{3}{2}}(V-1)],$$

$$S_{TTTT} = \frac{1}{E_{TT}} + \frac{1}{H_p}[\frac{3(\sigma_{TT} - \sigma_{RR})}{2\tilde{\sigma}} + \sqrt{\frac{3}{2}}(V-1)]^2$$

$$S_{TTRT} = \frac{6\sigma_{RT}}{H_p\tilde{\sigma}}[\frac{3(\sigma_{TT} - \sigma_{RR})}{2\tilde{\sigma}} + \sqrt{\frac{3}{2}}(V-1)],$$

$$S_{TTTL} = \frac{3BV^2\sigma_{TL}}{H_p\tilde{\sigma}}[\frac{3(\sigma_{TT} - \sigma_{RR})}{2\tilde{\sigma}} + \sqrt{\frac{3}{2}}(V-1)],$$

(A.1)

$$S_{TTLR} = \frac{3BV^2\sigma_{LR}}{H_p\tilde{\sigma}}[\frac{3(\sigma_{TT}-\sigma_{RR})}{2\tilde{\sigma}} + \sqrt{\frac{3}{2}}(V-1)],$$

$$S_{RTRT} = \frac{1}{G_{RT}} + \frac{1}{H_p}(\frac{6\sigma_{RT}}{\tilde{\sigma}})^2,$$

$$S_{RTTL} = \frac{18BV^2}{H_p\tilde{\sigma}}\sigma_{RT}\sigma_{TL},$$

$$S_{RTLR} = \frac{18BV^2}{H_p\tilde{\sigma}}\sigma_{LR}\sigma_{RT},$$

$$S_{TLTL} = \frac{1}{G_{TL}} + \frac{1}{H_p}(\frac{3BV^2\sigma_{TL}}{\tilde{\sigma}})^2,$$

$$S_{TLLR} = \frac{\sigma_{LR}\sigma_{TL}}{H_p}(\frac{3BV^2}{\tilde{\sigma}})^2,$$

$$S_{LRLR} = \frac{1}{G_{LR}} + \frac{1}{H_p}(\frac{3BV^2\sigma_{LR}}{\tilde{\sigma}})^2,$$

Other items of S_{ijkl}^{ep} can be obtained because of the symmetric matrix.

Appendix 2

The off-axis tension tests for *E. nitens* specimens were conducted on a Universal Testing Machine (Zwick Roell-Z100, capacity 100 kN) according to ASTM D143–09 [57] at temperature and relative humidity in the range of 15 - 25 $^{\circ}$C to and 55 to 70 %, respectively. The specimens were carefully clamped on either end (*Fig A.1*). The tensile testing was performed with displacement-control and at a constant loading rate of 0.3 mm/min for each testing and discontinued when the rupture failure was observed in the load-deformation curves. The forces and the deformations were measured in the axis of loading. Deformations were measured from the point at which tensile force first appeared. The distance between the two grips when tension was first developed was also measured as the original distance. The tensile strain was controlled by a moveable crosshead and calculated in the load direction from the relative position of the grips in relation to the original distance between the two grips. A computer connected to a data acquisition board was used to store and analyse the data. The load and deflection curves of small clear *E. nitens* with both low and high moisture contents in off-axis tension testing were obtained.

Fig. A.1 Test photo of off axis tension testing

Two dimensions of the samples were used, the first is 600 mm length (*L*) × 50 mm width (*W*) × 10 mm depth (*D*) with a narrow part with cross-sectional area of 10 × 10 mm^2 and a length of 100 mm, while the second is 600 mm (*L*) × 50 mm (*W*) ×10 mm (*D*) (*Fig 7.1c, d*). The first sample type was waisted to ensure that failure occurred within the central portion and to minimise stress concentration in the transition area and was used to-test grain angles of 0°, 10° or 45°, while the second sample type was used for testing in tension perpendicular to the grain as it is hard to manufacture waisted samples for tension perpendicular to the grain (i.e. at a grain angle of 90°). Small pieces cut from each specimen were oven dried for 72 hours to determine moisture content and basic density according to AS/NZS 1080.1 [85]. In total, 80 small clear *E. nitens* samples were used; half of each species was tested in a dry condition (i.e. 40 dry samples for *E. nitens),* and the rest of the samples were tested in a wet condition, and these were prepared using the same method described in a the previous study [57].